An Investigation of the Properties and Functions of Connexins in the Mammalian Inner Ear

John Joseph Kelly

Ear Institute

University College London

A thesis submitted for the degree of

Doctor of Philosophy

September 2011

Declaration

I, John Kelly, confirm that the work presented in this thesis is my own. Where information or assistance has been derived from other sources, I confirm that this has been indicated in the thesis.

Acknowledgements

First and foremost, I would like to thank my supervisors: Dr. Dan Jagger for your continued support, advice and patience throughout my Ph.D., and Prof. Andy Forge for all your help and guidance along the way. It's been a privilege to have you both as my mentors. I'd also like to thank other members of the group: Regina, for your expertise and friendship and for helping me integrate into the lab with ease; Ruth, for your help and advice over the years; Graham for your expertise and recommendations of areas to explore in the UK (one day….), and Nicole, for your company both inside and outside of the lab, and for the fond memories of our road trip around southern California with Cassy. Lisa, I've had the pleasure of working with you in two different labs. Thank you for all your help and advice and for your infectious positivity! I would like to thank Dr. Sally Dawson for introducing me to the world of molecular biology and to both Sally and Dr. Jonathan Gale for the advice you have both given me. Emily, you've been a fantastic lab, desk and tea-break buddy. Thank you for all your help and advice and for putting up with all my silly questions. Miriam, thank you for all your help in the lab. Tommy and Valentina, you both made me feel so welcome when I joined and your help in the lab was very much appreciated. It has been a pleasure working with you all.

I'd like to thank Deafness Research UK for funding my Ph.D. studies and giving me the opportunity to present my work in the USA. I am indebted to all the friends I have made at the Ear Institute over the past five years. Elena (BT/Mou) we started this together and we'll finish this together. It's been a long journey but I couldn't have asked for a better person to have shared it with. Freeman, you've been a constant source of entertainment and laughter. Marc Astick, you nearly ruined my Ph.D. after introducing me to stick cricket, but I forgive you. Zoë, you always made sure we were in the pub by 5.30pm (at the latest) on a Friday night. Bjorn and Lucy, we've enjoyed a drink (and a whiskey) or two! Amongst others, Greg, Pavel, Manu, Jason, Ghada, Joey, Joerg, Nico, and all those in the "back-office"; thank you all for your support and friendship over the years, it's been a pleasure getting to know you all.

Adam, thanks for being a fantastic mate and giving me sound advice along the way, and a huge thank you to my fellow Ph.D. buddies Clare (we made it!), Jenny, Mark, Fran, Maz and Andrew for adopting me as their unofficial 7th group member.

We've had some incredible and unforgettable times. I'd like to thank Ben, Mace, Kate, Steve, Emily, Mattea, Unyime, Phil, John, Tom and Kieran for giving me an escape-route from work and not giving up on me towards the end. I can't have asked for a better bunch of friends.

Last, but certainly not least, I'd like to thank my family. Mum, Dad, Maria, Sarah, Cath and Gel. Your support and encouragement has been amazing, without which this Ph.D. wouldn't have been possible.

John Kelly

September 2011

Abstract

Connexin 26 (Cx26) and Cx30 are the two predominant gap junction constituents expressed in the mammalian cochlea. Mutations in either gene cause hereditary deafness, indicating an essential role for connexins in auditory function. Gap junctions consisting of Cx26 and Cx30 have been implicated in several cochlear processes; however, the precise functions and life-cycle of connexins in the cochlea are poorly defined. Three aspects of inner ear connexin biology were investigated.

Most connexins traffic to the plasma membrane (PM) via the conventional secretory pathway. Conflicting data exists for Cx26 trafficking, whereas that of Cx30 had not been previously studied. Trafficking of Cx26 and Cx30 were investigated using stably-transfected HeLa cell lines. Treatment with brefeldin-A (a Golgi-disrupting drug) did not prevent targeting of Cx30 to the PM, whereas Cx26 was strongly inhibited. These data suggest that Cx30 may traffic to the PM via a Golgi-independent pathway, which is in contrast to a Golgi-dependent pathway for Cx26.

Gap junctional intercellular communication (GJIC) pathways are hypothesised to support K^+ recycling in the cochlea. This study investigated the development of GJIC in the lateral wall (LW) of live rat cochlear slices. Cx26 and Cx30 immunofluorescence revealed a progressive increase of gap junction expression from postnatal day 0 (P0) to P7-P8. Dye-coupling was compartmentalised between P2-P5, but was extensive by P7. These data suggest that GJIC matures several days in advance of hearing onset and provides anatomical evidence of a putative K^+-recycling pathway.

Finally, $Cx30^{-/-}$ mice are deaf and fail to develop an endocochlear potential (EP). This study investigated the expression of proteins involved in EP generation and found that the potassium channel $K_{ir}4.1$ was noticeably reduced in the stria vascularis (SV) of $Cx30^{-/-}$ mice. In contrast to a separate study, the SV endothelial barrier was intact. In addition, anatomical analysis was consistent with loss of Cx30 retarding maturation of SV.

Table of Contents

List of Figures

List of Tables

List of Abbreviations

aa	Amino acid
ATP	Adenosine triphosphate
BFA	Brefeldin-A
BLAST	Basic local alignment search tool
BPS	Bart-Pumphrey syndrome
BSA	Bovine serum albumin
Cx	Connexin
DAPI	4',6-diamidino-2-phenylindole
cAMP	Cyclic adenosine monophosphate
CFP	Cyan fluorescent protein
dB	Decibel
DMEM	Dulbecco's Modified Eagle medium
DMSO	Dimethyl sulphoxide
EDTA	Ethylenediamine tetra-acetic acid
eGFP	Enhanced green fluorescent protein
EDTA	Ethylenediaminetetraacetic acid
EGTA	Ethylene glycol-bis (β-aminoethyl ether)-N,N,N'N'-tetraacetic acid
EP	Endocochlear potential
ER	Endoplasmic reticulum
ERGIC	ER-Golgi intermediate compartment
FBS	Foetal bovine serum
FC	Fibrocyte
FD	Fluorescein-conjugated dextran
FITC	Fluorescein isothiocyanate

FRAP	Fluorescence recovery after photo-bleaching
FRET	Fluorescence resonance energy transfer
GLUT-1	Glucose transporter-1
GJ	Gap junction
GJIC	Gap junctional intercellular communication
HBSS	Hanks Balanced Salt Solution
HEPES	4-(2-hydroxyethyl)-1-piperazineethanesulfonic acid
HID	Hystrix-like ichthyosis-deafness
IHC	Inner hair cell
IP_3	Inositol 1,4,5-triphosphate
IRES	Internal ribosomal entry site
ITS	Insulin-transferrin-selenium
KID	Keratitis-ichthyosis deafness
LB	Luria-Bertani medium
LY	Lucifer yellow
MEM-α	Minimal essential medium alpha
MET	Mechanoelectrical transduction channel
MFA	Meclofenamic acid
2-NBDG	2-[N-(7-Nitrobenz-2-Oxa-1,3-Diazol-4-yl)Amino]-2-Deoxy-D-Glucose
NBN	Neurobiotin™
neo	Neomycin resistance cassette
NKCC1	Na^+,K^+,Cl^- co-transporter protein 1
OCT	Optimal cutting temperature
OHC	Outer hair cell
PBS	Phosphate buffered saline
PCR	Polymerase chain reaction
PFA	Paraformaldehyde

PM	Plasma membrane
PPK	Palmoplantar keratoderma
q-PCR	Quantitative real-time polymerase chain reaction
ROS	Reactive oxygen species
rpm	Revolutions per minute
RT-PCR	Reverse transcription polymerase chain reaction
SC	Supporting cell
SEM	Standard error of the mean
SV	Stria vascularis
TAE	Tris-actate-EDTA electrophoresis buffer
TEM	Transmission electron microscopy
TGN	*trans*-Golgi network
VS	Vohwinkel syndrome
YFP	Yellow fluorescent protein
ZO-1/2	Zona occludens protein 1/2

1 INTRODUCTION

As many as 3 in 1000 children are born deaf or develop profound hearing loss by the age of five years (reviewed by Morton and Nance, 2006) and at least 50-60% of these cases are genetically inherited, making hearing impairment the most common inherited sensory disorder (Marazita et al., 1993). Around 70% of cases are non-syndromic (where deafness is the only phenotype) and approximately half of these are attributed to recessive mutations in genes that encode "connexin" proteins that form "gap junctions" (Denoyelle et al., 1999). In addition, several dominantly inherited mutations in human connexin genes cause hearing loss that are also associated with other syndromes, such as skin disease (reviewed by Scott and Kelsell, 2011). Despite the high frequency of deafness, our understanding of the role of these proteins in the normal physiology of the inner ear remains to be clarified. This thesis investigates some of the properties and functions of connexins in the mammalian inner ear and discusses their potential role in hearing and deafness. This chapter broadly introduces the field of gap junctions and gives a general description of what gap junctions are and how they are formed. In addition, the general structure and function of the mammalian hearing system is introduced as well as the gap junction networks within the inner ear.

1.1 Gap Junctions

The evolution of multicellular organisms from primitive single-cell structures required the development of intercellular communication. Without such development, cells would act independently rather than in a cooperative syncytium where it "becomes possible to exploit resources that no single cell could utilize so well" (Alberts et al., 1994). The development of cell-cell communication allows multicellular structures to coordinate responses to external stimuli and determine the differentiation and function of individual cells as well as more complex tissues and organs in the animal kingdom. As well as extracellular signalling, direct intercellular communication is paramount for regulating the internal environment of a multicellular organism. This direct communication is mediated by gap junctions.

Gap junctions are clusters of pore-forming transmembrane channels that connect the cytoplasm of adjacent cells, providing pathways for the transfer of ions, metabolites

and second messengers up to ~1 kDa in molecular mass (reviewed in Bruzzone et al., 1996; Laird, 2006). Thus, gap junctions permit nutrient transfer between cells, metabolic coupling and buffering of ions. Gap junctions have also been implicated in the propagation of second messengers such as cAMP, growth regulation, differentiation and development in all vertebrate multicellular systems (Goodenough et al., 1996; Alexander and Goldberg, 2003; Bruzzone and Dermietzel, 2006).

1.1.1 Identification of intercellular communication and gap junctions

The first description of intercellular communication was suggested by Engelmann in 1877, who predicted that cardiac cells were in direct contact when alive, but became independent as they die – a process termed 'healing-over' (as mentioned in Weidmann, 1952; De Mello, 1983). Evidence of direct intercellular communication was not described until the 1950s through electrophysiological studies of Purkinje fibres of the mammalian heart (Weidmann, 1952) and motor synapses of the giant crayfish (Furshpan and Potter, 1959). Loewenstein (1966) then demonstrated ionic coupling between epithelial cells and showed gap junction sensitivity to changes in Ca^{2+} concentration for the first time.

Gap junction structures were first identified in thin-section electron micrographs (EM) of goldfish Mauthner cell synapses, where they were recognised as closely-packed, honeycomb-like hexagonal arrays (Robertson, 1963). These structures also found in negatively stained plasma membranes from rat liver fractions and Emmelot, 1965) (Image deleted due to copyright

Figure 1-1A). A subsequent study of mouse heart and liver tissue pre-treated with a membrane-impermeable, colloidal form of lanthanum showed electron dense material between two closely opposed plasma membranes (Revel and Karnovsky, 1967). These junctional structures resulted in a very narrow "gap" of ~20 Å (~2 nm) between membranes (Image deleted due to copyright

Figure 1-1B) and led to the eventual term “gap junction”. Confirmation that these junctions were composed of hexagonal gap junction units, rather than tight junctions was verified using the freeze-fracture technique (Chalcroft and Bullivant, 1970; Goodenough and Revel, 1970). In addition to the techniques described, X-ray diffraction analysis revealed that the extracellular “gap” between the membranes was bridged by two hexameric hemichannels (otherwise known as connexons) that dock together to form a complete intercellular channel or gap junction (Makowski et al., 1977).

In vertebrates, each hemichannel is composed of six connexin subunits (see below for detailed gap junction structure). The discovery that invertebrates also express gap junction proteins suggests that the ability for cells to communicate via gap junctions and hemichannels is evolutionarily conserved. Invertebrate gap junctions are composed of subunits called innexins, which share similar topography, but not sequence homology, to connexins (reviewed by Phelan, 2005). In addition, studies in the last decade have also identified a separate family of vertebrate proteins that share homology to invertebrate innexins, but not connexins. These proteins, called pannexins, are classed within the gap junction family of proteins due to their homology to innexins and similar topography to innexins and connexins. However, recent data has suggested that pannexins function mostly as membrane channels, termed pannexons, rather than functional intercellular channels (reviewed by Scemes, 2011; Sosinsky et al., 2011). Pannexon channels are suggested to participate in purinergic signalling and calcium-wave propagation by releasing ATP into the extracellular space. Thus, pannexins may be important for migratory patterns, regenerative signals, cell proliferation and development (reviewed by Barbe et al., 2006).

Figure 1-1. Early electron micrographs of gap junction channels.

(A) Negatively stained rat liver plasma membrane revealing the hexagonal configuration of gap junction channels (adapted from Benedetti and Emmelot, 1965). (B) A high magnification image of a mouse cardiac gap junction. The intercellular space (ics) is reduced to a gap about 20 Å (~2 nm) wide (g) in the junctional area (adapted from Revel and Karnovsky, 1967).

1.1.2 Connexin nomenclature

A variety of biochemical techniques developed in the 1970s led to the isolation and identification of gap junction constituents (Goodenough and Stoeckenius, 1972; Goodenough, 1974), and it was Goodenough (1974) who first proposed the term "connexin" as an amalgamation of the words 'connection' and 'nexus'. At the molecular level, connexins were first cloned in 1986 (Paul, 1986; Kumar and Gilula, 1986) and since then, a total of 21 connexin-coding genes have been identified in humans and 20 in mice (Willecke et al., 2002) (see Table 1-1). Historically, connexin genes were classified according to their phylogenetic homology, which took into account genetic structure, sequence homology and matching of specific genetic motifs (Kumar and Gilula, 1992).

Connexin genes are named with a prefix of Gj ('Gap Junction') followed by a Greek letter which represents the classification group (α, β, γ, δ, and ε). In addition, a number corresponding to the order of identification is also added. For example, connexin 43 (Cx43) has the gene name *Gja1*, indicating that it belongs to the α group of connexins and was the first α-connexin gene to be identified. The connexin protein name is based on the predicted molecular mass (in kDa) of the connexin (e.g. Cx43 has a molecular mass of 43 kDa). To distinguish human connexins from other species, connexin genes and proteins are written in upper-case letters, such as CX43 or *GJA1*, compared to Cx43 or *Gja1* for other species, including mouse.

Nineteen connexins can be grouped as sequence-orthologous pairs between humans and mice, however there are connexin genes that occur only in the mouse (Cx33) or in the human genome (Cx25 and Cx59). Further complexity in connexin nomenclature arises from orthologous connexins that have differing molecular masses. For example, Cx57 is the mouse orthologue of human Cx62. In addition, Cx23 is not expressed in primates due to a premature stop mutation in the *GJE1* gene, yet it is highly conserved across other species, including mice. This has led to the presumption that the primate *GJE1* gene is a non-functional pseudogene (Sonntag et al., 2009). These complexities mean that connexin nomenclature has been a matter of debate for some time (Sohl and Willecke, 2003; Kidder, 2009). The current classification of all known mammalian connexins is summarised in Table 1-1.

Mouse Connexins		Human Connexins	
Protein	Gene	Protein	Gene
Cx43	*Gja1*	CX43	*GJA1*
Cx46	*Gja3*	CX46	*GJA3*
Cx37	*Gja4*	CX37	*GJA4*
Cx40	*Gja5*	CX40	*GJA5*
Cx33	*Gja6*	-	-
Cx50	*Gja8*	CX50	*GJA8*
-	-	CX59	*GJA9 (GJA10)*
Cx57	*Gja10*	CX62	*GJA10*
Cx32	*Gjb1*	CX32	*GJB1*
Cx26	*Gjb2*	CX26	*GJB2*
Cx31	*Gjb3*	CX31	*GJB3*
Cx30.3	*Gjb4*	CX30.3	*GJB4*
Cx31.1	*Gjb5*	CX31.1	*GJB5*
Cx30	*Gjb6*	CX30	*GJB6*
-	-	CX25	*GJB7*
Cx45	*Gjc1*	CX45	*GJC1 (GJA7)*
Cx47	*Gjc2*	CX47	*GJC2 (GJC12)*
Cx29	*Gjc3*	CX30.2/CX31.3	*GJC3 (GJE1)*
Cx36	*Gjd2*	CX36	*GJD2 (GJA9)*
Cx30.2	*Gjd3*	CX31.9	*GJD3 (GJC1)*
Cx39	*Gjd4*	CX40.1	*GJD4*
Cx23	*Gje1*	CX23	*GJE1*

Table 1-1. Nomenclature of mouse and human connexins.

Information is organised so that corresponding orthologues are aligned in the same row. There are five main connexin families: alpha (*Gja*), beta (*Gjb*), gamma (*Gjc*), delta (*Gjd*) and epsilon (*Gje*). Genes in brackets indicate previously assigned gene names. Missing gene numbers have been assigned to other species that do not have orthologues in the mouse or human genomes. For example *Gja2* codes for Cx38 in *Xenopus laevis*. Data adapted from Beyer and Berthoud **(**2009) and from the HUGO Gene Nomenclature Committee website (http://www.genenames.org/genefamilies/GJ, accessed August 2011).

1.1.3 Structure of gap junctions

A model of the topological structure of the liver connexin (later identified as Cx32) was first demonstrated by Zimmer et al. (1987) using a combination of proteolytic digestion and site-directed antibodies. This model is thought to be consistent across all members of the connexin family. Each connexin spans the membrane four times forming four transmembrane domains (M1-M4), which are connected by two extracellular loops (E1, E2). On the cytoplasmic side of the membrane, one cytoplasmic loop (CL), an amino-terminus (NT) and a carboxyl-terminus (CT) complete the connexin structure (Figure 1-2).

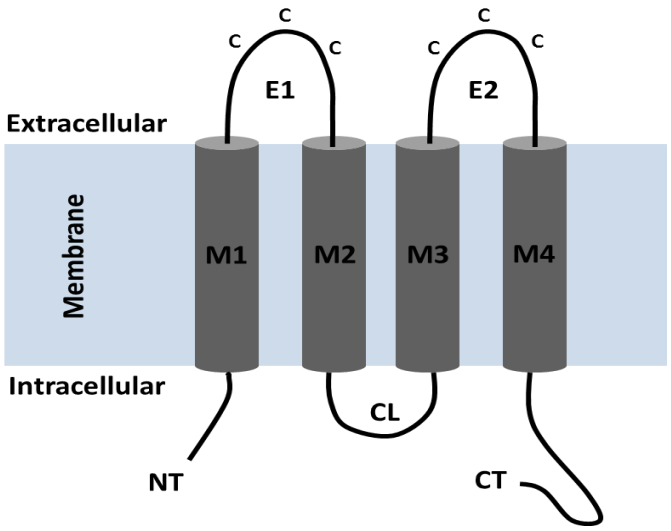

Figure 1-2. Connexin membrane topology.

The four transmembrane domains, the two extracellular loops and the amino-terminus are the most conserved regions between connexins, as determined by sequence analysis. In particular, E1 and E2 are amongst the most conserved regions, with each loop containing three cysteine residues (see Figure 1-2) separated by a set number of amino acids. E1 contains C-X_6-C-X_3-C and E2 contains C-X_4-C-X_5-C sequence motifs. The only exceptions to these rules are for Cx31, which contains a C-X_5-C-X_5-C motif in E2, and Cx23, which has only two cysteines in E1 and E2. The CL and CT domains have highly divergent amino acid (aa) sequences, with the CT having the greatest variability between connexins. Changes in the length of the CT are responsible for most differences in molecular mass and can vary drastically from 10 to 12 aa in Cx26, Cx30.3 and Cx31.1 to more than 310 aa in CX59 and CX62 (reviewed in Beyer and Berthoud, 2009).

Each connexin oligomerises with five other connexins to form a hexameric connexon (hemichannel). Adjacent cells each provide one hemichannel that dock together at closely associated apposing cell membranes to form an intercellular channel or gap junction (Image (C) deleted due to copyright

Figure 1-3A). Docking of opposing connexons is determined by the extracellular loops, with E2 influencing whether two connexons are compatible (White et al., 1995). The highly conserved cysteine residues form disulphide bonds between the extracellular loops (John and Revel, 1991) and are essential for the functioning of channel (Dahl et al., 1992). Connexons can be homomeric, consisting of only one connexin subtype; or heteromeric, consisting of more than one connexin type (Image (C) deleted due to copyright

Figure 1-3B). Likewise, gap junctions can be homotypic, with each connexon containing six identical connexins; or heterotypic, containing different connexons with varying composition and/or stoichiometry. The compatibility of different homomeric connexons to form heterotypic channels likely depends on specific motifs in the extracellular loops (reviewed by Koval, 2006).

The initial higher-order structure of gap junctions was first revealed by analysis of 2D crystals at 19Å resolution (Unwin and Ennis, 1984). Since then, advances in techniques used to detect high-resolution structures, such as atomic force and electron crystallography, have led to a great increase in knowledge of how hemichannels dock together and how the spatial resolution of single amino acids regulate gap junction permeability. Both techniques have revealed that the loops of a connexon form six alternating 'peaks and valleys' (Image (C) deleted due to copyright

Figure 1-3C) (Perkins et al., 1998). After a 30^{o} rotation, the peaks of one connexon fit into the valleys of the apposed connexon by a predicted "lock and key" mechanism, thus forming a tightly sealed channel (Image (C) deleted due to copyright

Figure 1-3D) (Hoh et al., 1993; Perkins et al., 1998). Further analysis has revealed a 3-dimensional model of a C-terminally truncated Cx43 channel at 7.5Å using cryo-electron-microscopy (Unger et al., 1999). More recently, the crystal structure of a Cx26 gap junction at 3.5Å resolution has been reported (Maeda et al., 2009). The authors propose that Cx26 gap junctions have a narrow funnel leading from the cytoplasmic entrance to the transmembrane pore. The funnel is regulated by conformational changes in the N-terminal regions of connexin subunits, and thus determines the molecular size restriction at the channel entrance. The conformational changes in the Cx26 N-termini are predicted to play a role in the gating of the channel by transjunctional voltage.

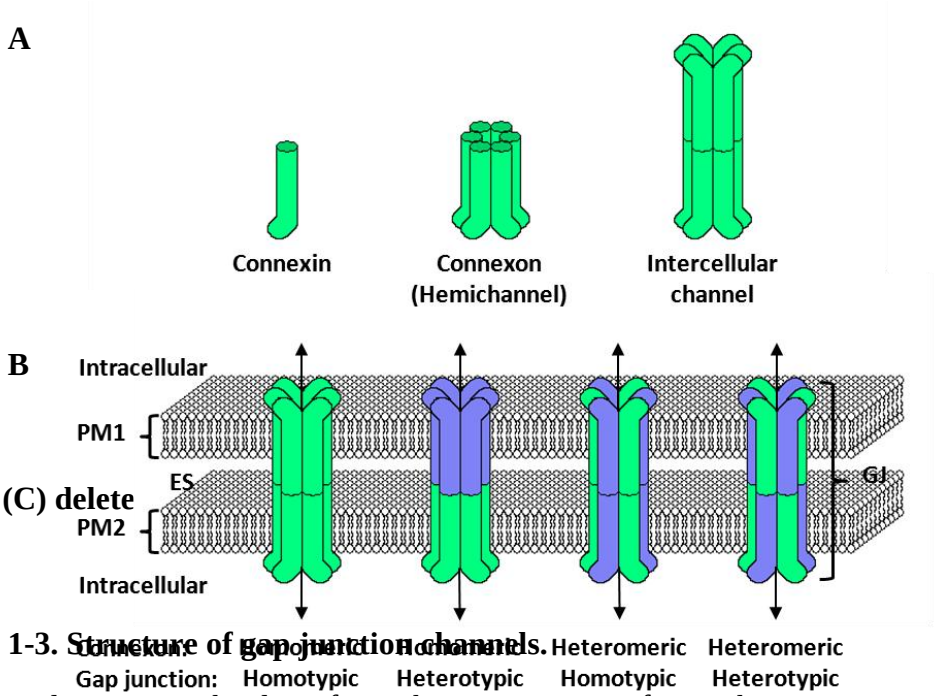

Image (C) delete

Figure 1-3. Structure of gap junction channels.
(A) A single connexin binds to five other connexins to form a hexameric connexon or hemichannel. Two connexons dock together to form an intercellular channel. (B) Intercellular channels bridge the 2 nm gap of extracellular space (ES) between two opposing plasma membranes (PM1, PM2). Thus, the intercellular channels are referred to as gap junctions (GJ), which can contain more than one connexin and a range of different hemichannel and gap junction configurations. (C) Computer reconstruction of a connexon, revealing the peaks and valleys on the extracellular surface. (D) A gap junction model of two docked connexons showing a tight seal between the peaks and valleys after a 30^{o} rotation. Images (C) and (D) were adapted from Perkins et al., 1998.

1.1.4 Gap junction expression and disease

Connexin expression and gap junctional intercellular communication (GJIC) exists in almost all mammalian cell types (reviewed by Saez et al., 2003; Laird, 2006). Cx43 has been detected in at least 35 distinct tissues and cells types, making it the most prevalent connexin subtype expressed in mammals (reviewed by Laird, 2006). In addition, many cells and/or tissues express more than one connexin, for example keratinocyte populations can express up to 10 different connexin isoforms (Di et al., 2001). These expression patterns allow for inter-mixing of connexins within family subgroups, and therefore, can lead to a large number of different gap junction configurations. This property allows gap junctions with different configurations to regulate certain properties, such as permeability, and confer sensitivities to changes in cellular cues, such as pH, voltage-gating and Ca^{2+} signalling (reviewed by Harris, 2001). In addition, over-lapping connexin expression could represent an evolutionary compensatory mechanism for the loss or mutation of a particular connexin, although this is not always the case, since some mutations can exert dominant-negative effects or develop a pathological gain-of-function (reviewed by Laird, 2006).

Mutations in connexin genes account for many inherited diseases, ranging from deafness to neuropathies, skin disease, cataracts and oculodentodigital dysplasia, the inheritance of which can be autosomal dominant, autosomal recessive or X-linked (reviewed by White and Paul, 1999; Beyer and Berthoud, 2009). Connexin mutants can confer disease through a variety of defects, including faulty protein folding and oligomerisation, trafficking defects, ER-associated cell death, aberrant hemichannel activity and non-functional channels. The first condition connected to a mutation in a connexin gene was that of the X-linked form of Charcot-Marie-Tooth disease (CMTX). The mutation was mapped to the X-chromosome region where the CX32 gene, *GJB1*, resides and was subsequently confirmed by direct sequencing (Bergoffen et al., 1993). More than 200 mutations associated with CMTX have since been identified in the *GJB1* gene, which cause a progressive neuropathy resulting in the degeneration of peripheral nerves.

More than 20 dominant mutations in the *GJA1* gene (codes for CX43) are associated with oculodentodigital dysplasia. This disease causes craniofacial abnormalities and malformations of fingers and teeth, as well as cardiac abnormalities

(reviewed by Paznekas et al., 2009). Other diseases linked to connexin mutations include cataracts, which are formed by precipitation of crystallins within the lens fibre cells. Cx46 and Cx50 are essential for lens homeostasis and mouse models with gene deletions form cataracts (reviewed by Mathias et al., 2010).

Connexin diseases can also be caused by more than one connexin isoform and can affect more than one system. For example, mutations in *GJB2* (Cx26), *GJB3* (Cx31), *GJB4* (Cx30.3) and *GJB6* (Cx30) can cause hearing loss (non-syndromic), skin disease, or hearing loss with skin disease (syndromic). Some of these mutations are described in further detail in chapter 5, and reviewed by Scott and Kelsell (2011).

1.2 The Mammalian Inner Ear

1.2.1 General structure of the inner ear

The ear is comprised of three compartments, namely the outer, middle and inner ear. The outer ear, including the pinna and the external auditory canal, is focusing acoustic energy towards the tympanic membrane (ear drum). Vibrations tympanic membrane are relayed to the connecting malleus, incus, and stapes, together form the middle ear ossicular chain. These bones, the smallest bones in body, amplify and transmit sound energy from the air-filled outer/middle ear to fluid-filled inner ear via the oval window (Images deleted due to copyright

Figure 1-4A).

The inner ear is a complex structure and consists of two sensory systems: the cochlea for hearing and the vestibular system for balance. In humans and higher primates, the structure is encased within the petrous portion of the temporal bone, the hardest bone in the body, and consists of a series of interconnected bony labyrinthine channels. In other mammals, the inner ear is contained within an easily-accessible auditory bulla (Forge and Wright, 2002). The bony labyrinth is filled with a fluid called perilymph, the composition of which is similar to other extracellular fluids (low in K^+ ions, high in Na^+ ions). Within the bony channels, and enclosed in perilymph, is a membranous, epithelial labyrinth. These epithelial tubes are filled with a fluid called endolymph, whose unusual composition more closely resembles that of intracellular fluid (high in K^+ ions, low in Na^+ ions). A more detailed description of these fluids can be found in chapter 4.

Images deleted due to copyright

Figure 1-4. Structure of the human ear.

(A) Anatomical diagram indicating the location and components of the outer (green), middle (blue/red) and inner (purple/yellow) ears in humans. Image adapted from Chittka and Brockmann, 2005. (B) A diagram of a cross-section through the human inner ear. The white spaces of the bony labyrinth are filled with perilymphatic fluid, whereas the grey-shaded membranous labyrinths are filled with endolymphatic fluid. The six sensory epithelia are shaded in black. (C) Cross-section of a slice through the cochlear duct (red box). The sensory epithelia (organ of Corti), ion transporting epithelia (stria vascularis) and less specialised epithelia (Reissner's membrane) lining the endolymphatic duct (scala media) are labelled. Images (B) and (C) adapted from Forge and Wright, 2002.

Three types of epithelium line the endolymphatic compartment: sensory epithelia, ion-transporting epithelia and relatively non-specialised epithelia. The mammalian ear uses six sensory epithelia to detect sound and head motion (Images deleted due to copyright

Figure 1-4B, C). The organ of Corti in the cochlear duct detects sound, cristae of the three semi-circular canals detect angular acceleration, and maculae of saccule and utricle detect linear acceleration and head tilt. Each sensory epithelium contains a highly ordered array of polarised mechanosensory hair cells. Each hair cell is surrounded and isolated from other hair cells by non-sensory supporting cells. This organisation requires exquisite developmental precision, described as "one of the most remarkable displays of precision micro-engineering in the vertebrate body" (Swanson et al., 1990). The apical surfaces between these cells are joined by tight junctions to form the reticular lamina, which acts as a diffusion barrier to prevent mixing of endolymphatic and perilymphatic fluids (reviewed by Raphael and Altschuler, 2003).

1.2.2 Sensory epithelium and mechanoelectrical transduction

Hair cells are the mechanosensory transducers of the inner ear, of which there are four types: inner hair cells (IHCs) and outer hair cells (OHCs) in the cochlear Corti, and type I and type II hair cells in the vestibular sensory epithelia. This will focus primarily on the cochlear sensory epithelium (organ of Corti), which of one row of IHCs and three rows of OHCs (see Image deleted due to copyright.

Figure 1-5).

Hair cells are named as such due to the actin-rich stereocilial bundles located at their apical surface. The individual cilia are arranged in rows of graded heights, resembling a staircase pattern (Lin et al., 2005). Between each row of stereocilia are a number of fibrillar extracellular cross-links. Numerous lateral and ankle links join the shafts of adjacent stereocilia, whereas a single filament, termed the tip link, stretches from the tip of the shorter stereocilium to the lateral membrane of the neighbouring, taller stereocilium (reviewed by Gillespie et al., 2005). First identified by Pickles in 1984, tip links are thought to interact with and directly open the mechanoelectrical transduction (MET) channel on the shorter stereocilia, when stretched (Pickles et al., 1984; Beurg et al., 2009). This mechanism is aided by an acellular matrix that sits atop the stereocilia of hair cells (except IHCs). This structure is known as the tectorial membrane in the organ of Corti; the otoconial membrane in the maculae; and the cupula in the cristae. The matrix provides a stable structure, which, upon sound stimulation or head movement, accentuates the displacement of the hair bundles towards the taller stereocilia.

The organ of Corti lies upon a resonant structure called the basilar membrane (BM). This structure is important for spatially dispersing sound waves to separate frequencies along the length of the cochlea. The mass and stiffness properties of the BM vary along a base-to-apex gradient: the BM is stiff and low in mass at the basal end of the cochlear coil and is therefore sensitive to high resonant frequencies, whereas at the apical end of the coil the BM is less stiff and high in mass, allowing for low frequency sensitivity. According to the place theory, sound-induced deflections of the basilar membrane cause vibrations of hair cells at particular tonotopic regions. This causes hair bundle deflection towards the taller sterocilia and forces the tip links to stretch and the cation-selective MET channels to open. The open state causes an influx of K^+ ions from endolymph into hair cells. This process is driven primarily by a high potential, the endocochlear potential (EP), in the scala media, which is +80 to +100 mV more positive in respect to perilymph (von Békésy, 1952). This unusually high potential is generated and maintained by the ion-transporting epithelium, the stria vascularis (see next section), and depends on tight junctions that electrically isolate endolymph from perilymph (reviewed in Hibino et al., 2010). The potential difference of ~140 mV between endolymph and the resting potential of a cochlear hair cell (~-60 mV) accounts for the driving force of K^+ entry, irrespective of the K^+ concentration. Therefore, the EP

is essential for hearing. A more detailed description of the EP is described in results chapter 4. It is of note to point out that the EP driving force for K^+ entry into hair cells only occurs in the organ of Corti, since an equivalent high potential is not present in the vestibular organ.

Image deleted due to copyright.

Figure 1-5. Illustration of the sensory epithelium of the mammalian inner ear.

The schematic shows the inner (IHC) and outer hair cells (OHCs) of the organ of Corti, surrounded by various supporting cells, including Deiters', Hensen's and Claudius cells. The tips of OHCs are usually embedded in the tectorial membrane. The apical surfaces of hair cells and supporting cells are bathed in endolymph that fills the scala media. Image modified from Raphael and Altschuler, 2003 (originally derived from Retzius, 1884).

Within the organ of Corti, IHCs receive ~95% of the afferent neurons (Spoendlin, 1972) and so are classed as the true sensory receptors of the cochlea. During sound stimulation, influx of K^+ ions through the MET channel causes IHC depolarisation and the opening of voltage-sensitive Ca^{2+} channels. The increase in intracellular Ca^{2+} then triggers the release of the neurotransmitter glutamate at the basal end of the IHC. Afferent auditory neurons, which surround the basal pole of hair cells, are then activated and relay action potentials to the auditory cortex. Conversely, the MET channels close when the stereocilia are angled in the opposite direction (towards the smallest stereocilia), which allows the cells to hyperpolarise and thus suppresses neurotransmitter release. IHCs are therefore described as mechanoelectrical transducers, converting mechanical sound stimuli into electrical nerve impulses. The transduction process in hair cells has been reviewed in detail by Fettiplace and Ricci, 2006.

In contrast, OHCs are innervated mostly by efferent neurons that do not convey electrical signals to the brain. Rather than transmitting acoustic information, OHCs have been implicated in the amplification of sound through the contraction and relaxation of their lateral membranes in response to K^+-induced voltage changes. This phenomenon occurs via the motor protein prestin, and is assumed to play a primary role in the "cochlear amplifier" effect (Ashmore, 1987; Liberman et al., 2002). These electromotile responses are thought to provide an active feedback to the basilar membrane, thus enhancing the sensitivity of IHCs at specific frequencies. The activity of prestin in OHCs has been shown to amplify sound by as much as 40-65 dB (Liberman et al., 2002). Thus, OHC amplification establishes the high frequency tuning and discrimination of the cochlea (Geleoc and Holt, 2003). The energy for the cochlear amplifier is provided by the EP, and therefore, loss of EP results in reduced functionality of OHCs and hearing impairment (Ruggero and Rich, 1991).

1.2.3 Ion transporting epithelium

The stria vascularis (SV) of the cochlea and the dark cell regions of the vestibular vestibular system constitute the ion transporting epithelia of the inner ear. The SV the upper boundary between the spiral ligament and scala media (Images deleted due to copyright

Figure 1-4) and functions mainly to generate and maintain the high endolymphatic K^+ concentration and EP (as reviewed by Hibino and Kurachi, 2006; Zdebik et al., 2009). Therefore, the SV unit can be described as a remote power source supplying the energy required for the mammalian cochlear amplifier (Zdebik et al., 2009). To perform this task, a rich blood supply is required, and is achieved by encompassing a network of thin capillaries between two epithelial sheets, hence the term "stria vascularis". The SV is composed of three cell layers: marginal cells which face the endolymphatic compartment, basal cells which face the spiral ligament, and intermediate cells, which are connected to basal cells and protrude through the intrastrial space (Image deleted **due to copyright.**

Figure 1-6). Tight junctions between marginal cells, between basal cells and between endothelial cells enclose the intrastrial space and electrically isolate the SV compartment from endolymph, perilymph and the lumen of blood capillaries (Souter and Forge, 1998). This feature is essential for generating and maintaining the EP.

The vestibular dark cells form a single layer on top of pigmented cells at the base of each crista and around the utricular macula. There is no dark cell region in the saccule (Forge and Wright, 2002). Dark cells function in an almost identical way to marginal cells in that both cell types are primarily involved in K^+ secretion into endolymph. However, in contrast to the cochlea, the ion-transporting epithelia of the vestibular system consist only of a single layer of dark cells. The specialised cells, namely basal and intermediate cells important for generating the EP in the cochlea, are absent in the vestibular epithelia. As a result, the potential of the vestibular endolymph

is on the order of only a few millivolts, yet the K^+ concentration remains around 150 mM.

The development of SV and generation of EP is described in more detail in chapter 4, but is introduced briefly here. In rodents such as mice and rats, the endolymphatic K^+ concentration (~150 mM) is established 6-7 days after birth (DAB). Concomitantly, the onset of EP occurs from 7-8 DAB, which continues to rise until maturation (+80 to +90 mV) around 16 DAB (Bosher and Warren, 1971). Marginal cells express ion transporters from birth (i.e. before the EP is detected) suggesting that these cells are primarily concerned with active K^+ transport rather than EP generation (Image deleted **due to copyright.**

Figure 1-6). The latter is attributed to maturation of intermediate cells and formation of tight junctions between basal cells (Souter and Forge, 1998). Intermediate cells are melanocytes (contain melanin pigment) that are derived from the neural crest and are entirely enclosed within the SV compartment. They are connected to basal cells through gap junctions and have extensive cellular processes that wrap around capillaries and inter-twine with those of marginal cell infoldings. Due to the expression of melanin and an inwardly-rectifying K^+ channel called $K_{ir}4.1$ (KCNJ10), intermediate cells are proposed to have two roles in the SV. Firstly, the presence of melanin and enzymes involved in detoxifying oxidative waste suggest that intermediate cells are important for protecting the SV under conditions of stress (Spector and Carr, 1979). Secondly, the expression of $K_{ir}4.1$ is essential for K^+ diffusion into the intrastrial space and for the generation of the EP (Ando and Takeuchi, 1999). The loss of intermediate cells and/or $K_{ir}4.1$ channels causes deafness and highlights the essential role of these cells in cochlear physiology (Steel and Barkway, 1989; Marcus et al., 2002).

Basal cells are flat and elongated and constitute the basal layer of the SV. During development, basal cells are derived from mesenchymal cells that also form the spiral

ligament. Formation of a tight junction barrier between basal cells isolates the intrastrial space from perilymph of the spiral ligament. This process coincides with and is essential for the onset and rise of EP (Souter and Forge, 1998). Transgenic mice with a knock-out of the basal cell tight junction protein, claudin-11, do not develop a tight junction barrier, nor do they generate an EP (Gow et al., 2004; Kitajiri et al., 2004), suggesting that basal cells, as well as intermediate cells, are vital for SV function. Gap junctions are found in large numbers between adjacent basal cells, basal and intermediate cells and basal cells and fibrocytes in the spiral ligament (Forge, 1984). Gap junctions allow transcellular transport into the SV, whereas tight junctions prevent paracellular flow of perilymph into the SV. Thus, basal cells form a cell-permeable partition between intermediate cells and fibrocytes. This is proposed to allow cycling of K^+ ions from the spiral ligament to marginal cells, whilst also electrically isolating the compartment from perilymph (Kikuchi et al., 2000).

Image deleted due to copyright.

Figure 1-6. Schematic diagram of the ion transporting epithelium

Inset, a transverse section through the cochlear duct. Blood vessels are represented in red. The stria is a highly vascularised tissue composed of numerous branched capillaries. Large diagram, the stria vascularis is a stratified epithelium consisting of three layers: marginal cells (M), intermediate cells (I) and basal cells (B). The apical surfaces of marginal cells face scala media and pump K^+ into endolymph via KCNQ1/E1 channels. Their basolateral membranes in contrast siphon K^+ from the intracellular space via Na^+,K^+-ATPase and Na^+,K^+,$2Cl^-$ transporters. Intermediate cells express the inwardly-rectifying K^+ channel $K_{ir}4.1$ (KCNJ10) and provide the K^+ for marginal cells. Basal cells line the spiral ligament and are connected to fibrocytes (F) and intermediate cells via gap junctions (double bars). The intrastrial space is filled with capillaries and processes emanating from marginal and intermediate cells. Tight junctions (black boxes) seal the SV compartment from endolymph and perilymph at the marginal and basal cell layers. K^+ concentration and electric potential are indicated for perilymph (taken as reference), intrastrial space and endolymph. The EP is generated across the basal and intermediate cell layers. Ion transporters are indicated by arrows. Image adapted from Cohen-Salmon et al., 2007.

1.3 Gap junctions in the mammalian inner ear

The majority of cells within the auditory and vestibular organs of vertebrates are extensively coupled by numerous and often large (more than 100,000 channels per plaque) gap junctions (Forge et al., 2003a). Evidence of these gap junctions first arose in the 1970s using the freeze-fracture technique. Supporting cells of the organ of Corti (Jahnke, 1975; Gulley and Reese, 1976; Iurato et al., 1976; Tachibana and Morioka, 1976), supporting cells of the maculae (Jahnke, 1975; Laciano et al., 1977), and cells of the spiral ligament and SV (Jahnke, 1975; Reale et al., 1975) were all discovered to contain gap junction plaques.

1.3.1 Gap junction networks

Based on immunohistochemical and ultrastructural analysis, two gap junction networks – the epithelial gap junction network and the connective tissue gap junction network – have been described within the mammalian cochlear duct (Kikuchi et al., 1995) and vestibular system (Kikuchi et al., 1994). The cochlear epithelial gap junction network consists of gap junctions between non-sensory epithelial cells, including interdental cells, inner sulcus cells, organ of Corti supporting cells, outer sulcus cells and root cells projecting into the spiral ligament (Kikuchi et al., 1995; Forge et al., 2003a) (Figure 1-7). In recent dye-transfer studies, it has been proposed that the mature epithelial gap junction network segregates into two directional pathways, separated by inner and outer pillar cells (Jagger and Forge, 2006). The lateral pathway connects outer pillar cells and OHC supporting cells with the outer sulcus. Whereas the medial pathway connects inner pillar cells, IHC supporting cells, and cells of the inner sulcus. No gap junctions have been identified between hair cells and supporting cells, as confirmed by electron microscopy, electrophysiology and dye transfer studies (Gulley and Reese, 1976; Santos-Sacchi and Dallos, 1983; Jagger and Forge, 2006). The connective tissue gap junction network consists of fibrocytes within the spiral ligament and spiral limbus, basal cells and intermediate cells of the SV and mesenchymal cells that line the scala vestibuli. No gap junctions have been identified between marginal cells or between marginal cells and intermediate cells, suggesting that, like hair cells, marginal cells are isolated from the gap junction syncytium (Kikuchi et al., 1995).

1.3.2 Connexin expression

In the mammalian inner ear, a variety of connexin subtypes have been detected by RT-PCR, cDNA macroarray and immunohistochemistry. In one study, the RNA transcription levels of 16 different connexin isoforms was quantified from mouse cochleae (Ahmad et al., 2003). Only Cx26, Cx29, Cx30 and Cx43 were consistently detected, and Cx31 occasionally detected in cochlear tissue, as also confirmed (except for Cx29) by Forge et al. (2003a). A recent study has reported the expression of Cx30.3 in the rat cochlea (Wang et al., 2010). However, Cx30.3 mRNA has not been detected in other studies (Forge et al., 2003a) and Cx30.3-null mice do not suffer any degree of hearing loss (Zheng-Fischhofer et al., 2007), suggesting that this connexin may not be essential for cochlear function. Cx31 has been detected in fibrocytes of the spiral ligament and spiral limbus, the expression of which increases with age, but decreases from base to apex (Xia et al., 2000; Forge et al., 2003a). Like Cx30.3-null mice, those with a deletion of the Cx31 gene, *Gjb3*, do not exhibit any degree of hearing loss (Plum et al., 2001). This suggests that other connexins in the cochlea can compensate for the loss of Cx30.3 and Cx31. However, human mutations of both Cx30.3 (Lopez-Bigas et al., 2002) and Cx31 (Xia et al., 1998; Kelsell et al., 2000) have been shown to cause hearing loss and/or skin disease, suggesting a dominant-negative or gain-of-function effect. In the mouse cochlea, Cx29 expression has been confirmed in myelinating cochlear Schwann cells and is important for the survival of spiral ganglion neurons (Tang et al., 2006; Eiberger et al., 2006). Weak Cx43 expression has been detected in the non-sensory epithelia, fibrocytes and stria vascularis with variable results (Lautermann et al., 1998; Liu et al., 2001; Suzuki et al., 2003). In contrast, Cx43 has not been detected in the organ of Corti of mice and is instead confined to the cells lining the inside of the bony wall (most likely type III fibrocytes) and the bone of the otic capsule (Forge et al., 2003a; Cohen-Salmon et al., 2004). A reporter gene approach has also identified Cx45 expression in the vasculature of the murine cochlea (Cohen-Salmon et al., 2004).

The two predominant connexin isoforms expressed in the cochlea and the vestibular system are Cx26 and Cx30, which are found in almost all cells comprising the epithelial and connective tissue gap junction systems (Kikuchi et al., 1994; Kikuchi et al., 1995; Lautermann et al., 1998; Ahmad et al., 2003; Forge et al., 2003a; Sun et al., 2005). In addition, many of the gap junction plaques reveal co-localisation patterns for

Cx26 and Cx30 (see Figure 1-8), suggesting that gap junctions might form heteromeric/heterotypic configurations (Lautermann et al., 1998; Forge et al., 2003a). This has since been confirmed by co-immunoprecipitation (Ahmad et al., 2003; Forge et al., 2003b; Yum et al., 2007) and electrophysiology (Zhao and Santos-Sacchi, 2000). Despite these findings, there is strong evidence to suggest that not all gap junctions are homogenous in the cochlea. For example, in the mature cochlea, Cx30 expression appears upregulated in Deiters' cells compared with Cx26 expression (Sun et al., 2005, Figure 1-8). In addition, electrophysiological and dye-transfer studies have led to the prediction that Cx26 and Cx30 are differentially distributed between supporting cells, which may lead to asymmetric coupling and formation of separate communication compartments (Zhao and Santos-Sacchi, 2000; Jagger and Forge, 2006).

1.3.3 Function of inner ear gap junctions

The arrangement of gap junctions into the epithelial and connective tissue gap junction networks has prompted the idea that gap junctions provide a route for K^+ recirculation from the hair cell vicinity to endolymph. This mechanism is described briefly, but has been reviewed extensively elsewhere (Kikuchi et al., 2000; Wangemann, 2002; Wangemann, 2006; Hibino and Kurachi, 2006; Zhao et al., 2006). The model suggests that K^+ ions released from hair cells during the mechanosensory transduction process are immediately siphoned by surrounding supporting cells to prevent continuous hair cell depolarisation. From here the ions are transported through the epithelial gap junction network to the outer sulcus. Potassium channels in the root processes are then predicted to secrete K^+ into the extracellular space of the lateral wall (Jagger et al., 2010). From here, K^+ ions enter the connective tissue gap junction network and diffuse through the syncytium where they are released by intermediate cells into the intrastrial space. The extracellular K^+ ions are siphoned by marginal cells and then secreted back into endolymph, thus completing the K^+ recycling pathway. The process of K^+ ion movement through the connective tissue gap junction network to intermediate cells is hypothesised to be crucial for the generation and maintenance of EP. This model is based primarily on indirect evidence from protein expression data and requires technological advances to conclusively prove a role for connexins in K^+ recycling.

Images deleted due to copyright.

Figure 1-7. Schematic diagram of the two gap junction networks within the mammalian cochlea.

The epithelial gap junction network (grey shaded cells) and the connective tissue gap junction network (black cells) are indicated. The connective tissue gap junction network can be sub-divided into lateral and medial regions, connected by mesenchymal cells lining the scala vestibuli. Image adapted from Kikuchi et al., 1995.

Figure 1-8. Co-expression study of Cx26 and Cx30 in the mammalian cochlea.

An illustration annotated with confocal images from various cochlear regions showing Cx26 (red) and Cx30 (green) immunolabelling. Numbers give the percentage of gap junction plaques that have Cx26 and Cx30 co-localisation. Note the lack of co-localisation (5%) and predominant expression of Cx30 in the Deiters' cell region. Image adapted from Sun et al., 2005.

In addition to the recirculation pathway, the gap junction networks create a substantial intracellular volume for a role in buffering K^+ ions away from the vicinity of hair cells (Nickel et al., 2009). This theory has been questioned since the loss of one connexin (either Cx26 or Cx30) cannot compensate for the loss of the other (Cohen-Salmon et al., 2002; Teubner et al., 2003b), even though both homotypic gap junctions have been shown to transfer K^+. However, the inability of one connexin to compensate for the other could be explained by asymmetric coupling. Electrophysiological studies have shown that asymmetrical voltage gating between coupled supporting cells induces a directional transjunctional current, which would facilitate funnelling of ions, such as K^+, away from sensory cells (Zhao and Santos-Sacchi, 2000; Zhao, 2000; Sun et al., 2005). This suggests an essential role for specific heterotypic/heteromeric gap junction configurations within the supporting cell network.

In addition to roles in K^+ diffusion, there is increasing evidence that cochlear gap junctions are important for biochemical coupling. Intercellular transfer of the Ca^{2+}-mobilising second messenger inositol 1,4,5-triphosphate (IP_3) is considered to be essential for calcium wave propagation in the immature organ of Corti, and deafness-causing Cx26 and Cx30 mutations lead to disrupted IP_3 transfer (Beltramello et al., 2005; Zhang et al., 2005; Anselmi et al., 2008). In addition, heteromeric Cx26/Cx30 gap junctions have been shown to permit faster intercellular Ca^{2+} signalling than Cx26 or Cx30 homotypic channels (Sun et al., 2005). As well as biochemical coupling, a recent report has suggested that cochlear gap junctions are also important for metabolite transfer. The intercellular transfer of a fluorescent glucose analogue (2-NBDG) between cochlear supporting cells was severely reduced in Cx30-null mice (Chang et al., 2008).

An emerging idea for inner ear connexins is a role in adenosine-5'-triphosphate (ATP) release through unpaired hemichannels (Gale et al., 2004; Zhao et al., 2005; Anselmi et al., 2008; Majumder et al., 2010). This purinergic signalling mechanism is proposed to occur in unison with second messenger transfer through gap junctions to sustain long-range intercellular Ca^{2+} signal propagation. ATP release through hemichannels is also suggested to have a role in reducing OHC electromotility, and thus hearing sensitivity, via P2 receptor activation (Zhao et al., 2005).

1.4 Scope of the thesis

Cx26 and Cx30 are the two predominant connexins expressed in the cochlea and are critically important for functional hearing and cochlear physiology. However, our understanding of how these proteins function in the inner ear is still lacking. Several reports have indicated cochlear gap junctions in asymmetric coupling, K^+ buffering and recycling, cochlear development and biochemical coupling. Although the bigger picture is now emerging for these connexins, certain aspects of their life-cycle and role in cochlear physiology remain unsolved. In the cochlea, it still remains to be seen why Cx26 or Cx30 cannot compensate for the loss of the other, and why certain mutations lead to hearing loss only, whereas others lead to syndromic hearing loss. Cx26 and Cx30 transgenic mouse models are deaf from birth (discussed in chapter 5), suggesting a role for these connexins in cochlear development and maturation. However, these roles have not been fully elucidated. For any possible therapeutic techniques in the future, it is essential we understand the exact role and properties of these connexins in cochlear development and physiology.

In light if these issues, this thesis investigates the properties and functions of inner ear connexins in three parallel studies, with each study utilising a different experimental system:

1) *In vitro* heterologous expression studies to investigate the trafficking pathways of Cx26 and Cx30.

2) *In situ* studies to investigate the development of gap junctional intercellular communication in the cochlear lateral wall.

3) *In vivo* studies to investigate the mechanism leading to hearing impairment and cochlear pathology in Cx30-knockout mice.

Since these three topics are somewhat dissimilar, each results chapter includes its own introduction, which describes the reasons for the investigation, and discussion sections. The last chapter is a short general discussion, in which the three parallel studies are discussed in relation to cochlear physiology and development.

2 MATERIALS AND METHODS

2.1 Materials

All materials and reagents were purchased from Sigma-Aldrich (UK) unless stated.

2.2 Cell Culture

2.2.1 HeLa cell culture

Human HeLa cervical carcinoma cells (OHIO, ECACC) were used for connexin expression studies. These cells are gap junction deficient making them ideal mammalian hosts for studying specific connexin properties. Cells were grown in tissue culture flasks (75 cm^2) under sterile conditions in Dulbecco's Modified Eagle medium (DMEM), supplemented with 10% foetal bovine serum (FBS), 1% penicillin/streptomycin, 0.5% Amphotericin B (FungizoneTM) and 2 mM glutamine, at 37^oC in a humidified 5% CO_2 incubator. To split the cells they were first rinsed with Hank's Balanced Salt Solution (HBSS) followed by a brief rinse with 1X trypsin/ethylenediaminetetraacetic acid (EDTA) solution and then incubated with 1 ml trypsin/EDTA for 3-5 mins at 37^oC to detach the cells. Trypsin activity was quenched by adding 8 mls of DMEM containing FBS. Cells were split into 1:10 dilutions and passaged every 4-7 days, changing the medium when required.

2.2.2 Connexin expression constructs

Wild-type (wt) rat Cx26 cDNA cloned into pCR3 (Invitrogen) was a gift from Prof. H. Evans and Dr. P. Martin Martin et al., 1999. Wt mouse Cx30 cDNA cloned into pCR3 was generated previously by Dr. N. Marziano (Marziano et al., 2003). These constructs were used for stable HeLa cell transfection (see below). The stably transfected mouse Cx43-HeLa cell line (cDNA inserted into pIREShyg, Clontech) was a gift from Prof. N. Severs (Imperial College, London). Mutant Cx26 constructs, D66H and G59A fused to an enhanced green fluorescent protein tag (eGFP), were created by Dr. N. Marziano (Marziano et al., 2003) and used for transient transfections.

2.2.3 Transient expression of connexin constructs

HeLa cells were grown on heat sterilised 13 mm glass coverslips in 24-well culture plates until 80-90% confluency. Cells were transfected with 0.8-1 µg of

connexin plasmids and 2 µl Lipofectamine™ 2000 (Invitrogen) according to manufacturer's guidelines and incubated for 24-48 hours. Cells were fixed in 4% paraformaldehyde for 20-30 minutes at room temperature, washed in PBS and prepared for immunofluorescence labelling as described below.

2.2.4 Stable expression of connexin constructs

Stably transfected Cx26-HeLa were produced previously by Dr. R. Nickel in our lab. To obtain a stably transfected Cx30 cell-line, HeLa cells were plated in 35 mm petri dishes and transfected as described above, but with DNA scaled up to 3 µg per well. After 24-48 hours, cells were harvested with 500 µl trypsin/EDTA solution and split 1:5 to several culture dishes (10 cm in diameter, Nunc) containing 10 ml DMEM and 500 µg/ml of the selection antibiotic Geneticin (G418). After seven days, by which time non-transfected and transiently transfected cells are thought to be dead, the concentration of G418 was reduced to 250 µg/ml to prevent cytotoxic effects. The selection medium was changed every 4 days for 2-3 weeks. Once cell clones reached a diameter of 2-3 mm, they were harvested using trypsin-soaked sterile cloning discs (3 mm) and transferred to a 24-well plate. Cells were grown to confluency in the presence of G418, harvested and transferred to increased sized culture vessels up to 75 cm^2 flasks. Cell samples were plated onto coverslips between harvesting, fixed and checked for connexin expression using immunocytochemistry. Both the Cx26 and Cx30 stably transfected cell lines were maintained in G418-containing medium. The Cx43-HeLa cell line was maintained in medium containing hygromycin (250-500 µg/ml).

2.2.5 Cryopreservation of cell lines

For freezing, cells were grown to near-confluency in a 75 cm^2 flask with fresh medium changed 24 hours prior to cryopreservation. Cells were harvested as above, resuspended in 10 ml medium and centrifuged at 1000 rpm for 5 minutes. The cell pellet was resuspended in a 5 ml solution of 50% FBS and 50% dimethyl sulphoxide (DMSO). Aliquots (1 ml) were placed into cryovials and frozen at -80^oC for 24 hours before being transferred to liquid nitrogen for long-term storage. To re-activate cell lines, vials were defrosted in a 37^oC waterbath, diluted in 5 ml medium and grown to confluency in 25 cm^2 flasks.

2.2.6 Drug treatment

Brefeldin-A (BFA), a Golgi-disrupting drug, was reconstituted in 100% ethanol to a stock concentration of 5 mg/ml and stored at -20^{o}C until required. Stably-transfected HeLa cells were grown to 60-70% confluency on 13 mm glass coverslips in 6 mm culture dishes. Medium was replaced with fresh DMEM containing 5 µg/ml BFA (or 0.01% (v/v) ethanol for control purposes) and incubated for 5-7 hours at 37^{o}C. Cells were then washed briefly in HBSS and then fixed in 4% PFA for 20-30 minutes at room temperature.

2.2.7 Temperature manipulation

Stably transfected HeLa cells were grown to 70-80% confluency on 13 mm glass coverslips in 6 mm culture dishes and then incubated in a CO_2 atmosphere at 19-20^{o}C for the hours indicated in the figure. The temperature was checked regularly and never reached higher than 20.3^{o}C or lower than 19.4^{o}C. Cells were rinsed briefly in HBSS and then fixed in 4% PFA for 20-30 minutes at room temperature.

2.3 Animals

Adult (P21+) tri-colour guinea pigs were used for cochlear fibrocyte cultures and Sprague-Dawley rats for live cochlear slicing. Animals were killed by cervical dislocation or by CO_2 inhalation followed by cervical dislocation in accordance with Schedule 1 of the United Kingdom Animals (Scientific Procedures) Act of 1986.

2.4 Primary Culture of Cochlear Fibrocytes

Fibrocyte cell culture was essentially carried out as described by Gratton et al. (1996), but with modifications. Decapitated heads were skinned, disinfected briefly in 70% ethanol and transferred to sterile ice cold HBSS supplemented with HEPES. All dissections from this point were performed under sterile conditions in a laminar flow hood with heat sterilized instruments. The heads were sagitally cut in half, lower jaws removed and brain and temporal bones removed. The bullae were excised and the outer bony casing trimmed away with forceps (rat) or bone nibblers (guinea pig). The cochlear bone was first scored with a No. 11 scalpel blade and then removed in small pieces from apex-to-base to reveal the intact spiral ligament. The cochlea was removed from the connecting vestibular system with the scalpel and spiral ligament peeled away

from the organ of Corti using a needle and fine forceps. The spiral ligament was cut into 3-6 segments and gently placed onto rat tail collagen type-I coated petri dishes. A minimal amount of fibrocyte culture media (MEM-α, supplemented with 10% fetal bovine serum (FBS), 1% insulin-transferrin-selenium (ITS) 1% penicillin/streptomycin and 0.5% Amphotericin B (FungizoneTM)) was dropped onto the tissue segments. To facilitate attachment the dishes were incubated at 37^{o}C for ~10 minutes until the culture medium had reduced in volume and the tissue had attached. In some instances a sterilized glass coverslip was placed over the tissue fragments to aid adhesion and cell growth. Further media was added to each well and incubated at 37^{o}C in a 5% CO_2, 95% air atmosphere, with fresh media changed every 3 days. After ~4 days in culture fibrocyte migration from tissue explants was visible. Full confluency was reached after 2-3 weeks at which point the cells were sub-cultured into 25 cm^2 flasks and allowed to grow to near confluency before being split 1:1 into a larger 75 cm^2 flask. Fresh media was changed every 3 days and cells split 1:10 once a week or when fully confluent. Cell stocks were prepared as described above (2.2.5).

2.5 Immunofluorescence labelling and confocal microscopy

Processing for immunofluorescence labelling was carried out in humidified chambers at room temperature on an orbital shaker, unless stated otherwise. Cell monolayers were fixed with 4% PFA for 20-30 minutes. Whole cochleae were fixed by making a small hole in apical region of the otic capsule and gently perfusing PFA through the round window. Fixation was continued on a rotator for 1 hour and cochleae processed for cryosectioning or slicing (see section 2.9 below). Live cochlear slices were fixed with 4% PFA for 30-45 minutes. Tissue sections/slices and cell monolayers were incubated for 1 hour in PBS containing 10% goat serum (or 10% horse serum for KCNQ1), 0.1% (monolayers) or 0.2% (tissue) Triton X-100 (TX-100) to block non-specific sites and permeabilise the cells. Specimens were incubated with various combinations of monoclonal and polyclonal primary antibodies (see Table 2-1) in PBS containing 0.1 M L-Lysine and 0.1%/0.2% TX-100 overnight at 4^{o}C. Primary antibodies were omitted for negative controls. Following three 10 minute washes with PBS, cells/tissues were incubated with appropriate secondary antibodies or other fluorescent probes (see Table 2-2) in PBS, 0.1 M L-lysine and 0.1% TX-100 for 40-60 minutes in the dark. After three 10 minute washes with PBS specimens were mounted

on coverslips with anti-fade medium (Vectashield, Vectorlabs) containing 4',6-diamidino-2-phenylindole (DAPI) to stain nuclei, and sealed with nail varnish.

Immunofluorescent samples were examined and imaged using a Zeiss Meta confocal laser scanning microscope with 20x (dry), 40x (oil) and 63x (oil and water) objectives. The fluorochromes Alexa 488 (excitation/emission 496/519 nm), Alexa 555 (ex/em 555/565 nm), rhodamine (ex/em 550/570 nm), Alexa 633 (ex/em 632/647 nm) and DAPI (ex/em 358/461 nm) were excited by wavelengths of 488, 568, 633 and 364 nm laser lines. Images were recorded by single- or sequential dual/triple-channel scanning. Z-series stacks were taken at ~1 µm intervals and transformed into projections of maximum pixel intensity. Settings for laser power, pinhole and photomultiplier tube were kept constant for comparative experiments.

Protein	Type; host	Concentration	Source	Antibody #
Acetylated tubulin	Monoclonal; mouse	1:1000	Sigma	T6793
Alpha tubulin	Monoclonal; mouse	1:400	Invitrogen	32-2500
Ca^{2+}-ATPase	Monoclonal; mouse	1:200	Sigma	A7952
Claudin-11	Polyclonal; rabbit	1:200	Invitrogen	36-4500
Cx26	Monoclonal; mouse	1:400	Invitrogen	33-5800
Cx26	Polyclonal; rabbit	1:200	W. H. Evans, Univ. of Wales, Cardiff, UK	GAP28H
Cx30	Polyclonal; rabbit	1:400	Invitrogen	71-2200
Cx31	Polyclonal; rabbit	1:100	D. P. Kelsell, Queen Mary, Univ. of London, UK	N/A
Cx43	Polyclonal; rabbit	1:400	Sigma	C6219
GLUT-1	Polyclonal; rabbit	1:300	Sigma	SAB4502803
GM130	Monoclonal; mouse	1:400	BD Biosciences	610823
KCNQ1	Goat; polyclonal	1:200	Santa Cruz	Sc-10646
K_{ir}4.1	Polyclonal; rabbit	1:400	Alomone Labs	APC-035
Na^+,K^+,ATPase	Monoclonal; mouse	1:300	Sigma	A-275
NKCC1	Monoclonal; mouse	1:300	C. Lytle, Developmental Studies Hybridoma Bank, Univeristy of Iowa	N/A
S100 alpha	Polyclonal; rabbit	1:200	Abcam	ab11428
Vimentin	Monoclonal; mouse	1:400	Sigma	V2258

Table 2-1. Primary antibodies used for immuno-labelling

Secondary antibody & other conjugated fluorophores	Host	Concentration	Source	Antibody #
Anti-goat Alexa Fluor 633	Donkey	1:200	Invitrogen	A21082
Anti-mouse Alexa Fluor 555	Goat	1:200	Invitrogen	A21422
Anti-mouse Alexa Fluor 633	Goat	1:200	Invitrogen	A21050
Anti-rabbit Alexa Fluor 488	Goat	1:200	Invitrogen	A11008
Anti-rabbit Rhodamine	Goat	1:200	Chemicon (Millipore)	AP132R
Phalloidin Alexa Fluor 633	N/A	1:400	Invitrogen	A22284
Streptavidin Alexa Fluor 555	N/A	1:1000	Invitrogen	S32355

Table 2-2. Secondary antibodies and other fluorescently-conjugated probes.

2.6 Reverse transcription PCR

Cells were grown to full confluency in 25 cm^2 flasks and RNA extracted using the RNeasy kit (Qiagen), with additional DNAse treatment, according to manufacturer's instructions. For positive control reactions, RNA was extracted from guinea-pig brain, and cochlea tissue using a rotor-stator homogeniser. RNA concentrations were recorded using a Nanodrop 1000 spectrophotometer (Thermo Scientific) and then reverse transcribed into complementary DNA (cDNA) using the Quantitect Reverse Trancription kit (Qiagen). cDNA concentrations were recorded and specific sequences amplified by polymerase chain reaction (PCR) using the *Taq* DNA polymerase kit (Qiagen) as described.

Specific primers for the following connexin sequences were designed with the aid of Primer3 (http://frodo.wi.mit.edu/primer3/). All primers were obtained from guinea-pig (*Cavia porcellus*) coding DNA, with the exception of Cx30; the guinea-pig sequence was not available at the time so primers were designed from mouse (*Mus musculus*) coding DNA. The functionality of mCx30 primers was confirmed by amplification of Cx30 from guinea-pig cochlear cDNA. Primer sequences (including coding DNA accession numbers): guinea-pig Cx26 (gCx26, NM_001172823.1) (forward: 5'- ACCGGAAGCATGAGAAGAAA-3'; reverse: 5'-CAAGCATTGCATTTCACCAG-3'), mCx30 (NM_001010937.1) (forward: 5'-AGGAAGTGTGGGGTGATGAG-3'; reverse: 5'-AGGTAACACAACTCGGCCAC-3'), gCx31 (ENSCPOT00000010722) (forward: 5'-TATACGTGGTGGCTGCAGAG-3'; reverse: 5'-TGCTCACCGTACTTCTGACG-3'), gCx43 (NM_001172748.1) (forward: 5'-AGGAGGAGCTCAAGGTAGCC-3'; reverse: 5'-GACCGACTTGAAGAGGATGC-3'). All connexin primer sequences were checked using the BLAST tool (http://blast.ncbi.nlm.nih.gov/Blast.cgi) to rule out cross-reactivity with other connexin types. Glyceraldehyde-3-phosphate dehydrogenase (gGAPDH, NM_001172951.1) (forward: 5'-GTCGGTTGTGGATCTGACCT-3'; reverse: 5'-TGCTGTAGCCGAACTCATTG-3') served as a positive control. Primers were purchased from Sigma-Aldrich and re-suspended at 100 µM in ddH_2O. PCR reactions were set up as follows: 1x PCR buffer, 1.5 mM $MgCl_2$, 200 µM of each dNTP, 2.5 units *Taq* DNA polymerase, 0.2 µM of each primer and 1 µg template DNA, made up to 20 µl with dH_20, per 20 µl reaction. Samples from reverse transcriptase

reactions without enzyme or dH_2O replaced the template DNA for negative control reactions. Optimal annealing temperatures for each primer pair were determined by a temperature gradient. Thermal cycling was performed using an Eppendorf Mastercycler Gradient under the following conditions:

1)	Initial denaturation	94°C	5 minutes
2)	Denaturation	94°C	30 seconds
3)	Annealing	60°C	(Cx26 primers) 63°C (all other primers) 1 minute
4)	Extension	72°C	1 minute
5)	Repeat steps 2-4, 35 times		
6)	Final extension	72°C	10 minutes
7)	Hold	4°C	Indefinitely

PCR products were run on a 2% agarose gel as described in section 2.8.3

2.7 Quantitative real-time PCR

Whole stria vascularis strips were isolated and pooled from each cochlea of age-matched *Cx30*$^{+/+}$ and *Cx30*$^{-/-}$ mice and transferred into RNAlater (Qiagen). RNA was extracted using the RNeasy kit (Qiagen) and reverse transcribed as mentioned in section 2.6. Gene expression was determined by quantitative real-time PCR (qPCR) using a $K_{ir}4.1$ gene expression assay (Applied Biosystems; Mm00445028_m1). Reactions were multiplexed with a primer-limited eukaryotic 18S rRNA endogenous control (Applied Biosystems; Mm03928990_g1). Each reaction was performed in triplicates or quadruplicates and amplified on a SDS7500 real-time PCR System (Applied Biosystems). Relative quantification analysis was performed with SDS1.2.1 software (Applied Biosystems).

2.8 Connexin 30 transgenic mice

2.8.1 Generation of Cx30 knockout mice

Connexin 30 knockout (*Cx30*$^{-/-}$) frozen embryos (EM:00323) were purchased from the European Mutant Mouse Archive (EMMA), CNR, Consiglio Nazionale delle Ricerche, Monterotondo Scalo, Roma, Italy. The re-derivation process was carried out by Ms. K. Gardner at the Transgenic Laboratory, Neural Development Unit, Institute of Child Health, UCL. The procedure returned three healthy *Cx30*$^{-/-}$ female mice which were then backcrossed with C57BL/6 wild-type mice to produce heterozygote litters and then intercrossed to produce homozygous *Cx30*$^{-/-}$ mice.

The *Cx30*$^{-/-}$ mice were originally created by Prof. K. Willecke's group at the Institute of Genetics, University of Bonn (Teubner et al., 2003a). Briefly, the coding region of the mouse *Gjb6* gene was replaced with the coding sequence of the *E. Coli* galactosidase reporter gene (*lacZ*) along with a nuclear localisation signal (NLS) neomycin resistance (neo) cassette (

Image deleted due to copyright.

Figure 2-1. **Generation of *Cx30*$^{-/-}$ mice.**

(A) The targeting vector containing the nuclear localisation sequence (NLS), *lacZ* reporter gene and the *neo* resistance cassette. Grey filled bars, Cx30 coding sequences homologous to wild-type DNA; thin line, vector backbone. (B) Wild-type *Cx30* gene. Thick line, genomic DNA. (C) Resulting allele after homologous recombination. Arrows represent primers used for genotyping. H, *Hind*III; N, *Not*I; S, *Sac*I restriction sites. Adapted from Teubner et al. (2003).

Image deleted due to copyright.

Figure 2-1). The NLS and neo sequences in the targeting vector were flanked by corresponding Cx30 sequences (

Image deleted due to copyright.

Figure 2-1, grey bars) which allowed for homologous recombination into genomic DNA (indicated by X). The targeting vector was linearised and electroporated into HM1 mouse embryonic stem cells, as described by (Theis et al., 2000). Cells that incorporated the targeting vector were selected for with geniticin (G418) and checked for homologous recombination by southern blot analysis. The cells were then injected into C57BL/6 blastocytes and implanted into pseudopregnant NMRI foster mothers. Chimeric mice were then backcrossed to C57BL/6 mice.

2.8.2 Genotyping

Genomic DNA was isolated from ear punches (live animals) or tail tips (sacrificed animals) using the Extract-N-Amp™ Tissue PCR Kit according to manufacturer's instructions. Custom made DNA oligo primers were designed to detect the presence of both wild-type *Cx30* (*Cx30*$^{+/+}$) and *lacZ* genes: Cx30 (forward: 5'-ATTGGTCAGATAATTCTGAGG-3'; reverse: 5'-AAACTTGTGATTGCATTCTGGC CAC); lacZ (reverse: 5'-AGCGAGTAACAACCCGTCGGATTC-3'). The forward primer lies outside of the *Cx30* coding region and the reverse primers of both *Cx30* and *lacZ* are located within the respective genes (Figure 2-1). *Cx30*$^{+/+}$ mice produce band sizes of 850 base-pairs, whereas *Cx30*$^{-/-}$ mice produce band sizes of 450bp (see Figure

2-2). Heterozygous mice ($Cx30^{+/-}$) contain bands of both sizes. Each 20 µl PCR reaction was set up as follows:

Extract-N-Amp PCR reaction mix (containing JumpStart Taq antibody for hot-start amplification)	10 µl
Tissue extract	5 µl
Cx30 wild-type 5' forward primer	1 µl (1 µM final conc.)
Cx30 wild-type 3' reverse primer	1 µl (1 µM final conc.)
Cx30 lacZ 3' reverse primer	1 µl (1 µM final conc.)
PCR grade water	2µl

Thermal cycling was performed using an Eppendorf Mastercycler Gradient under the following conditions:

1)	Initial denaturation	95°C	5 minutes
2)	Denaturation	95°C	30 seconds
3)	Annealing	57°C	30 seconds
4)	Extension	72°C	45 seconds
5)	Repeat steps 2-4, 35 times		
6)	Final extension	72°C	10 minutes
7)	Hold	4°C	Indefinitely

2.8.3 Agarose Gel Electrophoresis

Samples were loaded with 1x blue/orange DNA loading dye (Promega) and electrophoresed on a 1.3% agarose gel prepared with 1x TAE (2.0 M Tris, 1 M Glacial acetic acid, 50 mM EDTA, pH 8.0) buffer containing 0.25 µg/ml ethidium bromide. A 100 bp DNA ladder (Promega) was used as a molecular marker. DNA was viewed in a GelDoc-It 3UVTM Transilluminator Imaging system (Jencons-PLS) at 302nm (UV-B). Image acquisition and analysis was performed with LabWorksTM software (UVP BioImaging Systems).

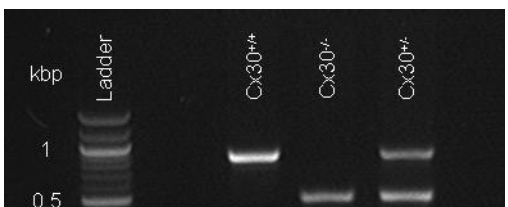

Figure 2-2. Cx30 genotyped samples.

Lane 1, 100 bp DNA ladder with size markers; lane 2, no template control; lane 3, a band at 850 bp ($Cx30^{+/+}$, wild-type); lane 4, a band at 450bp ($Cx30^{-/-}$, homozygous

2.9 Cochlear Preparations

2.9.1 Cryosectioning

After removing a small piece of bone from the very apical point of the cochlea, 4% PFA was gently perfused through the round and oval windows. Whole cochleae were then immersed in fixative and left on a rotor for a 1 hour at room temperature. PFA fixed mouse/rat cochleae were decalcified in 4.13% EDTA in PBS for 2-4 days at 4^{o}C. For cryoprotection, cochleae were rinsed in PBS and incubated in 30% sucrose in PBS overnight at 4^{o}C. Cochleae were embedded in low-gelling temperature agarose (Type VII) containing18% sucrose in PBS and 0.01% sodium azide (NaN_3). Gel was poured into 35 mm petri dishes and cochleae orientated so that the oval window was facing upwards and then allowed to set at room temperature. Dishes were sealed with Parafilm^{TM} and stored at 4^{o}C until required. Specimens were mounted onto cryostat chucks with a small amount of Tissue Tek OCT compound (Sakura, Netherlands) and frozen rapidly in liquid nitrogen. Tissue blocks were allowed to equilibrate to the temperature inside a Leica CM1900 cryostat (-20^{o}C) for 30 mins. Sections were cut at a thickness of 15 µm and mounted on poly-L-lysine coated slides (VWR, UK) and stored at -20^{o}C.

2.9.2 Cochlear slice preparation

Sprague Dawley rats aged P0 to P7 were used for live slices and P0 to adult for fixed slices. Rats were killed as described above. The developing bullae were excised, and the cochlear bones were exposed. Additional dissection was performed in cold artificial perilymph (in mM: 150 NaCl, 4 KCl, 2 MgCl2, 1.3 CaCl2, and 5 glucose, pH adjusted to 7.3 with NaOH). The cochlear bone was mounted on a vibratome block using cyanoacrylate glue (Roti-Coll 1; Carl Roth, Karlsruhe, Germany). Slices were cut at 200–400 µm on a semi-automatic vibratome (Vibratome 1000+; TPI, St. Louis, MO), fitted with a razor blade (Wilkinson Sword, High Wycombe, UK). The vibratome was adjusted to allow a very slow blade advance (<0.1 mm/s).

For fixed cochlear slices: cochleae were fixed with 4% PFA for 1 hour at room temperature and decalcified as described for cryosectioning and then mounted and sliced as described above.

2.10 Whole-cell patch clamp recordings/dye transfer

Live cochlear slices were stored in artificial perilymph (in mM: 145 NaCl, 4 KCl, 2 $MgCl_2$, 1.3 $CaCl_2$, and 5 glucose, pH adjusted to 7.3 with NaOH) on ice until use. For patching, slices were placed in a recording chamber (~400 µl) on an upright microscope (Axioskop; Zeiss, Oberkochen, Germany) and superfused with artifical perilymph. The flow rate (2-4 ml/min) was controlled by a peristaltic pump and slices secured with short lengths of platinum wire. All experiments were carried out at room temperature (20 – 24^{o}C). To view individual cells for patch-clamp recordings, the tissue was visualized with near-infrared videomicroscopy (as described in Jagger et al., 2000), using a CCD video camera (ICD 42E; Ikegami, Tokyo, Japan) and light from a 100W halogen bulb filtered at 750 nm (centre wavelength, ±10 nm).

2.10.1 Dye transfer in cochlear slices

Dye transfer and patch-clamp recordings in cochlear slices have been successfully used in our lab previously (Jagger and Forge, 2006). A 10 min whole-cell recording has been shown as sufficient time for Neurobiotin^{TM} Tracer (NBN, Vector Laboratories, Burlingame, CA) dye to pass throughout Köllicker's organ, which is the standard duration used for these experiments. Recordings were performed using a patch-clamp amplifier (Axopatch 200B; Axon Instruments, Union City, CA) and a Digidata board (Axon Instruments) under the control of computer software (pClamp version 8; Axon Instruments). Patch pipettes were fabricated on a vertical puller (P30; Sutter Instruments, Novato, CA) from capillary glass (GC120TF-10; Harvard Apparatus, Edenbridge, UK). Pipettes were filled with a potassium chloride intracellular solution (in mM: 140 KCl, 10 NaCl, 2 $MgCl_2$, 5 HEPES, 5 EGTA, and 5 glucose, pH adjusted to 7.3 with KOH). For dye transfer experiments, the pipette solution was supplemented with 1 mg/ml NBN (MW, 287 Da; charge +1) and either 2 mg/ml Lucifer yellow (LY; di-lithium salt; MW, 443 Da; charge -2, Sigma) or 2 mg/ml fluorescein-conjugated dextran (FD; anionic, lysine fixable; MW 10,000 Da; Invitrogen). These dyes have different permeabilities depending on the connexin composition of gap junction channels. NBN has been shown to pass through all functional gap junction channels, whereas LY is permeable to Cx26 homotypic channels, but not Cx30 homotypic or Cx26/Cx30 heterotypic channels (Jagger and Forge, 2006). FD is impermeable to gap junctions due to its high molecular weight and is useful for identifying patched cells and

studying cell morphology. Pipette solutions were filtered at 0.22 µm and centrifuged to remove insoluble debris. Pipettes had an access resistance of 2-4 MΩ, measured in artificial perilymph. A small amount of positive pressure was applied to the pipette tip to keep it free from blockages before the patch formation. Once a giga-seal was formed suction was applied to create the whole-cell configuration. The input resistance was measured during 10 mV hyperpolarizing pulses (10 ms duration). After 10 mins the pipette was gently removed to form a tight seal, which was confirmed by the formation of a high-resistance membrane patch. Upon removal of the pipette, slices were fixed in 4% PFA at room temperature for 30 mins.

2.10.2 Dye transfer in HeLa and fibrocyte cell lines

Essentially the same technique as described above was used for dye transfer in HeLa and fibrocyte cell lines grown to 85-95% confluency on 9 mm coverslips. For BFA experiments, cells were incubated in media containing 5 µg/ml BFA (or 0.01% (v/v) ethanol for control purposes) for 6-7 hours prior to dye injection. Cells were then fixed, NBN visualised by staining with streptavidin-conjugated to an Alexa Fluor 555 probe (as described in section 2.5) and imaged using a Zeiss LSM 510 confocal microscope. All image settings were kept constant between coverslips. To prevent bias, each coverslip was randomly assigned a letter by D. Jagger before imaging. Therefore, each image was counted blind. Counts were performed using ImageJ software and only included cells with NBN present in the cytoplasm and nucleus. Data was collated, presented as mean ± standard error of the mean (SEM) and statistically analysed using the Student's T-test in GraphPad Prism4.

2.10.3 Inward-rectifying potassium channel recordings

For $K_{ir}4.1$ recordings the intracellular pipette solution was supplemented with 3 mM ATP-Na_2. In some experiments, $BaCl_2$ or fluoxetine hydrochloride was added to artificial perilymph to block inward-rectifying K^+ channels. $BaCl_2$ was made up as a 1M stock solution in sterilised ddH_20 and diluted to 2 mM in artificial perilymph before the experiment. Fluoxetine hydrochloride was made up as a 10 mM stock in sterilised ddH_20 and diluted to 100 µM in artificial perilymph. For the $[K^+]$ test, artificial perilymph solutions were made by adjusting KCl and NaCl concentrations appropriately: 1 mM KCl, 148 mM NaCl; 10 mM KCl, 139 mM NaCl; 40 mM KCl, 109 mM NaCl.

2.11 Stria vascularis measurements

2.11.1 Stria vascularis thickness measurements

Measurements of stria vascularis thickness were taken from thin sections, imaged by TEM and cryosections, imaged by confocal microscopy. The thickness was calculated as the distance between the endolymphatic surface of marginal cells to the apical surface of basal cells directly abutting the spiral ligament. Three measurements were taken for each turn of the cochlea. Basal measurements were pooled together as were apical measurements (according to the animal's age) and averaged to obtain a mean thickness. Data are presented as mean ± SEM and were statistically analysed using Student's t-test in GraphPad Prism 4 software. Differences were considered significant when $p<0.05$.

2.11.2 Dimensions of marginal cell nuclei

Marginal cell nuclei dimensions were calculated by measuring the distance from one end of DAPI stained nuclei to the other (length) and divided by the height measured at the mid-point of the length. Distances were measured using Zeiss LSM Image Browser software (http://www.zeiss.de/micro). Measurements were taken from mid-modiolar cochlear cryosections and pooled according to age and genotype. Data are presented as mean ± SEM and were statistically analysed using Student's t-test in GraphPad Prism 4 software. Differences were considered significant when $p<0.05$.

2.12 Vascular permeability studies

2.12.1 FITC-conjugated bovine serum albumin tail-vein injections

Adult (P21+) *Cx30*$^{+/+}$, *Cx30*$^{+/-}$ and *Cx30*$^{-/-}$ mice were used for tail-vein injections. The animals were warmed in a 39^{o}C incubator for 5 minutes and held in a mouse restrainer so that the tail was accessible and the vein visible. A 50µl aliquot of 5% (w/v) FITC-conjugated bovine serum albumin (BSA-FITC) made up in sterilized PBS was injected into each mouse. The mice were left for 30-60 minutes at room temperature to allow the BSA-FITC to permeate all capillaries and to allow for any vessel leakage. The mice were then killed via CO_2 inhalation and cochleae excised as described above. For live whole-mount imaging the cochlear bone was removed and stria vascularis (SV) segments dissected onto a microscope slide with Vectashield tissue

mounting media. The segments were immediately imaged under a Zeiss epifluorescence microscope. For fixed SV imaging the cochleae were prepared and cryosections cut as described in section 2.9.1. Sections were immunolabelled for Cx30 (counter-stain) and viewed under a Zeiss LSM laser-scanning confocal microscope.

2.12.2 Semi-quantitative fluorescence analysis

All images were acquired using a Zeiss LSM 510 confocal microscope using the same detection settings for wild-type and transgenic samples. Images were taken from single plane sections, or combined stacks at the same thickness, as noted in figure legends. The green BSA-FITC channel was converted to greyscale and analysed using ImageJ software (http://rsbweb.nih.gov/ij/). Each 8-bit image could produce a maximum greyscale level of 256. Single line profile plots were measured along the width of the stria, traversing each capillary, in cochlear sections. For whole-mounts, line distances were kept the same and plotted in regions of highest fluorescence intensity. Pixel intensities measured along the line profiles were transferred to GraphPad Prism 4 software for further analysis. Graphs were plotted as distance vs fluorescence intensity or total average fluorescence intensity.

2.12.3 Diuretic injections

Adult (P21+), age-matched $Cx30^{+/+}$ and $Cx30^{-/-}$ mice were given a single subcutaneous intraperitoneal injection of a clinical preparation of the loop diuretic, bumetanide (Burinex injection, Leo-Pharma) at 0.05 mg/g. Animals were killed and cochlea tissue obtained 24 hours later.

2.12.4 Thin sections and transmission electron microscopy

Cochleae were perfused with, and then immersed in 2.5% gluataraldehyde in 0.1M cacodylate buffer (pH 7.3) with 3 mM $CaCl_2$. Fixation was continued for a minimum of 2 hrs at room temperature. The cochleae were then post-fixed in 1% OsO4 (osmium tetroxide) in 1 mM cacodylate buffer for 2 hrs at room temperature. The cochleae were then decalcified in 4.13% EDTA in cacodylate buffer (pH7.3) for 48-72h at 4°C. The cochleae were partially dehydrated in an ethanol series to 70% ethanol, then immersed in saturated uranyl acetate in 70% ethanol overnight at 4°C to “en bloc” stain the tissues. Dehydration was continued to 100% ethanol before embedding the entire cochlea in plastic (Epon). Sections parallel to the modiolus were cut at 1 µm thickness

and stained with toluidine blue for visualisation by light microscopy. A series of thin sections for transmission electron microscopy (TEM) were then cut (80-100 nm thick). This procedure was carried out by Mr. G. Nevill. TEM images were collected digitally using a Gatan camera.

3 TRAFFICKING PATHWAYS OF INNER EAR CONNEXINS

3.1 Introduction

The large number of possible configurations and the wide-spread expression of connexins in the mammalian system suggest specific functions for gap junctions in particular cells or tissues. Mutations in connexins cause up to 10 different diseases, including hearing loss, skin disease, cataracts and heart disease, amongst others (reviewed by Laird, 2010). It is therefore, imperative to understand how gap junctions are regulated and how connexin composition influences intercellular communication. In the inner ear, Cx26 and Cx30 are vital for hearing. The loss of either one of these connexins cannot be compensated for by the other, suggesting a functional requirement for heteromeric/heterotypic gap junction configurations. Mutations in the genes coding for Cx26 and Cx30 can lead to truncated proteins, oligomerisation defects, trafficking defects, non-functional channels or channels with aberrant permeabilities (reviewed by Martinez et al., 2009). In addition, dominant-negative mutations in either connexin can lead to cochlear dysfunction. Of interest are the many Cx26 (Martinez et al 2010) and Cx30 (Common et al 2002) mutations that impair trafficking of connexons to the plasma membrane, which lead to syndromic (associated with other diseases, i.e. skin disease) or non-syndromic hearing loss.

It is not clear how the co-assembly of Cx26 and Cx30 is regulated both temporally and spatially in the cochlea. In light of mutation-specific treatments for cystic fibrosis (discussed below) and for connexin-mutation specific therapies in the future, it is vital to investigate the molecular assembly, trafficking and life-cycle of Cx26/Cx30 gap junctions. At the time of this study, there had been conflicting data regarding the Cx26 trafficking pathway, whereas the Cx30 pathway had not been investigated. For Cx26, some studies suggest a trafficking route through the Golgi apparatus, termed the ‘conventional secretory (trafficking) pathway’, whereas others suggest a route that by-passes the Golgi, termed the ‘non-conventional trafficking pathway’ (discussed further in section 3.1.3). Since Cx26 and Cx30 bind together to form heteromeric channels in the cochlea, it seems likely that both connexins follow similar trafficking pathways. Therefore, this project set out initially to investigate the intracellular trafficking pathways of Cx26 and Cx30 *in vitro*, with particular attention to Golgi interactions. In the long-term, it would be beneficial to elucidate where in the cell

these proteins oligomerise into heteromeric connexons. This is with the future aim of identifying possible therapeutic substances that can rescue trafficking-defective mutations, as has been described for cystic fibrosis (see section 3.1.2). This section introduces the field of protein trafficking, the two general secretory pathways and our current knowledge about connexin trafficking.

3.1.1 The conventional secretory pathway

Most membrane-spanning proteins are transported from their site of translation to the cell surface via the conventional secretory ("trafficking") pathway. This process, originally described by George Palade (1975), involves insertion of nascent proteins into the endoplasmic reticulum (ER) membrane through binding of a signal-peptide recognition particle. From here proteins undergo folding, oligomerisation, addition of oligosaccharide chains and packaging into budding vesicles at ER exit sites (ERES). To continue transport along the secretory pathway these vesicles require binding of coat protein complex II (COPII), which directs the cargo to the *cis*-Golgi via the ER-Golgi intermediate compartment (ERGIC). The proteins are then modified, processed and sorted whilst being directed towards the *trans*-Golgi network (TGN) where they then bud off and fuse with the plasma membrane (PM). This process has been well documented (Rothman, 1994; Mellman and Warren, 2000; Lee et al., 2004) and was once thought to be the common pathway for all transmembrane proteins and secretory molecules (Palade, 1975).

3.1.2 Discovery of non-conventional secretory pathways

The discoveries of alternative trafficking pathways have only emerged in the last 20 years. The non-conventional secretory pathway has been described as a transport system for proteins that do not enter or pass through the ER and/or Golgi apparatus *en route* to the PM, and that do not contain post-translational modifications specific for these compartments (reviewed by Nickel and Seedorf, 2008). Originally, evidence for non-conventional secretion was shown for interleukin 1β (Rubartelli et al., 1990) and galectin-1 (Cooper and Barondes, 1990). These cytoplasmic and nuclear proteins lack an ER-signal peptide and have been shown to exit cells through ER- and Golgi-independent pathways. Since their discovery these molecules have been joined by other similar proteins such as fibroblast growth factors (FGF1 and 2), galectin-3, β-galactosidase-specific lectins and engrailed homeoprotein, amongst others, with up to

20 different soluble proteins making up this group. These proteins are often referred to as “soluble” or “cytoplasmic” proteins and are involved in various physiological processes, such as inflammation, angiogenesis, cell differentiation, or proliferation (reviewed by Nickel and Seedorf, 2008; Nickel and Rabouille, 2009).

An alternative group of proteins that traffic non-conventionally start their journey in the ER and transport to the cell surface in a COPII and/or Golgi-independent manner. Proteins that do not require COPII-coat components include yeast heat-shock protein Hsp150 (Fatal et al., 2004), K_v4 voltage-sensitive potassium channels (Hasdemir et al., 2005), EDEM1 and OS-9 (Zuber et al., 2007; Cali et al., 2008) – both of which are regulators of ER-associated degradation (ERAD). These pathways would most likely require novel coat complexes or have the ability to directly insert into the PM from ER-exit sites (for PM targeted proteins).

Various techniques have been used to show that the remaining non-conventional group of proteins bypass the Golgi apparatus (reviewed by Grieve and Rabouille, 2011): i) Brefeldin-A (BFA) treatment to destabilise the Golgi stacks and prevent ER-to-Golgi transport (discussed in chapter 3.1.4); ii) glycosylation state as detected by Endoglycosidase H (Medzihradszky, 2005); and iii) knock-down of Golgi SNARE (soluble *N*-ethylmaleimide-sensitive-factor attachment protein receptor) proteins required for vesicle docking. Examples of proteins identified to traffic non-conventionally using these techniques are described briefly.

Cystic fibrosis transmembrane conductance regulator (CFTR) is the most documented example of Golgi bypass. Although the general consensus is that CFTR exits the ER via COPII vesicles (Wang et al., 2004), Golgi bypass still occurs in baby hamster kidney (BHK) and Chinese hamster ovary (CHO) cells (Yoo et al., 2002). However, the authors suggest that CFTR trafficking may be cell-type specific, since Golgi bypass was not shown for HeLa or 293T cells. The predicted trafficking pathway is thought to incorporate fusion with endosomes or the TGN prior to PM insertion, thus bypassing the *cis* and *medial* Golgi stacks (Yoo et al., 2002). Understanding the protein trafficking pathway of CFTR has been instrumental in developing cystic fibrosis clinical trials. Recently, research has focused on the most common mutation, ΔF508-CFTR, which fails to fold correctly in the ER and is rapidly degraded via the proteasome. In addition, the mutation confers reduced capacity to transport Cl^- ions and decreases the

PM half-life (reviewed by Guggino and Stanton, 2006). Interest in the field stems from the discovery that certain chemicals and drugs can rescue, to an extent, the trafficking and functions of ΔF508-CFTR. Curcumin, a component of the spice turmeric, and S-nitrosoglutathione, a bronchodilator normally expressed in healthy lungs, can induce transport of this mutant to the PM (Zaman et al., 2001; Egan et al., 2004). Therefore, these compounds could potentially be used alongside drugs that increase ΔF508-CFTR activity. One such drug that is being investigated is a flavinoid called Genistein, which has been shown to activate both ΔF508-CFTR and another human mutation, G551D-CFTR. In combination, these drugs and compounds could be used to help reduce the symptoms of cystic fibrosis (Guggino and Stanton, 2006).

CD45 is a protein tyrosine phosphatase that has the ability to traffic to the PM in a BFA-insensitive manner. In T-cells, it has been shown that two glycosylated forms of CD45 reach the cell surface as detected by Endoglycosidase H (EndoH) sensitivity. EndoH functions by detecting proteins with a high mannose oligosaccharide core. The addition of high mannose oligosaccharides usually occurs within the ER. Upon entry into the Golgi apparatus, these sugars are modified to an extent where they are no longer a substrate for EndoH. Therefore, EndoH-resistant forms are thought to traffic through the Golgi, whereas EndoH-sensitive proteins are thought to bypass the Golgi. The pool of CD45 EndoH-sensitive proteins also traffic to the PM three times faster than the resistant form, leading to speculation that divergent trafficking pathways act as a control mechanism in regulating protein modifications and activity (Baldwin and Ostergaard, 2002).

Ist2 is a *Saccharomyces cerevisae* (yeast) integral PM protein that is synthesised from mRNA at localised, specific ER domains. Evidence suggests a novel trafficking pathway whereby Ist2 is directly transported from cortical ER exit sites into the PM, thus bypassing the Golgi apparatus and components of the conventional secretory pathway (Juschke et al., 2004; Franz et al., 2007).

3.1.3 Connexin trafficking pathways

Connexins, along with most integral membrane proteins are synthesised by bound ribosomes and are co-translationally inserted into the ER membrane. insertion into the PM, connexin subunits must oligomerise into hexameric Within the ER most connexins are sorted, assembled into connexons and trafficked

the conventional secretory pathway (Yeager et al., 1998; Segretain and Falk, 2004; Thomas et al., 2005; Laird, 2006). The exact intracellular location of connexon assembly may be unique to the connexin and cell type, with some studies oligomerisation in the ER (Falk et al., 1997; Ahmad et al., 1999; Maza et al., 2005) ERGIC (Diez et al., 1999). Other studies, however, have shown that Cx43 and present in their monomeric form in the Golgi apparatus and oligomerise in the (Musil and Goodenough, 1993; Koval et al., 1997; Maza et al., 2003; Das et al., Both pathways are summarised in

Image deleted due to copyright.

Figure 3-1. A recent study has also argued against Cx32 oligomerisation in the ER and suggested instead that connexon formation occurs at a post-ER site, likely to be the TGN (Vanslyke et al., 2009).

Cx43 is the most widely distributed connexin in the body and has roles in many organs, including the heart, skin, eye and brain (as reviewed by Laird, 2006). The trafficking pathway of Cx43 has been well characterised, with the common understanding that it traffics via the Golgi apparatus and oligomerises into connexons before insertion into the PM (Musil and Goodenough, 1993; Laird et al., 1995; Martin et al., 2001a; Thomas et al., 2005). These studies found that both endogenous and green fluorescent protein (GFP)-tagged Cx43 were sensitive to BFA treatment in a variety of mammalian cell lines. After a 6 hour incubation, gap junction plaques were removed from the cell surface and intracellular staining exhibited an ER-like localisation, suggesting that Cx43 required a functional Golgi unit for trafficking to the PM. Similar results were also found for tagged (Cx26-YFP) and Cx26-untagged protein trafficking in stably transfected mammary-tumour (BICR-M1Rk) and normal rat kidney (NRK) cell lines. In further support of this finding, Cx26 and Cx43 ER-to-Golgi transport was inhibited by expression of a dominant-negative form of Sar1 (secretion-associated and Ras-related protein 1), a guanine triphosphatase (GTPase) that is required for COPII coat formation on budding ER vesicles (Thomas et al., 2005). In addition, Cx43-GFP

delivery and gap junction regeneration was inhibited by the microtubule disrupting drug nocodazole, whereas Cx26-GFP trafficking was unaffected. These data point towards a conventional secretory pathway for both Cx26 and Cx43, and a microtubule-dependent pathway for Cx43, but not Cx26.

The studies mentioned in the previous paragraph suggest that Cx26 follows the same conventional trafficking pathway as Cx43 through the Golgi apparatus. However, Cx26 homomeric connexons have also been suggested to insert directly into PMs via a pathway that does not implicate the Golgi apparatus (Diez et al., 1999). In support of this finding, connexons composed of Cx26 have been demonstrated to traffic to the PM in the presence of BFA (George et al., 1999; Martin et al., 2001a; Martin et al., 2001b). In addition, Cx26 can also post-translationally insert into ER membranes, and possibly plasma membranes, in a cell-free translation system – a process that is rarely seen in eukaryotes and one that contrasts with the usual co-translational integration into ER membranes seen with most other proteins (Ahmad et al., 1999; Ahmad and Evans, 2002). These data suggest that Cx26 has the potential to reach the PM via a Golgi-independent pathway. In contrast to the study by Thomas et al. (2005), data presented by Martin et al. (2001a) also suggest that connexons composed of Cx26, but not those of Cx43, require microtubules to traffic to the PM. These contradictory results have raised many questions about the influence of cell type and exogenous expression systems used in the study of connexin trafficking.

Image deleted due to copyright.

Figure 3-1. **Oligomerisation and trafficking pathways of Cx32 and Cx43.**

Evidence suggests that connexins have the potential to oligomerise in the ER (in over-expression systems), ERGIC (Cx32, green) or the TGN (Cx43, mauve). Both these pathways include trafficking through the Golgi apparatus before insertion in the PM. From here, connexons dock with compatible connexons on the opposing PM to form gap junction channels, which cluster together to form semi-crystalline arrays known as gap junction plaques. Adapted from Koval, 2006.

3.1.4 Trafficking routes of Cx26 and Cx30 in vitro

Since gap junctions in the cochlea are often composed of Cx26/Cx30 heteromeric gap junctions (Forge et al., 2003b; Yum et al., 2007), it would seem likely that they oligomerise prior to insertion in the PM. Thus it would seem likely that Cx26 and Cx30 trafficking pathways show common features. The reports described in the previous section have revealed conflicting data regarding whether Cx26 travels through the Golgi apparatus en route to the PM. At the time of study, the trafficking pathway of Cx30 had not been investigated.

This chapter investigates the trafficking of rodent Cx26 and Cx30 *in vitro*, with particular attention to potential Golgi interactions. Immunofluorescence labelling was used to determine intracellular localisation and dye transfer studies to determine the extent of functional gap junctional coupling. The Golgi-disrupting drug Brefeldin-A (BFA) and temperature manipulation are commonly used to disrupt Golgi-dependent protein trafficking to the PM. The techniques and mechanisms are described briefly below.

3.1.4.1 Brefeldin-A

BFA is a fungal metabolite often used in protein trafficking studies due to its unique ability to disrupt protein trafficking from the ER to Golgi, and its relatively non-cytotoxic effects (Misumi et al., 1986; Klausner et al., 1992). It functions by inhibiting a guanosine triphosphate exchange factor (GEF) that catalyses the activation of a small GTPase called Arf1p on Golgi membranes. This process is essential for recruitment of coat proteins (COPs) to the membrane and subsequent formation of transport vesicles (Helms and Rothman, 1992; Nebenfuhr et al., 2002). In most cells, BFA treatment results in the absorption of the Golgi membrane into the ER (Lippincott-Schwartz et al., 1990). The discovery of unconventional protein secretion has been largely attributed to the effects of BFA on cultured cells. In recent years, research has suggested that PM cargo may segregate early in the secretory pathway, either in the ER, ERGIC or earliest Golgi cisternae and that these proteins traffic to the PM via unconventional (Golgi-independent) trafficking routes (Prydz et al., 2008; Nickel and Rabouille, 2009; Tveit et al., 2009).

3.1.4.2 Temperature regulation of trafficking pathways

Temperature manipulation is a common technique used to halt the transport of proteins in specific intracellular compartments. One of the first experiments to show temperature-dependent trafficking through the Golgi was carried out by Matlin and Simons (1983). They showed that influenza virus hemagglutinin was terminally glycosylated in the Golgi apparatus and trafficked to the cell surface via the TGN. Incubation at 20^{o}C resulted in continued glycosylation, but a lack of hemagglutinin detection at the cell surface, suggesting an accumulation in the Golgi apparatus. This process was reversible when the temperature was returned to 37 ^{o}C. Other studies have also used this technique to entrap proteins trafficking through the common secretory pathway in the TGN (Griffiths et al., 1989; Sato et al., 2009). Further studies have also established a lower temperature block of protein accumulation in the ERGIC. At 15^{o}C proteins exit the ER but fail to enter the Golgi stacks and accumulate in pre-Golgi vacuolar compartments (Saraste and Kuismanen, 1984; Lippincott-Schwartz et al., 1990; Klumperman et al., 1998; Martinez-Alonso et al., 2005). Using temperature manipulation, Musil and Goodenough (1993) were the first to show that Cx43 oligomerisation occurred within the TGN (at 20^{o}C), rather than in the ER (at 15^{o}C).

For the questions being asked here, temperature-blocking of Cx26 and Cx30 at 20^{o}C was utilised as a way of determining whether these proteins pass through the Golgi apparatus. At these lower temperatures one would expect an accumulation of protein within the Golgi stacks if trafficking is halted at the TGN. If the trafficking is Golgi-independent then temperature blocking at 20^{o}C should have no effect since these proteins are presumed to not pass through the TGN.

3.2 Results

3.2.1 Connexin 43 co-localises with the Golgi apparatus

Using BFA to disrupt the Golgi apparatus, previous reports have shown Cx43 traffics through the Golgi before inserting into the PM (Laird et al., 1995). For comparative reasons and to standardise our technique, HeLa cells stably expressing Cx43 were used to assess Cx43 intracellular localisation and the effect of BFA on gap junction formation.

Control Cx43-HeLa cells immunolabelled for Cx43 showed an abundance of gap junction plaques between cells and intracellular cytoplasmic accumulations (Figure 3-2Ai). Co-labelling with the *cis*-Golgi marker GM130 (Figure 3-2Aii) revealed co-localisation with the Cx43 cytoplasmic accumulations, as depicted by yellow pixels (Figure 3-2Aiii). To disrupt ER-Golgi trafficking, cultured cells were treated with 5 μg/ml BFA for 7 hours prior to fixation. This time was seen as sufficient to allow reduction of gap junction numbers, since most gap junctions have a half-life of 1.5-5 hours at the PM (Fallon and Goodenough, 1981; Laird et al., 1991). After 7 hours, the intracellular localisation Cx43 was diffuse throughout all cells (Figure 3-2Bi). The Golgi apparatus was completely disrupted and small GM130-labelled punctae were spread throughout the cell cytoplasm (Figure 3-2Bii). This labelling pattern was expected since disruption of COPII coat formation by BFA is known to disrupt the Golgi structure and cause regression of Golgi membranes into ER/ERGIC compartments (as described previously). Therefore, the expression patterns of GM130 and Cx43 after BFA treatment are likely due to ER localisation (Figure 3-2Biii).

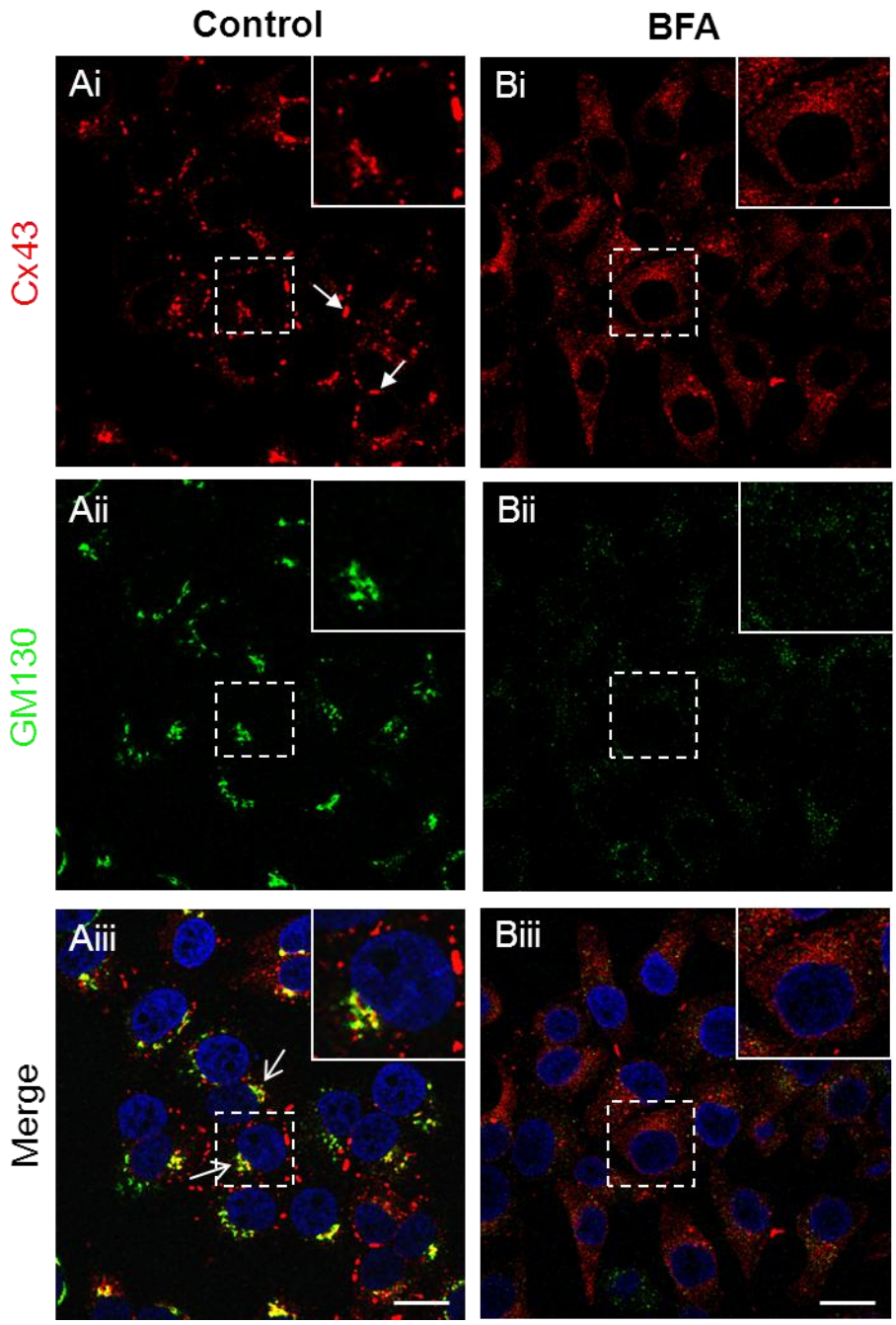

Figure 3-2. Cx43 co-localises with the *cis*-Golgi and is disrupted by BFA.

(Ai) Control HeLa cells stably expressing Cx43 (red) formed gap junction plaques at cell-cell boundaries (closed arrows). (Aii) Staining with anti-GM130 showed the structure of the *cis*-Golgi (green). (Aiii) Cx43 co-localised with GM130 in control cells (yellow, open arrows). Nuclei were counter-stained with DAPI (blue). (Bi) Cx43 localisation was diffuse throughout the cell along with an apparent reduction in gap junction numbers after treatment with BFA for 7 hrs. (Bii) Confirmation of Golgi apparatus disruption (note the dispersed green staining). (Biii) Cx43 no longer accumulated in a specific sub-cellular region after Golgi dispersal. Insets show detail in regions delineated by dashed boxes. Scale bars 20 µm.

3.2.2 Connexin 26 localises to the Golgi apparatus

HeLa cells stably expressing Cx26 showed less intracellular staining compared with Cx43-HeLa cells, and had only small Cx26 punctae within the cell cytoplasm (Figure 3-3Ai). Co-labelling with GM130 did not reveal any direct co-localisation, as determined by yellow pixels (Figure 3-3Aii-iii). However, upon closer inspection, many of the Cx26-labelled granules were localised to the vicinity surrounding the *cis*-Golgi cisternae (Figure 3-3Aiii, inset). After 7 hours of BFA treatment, Cx26 appeared dispersed throughout the cells' cytoplasm (Figure 3-3Bi), in a similar, but not identical pattern to the disrupted GM130 labelling (Figure 3-3Bii-iii). These data suggest that Cx26 is localised to the Golgi region and possibly locates to an ER-like compartment upon BFA treatment. It is difficult to determine conclusively that Cx26 was localised within the Golgi compartment due to a lack of direct co-localisation with GM130 (i.e. lack of yellow pixels). However, the Cx26-labelled granules that localised specifically around the GM130 marker could represent budding vesicles from the *cis*- or *medial*-Golgi stacks.

To further investigate whether Cx26 traffics through the Golgi apparatus, normal HeLa cells were transiently transfected with two mutant constructs that confer syndromic hearing loss (i.e. also cause skin disease). These were developed previously by Marziano et al. (2003), and contain a single dominant mutation in the *GJB2* gene (G59A and D66H). D66H does not traffic to the PM and instead accumulates in an intracellular compartment localised to the perinuclear region. G59A also accumulates in an intracellular compartment, but a proportion can traffic to the PM to form non-functional gap junctions (Marziano et al., 2003; Thomas et al., 2004). These mutations were used to determine whether accumulation occurs in the *cis*-Golgi compartment. HeLa cells transfected with D66H-eGFP showed accumulation in the *cis*-Golgi apparatus as shown by the strong co-localisation (yellow pixels) with GM130, and did not form gap junction plaques (Figure 3-3Ci-iii). The G59A-eGFP mutant formed small, gap junction plaques and also accumulated in the *cis*-Golgi apparatus as shown by its co-localisation with GM130 (Figure 3-3Di-iii). It is evident that the trafficking of these two Cx26 mutants accumulates (G59A) and stalls (D66H) at the *cis*-Golgi apparatus. These data suggest further that Cx26 must travel through the Golgi before reaching the PM and that mutations in this gene can affect the normal trafficking route through the secretory pathway.

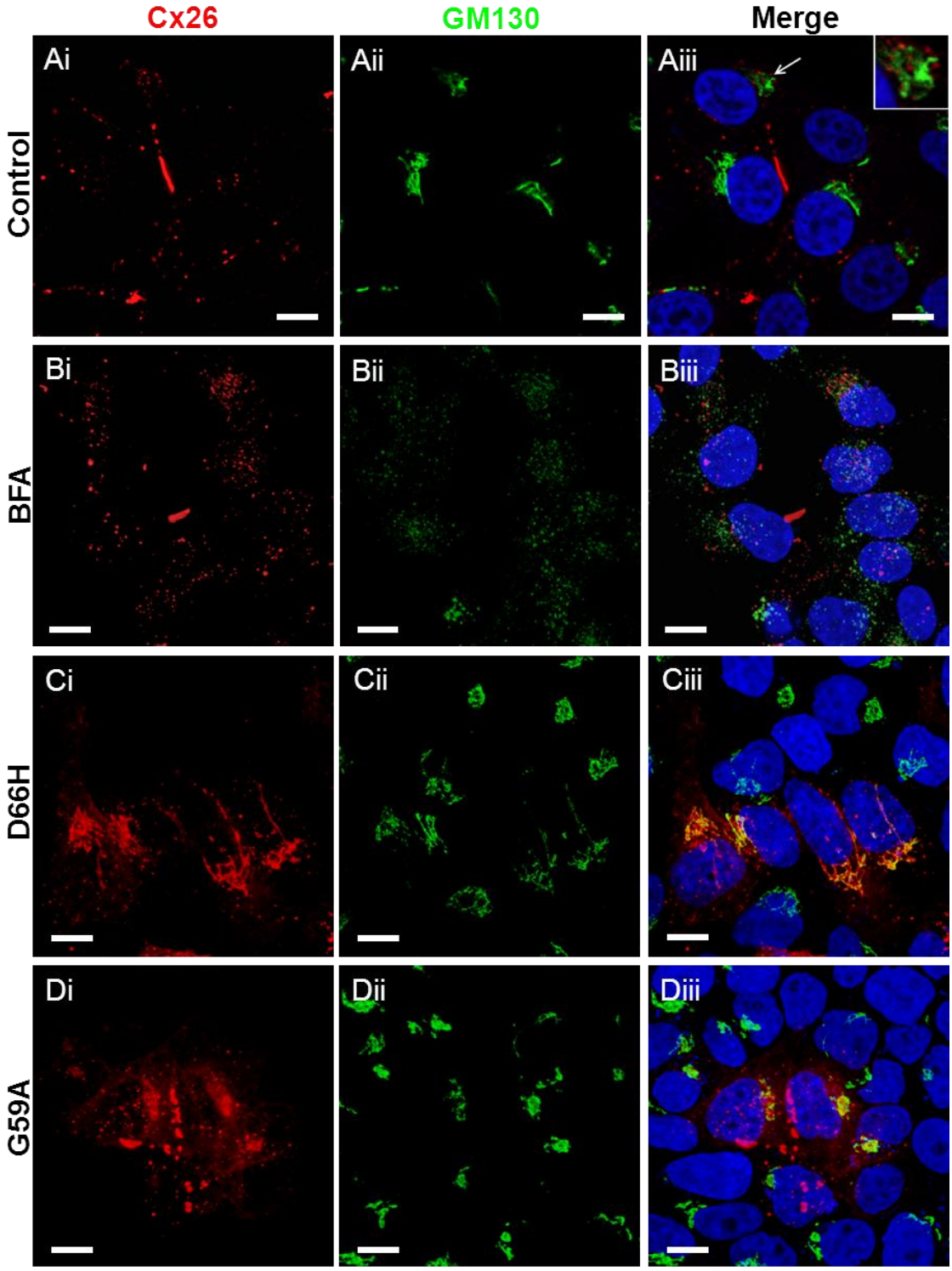

Figure 3-3. Connexin 26 mutants co-localise with the *cis*- Golgi

(Ai-iii) HeLa cells stably expressing Cx26 (red) show Cx26-labelled granules surrounding the *cis*-Golgi marker GM130 (green). Arrow, enlarged region within the inset. Nuclei were counterstained with DAPI (blue). (Bi-iii) Cx26 was dispersed along with the Golgi apparatus after 7 hrs BFA treatment. (Ci-iii, Di-iii) HeLa cells were transiently transfected with two different constructs that contain a single, dominant mutation in the *GJB2* gene (D66H and G59A) – both of which cause syndromic deafness. Both mutations show co-localisation with the *cis*-Golgi compartment (yellow). Scale bars 10µm.

3.2.3 Connexin 30 does not co-localise with the Golgi apparatus

At the time of study, no other publications had reported the trafficking pathway of Cx30. Immunofluorescent labelling was investigated in HeLa cells stably expressing Cx30. The cells displayed distinct gap junction plaques, but, in contrast to Cx26 and Cx43, had no discernible intracellular labelling when the detection levels were comparable to those used for Cx26 (Figure 3-4Ai-iii). However, when the detector gain levels were increased so that immunofluorescence levels were saturated, some Cx30 intracellular localisation became apparent (Figure 3-4Bi-iii). Although both Cx30 and GM130 labelling were localised in similar regions of the cell, they did not exhibit any direct co-labelling (determined by yellow pixels) and appeared to segregate into separate compartments. Gap junction plaques were still visible after treatment with BFA for 7 hours, and some intracellular Cx30 vesicle-like structures were apparent in the cytosol (Figure 3-4Ci-iii). The Cx30-labelled vesicles were distinct from GM130-labelled punctae and could have been formed by endocytosis from gap junction plaques. Thus, Cx30 intracellular labelling, although present at much lower levels, exhibited different patterns to both Cx26 and Cx43 and did not co-localise with the *cis*-Golgi compartment.

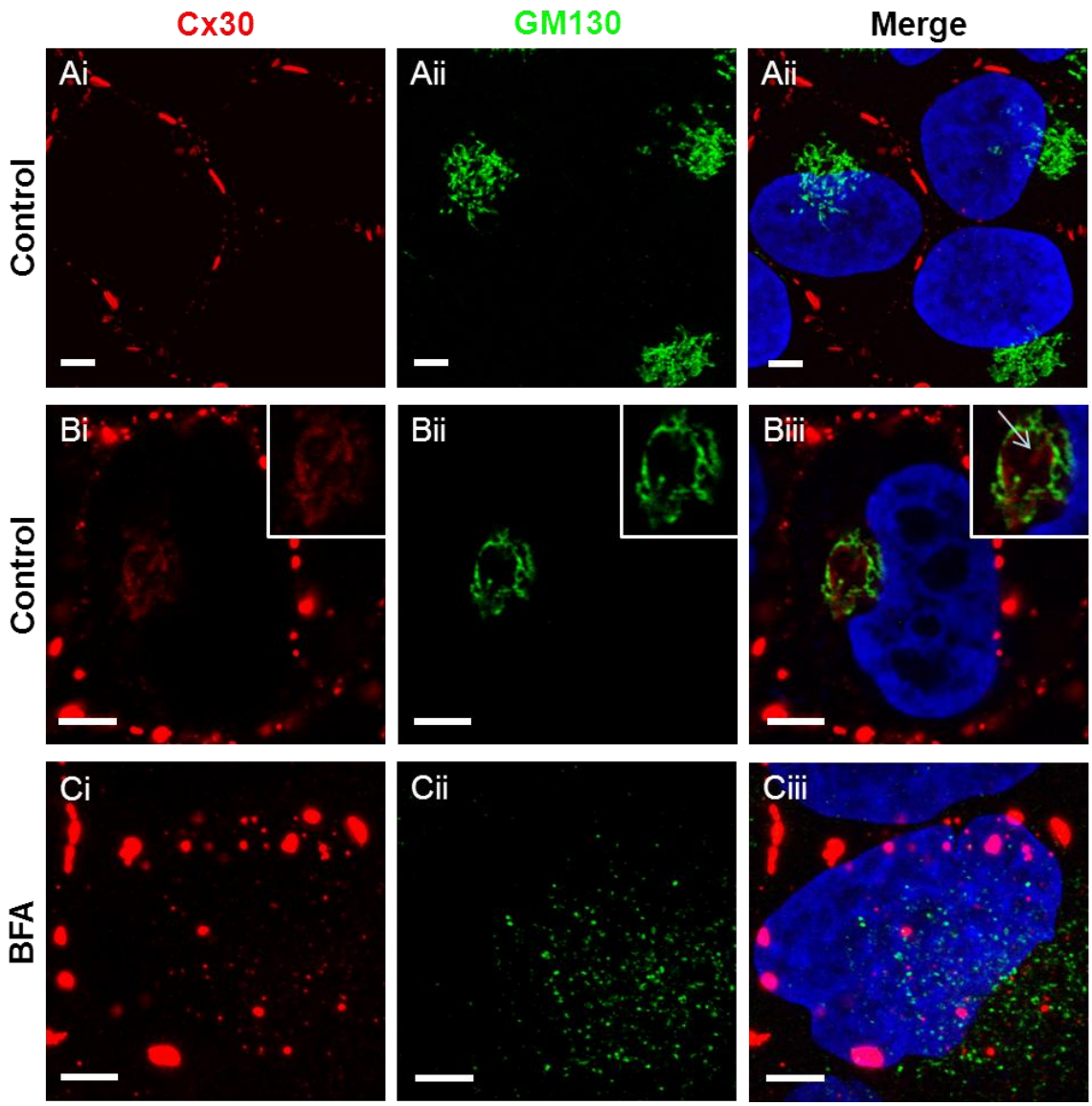

Figure 3-4. Connexin 30 does not co-localise with the Golgi apparatus.

(Ai-iii) Immunostaining of HeLa cells stably expressing Cx30 (red) did not show intracellular localisation in the cytoplasm or in the *cis*-Golgi (green) when the detector levels were comparable to those used for Cx26 (Figure 3-3A). Nuclei were counterstained with DAPI (blue). (Bi-iii) However, faint intracellular localisation was visible when focused on one cell and with the detector of the red channel raised to a saturation level. Insets show a more detailed image of the *cis*-Golgi region and revealed that the faint Cx30-labelling was distinct from GM130 labelling (arrow). Note the lack of yellow pixelation. (Ci-iii) Cells treated with BFA for 7 hours revealed similar gap junction plaques (bright red patches) and possibly more Cx30 positive granules in the cytoplasm. Scale bars 5 µm.

3.2.4 BFA effect on dye transfer in Cx43, Cx26 and Cx30-HeLa cells

Injection of small molecular dyes and subsequent intercellular transfer can be a useful technique for determining the presence of functional gap junctions between cells in culture or *in situ* (Jagger and Forge, 2006). This technique was used here to quantify the extent of gap junctional intercellular communication (GJIC) in Cx-HeLa cells before and after BFA treatment. HeLa cells were used for *in vitro* studies since these cells do not express any known connexins (Eckert et al., 1993; Elfgang et al., 1995), which permits the use of dye transfer as a quantitative way of measuring functional gap junction coupling. Cells were plated onto 9 mm glass coverslips and grown to a monolayer confluency of 85-95%. Intracellular recording solution containing the gap junction permeable dye neurobiotin (NBN; charge, +1; MW, 287 Da) was introduced into a single cell using the whole-cell patch clamp method. Previous studies have shown that a 10 minute period is sufficient to permit extensive dye spread (Jagger and Forge, 2006). After this period, cells were fixed and fluorescently labelled (as described in materials and methods). For BFA treatment, cells were incubated with media containing 5 µg/ml BFA for 6-7 hours before whole-cell dye injections were performed. BFA was also included in the bath solution to maintain Golgi disruption.

In control Cx43-HeLa cells, NBN introduced into a single cell spread extensively between gap junction-coupled cells (average of ~150 cells, Figure 3-5Ai-iii). Incubation with BFA for 7 hours caused a 60% decrease in the number of cells containing NBN (average of ~60 cells), suggesting a strong reduction in the number of gap junctions. These data, taken together with the immunofluorescence labelling, agree with previous reports that Cx43 traffics through the Golgi apparatus en route to the PM, and standardises our experimental technique for investigating Cx26 and Cx30 trafficking. Control Cx26-HeLa cells exhibited wide-spread NBN transfer (average of ~290 cells) after 10 minutes of dye injection (Figure 3-5Bi-iii). The amount of dye spread was reduced by 86% (to ~40 cells) after 7 hour incubation with BFA. These data, along with the Cx26-HeLa immunofluorescence labelling and mutant transfections, strongly indicate that Cx26 traffics through some component of the Golgi apparatus en route to the PM in HeLa cells. Immunofluorescence labelling did not yield definitive results regarding Cx30 localisation at the Golgi. Dye transfer studies have, however, helped to elucidate that Cx30 may traffic to the PM via a Golgi-independent route.

There was no significant difference between the number of cells containing NBN after 7 hours BFA treatment (~60 cells) in comparison to control cells (~65 cells, Figure 3-5Ci-iii), suggesting that Cx30 trafficking is not dependent on an intact Golgi apparatus in HeLa cells.

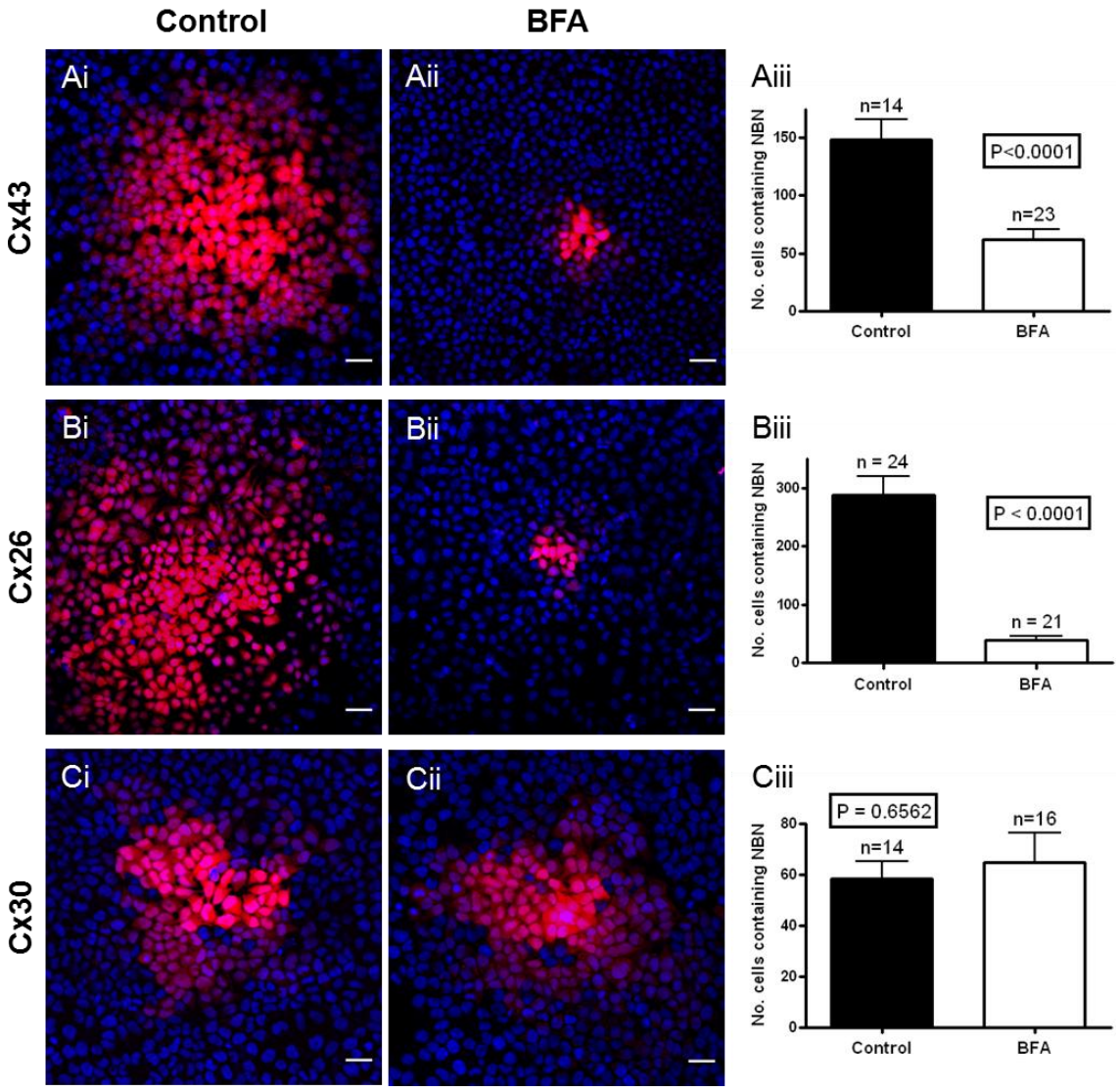

Figure 3-5. Dye transfer in Cx30-HeLa cells is not inhibited by BFA.

Neurobiotin (NBN, red) was introduced into single Cx43 (Ai), Cx26 (Bi) and Cx30 (Ci) HeLa cells via a patch pipette and allowed to diffuse through gap junctions for 10 minutes before fixation. Nuclei were labelled with DAPI (blue). Representative images of NBN transfer in Cx43 (Aii), Cx26 (Bii) and Cx30 (Cii) HeLa cells after 7 hrs BFA treatment. (Aiii) BFA caused a significant reduction ($P<0.0001$) in the number of Cx43-HeLa cells containing NBN. (Biii) BFA also significantly reduced ($P<0.0001$) NBN transfer in Cx26-HeLa cells. (Ciii) There was no significant difference ($P=0.6562$) in the number of Cx30-HeLa cells containing NBN after BFA treatment. *n* = number of dye injections. Scale bars 50 µm.

3.2.5 Cx26 and Cx30 do not accumulate in the Golgi apparatus when TGN exit is blocked

Incubation of cells at temperatures of 15-20^{o}C have been used to block trafficking at certain points along the secretory pathway. Cells cultured at 15^{o}C accumulate newly synthesised proteins in the ER/ERGIC (Klumperman et al., 1998; Martinez-Alonso et al., 2005), whereas cells incubated at 19-20^{o}C permit exit from the ERGIC into the Golgi stack, but block release from the TGN (Matlin and Simons, 1983; Saraste and Kuismanen, 1984; Griffiths et al., 1989; Lippincott-Schwartz et al., 1990). Temperature manipulation was used here to try and elucidate whether Cx26 and Cx30 traffic through the Golgi apparatus. The aim of the experiment was to determine whether either connexin accumulates in the Golgi stack upon temperature reduction.

Transfected HeLa cells stably expressing Cx26 or Cx30 were incubated at 19^{o}C for 2, 4 and 8 hours before fixation and immuno-staining. In control cells (37^{o}C), gap junction plaques were visible between cell-cell contacts, but intracellular staining was minimal (Figure 3-6A, E). After 2 hour incubation at 19^{o}C, the *cis*-Golgi apparatus in both cell lines appeared to condense and lose its tubular structure. However, no accumulation or co-localisation with the GM130 marker was noticeable for Cx26 or Cx30 (Figure 3-6B, F). Increasing the incubation times to 4 (Figure 3-6C, G) and 8 (Figure 3-6D, H) hours at 19^{o}C did not induce any changes in connexin localisation. In addition, most cells were still connected by large gap junction plaque. Consequently, there was no apparent accumulation of Cx26 or Cx30 in the Golgi at 19^{o}C.

These data are difficult to interpret. For Cx26, which is BFA-sensitive, it was expected that blocking TGN exit at 19^{o}C would lead to an accumulation in some part of the Golgi compartment and a stark reduction in gap junction plaques after 8 hours. In comparison, Cx30 was not expected to accumulate in the Golgi if it is trafficked to the PM in a Golgi-bypass manner. It could be that the amount of time required for significant Cx26 accumulation to occur in the Golgi is longer than the incubation times used. Therefore, Cx26 accretion would not be apparent with immuno-localisation studies. It is also possible that Cx26 buds off from *cis* or *medial*- Golgi compartments, rather than trafficking through to the TGN. This would explain why Cx26 is sensitive to BFA, yet does not show any localisation within the Golgi stack. Cx30 on the other hand might not accumulate in any of the Golgi stacks due to its possible Golgi-bypass

route. A positive control that shows protein accumulation in the Golgi is required to determine whether TGN exit was significantly blocked in these cells. Cx43-HeLa cells were not used as a positive control since they localise strongly to the Golgi complex in normal conditions, therefore, immuno-labelling would not yield informative results. Ideally dye transfer experiments would have been implemented to allow quantification of the extent of gap junctional coupling. Connexins that traffic through the Golgi and are blocked from TGN exit would, in theory, have a reduction in the number of gap junctions, thus reducing the extent of gap junctional intercellular communication. This experiment was not possible due to problems of maintaining the cells at 19^{o}C on the electrophysiology rig.

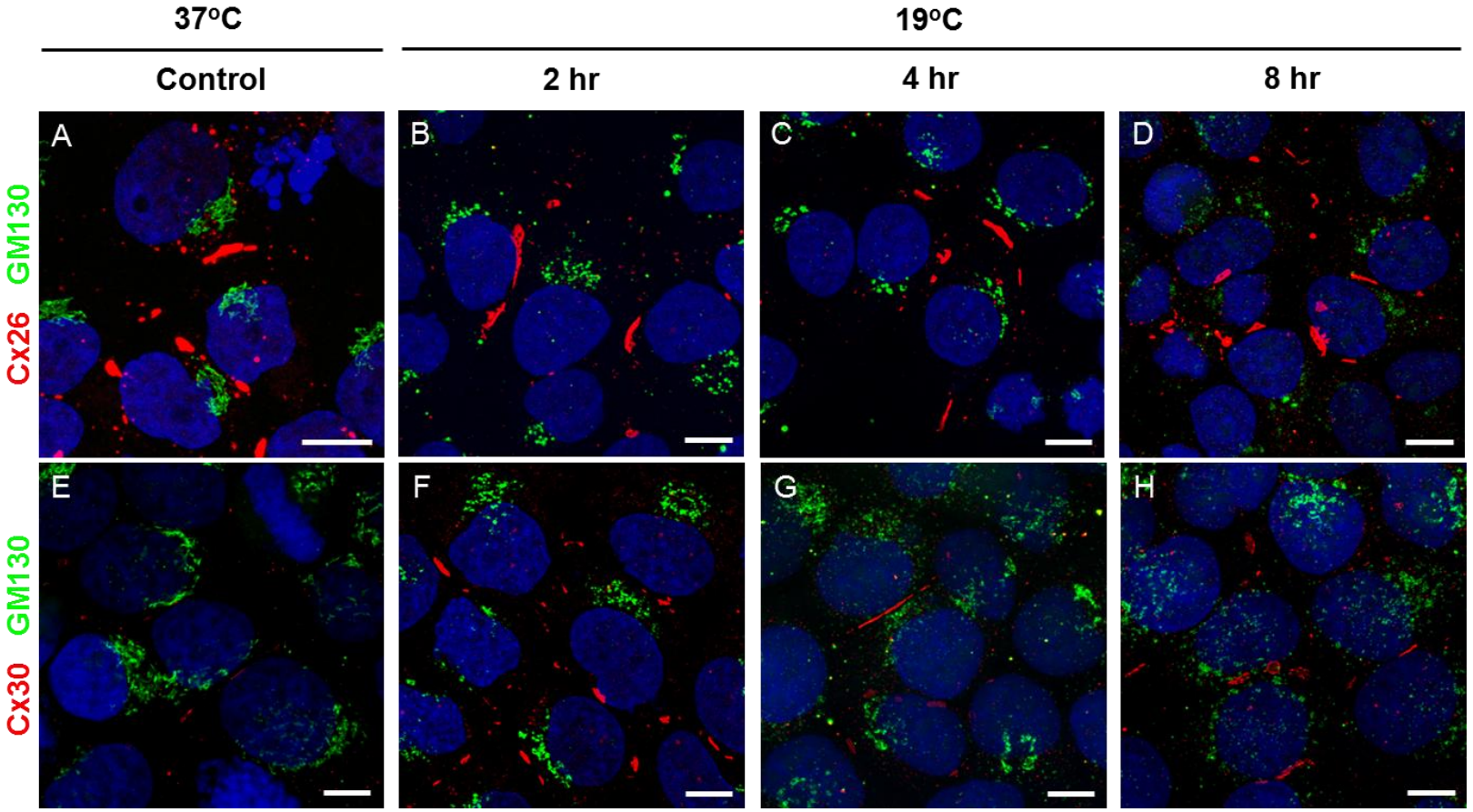

Figure 3-6. Cx26 and Cx30 do not accumulate in the Golgi at temperatures that inhibit TGN exit.

(A) At 37°C, small Cx26-labelled vesicles (red) were localised around the *cis*-Golgi marker GM130 (green). (E) These vesicles were less evident in Cx30-HeLa cells as described previously. (B, F) There were no visible differences in connexin localisation or connexin accumulation in the Golgi after 2 hours at 19 °C. (C, D, G, H) At further time points, the Golgi apparatus appeared to fragment. Gap junction plaques were still visible and there were no apparent intracellular accumulations of either connexin. Nuclei were counterstained with DAPI (blue). Scale bars, 10 μm.

3.2.6 Trafficking routes of native Cx26 and Cx30: the quest for endogenous Cx26/Cx30 expressing cells

Stably-transfected cell lines are useful models for trafficking experiments as these systems allow the researcher to directly regulate the expression of genes of interest. There are, however, conflicting results in the literature (especially for Cx26) when using *in vitro* techniques (for example, Martin et al., 2001a; Thomas et al., 2005). With this in mind, and to verify results obtained from heterologous expression systems, cell lines were also created from both adult guinea-pig and rat cochlear lateral wall fibrocyte cultures. These cells express significant amounts of Cx26 and Cx30 *in vivo*. Five different fibrocyte subtypes have been classified in the lateral wall according to their immunohistochemical expression and localisation within the spiral ligament (see Table 3-1). This profile was used to ascertain which subtype had been cultured, with the view of using these cells to repeat the trafficking experiments. Given that fibrocytes express both Cx26 and Cx30 *in vivo* these cells would represent an excellent model system to assess whether the trafficking properties of these connexins match those *in vitro* or change when expressed simultaneously in the same cell type. These cells were also identified as a possible model to investigate the intracellular location of Cx26/30 oligomerisation.

In vitro techniques have been invaluable for studying protein trafficking and intracellular localisation, but they may not represent the true *in vivo* expression pattern. Accordingly it would be beneficial to confirm the trafficking results seen so far by repeating the experiments on a cell line that endogenously express Cx26 and Cx30. Most of the fibrocytes in the lateral wall express both these connexins and can be cultured readily (Gratton et al., 1996; Yoshida et al., 1999; Suko et al., 2000; Shen et al., 2004). However, connexin expression in cultured fibrocytes has not been reported previously. This was investigated here using adult guinea-pig preparations. Lateral wall sections were plated onto collagen coated coverslips and cultured as described in material and methods (Figure 3-7A-C). Healthy cell lines were maintained for up to ~20 passages.

Immunohistochemical Profile of Lateral Wall Fibrocytes (*in vivo* expression data)					
Antigen	**Type I**	**Type II**	**Type III**	**Type IV**	**Type V**
Vimentin	+	-	+	+	-
Cytokeratins	-	-	-	-	-
Carbonic anhydrase II	+	-	+	+	+
Creatine Kinase-BB	+	-	+	+	+
Ca-ATPase	+	-	-	-	-
Na-K-ATPase	-	+	-	+	+
Caldesmon	+	+	+	N/D	N/D
S-100	+	+/-	-	+	+
Aquaporin-1	-	-	+	-	-

Table 3-1. Immunohistochemical profile of lateral wall fibrocytes.

Cultured fibrocytes can be classed into subgroups depending on their location in the lateral wall (Spicer and Schulte, 1991) and by the expression of the above proteins (*in vivo*). From Gratton et al., 1996, Suko et al., 2000, Liang et al., 2003 Qu et al., 2007 Mutai et al., 2009. See Figure 3-7 for a diagram of fibrocyte locations in the lateral wall. N/D, not described.

Immunofluorescence experiments on subcultured fibrocytes showed labelling for both S-100 (Figure 3-7D) and vimentin (Figure 3-7E), but not for Na^+-K^+-ATPase (Figure 3-7F). This indicated that the cells mostly resembled type I fibrocytes (according to the immunohistochemical profile in table 1), and would be expected to express both Cx26 and Cx30. However, neither the mRNA (data not shown) nor the protein of Cx26 (Figure 3-7G) or Cx30 (Figure 3-7H) were detected in these cells. Gap junctional intercellular communication was confirmed though by dye injection of NBN and Lucifer Yellow (LY), both of which transferred between numerous fibrocytes (Figure 3-7I). Accordingly, the connexin expression of the fibrocytes was investigated.

Reverse-transcription PCR (RT-PCR) confirmed the absence of Cx26 and Cx30 mRNA (data not shown), but revealed bands for both Cx43 (167 bp) and Cx31 (232 bp) in cultured fibrocytes (Figure 3-8A, C). Immunofluorescence labelling of Cx43 revealed extensive staining at cell-cell boundaries and strong co-localisation with the Golgi apparatus (Figure 3-8B) in a similar pattern to that in Cx43-HeLa cells. Cx31 staining was not as uniform compared to Cx43, but did reveal strong intracellular and possible PM localisation (Figure 3-8D). Consequently the fibrocytes did not express endogenous Cx26 or Cx30 in culture and so could not be used for trafficking experiments. Similar results were obtained with cultured rat fibrocytes (data not shown).

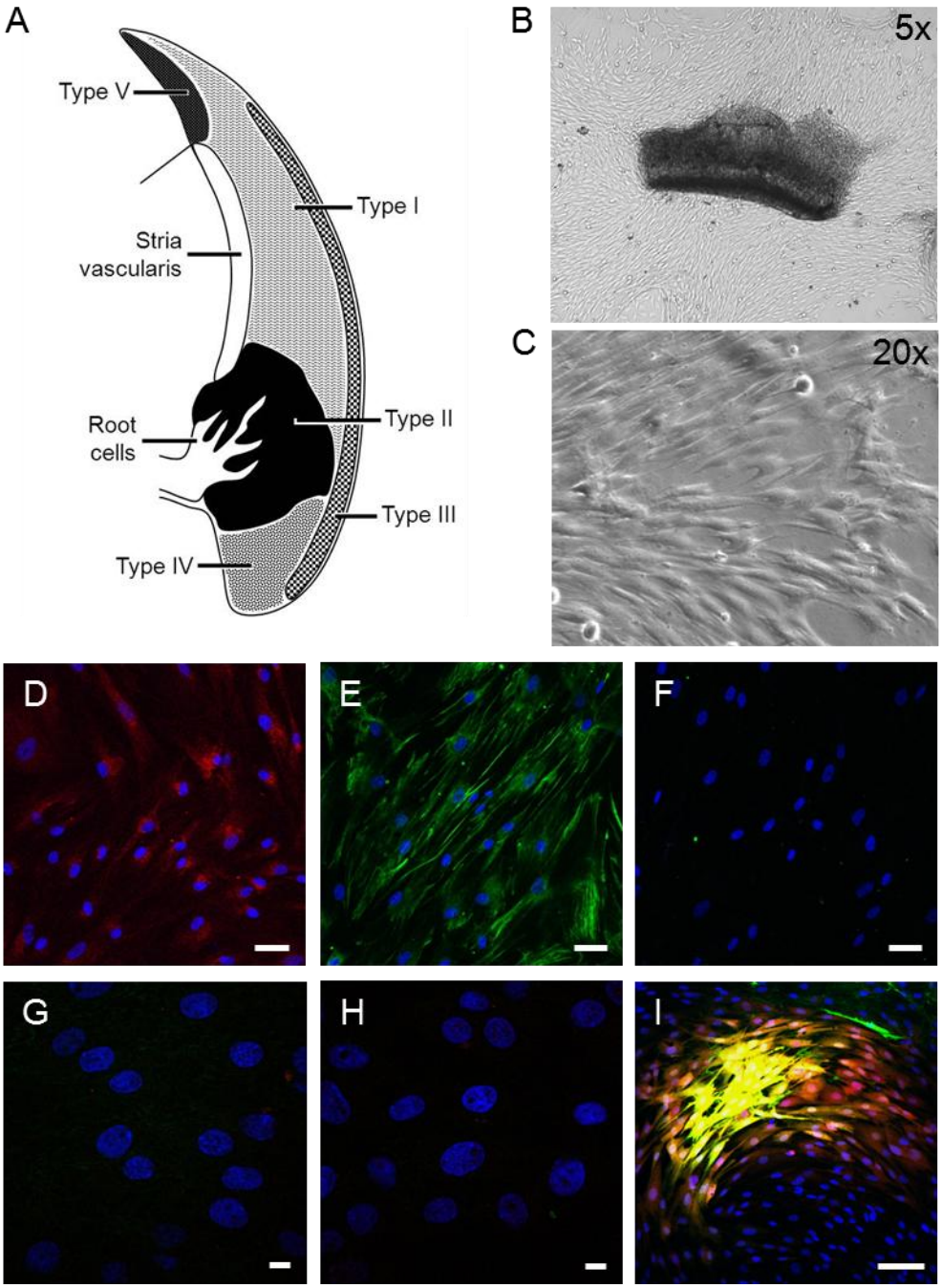

Figure 3-7. Cultured fibrocytes express type I markers, but not Cx26 or Cx30 *in vitro*.

(A) Lateral wall fibrocytes are classified into five subgroups according to their protein expression (see Table 1) and location. (B) Primary cell cultures were obtained from lateral wall dissections and (C) subcultured onto coverslips. Secondary cultures labelled for S-100 (D, red) and vimentin (E, green), but not Na^+-K^+-ATPase (F) indicating that these cells were most likely type I fibrocytes. Cx26 (G) and Cx30 (H) protein expression was absent, despite being ubiquitously expressed by type I fibrocytes *in vivo*. (I) Following a whole-cell patch clamp recording, NBN and Lucifer Yellow dyes were detected in numerous fibrocytes, suggesting the presence of gap junctions (NBN, red; LY green). Scale bars; D-F, 50 μm; G, H, 10 μm; I, 100 μm.

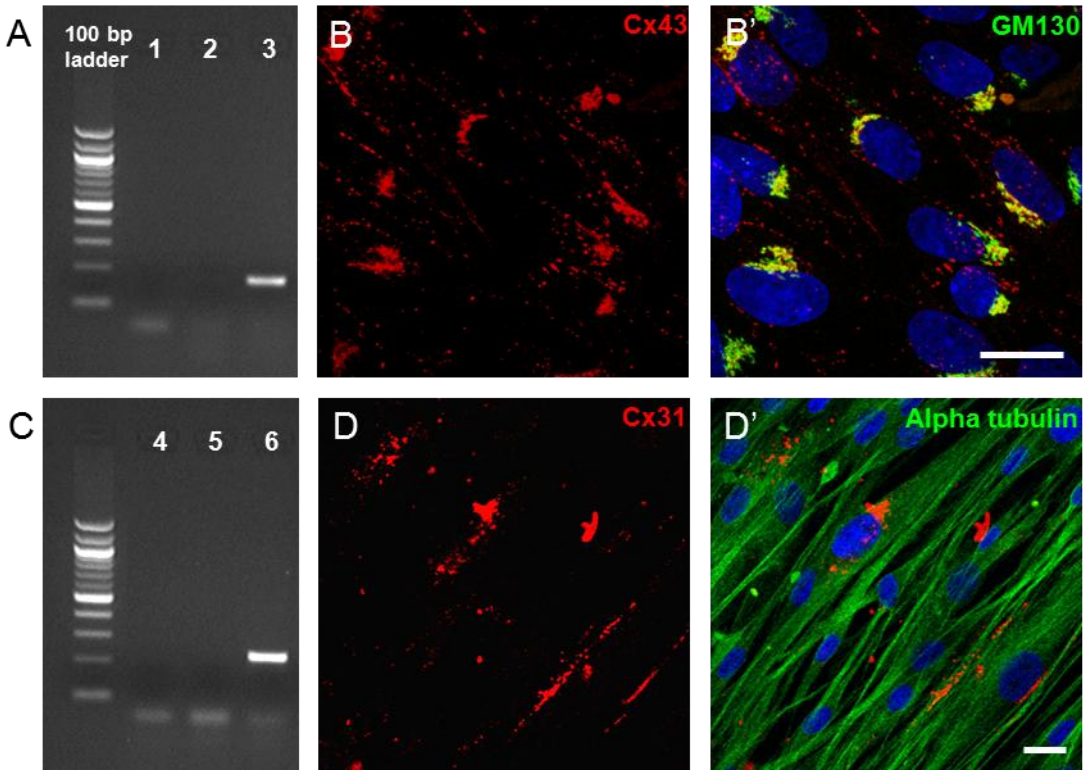

Figure 3-8. Cultured fibrocytes express Cx43 and Cx31.

(A) RT- PCR of cultured fibrocyte lysates revealed the presence of Cx43 (lane 3, 167 bp) and Cx31 (lane 6, 232 bp) mRNA. Lanes 1 + 4, water controls; lanes 2 + 5, no reverse transcriptase controls. (B) Cx43 expression (red) was confirmed by immunofluorescence labelling and was localised at cell-cell boundaries. (B') In addition, Cx43 strongly co-localised with the *cis*-Golgi marker, GM130. (D) Cx31 was detected by a polyclonal antibody raised against human Cx31 (from Prof. D. Kelsell). (D') Merged image, counterstained with alpha-tubulin. Cx31 was evident intracellulary and at cell-cell boundaries. Nuclei were counterstained with DAPI (blue). Scale bars 20 μm.

3.3 Discussion

Our understanding of the life-cycle of Cx26 and Cx30 proteins and gap junction regulation in the inner ear is lacking. This chapter has investigated the *in vitro* trafficking pathways of Cx26 and Cx30, with the future aim of understanding how and where these connexins oligomerise within the cell. Stably transfected Cx26-, Cx30- and Cx43-HeLa cells were immuno-stained to determine the intracellular localisation of connexins. BFA was used to disrupt the Golgi apparatus and thus block ER-to-Golgi transport and dye transfer studies were used to quantify the effect of BFA on gap junctional coupling. The results indicated a Golgi-dependent pathway for Cx26 and Cx43 transport to the PM, whereas Cx30 data suggested a Golgi-independent pathway. These data were unexpected since Cx26 and Cx30 form heteromeric connexons and so, were expected to follow similar pathways. These findings are discussed below. Attempts were also made to culture a cell line that would express native Cx26 and Cx30, and thus avoid possible issues with connexin overexpression.

3.3.1 Cx26 and Cx43 are trafficked via the Golgi apparatus

Proteins that travel along the conventional secretory pathway are transferred from the ER via ER exit sites to the *cis*-Golgi, through the Golgi stacks and then onwards to the PM via small vesicles that bud off from the *trans*-Golgi network (Rothman, 1994; Lee et al., 2004; Nakano and Luini, 2010). Trafficking of Cx43 is well-documented, and has been shown to transport through the Golgi apparatus, with oligomerisation occurring in the TGN before insertion into the PM (Musil and Goodenough, 1993; Koval et al., 1997). Considering the short half-life (1-2 hours) of Cx43 at the PM (Laird et al., 1991; Beardslee et al., 1998), it would seem likely that a continual production line of Cx43 protein, passing from the *cis*- to *trans*-Golgi compartments, is required to maintain gap junction formation. This was apparent in the immunofluorescence labelling shown in Figure 3-2. In addition, BFA treatment dispersed Cx43-labelling within the cytoplasm and caused a significant reduction in dye transfer. Consequently Cx43-HeLa cells were a useful model system for BFA sensitivity experiments, and results matched those of others (Musil and Goodenough, 1993; Laird et al., 1995; Martin et al., 2001a; Thomas et al., 2005).

As suggested elsewhere (Thomas et al., 2005), data presented here indicates that Cx26 trafficking depends on a functional Golgi apparatus. In comparison to Cx43, there was no direct overlap in expression (co-localisation) with the *cis*-Golgi marker GM130. There was also a lack of condensed intracellular accumulation, however small Cx26-positive granules were clearly visible and were concentrated around the *cis*-Golgi compartment. This localisation may represent Cx26-vesicle budding from early Golgi stacks before they reach the TGN. Budding and trafficking of vesicles to the PM before entering the TGN would represent a unique trafficking pathway for Cx26 and one that would require less time to reach the PM. These ideas are discussed in more detail below. In addition, since Cx26 labelling was only found in small granules, these regions may represent areas of Cx26 oligomerisation. The close proximity and clustering of connexins during this process may enhance the immunofluorescence signal and may explain why Cx26 fluorescence was not observed in the rest of the Golgi stack. However, it cannot be ruled out that differences in the intracellular localisation of connexins (i.e. Cx43 v Cx26) in these transfected cell lines may be due to differences in the amount of protein expression.

One explanation for the lack of direct co-localisation with the *cis*-Golgi marker GM130 could be that Cx26 spends less time within the Golgi or might not actually enter the late Golgi compartments (Figure 3-9). Diez et al. (1999) show in liver subcellular fractions that Cx26 is present in much lower amounts in the Golgi heavy fraction (compared to Cx32), but is present in the ER and ER-Golgi-intermediate compartment (ERGIC). The authors suggest that oligomerisation may occur in the ER or ERGIC (as in agreement with Falk et al., 1994) since these fractions contain monomeric and oligomeric configurations and that these have the potential to traffic to the PM via a pathway that does not implicate the Golgi apparatus. In contrast, the dye transfer experiments presented here showed that Cx26 trafficking was sensitive to BFA treatment, as in agreement with (Thomas et al., 2005), which suggests a reduction of Cx26 gap junction plaques at the PM. Cx26 immuno-labelling revealed small vesicles surrounding the *cis*-Golgi, which could represent regions of Cx26 oligomerisation before budding off and transporting to the PM. Alternatively, oligomerisation could occur within the ER/ERGIC compartment and then transfer to the *cis*-Golgi. From this point connexons could rapidly bud off from the stack, thus preventing a build-up of Cx26 in the Golgi apparatus (Figure 3-9). This observation can be supported by a study

by George et al. (George et al., 1999) which showed that Cx26 delivery to the PM occurred within 5 minutes. In contrast Cx43 (10 mins) and Cx32 (15 mins), which both traffic to the TGN, had slower rates of appearance at the PM. Therefore, Cx26 could be adapted to traffic via a pathway that is less time-limiting, which may involve budding from the classical secretory pathway before trafficking to the TGN. This hypothesis would fit with the data shown here since Cx26 immuno-labelling did not directly co-localise or accumulate with GM130-labelled compartments. In addition, Cx26 did not accumulate at a temperature that blocks TGN exit (19^{o}C), yet gap junctional communication was dependent on a functional Golgi apparatus as seen by its sensitivity to BFA.

The debate regarding the Cx26 trafficking pathway persists. The disparity between different studies could be due to various experimental conditions and systems used. For example, exogenous over-expression of connexins can induce changes in their trafficking and/or oligomerisation. A recent study by Van Slyke et al. (2009) found that Cx43, Cx32 and Cx26 subunit assembly into connexons can be influenced to take place in the ER of cells by strong over-expression. In contrast, the authors suggest that with endogenous levels of expression, oligomerisation occurs in the Golgi apparatus. Therefore, the number of over-expressed connexin 26 units in those studies that suggest Cx26 is BFA-insensitive, could have influenced the site of oligomerisation and their finding of direct trafficking to the PM from the ER (George et al., 1999; Martin et al., 2001a; Martin et al., 2001b).

Variations in protein trafficking can also be dependent on cell type (reviewed by Nickel and Rabouille, 2009). One example where this has been shown involves the cystic fibrosis trans-membrane conductance regulator (CFTR). CFTR has been shown to bypass the Golgi in a non-conventional pathway in both baby hamster kidney (BHK) and Chinese hamster ovary (CHO) cells (Yoo et al., 2002; Okiyoneda et al., 2004; Wang et al., 2004). However, the same results were not found in HeLa or 293T cells (Yoo et al., 2002). The authors note that CFTR transport from the ER is cell-type specific, which has also been shown by cAMP stimulating CFTR vesicle trafficking to the cell surface in some cell types, but not others. Consequently it is essential to note that *in vitro* experiments utilising genetic expression vectors may not replicate the *in*

vivo state. It would be advisable to repeat future experiments on other cell lines or use systems that express the protein/s of interest endogenously.

The results with Cx26 seen by Thomas et al. (2005) tend to agree with the results shown here, which suggest that Cx26 is sensitive to BFA and, therefore, passes through some component of the Golgi apparatus en route to the PM. Thomas et al. use normal rat kidney (NRK) and rat mammary BICRM1Rk tumour cells for their experiments, both of which express Cx43 endogenously. Expression of untagged and GFP/YFP-tagged Cx26 had almost identical results to Cx43 in both of these cells lines. Cx26 trafficking was disrupted upon treatment with BFA, and revealed results similar to those seen here, with noticeable Cx26 immuno-labelled vesicles surrounding the apparent *cis*-Golgi localisation. The influence of endogenous Cx43 on Cx26 should be minimal since Cx26 belongs to the β group of connexins and Cx43 to the α group. There is no evidence of co-assembly between connexins of different families – apart from point mutations that lead to a gain-of-function effect (Rouan et al., 2001). A separate study by Thomas et al. (2004) also suggests that Cx26 traffics all the way through the Golgi apparatus to the TGN. This is based on their finding that when cells transfected with Cx26-D66H (Golgi localised) were treated with BFA, a small compartment labelled by BODIPY did not retract into the ER. BODIPY is a dye used to label all parts of the Golgi network. The *cis*-Golgi, labelled with GM130, retracted into the ER system along with the Cx26-D66H contained in these compartments, leaving the remaining BODIPY structures (presumed TGN) co-labelled with Cx26-D66H intact. This would contradict the hypothesis that Cx26 buds off from the Golgi stacks before reaching the TGN. However, since this is a mutant protein which fails to leave the Golgi, the resultant accumulation could be expected to spread between all compartments.

Together, the data presented here points towards a Golgi-dependent trafficking pathway for Cx26 transport to the PM.

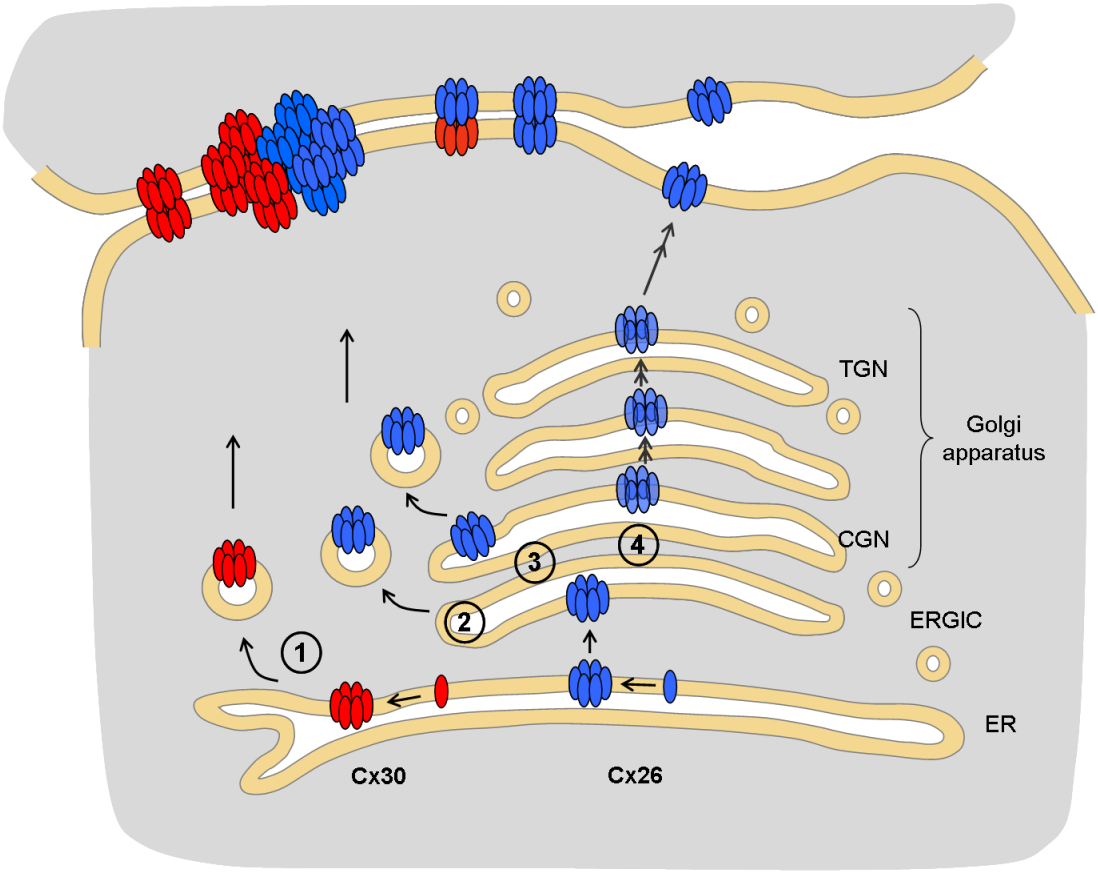

Figure 3-9. A preliminary summary of potential Cx26 and Cx30 trafficking pathways.

Based on the data shown here, and in combination with other studies, there are four likely candidates for Cx26 and Cx30 trafficking to the PM. 1) Evidence points towards a Golgi bypass route for Cx30 since there was no co-localisation with the *cis*-Golgi and BFA did not reduce GJIC. In addition, impermissible exit from the TGN at 19 ^{o}C did not result in Cx30 accumulation in the Golgi. 2) and 3) Cx26 transport to the ERGIC is dependent on COPII formation at the ER (Thomas et al., 2005). Cx26 is also highly sensitive to BFA, suggesting that it traffics through some part of the ERGIC/Golgi system. Since immuno-labelling revealed distinct Cx26 punctae surrounding the *cis*-Golgi and incubation at 19 ^{o}C did not induce intracellular accumulation, one could postulate that Cx26 buds off from the ERGIC or early Golgi compartments without passing through to the TGN. 4) Alternatively, Cx26 may traffic conventionally to the TGN; however, the lack of Cx26 accumulation at reduced temperature shifts suggests that this pathway is questionable (faded connexons).

3.3.2 Cx30 trafficking may bypass the Golgi apparatus

At the time of study, the trafficking pathway of Cx30 had not been examined previously. To elucidate whether Cx30 traffics through the Golgi apparatus HeLa cells stably expressing Cx30 were treated with BFA and processed for immunofluorescence-localisation or dye transfer as discussed above. Immuno-labelling initially revealed extensive gap junction-like plaques at cell-cell boundaries with very little discernible intracellular staining. There was no apparent localisation in Golgi structures, nor were there any Cx30-containing vesicles emanating from the Golgi stacks. However, when the detection levels were increased so that gap junctions were saturated, faint intracellular labelling became visible in some cells. The pattern of staining was unexpected since it did not show co-localisation with GM130 and was not vesiculated as seen with Cx26. Instead, the pattern appeared to follow a tubular, organelle-like labelling that was distinct from the *cis*-Golgi. This pattern of labelling could represent the ERGIC or ER compartments and could be tested by co-labelling with ER or ERGIC-specific markers. Upon BFA treatment, gap junctions persisted at the PM and some Cx30-labelled vesicles could be seen in the cell's cytoplasm. These vesicles did not co-localise with the vesiculated GM130-labelled Golgi membranes, and could represent endocytosed regions of the PM containing Cx30 gap junctions.

Cx30-HeLa dye transfer experiments revealed a stark difference in the extent of NBN transfer after BFA treatment, compared with Cx26 and Cx43. The number of cells containing NBN after 7 hours BFA did not change in comparison to untreated cells and actually showed a small (but insignificant) increase. This suggests that connexons were transported to the PM in a pathway that was unaffected by BFA treatment. This was somewhat unexpected since Cx26 and Cx30 have been shown to co-assemble into heteromeric connexons, which would suggest that the trafficking pathways follow similar routes.

During the course of this study, and in agreement with the results shown here, a publication by Qu et al. (2009) also showed that Cx30 gap junctions were insensitive to BFA treatment. The authors showed that the percentage of Cx30 gap junction-paired cells versus the total paired Cx30-expressing cells did not differ between control and BFA treated cells (5 μg/ml, 5 hours). In comparison, cells treated with cytochalasin B, a drug that disrupts actin filaments by blocking monomer addition at the fast-growing

end, caused a marked decrease in the percentage of gap junction-paired cells (from 70% to 10%). The observed insensitivity of Cx30 to BFA treatment supports the data shown here. In addition, cytochalasin B sensitivity suggests that actin filaments play a role in anchoring and stabilising Cx30 gap junctions at the PM. The authors also propose that a portion of Cx30 may traffic a short-distance directly from the ER to the PM in an actin-dependent manner (Figure 3-9). In addition, the presence of ER-plasma membrane "bridges" (Levine and Rabouille, 2005), may allow direct transportation of Cx30 connexons from the ER to the plasma membrane without passing through the Golgi apparatus (Qu et al., 2009).

3.3.3 Alternative explanations for Cx30 BFA-insensitivity

Cx30 turnover dynamics have not yet been studied. Even though most gap junctions have a half-life of 1.5-5 hours at the PM (Fallon and Goodenough, 1981; Traub et al., 1987; Laird et al., 1995; Darrow et al., 1995; Laing and Beyer, 1995; Beardslee et al., 1998), the possibility that Cx30 may have an unusually long half-life cannot be ruled out. If this is the case then trafficking of Cx30 may appear to be BFA-insensitive. A recent study has shown that pannexins (Panx) are insensitive to BFA, yet evidence also points towards a conventional trafficking route. Penuela et al. (2007) have shown that cell surface expression of Panx1 and Panx3 was unaffected by 6 hours of BFA (5 μg/ml) treatment, whereas Cx43 expression was lost from the PM with a concomitant increase in intracellular labelling. These data indicate that pannexins may be able to traffic to the membrane unconventionally. However, in the same study, treatment with cycloheximide (CHX), which is a potent inhibitor of protein synthesis, for up to 8 hours did not affect the amount of Panx1 protein, whereas Cx43 levels were decreased. If pannexins had a short half-life (like connexins) it would be expected that the protein level would decrease with time during CHX treatment. These data suggest that pannexins have distinct properties from Cx43 in that they have much slower turn-over kinetics and a longer half-life. An unusually long half-life at the PM could also explain why Cx30 was not affected by BFA treatment. CHX could be a useful tool for future experiments to determine the half-life of Cx30 protein at the PM in HeLa cells.

Alternatively, Cx30 may have the capacity to recycle via endosomal structures. Instead of internalised gap junctions being degraded, the vesicles may be transported to the endosome and then recycled back to the cell surface. Although this process has not

been shown for connexins, studies of other proteins have shown endosomal recycling (Maxfield and McGraw, 2004).

To verify these hypotheses, an ideal experiment would be to look at the turn-over rate and trafficking of Cx30 using live-cell fluorescence imaging. To do this, a fluorescently tagged connexin construct would be required and would need to be expressed in a cell line such as HeLa. Fluorescence recovery after photobleaching (FRAP) on a gap junction plaque could then be used to distinguish the rate of turnover of Cx30 homotypic gap junctions. Alternatively, a system implementing the bi-arsenical labelling of connexins would give a more accurate determination of half-life (Gaietta et al., 2002). This system would involve creating recombinant connexin proteins containing a tetracysteine (TC) motif (Cys-Cys-Pro-Gly-Cys-Cys) either at the C- or N-terminus. Visualisation of transient gap junction plaques during live cell imaging would be accomplished by incubating the cells in media containing a cell permeable, bi-arsenical reagent called FlAsH. Upon interaction with the TC motif, the fluorescein derivative emits green fluorescence, thus "lighting up" any connexin-TC proteins. Once FlAsH is bound, excess reagent can be washed off and changed for media containing a red-fluorescent bi-arsenical derivative called ReAsH. Any new connexin-TC proteins that form will then incorporate ReAsH. This process will enable the researcher to measure the time it takes for the green pre-existing gap junction plaque to be replaced by the red connexon units, thus giving a very accurate measurement of turn-over rates. BFA experiments could also be repeated using this system, allowing the researcher to disrupt the Golgi apparatus before tracking the transport of newly synthesised connexins. This will help to elucidate whether the extensive dye transfer seen in Cx30 HeLa cells during BFA treatment was a result of connexins that traffic via a Golgi-independent pathway, or whether Cx30 has a much longer half-life at the PM. If the latter is true, then Cx30 could function as a "stabilising" connexin. Some of the largest gap junction plaques in the mammalian system are found in cochlear regions where both Cx26 and Cx30 are co-expressed (Forge et al., 2003a). Thus, Cx30 could have a role in extending the life of cochlear gap junctions.

Either way, it appears that the functional properties of Cx30 are remarkably different in comparison to other connexin isoforms.

3.3.4 The on-going quest for endogenous Cx26/Cx30 expression

Most gap junction studies use cell lines devoid of connexin expression (e.g. HeLa cells), thus allowing the researcher to regulate specific connexin subtypes. This system is extremely useful for looking at protein dynamics and live-cell imaging, but exogenous over-expression may affect normal protein behaviour (as discussed in section 3.3.1). Consequently, *in vitro* trafficking results can vary quite significantly between different groups, as is the case with Cx26. To answer the questions of connexin trafficking one would ideally want to use cell lines that already express connexins endogenously. Unfortunately there are no known cell lines that express just Cx30 or both Cx26 and Cx30 endogenously, making these studies difficult. Keratinocytes were explored as a possible model, since these cells express both Cx26 and Cx30 and can be readily cultured. However, keratinocytes also express Cx30.3, Cx31, Cx31.1 and Cx43 (Di et al., 2001). The binding of these connexins may alter trafficking routes and would pose a problem for dye transfer experiments. Additionally, it has been noted that cultured keratinocytes have much lower expression of Cx26 and Cx30, making immuno-labelling difficult (personal communication, Dr. D. Becker, UCL). Another possible alternative presents in the form of cultured astrocyte cells, which express Cx26, Cx30 and Cx43 *in vivo*. Although some studies suggest the presence of Cx30 in cultured glial cells (Kunzelmann et al., 1999), others show that expression of Cx26 or Cx30 were almost undetectable (personal communication, Prof. B. Barres, Stanford). In addition the glial cultures that did express Cx30 were not uniform throughout - with measurements by Kunzelmann et al. (1999) suggesting up to only 15% of cells might express Cx30. This low expression number would pose problems for dye transfer experiments; therefore it was not viable to culture these cells.

Fibrocytes of the cochlear lateral wall were identified as a potential source for endogenous expression and were cultured according to Gratton et al. (1996). Cultures grew well and immunofluorescence labelling suggested that the cells resembled type I fibrocytes. These were expected to express both Cx26 and Cx30 since type I fibrocytes express both connexins *in vivo*. Disappointingly, immunostaining and RT-PCR revealed no expression of Cx26 or Cx30. Interestingly however, Cx43 and Cx31 mRNA were detected with RT-PCR. Immunostaining revealed distinct Cx43 and possible Cx31-labelled gap junctions. This finding is intriguing as it suggests that cultured fibrocytes

do not maintain the same profile *in vitro* as they do *in vivo*. It may suggest that cochlear fibrocytes undergo a de-differentiation step to a more primitive, fibroblast-like state when in culture. Alternatively the extra space or culture conditions might activate the expression of other connexins, whilst down-regulating both Cx26 and Cx30. Another explanation could be that a small sub-population of Cx43/Cx31 expressing fibrocytes was cultured. For example, type III fibrocytes express Cx43 (Forge et al., 2003a), and type II/IV fibrocytes express Cx31 (Xia et al., 2000; Forge et al., 2003a). Consequently, cultured fibrocytes, although interesting for their apparent "switch" in connexin expression, were not useful for Cx26/Cx30 trafficking studies.

Much of the work was spent trying to find and produce a cell line that expressed both Cx26 and Cx30 endogenously to address the issues noted. From the cell lines researched and cell lines created here, it would appear that Cx26 and Cx30 are down-regulated in dividing, cultured cells, as is the case with keratinocytes and astrocytes. There are some cell lines that either express or can be induced to express Cx26 in culture. These include rat liver hepatocytes and a porcine kidney epithelial cell line (LLC-PK1-CL-4). In primary hepatocyte cell cultures Cx26 expression is reduced. However, addition of S-Adenosylmethionine (Yamaji et al., 2010) or glucagon (Kojima et al., 1995) to the culture media can induce both Cx26 mRNA and protein expression. On the contrary, both authors point out that PM localisation and GJIC is not increased after these treatments, leading to the question of whether these Cx26 subunits are functional? The study by Kojima et al. (1995) showed an apparent increase in Cx26-containing gap junction plaques, so it may be possible to use these cells to study endogenous Cx26 trafficking pathways. However, the co-expression of Cx32 in these cells may affect intracellular transport and dye transfer studies. Alternatively the LLC-PK1-CL-4 cell line has been shown to express Cx26 mRNA (D'Souza et al., 2008), but to date, no journal publication has shown functional Cx26 gap junctional coupling in these cells. These cell types may provide some options for studying endogenous Cx26 trafficking in the future. To my knowledge, there are no cultured cell lines that express Cx30 endogenously, at least to a level required for these experiments.

3.4 Conclusion

The divergence of trafficking pathways could be an evolutionary mechanism designed to prevent certain proteins inter-mixing or a process that allows differential trafficking routes and turn-over rates for proteins in particular cell types. The work outlined in this chapter seems to point towards separate trafficking pathways for Cx26 (Golgi-dependent) and Cx30 (Golgi-independent). However, due to the issues and problems noted with *in vitro* techniques these results need to be clarified. If these findings prove to be correct, it raises an interesting question as to where in the cell these connexins oligomerise into heteromeric connexons. It is possible that in separate expression systems homomeric connexons have distinct trafficking properties. Upon inter-mixing, Cx26 or Cx30 might have the potential to over-ride a certain trafficking pathway dependent upon the hexameric conformation and/or ratios of Cx26 to Cx30. If these were true, it would reveal a unique and novel way of regulating many properties of the gap junction life cycle, including: turn-over rate, homomeric/heterotypic/ heteromeric gap junction configurations and regulation of intermixing between different connexin subtypes. Various mutations in Cx26 and Cx30 cause syndromic or non-syndromic deafness. Changes in trafficking, heteromeric ratios and intermixing as caused by mutation may explain why some cases of deafness are non-syndromic whereas others associate with syndromic phenotypes i.e. skin disease.

4 DEVELOPMENT OF GAP JUNCTIONAL INTERCELLULAR COMMUNICATION WITHIN THE LATERAL WALL OF THE RAT COCHLEA

4.1 Introduction

Functional gap junctions are vital for cochlea function. The previous chapter highlighted the possibility that altered trafficking pathways could help regulate connexin-intermixing. This effect, and those of mutations, could have consequences on gap junctional intercellular communication (GJIC) in both the epithelial and connective tissue gap junction networks of the cochlea. It has already been shown that the physiological properties of Cx26/Cx30 gap junctions vary depending on their connexin composition. In heterologous expression systems, dyes of varying charge and size, such as NBN (NBN) (charge, +1; MW, 287 Da) and Lucifer yellow (LY) (charge, -2; MW, 443 Da), have been used to investigate the permeabilities of gap junctions composed of Cx26 alone, Cx30 alone or Cx26 and Cx30 (Manthey et al., 2001; Marziano et al., 2003). Cx26 homotypic gap junctions are permeable to both LY and NBN, whereas Cx30 homotypic gap junctions are permeable to NBN, but not LY. Similarly, Cx26/Cx30 heteromeric gap junctions permit NBN transfer, but are impermeable to LY. Utilising slices of the rat cochlea, similar techniques have identified areas of compartmentalised gap junctional coupling between cells of the epithelial gap junction system (Jagger and Forge, 2006). In the hearing cochlea, these compartments are separated into medial and lateral GJIC pathways between supporting cells surrounding inner and outer hair cells, respectively. These pathways are formed progressively through postnatal development and are likely to be involved in buffering or cycling excess K^+ away from the vicinity of hair cells. Importantly, changes in gap junction selectivity and conductance during postnatal development correspond to changes in Cx26/Cx30 protein expression and gap junction plaque distribution.

4.1.1 Cochlear fluid compartments

The mammalian cochlea is composed of three tube-like structures; the scala tympani, scala media and scala vestibuli (see Image deleted due to copyright.

Figure 4-1), each of which are filled with extracellular fluid. The scala tympani and scala vestibuli are filled with perilymph, and scala media with an unusual fluid termed endolymph. The mechano-sensitive hair cells in the organ of Corti epithelium are bathed in both of these extracellular fluids; endolymph at the apical surface and perilymph surrounding the baso-lateral surface.

Endolymph is a unique extracellular fluid found only in the inner ear. K^+ represents the main cation, with an unusually high concentration of ~150 mM, whereas Na^+ (~1-2 mM) and Ca^{2+} (~20 μM) in comparison are unusually low in concentration. In contrast, perilymph has an ionic balance that resembles most other extracellular fluids in the body, such as plasma and cerebrospinal fluid. This fluid fills the scala tympani and vestibuli compartments and any other extracellular space (excluding the intrastrial space). Na^+ represents the main cation in perilymph, with a concentration of ~145 mM, $[Ca^{2+}]$ is also elevated (0.6-1.3 mM), whereas $[K^+]$ is significantly lower (4-6 mM) in comparison to endolymph (reviewed by Wangemann and Schacht, 1996; Wangemann, 2006). The intrastrial space represents a third extracellular fluid within the cochlea and fills the small extracellular spaces between basal, intermediate and marginal cells of the stria vascularis. This tightly packed compartment has a very low $[K^+]$ (1-2 mM), and slightly lowered $[Na^+]$ (~85 mM) in comparison to endolymph and perilymph respectively (Salt et al., 1987).

Auditory transduction depends on the flow of K^+ from endolymph into hair cells via mechano-sensory transducer channels located within hair cell stereocilia. Thus, the cochlear partition between endolymph and perilymph is essential for sensory transduction. Leakage of perilymph into endolymph, and vice versa, disrupts normal K^+ homeostasis and results in hair cell death (Nakano et al., 2009).

4.1.2 The endocochlear potential

Other than differences in ion composition, endolymph differs from perilymph in that it generates a very large, positive extracellular potential of around +80-100 mV, in respect to perilymph. This positive potential, termed the endocochlear potential (EP), was first measured by Georg von Békésy (von Békésy, 1952). The EP, along with the high endolymphatic [K^+], increases the driving force for K^+ entry into hair cells upon mechanical deflection of hair bundles (reviewed by Dallos, 1978). The ionic composition of endolymph and development of the EP have been shown to arise independently and in succession during cochlear maturation. Before the onset of hearing in rats (usually around postnatal day 12, P12), EP has been measured below +20 mV (Bosher and Warren, 1971; Rybak et al., 1992). Around P10-P12 there is a rapid upswing of the measured value of EP, which increases to a mature level of around +80-90 mV by P16. Importantly, the ionic composition of endolymph within scala media is established earlier in development. The [K^+] and [Na^+] reach near mature levels by P7 (Bosher and Warren, 1971). Comparable development has been observed for the mouse cochlea (Yamasaki et al., 2000).

The source of the EP generating machinery was identified as the stria vascularis in 1959 (Tasaki and Spyropoulos, 1959). It comprises of a tripartite structure of mesenchyme-derived basal cells, neural crest-derived intermediate cells (melanocytes) and epithelial marginal cells (Forge and Wright, 2002). Studies have since found a plethora of ion channels, transporters and junctional proteins within both the stria vascularis and spiral ligament that are important for maintaining both EP and high endolymphatic [K^+] (Wangemann, 2006; Zdebik et al., 2009; Hibino et al., 2010).

The potassium channel $K_{ir}4.1$ and tight junction proteins between apical surfaces of basal cells and marginal cells are two components that are essential for EP generation. The inwardly-rectifying $K_{ir}4.1$ channel was first detected in stria vascularis tissue by Hibino and colleagues (Hibino et al., 1997) and was thought to localise to epithelial marginal cells. However, the correct localisation to intermediate cells was later discovered by Ando and Takeuchi (Ando and Takeuchi, 1999), who suggested a role for $K_{ir}4.1$ in K^+ secretion into the intrastrial space. Knock-out of $K_{ir}4.1$ (Marcus et al., 2002) or treatment with Ba^{2+} (Marcus et al., 1985; Nin et al., 2008) - a reversible K_{ir} channel blocker - both abolish the EP and reduce endolymphatic [K^+]. Incidentally, the

expression profile of $K_{ir}4.1$ within intermediate cells coincides with development of EP from postnatal day 8 onwards (Hibino et al., 1997). These data taken together confirm an essential role for $K_{ir}4.1$ channels in production of the EP and suggest that the potential is formed across the intermediate cell membrane.

Tight junctions between basal cells have also been shown to correlate temporally with the period of onset and rise of EP (Souter and Forge, 1998). Claudin-11 is the only tight junction protein detected in basal cells, and mice with a deletion of this gene do not develop an EP (Gow et al., 2004; Kitajiri et al., 2004). This finding confirms the importance of sealing between basal cells and electrical isolation of the intrastrial compartment from perilymph. Consequently, the intrastrial space can generate a potential of ~+90-100 mV in respect to perilymph, termed the intrastrial potential.

4.1.3 K^+ recycling pathway

To maintain the EP and high endolymphatic [K^+] and to prevent pathological build-up of K^+ ions around hair cells, it has been postulated that supporting cells spiral ligament fibrocytes play a role in recycling extracellular K^+ away from the of Corti to the stria vascularis (Weber et al., 2001; Wangemann, 2006). The proposal for K^+ circulation arose from observations that radioactive K^+ was more readily detected in endolymph after application to perilymph rather than blood (Konishi et al., 1978; Sterkers et al., 1982). In addition, perilymphatic, but not perfusion of K^+-free solution severely suppressed the EP (Wada et al., 1979; al., 1981). The authors therefore suggest that the source of K^+ is more likely to from perilymph via a recirculation pathway, rather than from the vasculature. proposed pathway consists of gap junction coupled supporting cells within the gap junction network and connective tissue gap junction network (Kikuchi et al., The expression of certain ion transporters within these networks adds further for a trans-cellular K^+ pathway (see Image deleted due to copyright.

Figure 4-1).

The proposed mechanism for K^+ cycling has been described in detail elsewhere (Kikuchi et al., 2000; Wangemann, 2006; Hibino and Kurachi, 2006; Mistrik and Ashmore, 2009; Zdebik et al., 2009; Hibino et al., 2010), but is described only briefly here. The general consensus for K^+ cycling supports the following model: 1) K^+ from endolymph enters hair cells through the stereocilia MET channel in response to sound stimulation. Excess K^+ is extruded into the extracellular space (sometimes referred to as cortilymph) from hair cells most likely via KCNQ4 (Kharkovets et al., 2006) and Ca^{2+}-activated BK channels located in their basolateral membrane. 2) Supporting Deiters' cells immediately siphon extracellular K^+ to prevent hair cell depolarisation and toxic K^+ accumulation. This process likely occurs through K^+,Cl^- co-transporters (Kcc3 and Kcc4, Boettger et al., 2002; Boettger et al., 2003) and inwardly rectifying $K_{ir}4.1$ channels. 3) K^+ diffuses between supporting cells through the Cx26/Cx30 epithelial gap junction system towards outer sulcus cells. Root cell processes then release K^+ into the perilymphatic space of the spiral ligament most likely via $K_{ir}4.1$ channels (Jagger et al., 2010). 4) Type II fibrocytes that surround root cell processes absorb K^+ from the extracellular space through two K^+-uptake apparatuses; Na^+,K^+-ATPase and Na^+,K^+-$2Cl^-$ co-transporter (NKCC1). Expression of $K_{ir}5.1$ in these cells is thought to negatively regulate cochlear circulation and prevent its overshoot (Hibino et al., 2004). K^+ then passes through the connective tissue gap junction network towards stria vascularis. 5) $K_{ir}4.1$ channels in intermediate cells continuously secrete K^+ down its electrochemical gradient into the intrastrial space, which is then absorbed through Na^+,K^+-ATPase and NKCC1 at the basolateral membranes of marginal cells. This process maintains a low [K^+] in the fluid of the intrastrial space and thus facilitates K^+ diffusion through $K_{ir}4.1$ channels. The intrastrial potential has been recorded at +90-100 mV in respect to perilymph (Salt et al., 1987), which then decreases by ~10 mV across the apical membrane of marginal cells, resulting in a potential of +80-90 mV in endolymph (Prazma, 1975; Melichar and Syka, 1987). K^+ absorbed by marginal cells is finally secreted back into endolymph via K_v channels composed of KCNQ1 and KCNE1 subunits, thus completing the K^+ cycle.

Image deleted due to copyright.

Figure 4-1. Illustration demonstrating the potassium circulation model and formation of endocochlear potential.

(A) K+ is taken up by cochlear hair cells upon deflection of stereocilia and then extruded into "cortilymph". Deiters' cells absorb excess K+ and transfer it through the epithelial gap junction network to outer sulcus/root cells. K+ is extruded and taken up by spiral ligament fibrocytes and transferred to the stria vascularis through gap junction channels (see detail in B). (B) K+ and Na+ transporters (Na^+,K^+-ATPase and NKCC1) absorb excess K+ in extracellular space surrounding root cell processes (outer sulcus cells). GJIC (purple channels) permits movement of K+ towards basal cells and penultimately into intermediate cells. From here, Kir4.1 channels release K+ into the intrastrial space. Ion transporters (Na^+,K^+-ATPase and NKCC1) located in the basolateral membranes of marginal cells siphon excess K+. KCNQ1/KCNE1 channels secrete K+ back into the endolymph. Electrical isolation of the stria vascularis from perilymph and endolymph, thus permitting high endocochlear and intrastrial potentials, is maintained by tight junctions (TJ) between marginal cells and between basal cells. Image reproduced from Hibino and Kurachi, 2006.

The connective tissue gap junction network is composed of spiral ligament fibrocytes, and basal and intermediate cells of the stria vascularis. All these cells are inter-connected via gap junction plaques, which are constructed mostly from Cx26 and/or Cx30 subunits (Ahmad et al., 2003; Forge et al., 2003a; Forge et al., 2003b; Sun et al., 2005; Jagger and Forge, 2006; Nickel et al., 2009). Mutations within the genes for Cx26 (*GJB2*) and Cx30 (*GJB6*) cause inherited hearing loss in humans (Kelsell et al., 1997; Kelsell et al., 2001; Nickel and Forge, 2008), thus it appears likely that deficits in GJIC within the connective tissue gap junction network may contribute to this impairment. In addition, fibrocyte degeneration is a cause of one form of hereditary deafness (DFN3) (Minowa et al., 1999) and is a major cause of presbyacusis and loss of EP (Hequembourg and Liberman, 2001; Wu and Marcus, 2003). Consequently, fibrocytes are essential for cochlear homeostasis and normal hearing (Furness et al., 2009).

4.1.4 Cochlear slice preparation

Slices of the viable cochlea represent a unique way of identifying and recording changes in cochlea tissue during postnatal development. Cross sections through the modiolus provide access to cells in the lateral wall for patch clamping and dye experiments. This technique was originally developed in the neonatal rat (postnatal 4-14) and was successfully used to record from a variety of cochlear cells (Jagger et 2000). It has since been used for numerous studies investigating properties of supporting cells in the organ of Corti (Jagger and Forge, 2006), fibrocytes of the ligament and limbus (Furness et al., 2009) and root cells (Jagger et al., 2010). The advantage of using the cochlear slice technique over other preparations is that cell morphology and structure can be readily distinguished using infrared video-
(Image deleted due to copyright.

Figure 4-2). The technique also permits live cell imaging of intracellular fluorescent dye injections.

The rat cochlea undergoes extensive morphological development between birth and hearing onset (around P12). At P0, cochlear landmarks such as hair cells and supporting cells in the sensory epithelium, adjacent Kölliker's organ and overlying tectorial membrane were all clearly distinguishable (Image deleted due to copyright.

Figure 4-2A). Within the lateral wall, marginal cells formed an epithelial layer at the lumenal border facing scala media. At this young age, other cell-types in the posterior region of the lateral wall were hard to identify. Cells immediately abutting the marginal cell epithelium originate from the mesenchyme, and appeared rounded and tightly packed together (Image deleted due to copyright.

Figure 4-2B). This region is henceforth referred to as the "condensing mesenchyme" up until ~P5-P7, when characteristic fibrocyte morphologies appear.

Around the onset of hearing, cochlear tissues have fully matured; Kölliker's organ organ has receded, the spaces within the organ of Corti have opened and stria is clearly identifiable (Image deleted due to copyright.

Figure 4-2C). Lateral wall type I fibrocytes are clearly distinguishable from the stria vascularis, of which, three separate layers have formed, surrounding a network of fine capillaries (Image deleted due to copyright.

Figure 4-2D). Between the fibrocytes, numerous dense fibrillar strands were apparent, running parallel to stria vascularis (Spicer and Schulte, 1996).

Image deleted due to copyright.

Figure 4-2. Postnatal development of cochlear tissues.

(A) Differential interference contrast (DIC) photomicrograph of a mid-turn of a fixed vibratome slice cut from the cochlea of a P0 rat. Various tissues and structures are highlighted: spiral limbus (lim), Reissner's membrane (rm), Kölliker's organ (Ko), scala media (sm), lateral wall (lw), and otic capsule (oc). Hair cells and surrounding supporting cells were evident in the sensory epithelium (arrow). (B) Detail of the lateral wall at P0. A single layer of marginal cells (mc) are clearly distinguishable lining the lumenal border. Posterior to the marginal cells are a mass of mesenchyme derived cells which do not have a clearly definable morphology. This region is termed the "condensing mesenchyme". (C) DIC mid-turn of a P15 rat cochlea. Kölliker's organ had retracted, spaces within the organ of Corti had opened and the stria vascularis (sv) was visible. The approximate locations of fibrocyte subtype (fc1-fc5) are labelled. (D) Detail of the lateral wall at P15. Marginal cells, intermediate cells (ic) and basal cells (bc) of the stria vascularis were identified. Posterior to the basal cell layer, type I fibrocytes were distinguishable within the spiral ligament. Numerous, dense fibrillar strands running parallel to stria vascularis were apparent between fibrocytes. Scale bars, 20 µm. Image from Kelly et al., 2011.

4.1.5 Functional GJIC between fibrocytes and basal/intermediate cells

This chapter investigates the development of GJIC in the connective tissue gap junction system of the lateral wall during postnatal development, using immunofluorescence, dye injection and whole-cell patch clamp recordings. The majority of the data presented here has been published in the journal *Neuroscience* (Kelly et al., 2011). The data described in this sub-section (4.1.5 and Figure 4-3) was acquired by D. Jagger before the start of this project.

GJIC, as determined by neurobiotin (NBN) injection, was evident throughout the connective tissue gap junction network by post-natal day 7 (Figure 4-3A), suggesting a continuous syncytium throughout the lateral wall. NBN injected into type V fibrocytes was detected in distant regions such as in the cells lining the scala vestibuli (Figure 4-3B). NBN injected into type I fibrocytes was detected throughout the lateral wall and within intermediate cells counter-stained for $K_{ir}4.1$ (Figure 4-3C-D). Dye transfer to marginal cells was not detected in any of these experiments, confirming the absence of gap junctions in these cells (Forge et al., 2003a). These data reveal that GJIC matures in advance of hearing onset in rats (~P12). Therefore, a detailed examination of GJIC during earlier stages of development (before maturity) was carried out.

Image deleted due to copyright.

Figure 4-3. GJIC between lateral wall fibrocytes and stria vascularis.

(A-D) Dye transfer carried out in P7-P8 cochlear slice preparations. (A) NBN (red) injection into a type I fibrocyte cell in a basal turn region of a P7 cochlear slice. Dye was detected in almost all fibrocyte types within the lateral wall. (B) In a P8 apical turn slice, NBN injected into a type V fibrocyte could be detected in cells lining the scala vestibuli. (C) In a P10 slice, NBN injected into a type I fibrocyte was detected throughout the lateral wall syncytium and within intermediate cells (labelled for K_{ir}4.1; green). (Di-iii) In a separate experiment, NBN injected into a type I fibrocyte was detected in many other type I cells (fc1). K_{ir} 4.1 labelling of intermediate cells is shown again (green). The overlay of both images revealed NBN in strial basal cells (bc) and intermediate cells (ic). Scale bars, 20 μm. Image from Kelly et al., 2011.

4.2 Results

4.2.1 Development of gap junction plaques within the cochlear lateral wall

Gap junction plaques were detected using antibodies specific for Cx26 (GAP28H) and Cx30. This immuno-labelling was important to demonstrate the development of gap junctional intercellular communication (GJIC) during postnatal cochlear development. The following subsections then display dye transfer studies to show that these cells are functionally connected by gap junction channels.

Cx26 and Cx30 are the two predominant connexin isotypes expressed in the adult cochlea. Other studies have investigated co-localisation of these connexins during cochlear development (Lautermann et al., 1998; Lautermann et al., 1999; Ahmad et al., 2003; Forge et al., 2003a; Sun et al., 2005) and so are not described in detail here. The developmental expression of Cx30 (Figure 4-4A-D) and Cx26 (Figure 4-4Ai-Di) from post-natal day 0 (P0) to P12 was detected in rat cochlear slices using polyclonal anti-Cx30 and polyclonal GAP28H anti-Cx26 antibodies.

In the P0 cochlea (Figure 4-4A, Ai), Cx26 and Cx30 gap junction plaques were most prominent in Kölliker's organ. These cells are dye-coupled extensively at this age (Jagger and Forge, 2006). Smaller puncta were present in the spiral limbus and apical regions of Claudius and outer sulcus cells. Within the lateral wall, small puncta were visible in the suprastrial region (arrow head), close to where Reissner's membrane attaches to the lateral wall and within the condensing mesenchyme lateral to marginal cells. By P4, expression of both Cx26 and Cx30 was up-regulated in the condensing mesenchyme and also between cells within the stria vascularis (Figure 4-4B, Bi). The extent of Cx26 and Cx30 immunofluorescence was increased further by P8 (Figure 4-4C, Ci). Numerous gap junction plaques were detected between spiral limbus fibrocytes and between supporting cells extending to the outer sulcus. There was a marked increase in labelling for both Cx26 and Cx30 in the region around the developing basal cell layer of the stria vascularis, with smaller puncta scattered throughout the lateral wall. By P12 (corresponding to the onset of hearing in rats), both connexins were detected throughout the spiral ligament (Figure 4-4D, Di). Large and numerous gap junction plaques were present between type I, II and V fibrocytes and smaller plaques in the region where basal and intermediate cells of the stria vascularis

reside. These events reveal the progressive nature of connexin expression through postnatal development and compare closely to that discovered in the murine cochlea (Sun et al., 2005).

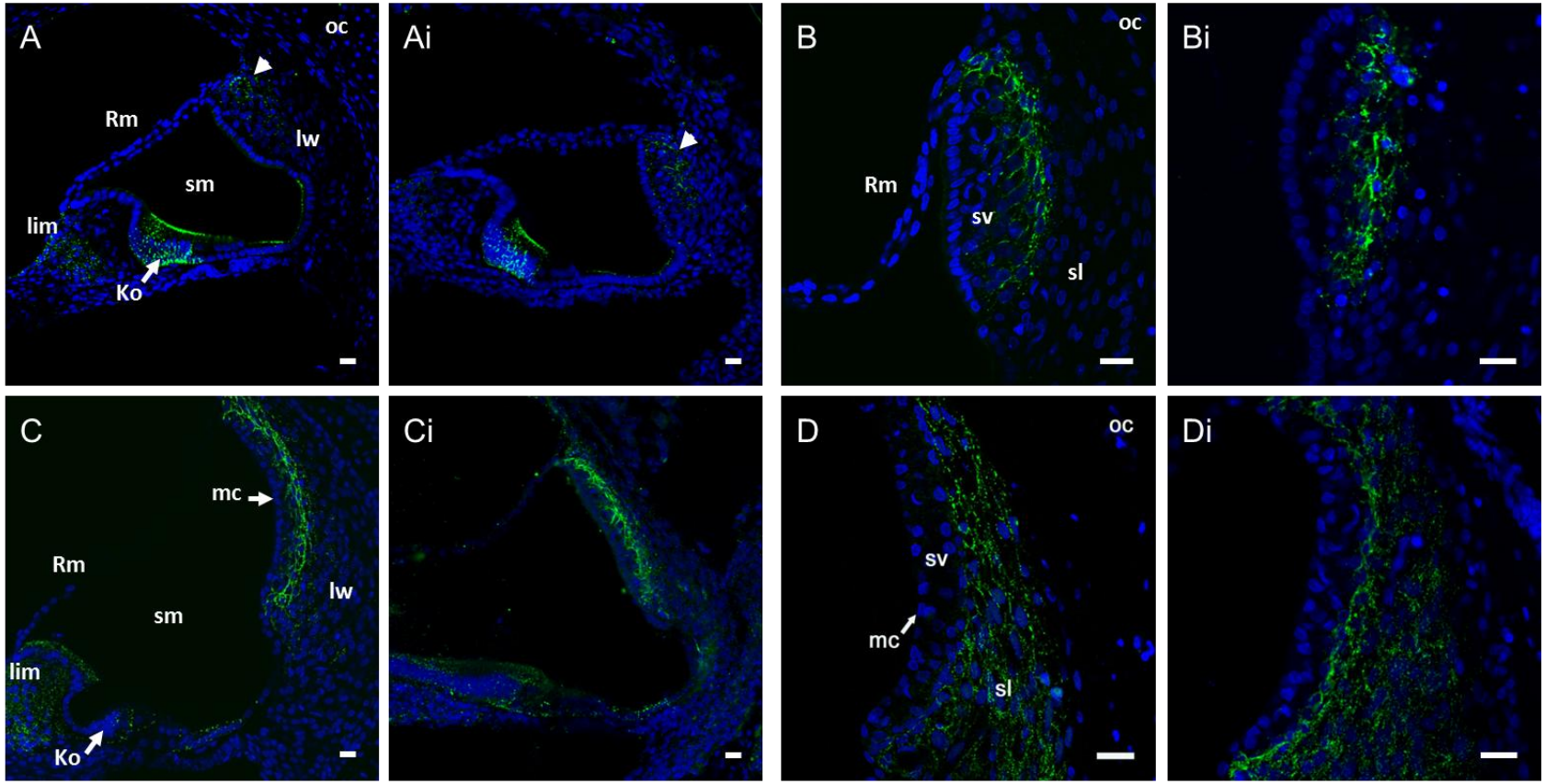

Figure 4-4. Postnatal development of gap junction plaques in lateral wall tissue of the rat cochlea.

(A-D) Cochlear slices stained for Cx30 (green). (Ai-Di) Cochlear slices stained for Cx26. Nuclei were counter-stained with DAPI (blue). (A, Ai) A P0 basal turn slice. Several tissues and structures are labelled: spiral limbus (lim), Reissner's membrane (Rm), Kölliker's organ (Ko), scala media (sm), lateral wall (lw) and otic capsule (oc). Gap junction plaques were present in Kölliker's organ, with smaller and sparser puncta in the superior region of the lateral wall (arrow head) and spiral limbus. (B, Bi) A magnified view of the lateral wall in a P4 slice. Gap junctions were present within the condensing mesenchyme adjacent to the developing stria vascularis (sv). Few puncta were seen elsewhere in the spiral ligament (sl). (C, Ci) Basal turns of a P8 cochlear slice show an increase in both Cx30 and Cx26 expression in the spiral limbus, sensory epithelium and lateral wall. Sparse puncta were visible in the inferior region of the spiral ligament. (D, Di) Detail of the lateral wall in the P12 cochlea. Fibrocytes throughout the spiral ligament were labelled for both connexins. Scale bars, 20 µm.

4.2.2 Functional GJIC in the early postnatal cochlear lateral wall (P2)

GJIC communication in the supporting cell region of the organ of Corti has been investigated previously using the whole cell patch clamp technique (Forge et al., 2003b; Jagger and Forge, 2006). This method is useful for dye transfer studies (as described in the preceding chapter) and simultaneous electrophysiological recordings. These techniques were used here to functionally determine the pattern and extent of GJIC during early postnatal lateral wall development.

The pattern of dye transfer in P2 live cochlear slice preparations varied depending on the location of the injected cell in the lateral wall. Cells within the condensing mesenchyme were clearly defined using infra-red DIC video-microscopy and could be distinguished from the marginal cells (Figure 4-5A). NBN injected into a single cell within this region passed to many cells in all directions, but was confined to a distinct, crescent-shaped zone (Figure 4-5B-D; n=8 injections). All cells within this zone were labelled for Cx30 (excluding marginal cells), indicating the presence of gap junction plaques. In agreement with the absence of gap junction plaques between marginal cells, NBN did not spread into the epithelial layer, thus confirming the absence of GJIC between these cells and mesenchymal cells. Simultaneous whole-cell current responses to 10 mV hyperpolarising steps (Figure 4-5Ci-Di) measured a very low input resistance, consistent with functional GJIC (Jagger and Forge, 2006). The pattern of dye spread was consistent between apical (Figure 4-5A-C) and basal (Figure 4-5D) turns.

Single cell recordings were then performed in the superior and inferior regions of the lateral wall outside of the main condensing mesenchyme zone where Cx30 immunofluorescence was restricted to small, sparse intercellular puncta. Immature cells within the superior region, located near to the attachment point of Reissner's membrane could be distinguished (Figure 4-6A). Live cell video-microscopy revealed a distinct column of Lucifer yellow transfer in a direction inferior to the patched cell and posterior to the condensing mesenchyme (Figure 4-6B). After processing the slice for immunofluorescent labelling, NBN had spread to a greater number of cells, but was still confined in a distinct columnar pattern (Figure 4-6C). Dye did not pass laterally to cells within the condensing mesenchyme. The input resistance (Figure 4-6D) was similar in comparison to recordings from cells within the condensing mesenchyme.

Cells injected in the developing type II fibrocyte region, inferior to the condensing mesenchyme, also revealed dye coupling in characteristic columns of 10-30 spindle-shaped cells (Figure 4-7A,D; *n*=9 injections). These columns were located parallel to the rear border of the condensing mesenchyme and towards the root cell processes adjacent to the outer sulcus. A more detailed image including fluorescein-dextran revealed characteristic spindle-shaped morphologies (Figure 4-7B,E). Processes extended from the polar ends and wrapped around cells above and below the injected cell. As a consequence, NBN spread between cells in a columnar direction and was not readily detected within the condensing mesenchyme. The input resistances measured from the two cells (asterisks) recorded in separate slices (Figure 4-7C, F) indicated a similar extent of GJIC in comparison to cells in the condensing mesenchyme. In five recordings at P2, there was a higher input resistance (50-500 MΩ) and a low membrane capacitance (3-20 pF), consistent with an absence of GJIC. After these recordings NBN was detected in single, spindle-shaped cells.

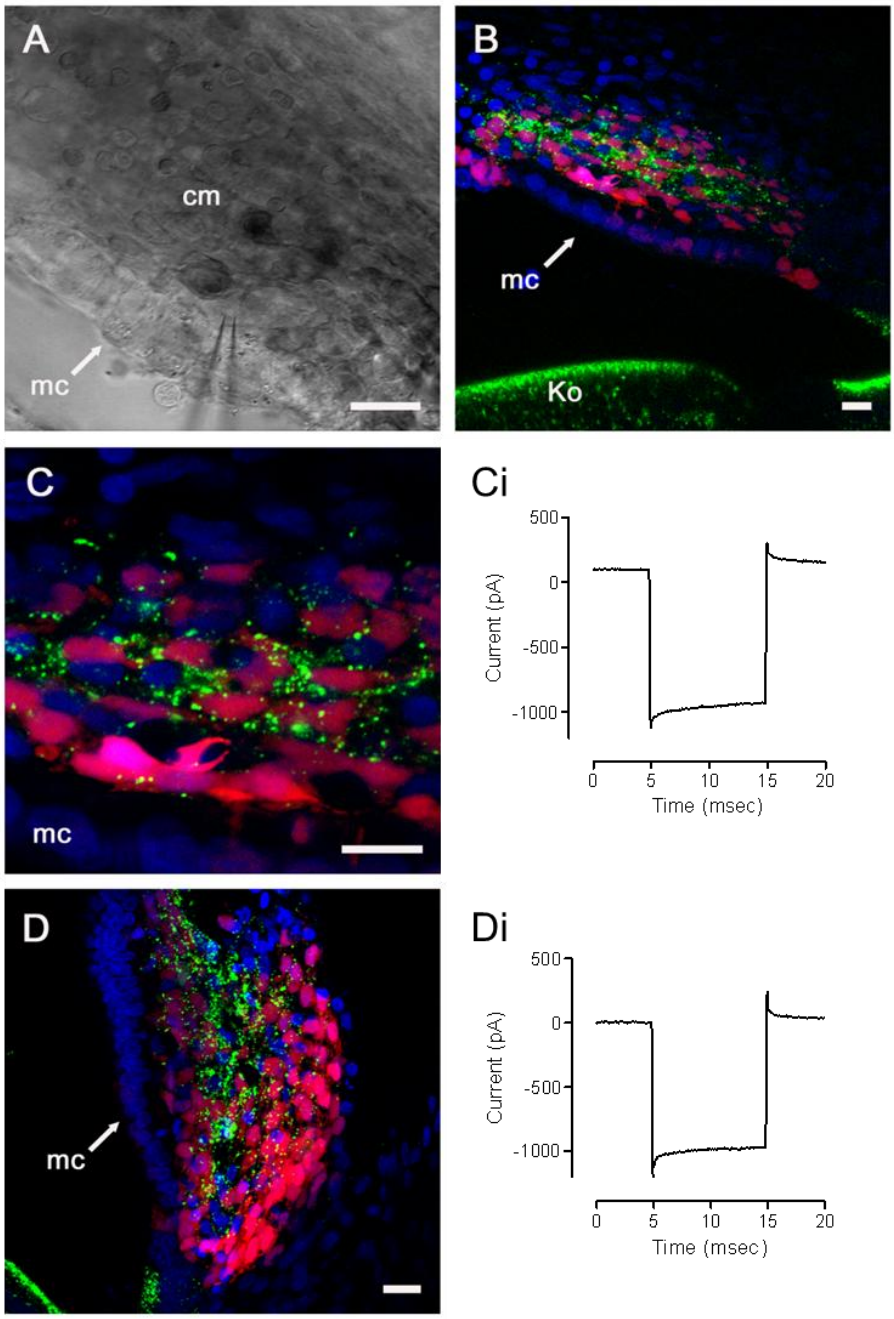

Figure 4-5. GJIC in the condensing mesenchyme of P2 cochlear slice preparations.

(A) Infra-red differential interference contrast (IR-DIC) video micrograph taken during a whole-cell patch clamp recording. The patch pipette is visible in the lower part of the micrograph whilst recording from a cell in the condensing mesenchyme (cm), behind the marginal cells (mc). (B) A confocal projection (10 µm depth) reveals the extent of NBN spread (red) following the recording in (A). The slice was counterstained for Cx30 (green) and DAPI (blue). (C) A magnified image from (B) showing detailed gap junction plaques between cells containing NBN. (Ci) Whole-cell current recording corresponding to (C) in response to 10 mV hyperpolarising pulses (input resistance, 10 MΩ). (D, Di) Extensive spread of NBN throughout the condensing mesenchyme in a different slice and the corresponding whole-cell recording (input resistance, 10M Ω). Scale bars, 20 µm.

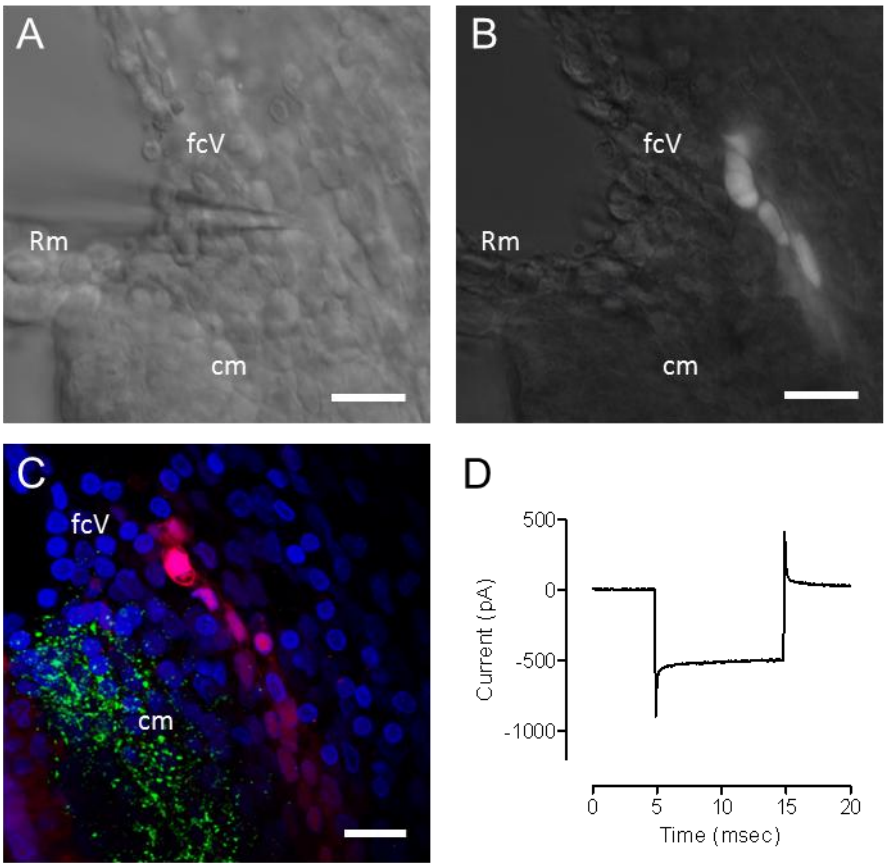

Figure 4-6. GJIC between developing type V/I fibrocytes of a P2 cochlear slice.

(A) Infra-red differential interference contrast (IR-DIC) video micrograph taken during a whole-cell patch clamp recording in the developing type V fibrocyte region (fcV). Reissner's membrane, Rm; condensing mesenchyme, cm. (B) Live fluorescent image of lucifer yellow (LY) showed directional coupling in a column of cells inferior to the patched cell and posterior to the cm. (C) A confocal projection (10 µm depth) labelled for Cx30 (green) and DAPI (blue) revealed further spread of NBN (red) in a discrete column of cells behind the condensing mesenchyme. (D) Whole-cell current recording in response to 10 mV hyperpolarising pulses (input resistance, 18 MΩ). Scale bars, 20 µm.

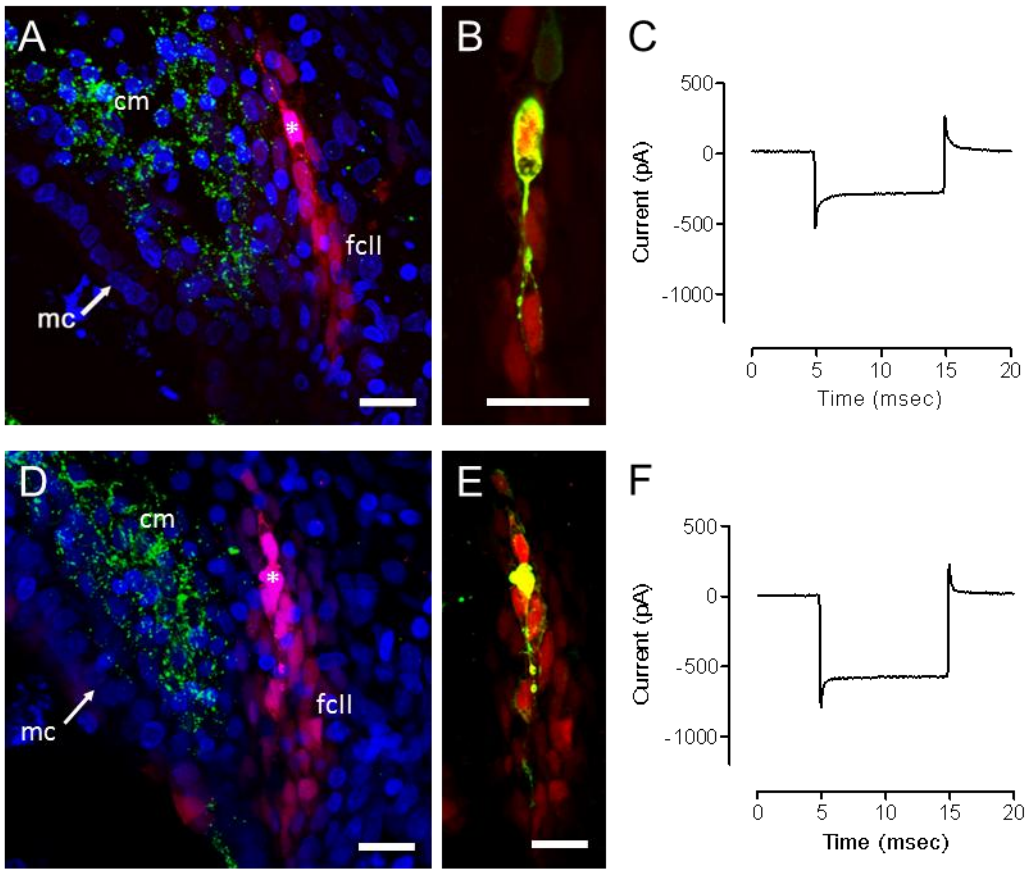

Figure 4-7. GJIC between developing type II fibrocytes in P2 cochlear slices.

(A) NBN (red) transfer from a patched cell (asterisk) in the developing type II fibrocyte region (fcII), posterior to the condensing mesenchyme (cm). Marginal cells (mc) indicate the apical surface of the stria vascularis. NBN was detected in a column of spindle-shaped cells, but not in the condensing mesenchyme. Slices were counterstained for Cx30 (green). (B) Detail of the injection in (A). Fluorescein-dextran (green), a GJ impermeable dye, did not spread from the patched cell and revealed long spindle-like processes contacting coupled cells. (C) Whole-cell current recording in response to 10 mV hyperpolarising pulses (input resistance, 19 MΩ). (D-F) Similar patterns of dye-transfer were seen consistently between slices from other P2 animals, with only slight variations in the extent of coupling. Scale bars, 20 µm.

4.2.3 Functional GJIC in the postnatal cochlear lateral wall (P5)

In P5 rat cochlear slices, the columns of dye-coupled fibrocytes seen at P2 were no longer observed. Cells injected in the type V fibrocyte region (Figure 4-8A) were dye-coupled to cells in the condensing mesenchyme/type I fibrocyte region, as demonstrated by extensive NBN transfer. In a more detailed image, Cx30 puncta were visibly aligned along the process of the injected cell (arrows, Figure 4-8B). As well as NBN, intracellular recording solutions were supplemented with fluorescein dextran, a gap junction impermeable dye, to reveal cell morphologies (Figure 4-8Bi). This dye does not pass through gap junction channels because of its high molecular weight (~10 kDa), which is useful for delineating the injected cell. It also confirmed that dye transfer occurred via gap junctional coupling, as opposed to other mechanisms, such as cytoplasmic bridging. The low input resistance recorded (Figure 4-8C) was consistent with the increase in GJIC. NBN spread within the type II fibrocyte region was multi-directional, though locally restricted, and corresponded with sparser anti-Cx30 labelling (Figure 4-8D-E). Fluorescein dextran co-injection revealed the morphology of the patched cell. Extensive projections extended to distant cells containing transferred NBN and had the appearance of wrapping around what could be a root cell process (Figure 4-8Ei), though this has not been verified. The input resistance measured (Figure 4-8F) corresponded with the extent of NBN transfer.

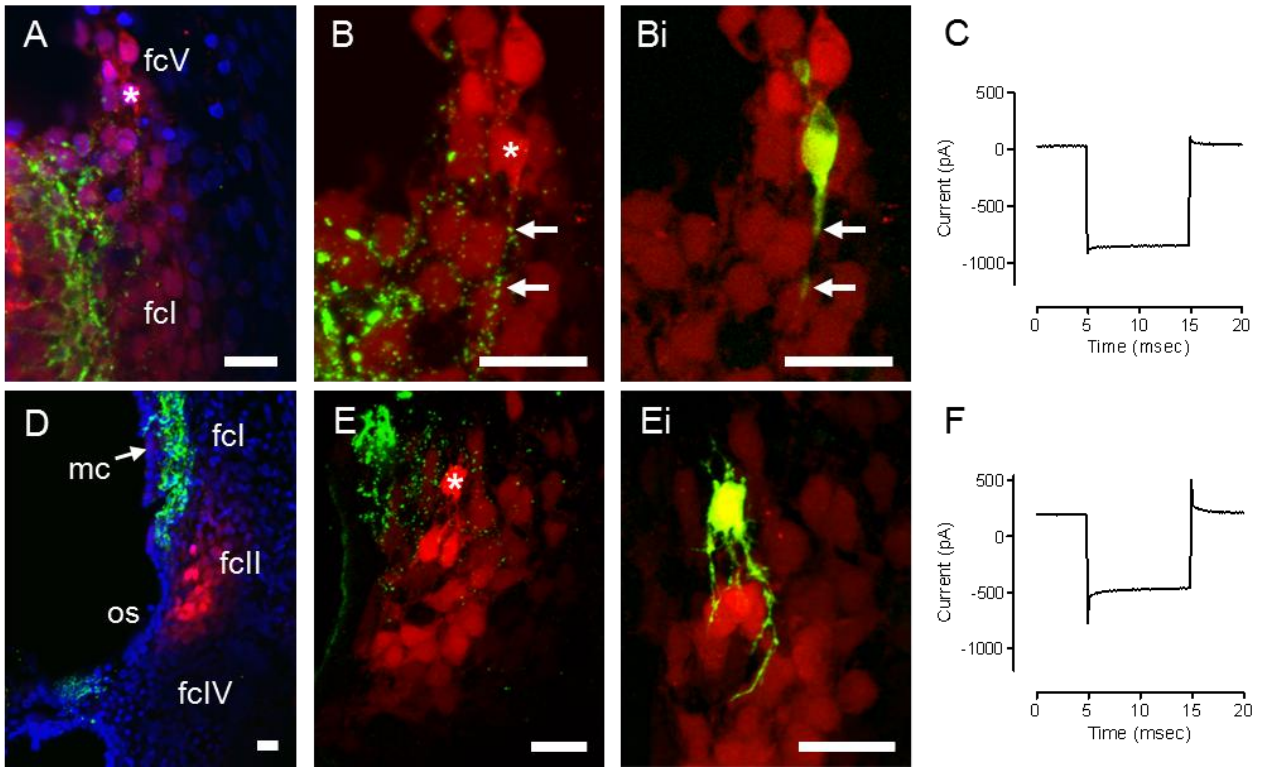

Figure 4-8. GJIC in P5 cochlear slice preparations.

(A) NBN (red) injection into a type V fibrocyte (fcV; asterisk) in a P5 cochlear slice. Dye spread to many cells linking the type V region to the condensing mesenchyme/developing type I region (fcI). The slice was counter-stained for Cx30 (green). (B) Detail of the injection in (A) shows the presence of small Cx30 gap junction plaques (green) between the NBN-coupled cells. (Bi) Fluorescein-dextran (FD, green), co-injected with NBN, did not pass into any surrounding cells. Arrows indicate distinct Cx30-labelled puncta dotted along the cell process that protrudes into the type I fibrocyte region. (C) Whole-cell patch clamp recording in response to 10 mV hyperpolarising steps (input resistance 11 MΩ) corresponds with the increase in dye-coupling. (D) NBN spreads following an injection into a P5 lateral wall fibrocyte located posterior to the outer sulcus (os). The cell was in the type II region (fcII), located superior to the type IV region (fcIV), but inferior to the type I region (fcI). (E) Detail of NBN spread from panel (D), showing Cx30-labelled puncta between type II coupled fibrocytes. (Ei) FD fluorescence revealed multiple cytoplasmic projections extended to distant cells containing NBN. (F) Whole cell recording (input resistance 15 MΩ) from (D). Scale bars 20 µm.

As described, co-injection of fluorescein dextran during recordings enabled the assessment of GJIC, whilst also describing the morphology of the injected cell. A comparison of the morphology of different fibrocyte subtypes from P5-P6 cochlear slices is shown in Figure 4-9. Fluorescence from a cell in the type II fibrocyte region revealed a multi-polar morphology that had numerous cytoplasmic extensions contacting cells some distance away from the cell body (Figure 4-9A). Similar to the cell shown in Figure 4-8Ei, the projections give the impression of wrapping around what could be the shape of a root cell process (located inferior to the cell body). Morphologies from other subtypes were also revealed. Type I fibrocytes were monopolar or bipolar spindle-shaped cells (Figure 4-9B), whereas some type V fibrocytes had a multi-polar morphology with numerous large diameter processes extending from the cell body (Figure 4-9C).

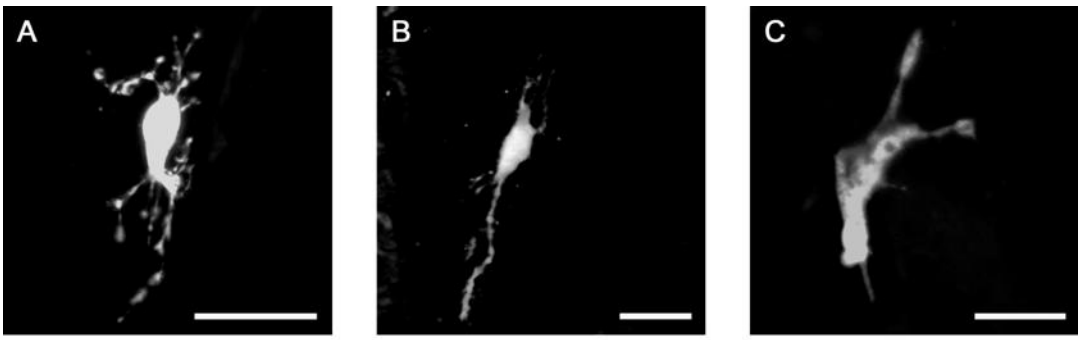

Figure 4-9. Characteristic morphology of fibrocyte subtypes in the postnatal spiral ligament.

(A-C) Neurobiotin fills of uncoupled fibrocytes in P5-P6 cochlear slices. (A) Multipolar cell in the type II fibrocyte region lateral to the outer sulcus. (B) Monopolar cell in the type I fibrocyte region to the rear of stria vascularis. (C) Multipolar cell in the type V fibrocyte region superior to where Reissner's membrane attaches to the lateral wall. Scale bars, 20 μm.

4.2.4 Fibrocytes in the early postnatal lateral wall have fluoxetine-sensitive, weakly rectifying currents

Single-cell lateral wall fibrocytes were determined by the lack of dye spread (using live IR-DIC video-microscopy), high input resistance (>50MΩ) and low membrane capacitance (3-20 pF, estimated from the patch clamp amplifier). These uncoupled cells permitted recordings of current-voltage (*I-V*) relationships during dye injection in the whole-cell patch clamp configuration. Previous studies have suggested that type I fibrocytes (cultured from gerbil lateral wall explants) have a K^+ membrane conductance that is mediated by BK channels (Liang et al., 2003; Shen et al., 2004). The authors propose that these channels are important in regulating the electrochemical gradient inside the lateral wall, which in turn is vital for K^+ recycling. The present study examined single, uncoupled fibrocytes to determine whether any voltage-dependent currents were present in early postnatal development.

During whole-cell recordings from single cells in P2 rat slices, the majority of fibrocytes had resting membrane potentials of -70 to -75 mV. *I-V* relationships were recorded in response to a voltage step command (Figure 4-10A). The corresponding recording (Figure 4-10B) is shown as a representative of several recordings in the P2 lateral wall (n=6). In response to both hyperpolarising and depolarising steps, inward and outward currents were activated respectively. The steady-state currents were plotted to produce an *I-V* curve that showed weak inward-rectification (Figure 4-10C). Inward rectification usually indicates that the main conductance is mediated by K_{ir} channels. To determine whether the membrane potential (E_m) was dependent on K^+, E_m was recorded in zero-current clamp mode in response to increasing $[K^+]_{bath}$ (Figure 4-10D). An increase in $[K^+]_{bath}$ caused cell depolarisation, suggesting that K^+ conductance is the major determinant of E_m.

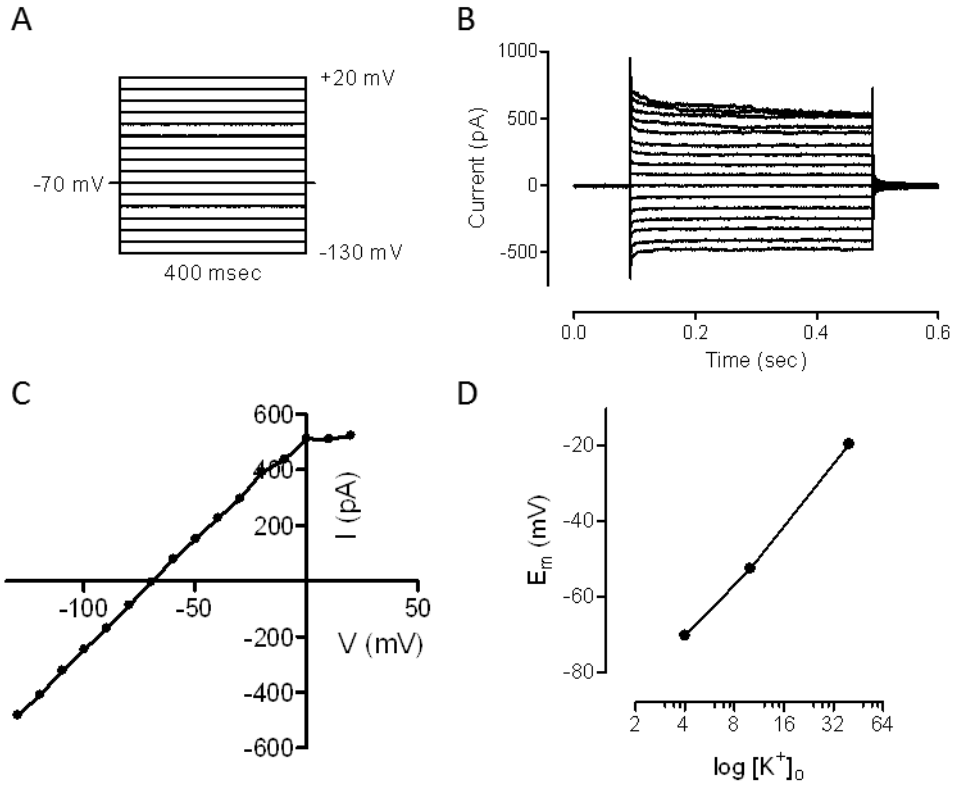

Figure 4-10. The resting potential of post-natal fibrocytes is dependent on K^+.

(A) Voltage (*V*) command used to record from a type II fibrocyte cell. The cell was voltage-clamped at -70mV in 4mM $[K^+]_e$ artificial perilymph with 400-ms steps in 10mV increments from -130mV to +20mV. (B) Current (*I*) trace in response to the voltage command. (C) *I-V* plot reveals a weak inwardly rectifying current, indicative of a K_{ir} channel. (D) The resting membrane potential (E_m), in *I*=0 mode, is highly dependent on $[K^+]_e$.

Candidate ion channels responsible for the rectifying currents include members of the K_{ir} family. However, there is no published evidence of inward-rectifying potassium channel expression in early (P0-P6) post-natal lateral wall fibrocytes. K_{ir}4.1 (KCNJ10) channel subunits, which conduct weakly inwardly rectifying currents in glia (Kofuji and Newman, 2004) and intermediate cells of the stria vascularis, are vital for generating the endocochlear potential (Takeuchi and Ando, 1998b; Takeuchi et al., 2000). Expression of K_{ir}4.1 in lateral wall fibrocytes, however, has not been reported. Alternatively, a study has shown the expression of K_{ir}5.1 (KCNJ16) within type II and type V fibrocytes of the lateral wall (Hibino et al., 2004). Although the authors show no immuno-detectable protein before P10, there remains the possibility that undetectable amounts may be present at younger postnatal ages. Electrophysiological recordings suggest this might be the case (Figure 4-10). Consequently, expression of Kir4.1 was investigated in rat cochlear cryosections using a polyclonal anti-K_{ir}4.1 antibody. P8 cochlea sections revealed expression in cells within the sensory epithelium and less strongly in outer sulcus and intermediate cells (Figure 4-11A). In a more detailed image of the outer sulcus/type II fibrocyte region, K_{ir}4.1 immuno-labelling was clearly visible in root cell processes and in puncta between type II fibrocytes (Figure 4-11B). By P12, intermediate cells strongly expressed K_{ir}4.1 (Figure 4-11C) and, surprisingly, relatively high levels in both type II (Figure 4-11Di) and type V fibrocytes (Figure 4-11Dii).

To further confirm that the currents were elicited by K_{ir} channels, single cells demonstrating the characteristic weekly rectifying properties were treated with Ba^{2+} – a potent K_{ir} channel blocker (Takeuchi and Ando, 1998b). Surprisingly, application of 2 mM Ba^{2+} had no inhibitory effect and even caused a slight increase in the peak current (Figure 4-12). In contrast, cells exposed to the selective serotonin reuptake inhibitor (SSRI) fluoxetine – previously shown to inhibit K_{ir}4.1 channels (Ohno et al., 2007) – had almost complete blockage of whole-cell currents (Figure 4-13). This effect was reversible after washout with fresh artificial perilymph. Fluoxetine also shifted the zero-current potential (V_z) from -70 mV to -25 mV, which provides further evidence for a potassium channel conductance in the regulation of E_m.

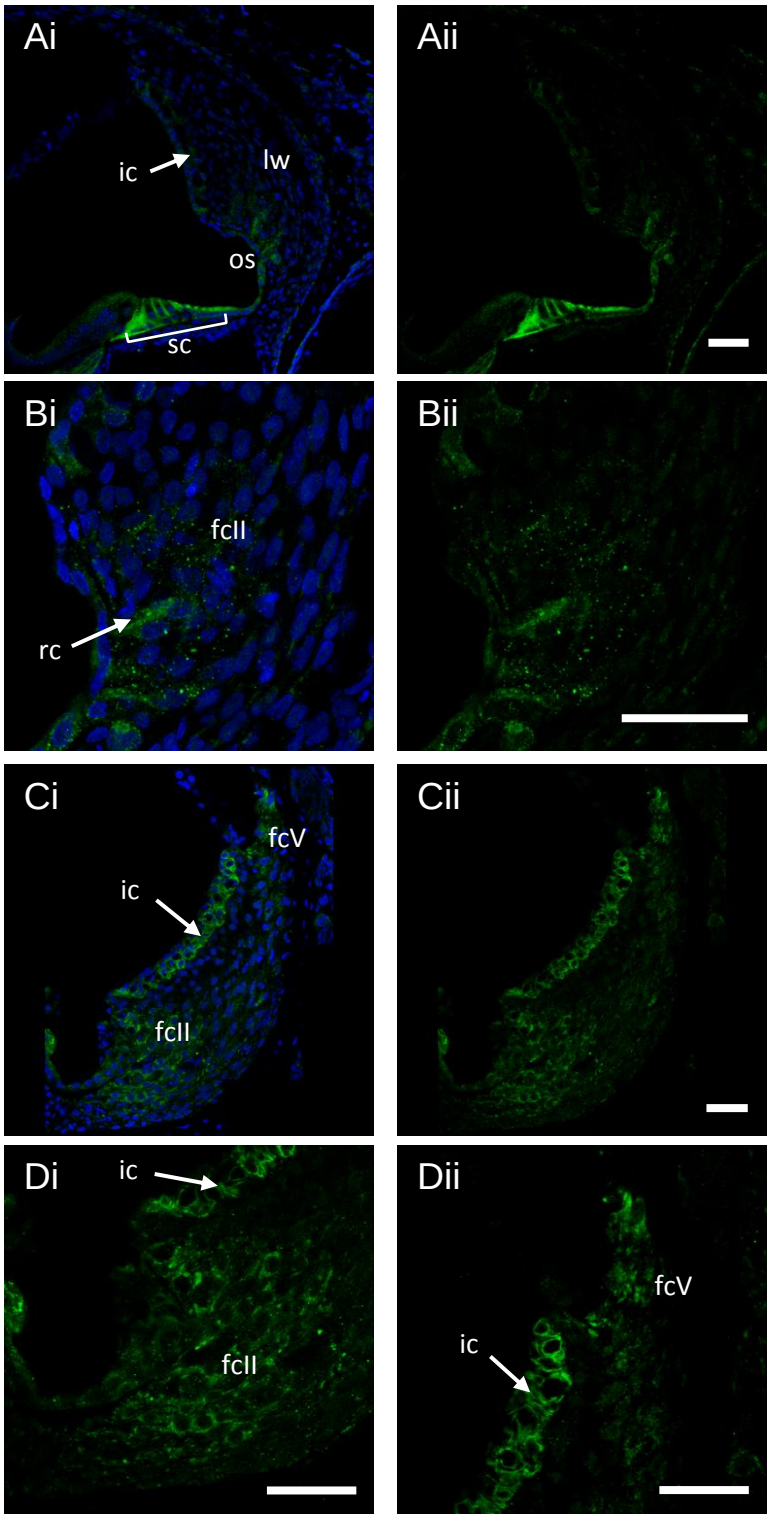

Figure 4-11. Kir4.1 immunofluorescence in P8 and P12 rat cochlea sections.

(Ai-ii) Single confocal image from a P8 rat cochlear section labelled for Kir4.1 (green). Nuclei were counterstained with DAPI (blue). Expression of Kir4.1 was detected in supporting cells (sc), and less strongly in outer sulcus (os) and intermediate cells (ic). (Bi-ii) Confocal projection (3 µm depth) of the type II fibrocyte (fcII) region from (A) revealed diffuse staining in root cell processes (rc). Diffuse and small puncta labelling was also detected in type II fibrocytes. (Ci-ii) A montage of single confocal images from a P12 rat cochlear section. Expression of Kir4.1 was detected in intermediate cells, and fibrocytes in the type II and V (fcV) regions of the lateral wall. Detailed Kir4.1 expression detected in type II (Di) and type V fibrocytes (Dii). Scales bars, 50 µm.

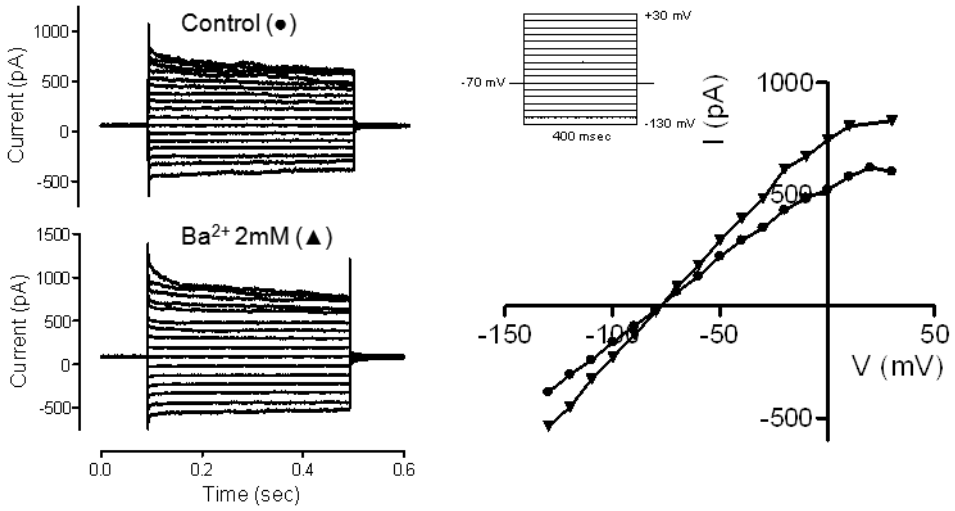

Figure 4-12. Fibrocyte currents are resistant to Ba^{2+}.

Current trace from a single spindle-shaped fibrocyte in the developing type II fc region bathed in 4 mM $[K^+]_o$ artificial perilymph (control, upper left panel) plus 2 mM Ba^{2+} (lower left panel). The cell was voltage-clamped at -75 mV and currents recorded in response to the voltage command shown. *I-V* relationship (right panel) shows a weakly rectifying current (control, ●). Ba^{2+} did not inhibit the current, and even caused a slight increase in current amplitudes (▲).

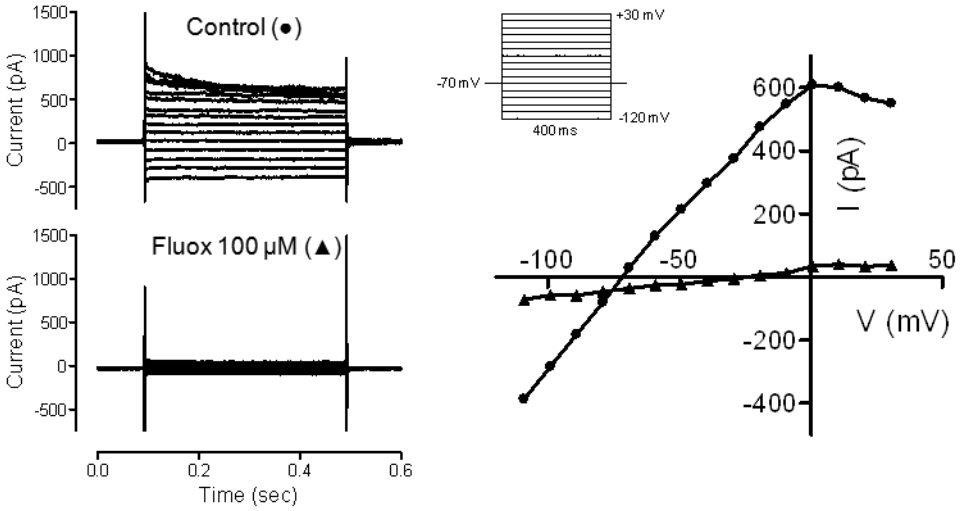

Figure 4-13. Fibrocyte currents are inhibited by fluoxetine.

Current trace from a single spindle-shaped fibrocyte in the developing type II fc region bathed in 4 mM $[K^+]_o$ artificial perilymph (control, upper left panel) or in response to 100 µM fluoxetine (lower left panel). The cell was voltage-clamped at -70 mV and currents recorded in response to the voltage command shown. *I-V* relationship shows a weakly rectifying current (control, ●), which was inhibited by 100 µM fluoxetine (▲).

4.3 Discussion

GJIC during development of the organ of Corti has been studied previously (Jagger and Forge, 2006). The results presented in this chapter reveal previously uncharacterised patterns of GJIC during early postnatal lateral wall development and document changes in the extent of GJIC up to the point of maturation (~P8). These data suggest that GJIC occurs in distinct compartments in the early stages of development and that by the end of the first postnatal week most of the fibrocytes are coupled by gap junctions. At this stage, there was also noticeable GJIC between fibrocytes and cells of the stria vascularis, indicating that lateral wall maturation is reached several days in advance of hearing onset. This study also utilised electrophysiogical recordings during whole-cell patch clamp mode *in situ*. These data suggest a previously undetermined role for weakly rectifying K^+ channels during early postnatal development of fibrocytes.

4.3.1 Morphological and functional maturation of the cochlear lateral wall

Studies performed on altricial rodents including mice, rats and gerbils, have documented the maturation of cellular architecture in the lateral wall from birth up until the onset of hearing (Kikuchi and Hilding, 1966; Steel and Barkway, 1989; Rybak et al., 1991; Souter and Forge, 1998). At birth, most of the structures and compartments within the lateral wall are ill-defined and immature. In the 7-12 days subsequent, there is a dramatic maturation of these compartments and differentiation into cell types equivalent of the mature form. The basic architecture noticeable at birth is that of the cuboidal epithelium of marginal cells, and cells derived from the periotic mesenchyme located posterior to the epithelium. At this stage the basolateral membrane infoldings of marginal cells do not extend beyond the basal lamina (Steel and Barkway, 1989). Na,K-ATPase activity, essential for K^+ uptake from the intrastrial space, can be detected in gerbil marginal cells by P2 (Souter and Forge, 1998). In addition, KCNQ1 expression is detected on the apical surface of marginal cells in rats at this developmental stage (D. Jagger, unpublished). Both proteins are essential for K^+ secretion into endolymph and EP generation (Wangemann, 2006).

Intermediate cells, which are melanocytes derived from the neural crest, are present in the lateral wall at P2, but have an immature morphology (Steel and Barkway, 1989). Concurrently, there is vigorous mitotic activity within the condensing

mesenchyme (Mutai et al., 2009). Strial basal cells are derived postnatally from the fibroblasts via a mesenchyme-epithelial transition (Trowe et al., 2008). By the end of the first postnatal week the basal lamina has disintegrated and marginal cell infoldings begin to penetrate and lengthen towards the strial inner layers. At the same time, intermediate cells begin to interdigitate with marginal cell outfoldings. By P7-P8, stria vascularis has formed three distinct layers composed of marginal cells, intermediate cells and basal cells (Steel and Barkway, 1989; Souter and Forge, 1998). At this stage, intermediate cells express Kir4.1, which likely increases after the onset of hearing, as has been shown in the murine lateral wall (Singh and Wangemann, 2008).

Dye injection into single fibrocytes of the lateral wall at P5-P6 revealed characteristic location-specific morphologies. Type II fibrocytes are multi-polar with extended processes that contact distant cells and wrap around what could be root cell projections. Type I fibrocytes have characteristic monopolar or bipolar, spindle-shaped morphologies and type V fibrocytes have multiple processes. This suggests that these cells have differentiated morphologically to carry out their roles in ion transport and neurotransmitter uptake (Spicer and Schulte, 1991; Spicer and Schulte, 1996; Furness et al., 2009; Jagger et al., 2010), around a week in advance of hearing onset. It has also been shown elsewhere that there is a rapid decrease in mitotic activity within the spiral ligament of rats between P7 and P10, suggesting that cells have matured before hearing onset. However, it remains possible that migration of differentiated cells within the ligament could occur during this period (Mutai et al., 2009).

4.3.2 Functional GJIC in the neonatal lateral wall

Previous studies have documented the immuno-reactive expression of Cx26 and Cx30 in the lateral wall during development of the cochlea (Lautermann et al., 1999; Sun et al., 2005). Functional GJIC studied here has revealed that otic fibrocytes are extensively coupled in the early postnatal period (P0-P7). In the early postnatal cochlea (P2), compartmentalised regions of GJIC were discovered. Cells within the condensing mesenchyme (posterior to the marginal cell layer) were coupled within a distinct, crescent-shaped zone. During this early stage, columns of dye transfer between spindle-shaped cells in the region equivalent to the type II fibrocyte region were also discovered, and which had no apparent spread of dye into the condensing mesenchyme zone. This suggests that GJIC within the lateral wall develops in compartmentalised

regions as previously reported for supporting cells in the organ of Corti (Jagger and Forge, 2006). By P5, the pattern of GJIC between type II fibrocytes became more radial. The discreet columns of dye transfer were no longer seen, yet dye-coupling still did not extend into the type I fibrocytes. However, by P7, NBN had spread throughout the spiral ligament and into cells of the stria vascularis, suggesting that compartmentalisation is not a feature of the mature lateral wall. This finding contrasts to that found in the organ of Corti, in which GJIC maturation occurs around hearing onset (Jagger and Forge, 2006). The maturation of GJIC in the spiral ligament by P7 suggests that the connective tissue gap junction network is capable of re-circulating cytoplasmic K^+ in advance of hearing onset, and so is primed for buffering K^+ upon hair cell activation.

It is not known whether GJIC is essential for proliferation and differentiation within developing fibrocytes. There have been no reports of gross morphological defects in fibrocytes of mouse mutants in which either Cx26 or Cx30 have been deleted or mutated (Cohen-Salmon et al., 2002; Kudo et al., 2003; Teubner et al., 2003b; Sun et al., 2009; Schutz et al., 2010). As early as P2 there was direct dye-coupling between cells within the condensing mesenchyme immediately abutting the basolateral membrane of marginal cells (possibly including developing intermediate cells). Gap-junctional coupling during this period of development may be required for physiological signalling mechanisms. It has been shown elsewhere that cochlear gap junctions play a role in the intercellular transfer of metabolites such as IP_3 (Beltramello et al., 2005), and glucose (Chang et al., 2008), and their impaired permeability may be the cause of human connexin-related deafness (Beltramello et al., 2005; Chang et al., 2009). These studies focused only on 1) cells of the epithelial gap junction system in neonatal rat pups (Beltramello et al., 2005), or 2) a variety of cells, including those within the connective tissue gap junction system, but only from P8 onwards (Chang et al., 2008). Future experiments could involve similar studies to investigate the contribution of GJIC to metabolite signalling in the lateral wall from P0 up to the point of GJIC maturity (~P7-P8).

Previous studies have used molecular dyes of varying size and charge to investigate the selective permeability of gap junctions (Marziano et al., 2003). The permeability of gap junctions between supporting cells has been shown to vary through development. In particular, gap junctions between Deiters' cells show a distinct increase

in selectivity beyond P12, which is thought to relate to changes in Cx26 and Cx30 expression (Jagger and Forge, 2006). Cx26 and Cx30 are expressed extensively in the lateral wall and co-localise in most regions, therefore, the possibility of selective permeability in the spiral ligament may also exist. Hardening of the otic bone, coupled with an increase in extracellular stroma surrounding cells later in development (>P10), meant recordings from fibrocytes past this age were unreliable. Consequently a study of gap junction permeability was not conducted here. A possible alternative to this problem might be to use a sharp electrode to microinject dyes of varying size and charge, rather than the whole-cell patch clamp configuration.

4.3.3 Dye coupling in the mature lateral wall supports K^+ re-circulation

The K^+ recycling pathway is a proposed mechanism that involves recirculation of extruded K^+ from hair cells through gap junctions of the epithelial and connective tissue networks and pumped back into endolymph via the stria vascularis. It is a topic that is widely discussed in the hearing field (Kikuchi et al., 2000; Wangemann, 2006; Hibino and Kurachi, 2006; Zhao et al., 2006; Mistrik et al., 2009), yet no direct functional evidence exists to verify the hypotheses. There are, however, many indirect findings that support such a mechanism. These include observations of sub-cellular anatomical specialisations (Spicer and Schulte, 1996), protein expression patterns *in vivo* (Spicer and Schulte, 1991; Sakaguchi et al., 1998; Ando and Takeuchi, 1999; Hibino et al., 2004) and *in vitro* (Shen et al., 2004), and the compatible biophysical properties of cells located at key loci within the suggested pathway (Jagger et al., 2010). Together, the data presented in this chapter confirms the presence of a continuous gap junction pathway through the lateral wall and provides further support for the K^+ recycling hypothesis. Type II fibrocytes, which are predicted to absorb K^+ secreted by root cell processes (Spicer and Schulte, 1996; Jagger et al., 2010), are connected to type I fibrocytes. In turn, type I fibrocytes are connected to basal cells of the stria vascularis, which are themselves coupled to intermediate cells.

The endolymphatic [K^+] in rats reaches almost adult levels by P7, and the ionic composition remains unchanged during the phase of rapid increase in EP (Bosher and Warren, 1971). This led to the suggestion that the ionic composition of endolymph and EP arise independently, and that they arise in succession during postnatal development. The fact that endolymphatic [K^+] almost reaches adult levels by P7, yet the levels of

connexin expression continue to increase up to and beyond the onset of hearing, points further to surplus capacity in ion transport within the mature cochlear lateral wall (Schulte and Schmiedt, 1992; Jagger et al., 2011). Marginal cells mature well in advance of EP generation, whereas basal cells mature to express tight junctions just prior to the onset of EP (Souter and Forge, 1998). The observation that GJIC in the lateral wall is effectively mature by P7, and that intermediate cells are known to express $K_{ir}4.1$, both suggest that endolymphatic K^+ could be derived from the connective tissue gap junction network in advance of hearing onset. These data add further, indirect evidence, to other reports suggesting the presence of a K^+ recirculation pathway. However, direct proof of such a mechanism is still lacking. Improvements in future techniques involving K^+-specific fluorescent indicators and electrophysiological techniques are required before direct measurements can confirm transfer of K^+ ions from the epithelial gap junction network to the connective tissue gap junctions network and consequently to the stria vascularis.

4.3.4 Early postnatal lateral wall fibrocytes have weak inwardly-rectifying potassium currents

Kunzelmann et al. (1999) have shown that Cx30 expression increases in rat hippocampal astrocytes during the first 3 weeks after birth and reaches fully mature levels by 4 weeks. The authors suggest that changes in the functional properties of astrocytes coincide with Cx30 expression, which may be important for meeting the demands of the maturing brain. These processes include spatial buffering, transfer of metabolites and second messengers or compounds that accumulate in extracellular space. Electrophysiological recordings also revealed inwardly rectifying K^+ channels (K_{ir}), which are indicative of mature astrocytes (Kunzelmann et al., 1999). K_{ir} channels are up-regulated in a similar temporal pattern to Cx30 (Kressin et al., 1995). Here, similar changes were observed with the zero-current potential shift (~52 mV) in response to high $[K^+]_o$ in early postnatal fibrocytes. This shift is close to that predicted by the Nernst equation for a K^+ selective membrane and suggests that the channels are predominantly permeable to K^+ ions. In addition, the conductance also increased in response to high $[K^+]$ (data not shown), which is typical of inward rectifying K^+ channels (Kressin et al., 1995). These channels are thought to play a vital role in K^+ buffering in the adult brain and, according to the spatial buffering hypothesis (Orkand et al., 1966), require cell-cell coupling via gap junctions (Kunzelmann et al., 1999). The

authors speculate that Cx30 is involved in K^+ homeostasis of the neuronal microenvironment since the temporal expression of both K_{ir} and Cx30 is highly co-ordinated in astrocyte development.

The findings presented here for postnatal fibrocytes show similarity to those of astrocytes. Like astrocytes, the expression of rectifying channels and gap junctions in fibrocytes might be important for early spatial buffering and/or the transfer of metabolites and second messengers during lateral wall development. Whether adult cochlear fibrocytes exhibit the same properties as early postnatal fibrocytes has yet to be determined. It has been suggested by that the resting membrane potential of adult fibrocytes is approximately ~-5 mV (Salt et al., 1987). This potential was recorded by advancing electrodes through the cochlear lateral wall in the horizontal plane towards stria vascularis and, therefore, may only be relevant for type I fibrocytes. As is now known, there are five main fibrocyte subtypes in the lateral wall and each subtype has different expression patterns of ion channels and transporters. In the recordings presented here, most of the developing fibrocytes were recorded from the developing type II region and had resting potentials of -70 to -75 mV. In agreement with the strong negative potentials found here, a study by Prazma (1975) also identified intracellular potentials of ~-80 mV in lateral wall fibrocytes in the region of the spiral prominence (type IIs). In type II fibrocytes expression of K^+ ion transporters, such as Na^+,K^+-ATPase, NKCC1 and K_{ir} channels (which are not expressed in type I fibrocytes), may account for the differences seen in the reported resting potential.

The finding of weakly rectifying currents and expression of K_{ir}4.1 in developing fibrocytes was surprising. Initially, expression of K_{ir} channels in the cochlea was thought to occur in intermediate cells and supporting cells only. However, data in the last few years has revealed that K_{ir} channels may have a wider role in cochlear physiology. For example, root cells express K_{ir}4.1 subunits and have weak inwardly-rectifying currents, which may serve as a mechanism of K^+ ion transport into the extracellular space (Jagger et al., 2010). In addition, Kir5.1 expression has been found in type II, IV and V lateral wall fibrocytes from P10 onwards (Hibino et al., 2004). The recordings presented here could be due to K_{ir}5.1-expression (at levels undetected by immunofluorescence) in developing type II fibrocytes. In heterologous expression systems K_{ir}5.1 homomeric channels are rapidly internalised from the plasma membrane and, consequently, do not form functional units (Tanemoto et al., 2002). Functional

channels would require heteromerization with another K_{ir} subunit (such as $K_{ir}4.1$) or binding to PSD-95 (Hibino et al., 2004). Whether $K_{ir}5.1$ is expressed alone in cochlear fibrocytes, or in combination with $K_{ir}4.1$/PSD-95, remains to be determined. PSD-95 is a PDZ-binding protein member of the membrane-associated guanylate kinase (MAGUK) family. These proteins are involved in clustering of ion channels, including K_{ir} channels, at the membrane (Nehring et al., 2000). It is possible that the currents detected in early post-natal fibrocytes are formed from homomeric Kir5.1 channels, which would suggest that these cells also express PSD-95. Detection of PSD-95 has only been identified in inner and outer hair cells and afferent nerve terminals in the organ of Corti (Davies et al., 2001), but has not been examined in the lateral wall.

Alternatively, the unexpected expression of $K_{ir}4.1$ found in type II and V fibrocytes before hearing onset may account for the currents recorded here. These could be generated from heteromeric Kir4.1/Kir5.1 complexes, which have been shown to form functional inwardly-rectifying currents and are thought to be highly sensitive to internal pH levels (Tanemoto et al., 2000). An alternative mechanism for K^+ uptake by type II fibrocytes could involve combinations of hetero- and homomeric K_{ir} channels and pH_i regulation. This can be explained using the Müller cell as a model system. Müller cells are a type of glial cell found in the retina and function in a similar way to astrocytes by siphoning extracellular K^+ away from the neuronal microenvironment (Newman et al., 1984). A study by Ishii and colleagues (Ishii et al., 2003) suggested that Müller cells differentially utilize at least two types of K_{ir} channel for K^+ regulation; Kir4.1 homotetramers for K^+ extrusion at Müller cell endfeet and $K_{ir}4.1/K_{ir}5.1$ heterotetramers for pH_i-dependent K^+ uptake at the distal regions of Müller cells. The authors note that $K_{ir}4.1/K_{ir}5.1$ heteromeric channels are sensitive to physiological ranges of pH, whereas $K_{ir}4.1$ homomeric channels are more resistant. This discrepancy is what allows the channels to function independently. The mechanism proposes that Müller cells possess an electrogenic Na^+-HCO_3^- co-transport system. An increase in extracellular K^+ would depolarize the cell and increase the inward transport of Na^+ and HCO_3^-. As a result of HCO_3^- influx, the pH_i would become more alkalinized. The authors propose that this would lead to an increase in the open probability of $K_{ir}4.1/K_{ir}5.1$ heteromeric channels and enhance K^+ uptake. Although it hasn't been verified here, a similar mode of action could be applied to the junction between cells of the epithelial system and connective tissue system. It has been shown that root cell

processes express $K_{ir}4.1$ and that this channel may be responsible for extruding K^+ into the extracellular space between lateral wall fibrocytes (Jagger et al., 2010). Immuno-labeling for $K_{ir}5.1$ has been reported in type II fibrocytes (Hibino et al., 2004), which taken with the immuno-labeling for $K_{ir}4.1$ shown here, may suggest the presence of $K_{ir}4.1/K_{ir}5.1$ heteromeric channels. It has also been shown that root cell processes express Pendrin, which is a member of the solute-carrier (*SLC26A*) family of anion transporters and has been suggested to secrete HCO_3^- (Wangemann et al., 2004). In addition, type II fibrocytes have been shown to express a sodium bicarbonate co-transporter (NBC3), which has the capacity to uptake Na^+ and HCO_3^- (Bok et al., 2003). Theoretically, the Müller cell model could then be applied: firstly, root cell processes may secrete K^+ through $K_{ir}4.1$ channels and HCO_3^- through Pendrin transporters into the extracellular space. Type II fibrocytes could then take up HCO_3^- through NBC3 co-transporters and cause alkalization of the pH_i. The change in pH_i may then increase the open probability of $K_{ir}4.1/K_{ir}5.1$ heteromeric channels and enhance K^+ uptake into the connective tissue gap junction system. Both NBC3 and $K_{ir}5.1$ have been shown to bind PSD-95 through their PDZ binding domains. Therefore, PSD-95 could act as an intrinsic regulator of this process.

This theory, however, is complicated somewhat by the observed insensitivity to high $[Ba^{2+}]$ exposure – a potent K_{ir} channel blocker. In contrast, exposure of cochlear slices to fluoxetine caused a complete blockage of channel activity and depolarized the resting membrane potential. Although this drug has been shown to block $K_{ir}4.1$ channels (Ohno et al., 2007), it is not specific. These data are difficult to interpret. One explanation could be that a novel, Ba^{2+}-resistant, K_{ir} channel is expressed in postnatal fibrocytes or that $K_{ir}4.1/K_{ir}5.1$ heteromeric or $K_{ir}5.1$ homomeric channels are resistant to Ba^{2+} in this system.

4.4 Conclusion

The data presented in this chapter has revealed compartmentalized intercellular dye-coupling in the rat lateral wall between P2 and P5. By P7, there was extensive dye-coupling throughout the connective tissue syncytium. Dye was detected in fibrocytes, basal cells and intermediate cells suggesting that lateral wall function matures several days in advance of hearing onset. Therefore, the lateral wall appears to be capable of re-circulating cytoplasmic K^+ as early as P7, and so is primed to receive and buffer K^+ ions when the pathway is activated by air-borne sound.

The detection of a negative resting potential sensitive to changes in $[K^+]_o$, weakly rectifying currents and immuno-labelling of $K_{ir}4.1$ in developing lateral wall fibrocytes may suggest additional roles for K^+ channels in the K^+ cycling pathway. The combination of K_{ir} channels and gap junction expression might also play a pivotal role in lateral wall maturation and EP generation. These data have only been studied in neonatal rat slices and need to be verified in the adult system.

These data add further indirect evidence to the hypothesis of K^+ recirculation in the cochlea. In despite of the growing support for recycling of K^+ ions, there remains a lack of direct proof for such a system. Direct measurements of K^+ flux from the epithelial gap junction network to the connective tissue gap junction network and to the stria vascularis will be required to finally deduce the existence of cochlear K^+ cycling.

5 ROLE OF CX30 IN THE DEVELOPMENT OF COCHLEAR FUNCTION

5.1 Introduction

The previous chapter described GJIC during cochlear lateral wall development and showed that lateral wall cells are functionally coupled in the early stages of post-natal development. This, together with previous work carried out in our lab (Jagger and Forge, 2006) suggests an important role for cell-cell communication before hearing onset. These studies, along with other clinical and functional analyses have helped to decipher some of the functions of inner ear connexins. However, our knowledge of the exact role of gap junctions in the inner ear and how connexin mutations specifically cause deafness is still lacking. This chapter discusses the genetics and animal models of connexin-related deafness and investigates the pathology and potential causes of EP loss in a *Cx30*-null (*Cx30*$^{-/-}$) mouse model.

5.1.1 Genetics of connexin-related hearing loss

The requirement for functional gap junctions in the inner ear has been highlighted by the discoveries of mutations in genes encoding Cx26 (*GJB2*) (Kelsell et al., 1997), Cx30 (*GJB6*) (Grifa et al., 1999) and Cx31 (*GJB3*) (Xia et al., 1998), all of which cause hereditary deafness in humans (Ballana et al. 2011, http://davinci.crg.es/deafness/). In addition, other connexins linked to deafness include Cx29 (*GJE1*) (Yang et al., 2007) and Cx32 (*GJB1*) (Bergoffen et al., 1993), both of which cause peripheral neuropathies. There has also been a report linking sensorineural deafness with mutations in Cx43 (*GJA1*) (Liu et al., 2001). This has since been shown to involve the pseudogene of Cx43 (Paznekas et al., 2003), however a more recent study has suggested that mutations in both *GJA1* and its pseudogene (*pGJA1*) may cause hearing loss (Hong et al., 2010). These types of deafness are associated with both recessive and dominant forms of inheritance and can cause deafness alone (non-syndromic) or present with other clinical problems (syndromic), such as skin disease (Rabionet et al., 2002).

Around 70% of prelingual hereditary deafness is of the non-syndromic sensorineural type, of which autosomal recessive traits (DFNB) make up ~85% and dominant traits (DFNA) ~15% of cases (Denoyelle et al., 1998). To date, at least 70 DFNB and 53 DFNA non-syndromic loci have been mapped. Of these loci, 41 genes

have been linked to DFNB and 25 genes to DFNA (Van Camp and Smith 2011, http://hereditaryhearingloss.org/).

5.1.1.1 Non-syndromic deafness; GJB2 mutations

Mutations at the DFNB1 locus account for up to 50% of all autosomal recessive non-syndromic hearing loss cases in many, but not all, populations studied (Bitner-Glindzicz, 2002; Dodson et al., 2011). DFNB1 is located on chromosome 13q11-12 (Guilford et al., 1994) and encompasses both the *GJB2* (Kelsell et al., 1997) and *GJB6* (del Castillo et al., 2002) genes within 50 kb of each other (Ortolano et al., 2008). To date, more than 100 missense, nonsense, insertion, deletion and frame-shift mutations have been discovered in the *GJB2* gene (Hoang et al., 2009). In European and North American populations the most common mutation is a recessive deletion of a single guanine nucleotide within a stretch of six guanines at position 35 of the *GJB2* cDNA (termed 35delG). This causes a frameshift and subsequent premature termination of protein translation (Zelante et al., 1997). It has been proposed that the 35delG mutation may account for up to 70% of *GJB2* mutant alleles and has a 1 in 50 carrier frequency in European populations, but is considerably higher in others (Bitner-Glindzicz, 2002). Additional *GJB2* mutations are highly prevalent in other populations and account for most cases of autosomal recessive non-syndromic deafness. For example, the 167delT mutation, which causes a premature stop codon, has a carrier rate of 4% in the Ashkenazi Jewish population (Morell et al., 1998), whereas the most common deafness-causing mutation in Japan is 235delC, with a carrier rate of ~1% (Abe et al., 2000; Kudo et al., 2000). A recent comprehensive review of various disease-causing Cx26 mutations has estimated the carrier frequency to be 1-4% in many populations, making *GJB2* one of the most common disease-linked genes in humans (Hoang et al., 2009).

The high carrier frequency of certain *GJB2* recessive mutations suggests there may be heterozygote advantage. For example, the most common recessive mutation found in the African population, R143W (Brobby et al., 1998), causes a thicker epidermis in both heterozygotes and homozygotes, which is thought to offer extra protection against pathogen invasion (Meyer et al., 2002). A separate study demonstrated that other non-syndromic *GJB2* mutations increase cell survival, and thus, may explain the thicker epidermis (Common et al., 2004). In addition, organotypic skin

cultures engineered to express the Cx26R143W mutation were less susceptible to bacterial invasion (Man et al., 2007).

Non-syndromic mutations are scattered throughout the Cx26 protein sequence (purple dots, Figure 5-1) and have been investigated using *in vitro* expression systems. Many of the recessive non-syndromic mutations have the ability to form gap junctions, but demonstrate a loss-of-function. These can include non-functional gap junctions (such as the R143W mutation), those with impaired electrical and biochemical coupling, and those with altered voltage gating (reviewed by Nickel and Forge, 2010). Others have impaired transcription due to large deletions of promoter elements or partial deletion of the gene itself (see section 5.1.1.3). The most common non-syndromic *GJB2* mutations mentioned above (35delG, 167delT and 235delC) are all caused by a single nucleotide deletion, which inserts a premature stop codon and thus leads to impaired translation. In addition to the common autosomal recessive non-syndromic forms of deafness, various dominant *GJB2* mutations (DFNA3) have also been implicated in both non-syndromic and syndromic deafness (Nickel and Forge, 2008; Hoang et al., 2009).

Image deleted due to copyright.

Figure 5-1. Location of deafness and skin-disease causing Cx26 mutations.

The Cx26 amino acid sequence is highlighted for mutations associated with deafness only (non-syndromic, purple dots) and those associated with deafness and skin disease (syndromic, orange dots). Reproduced from Laird 2006.

5.1.1.2 Syndromic deafness; GJB2 mutations

Almost all Cx26 mutations discovered to date are associated with some degree of hearing loss. Interestingly, several Cx26 mutations have also been shown to cause deafness and skin-disease syndromes (Kelsell et al., 2001). In human skin, mRNA expression of 10 different connexins has been reported, including Cx26 and Cx30 (Di et al., 2001). It is likely then, that the high number of connexins and complex overlapping distributions found across the keratinocyte sub-populations can accommodate for recessive or loss-of-function Cx26 mutations. Dominant mutations in the *GJB2* gene account for most forms of syndromic hearing loss. These mutations can associate with various skin disorders, including palmoplantar keratoderma (PPK), Vohwinkel syndrome (VS), Bart-Pumphrey syndrome (BPS), Keratitis-ichthyosis deafness (KID) syndrome and hystrix-like ichthyosis-deafness (HID) (reviewed in Nickel and Forge, 2008; Scott and Kelsell, 2011).

All dominant, syndromic *GJB2* mutations discovered so far are located in the first third of the Cx26 molecule incorporating the amino-terminus and first extracellular loop (orange dots, Figure 5-1). It has been speculated that this region of the molecule is important for regulating Cx26 oligomerization with its wild-type counterpart or other connexin members and for correct transport to the plasma membrane (Thomas et al., 2004; Laird, 2006). It has also been reported that some dominant Cx26 mutations can oligomerize with other connexins that do not normally form channels together. For example, R75W (Rouan et al., 2001) and G59A (Thomas et al., 2004) both of which have been linked to PPK; and D66H (Thomas et al., 2004) which causes VS, have all been shown to exert a trans-dominant effect on Cx43. In possible agreement with these findings, Cx26-R75W transgenic mice (Kudo et al., 2003) studied in our lab presented with cataracts (data not included in this thesis). In wild-type animals, alpha connexins Cx46 and Cx50 are expressed in the fibre cells and Cx43 and Cx50 in the epithelial cells of the lens and mutations in these connexins cause cataracts (Mathias et al., 2010). Ectopic R75W expression was found in all cataract lenses. Thus, expression of R75W under the control of the ubiquitous CAG promoter may be exerting a trans-dominant effect on alpha-connexins found in lens tissue (unpublished data).

In addition to trans-dominant effects, some dominant Cx26 mutations cause a gain-of-function effect. For example, G45E has been linked to a fatal form of KID

syndrome (Janecke et al., 2005). This mutation, along with others (Lee et al., 2009) has been implicated in cell death via 'leaky' hemichannels at the cell membrane. These studies highlight the complex nature of connexin biology and reveal a vast range of Cx26-linked pathologies associated with hearing loss and skin disease.

5.1.1.3 GJB6 mutations and large deletions

In addition to Cx26 mutations, studies have also identified mutations in the Cx30 gene *GJB6* that are linked to dominant and recessive forms of non-syndromic and syndromic (Clouston syndrome) hearing loss. Two deletions in the *GJB6* gene have been linked to non-syndromic deafness at the DFNB1 locus. A 309 kb deletion, del(*GJB6*-D13S1830), is the second most common mutation after *GJB2*/35delG in certain populations (del Castillo et al., 2002). A separate study identified another *GJB6* deletion resulting in a loss of a 232 kb DNA fragment termed del(*GJB6*-D13S1854), which has a carrier frequency of 2% in the Spanish population (del Castillo et al., 2005). These deletions were initially discovered after screening *GJB2* heterozygotes who presented with mild to severe hearing impairment (Lerer et al., 2001; Pallares-Ruiz et al., 2002). This has led to the prediction of a digenic mode of DFNB1 inheritance where the truncation of *GJB6* augments the effects of a single copy *GJB2* mutated allele *in trans* (del Castillo et al., 2005). In addition, the large deletions are predicted to remove regulatory elements important for Cx26 expression, which may act as a key factor in the severe deafness phenotype (Common et al., 2005). A more recent study by Feldmann et al. (2009) has reported the first known deletion of the *GJB2* gene. In this instance a heterozygous deletion of a region spanning at least 920 kb was found *in trans* with a rare V84M *GJB2* mutation leading to profound prelingual deafness.

Thus far, only one missense mutation in the *GJB6* (T5M) has been shown to cause non-syndromic hearing loss. This mutation has a dominant mode of inheritance and was the first Cx30 mutation linked to the DFNA3 locus (Grifa et al., 1999). In recombinant expression systems, Cx30T5M was localised to gap junction plaques at the plasma membrane and formed normal electrical coupling, but had impaired permeability to dye tracers and IP_3 (Common et al., 2002; Zhang et al., 2005). In addition, a mouse model engineered to express the Cx30T5M mutation has been suggested to have impaired ATP release through hemichannels during cochlear development (Schutz et al., 2010).

Dominant Cx30 mutations also cause a syndromic form of hearing loss associated with Clouston syndrome, also referred to as hidrotic ectodermal dysplasia (HED) (Lamartine et al., 2000; Smith et al., 2002). These mutations have impaired trafficking to the cell surface when expressed alone, but are rescued by co-expression of wild-type Cx30. The electrophysiological properties and dye transfer permeabilites differ only slightly between wild-type and mutant/wild-type channels. The mutations are thought to confer a gain-of-function, leading to ATP leak through hemichannels at the cell surface (Essenfelder et al., 2004).

5.1.2 Mouse models of connexin-related deafness

Mouse models of connexin-associated disease have proven to be valuable tools in the pursuit of understanding the complex nature of connexin biology. Deafness phenotypes associated with human connexin mutations correlate relatively well with mouse models of connexin-related deafness, although there are some differences between the two systems. To date, nine different Cx26 or Cx30 transgenic mouse lines have been developed with the aim of investigating the role of gap junctions in cochlear development and physiology. These include seven Cx26 and two Cx30 transgenic lines (see Table 5-1 for summary). One mutant mouse line (Cx26 double knockout) is embryonically lethal and causes death at around embryonic day 6. In contrast, patients homozygous for the 35delG mutation, who are effectively Cx26 knockouts, survive well and present with a non-syndromic form of hearing loss. The survival of these patients is due to inter-species variations in the placental syncytiotrophoblast layers. Humans have only one syncytiotrophoblast layer, whereas mice have two. Gap junctions composed of Cx26 are important for bridging the gap between the two layers in mice and permitting the transfer of glucose from the maternal side of the placenta to the foetal blood circulation. Deletion of *Gjb2* leads to ~60% decrease of glucose transfer in mice (Gabriel et al., 1998). Therefore, homozygous Cx26-null mice are not viable and cannot be used for cochlear studies.

5.1.2.1 Conditional Cx26 deletion and Cx26-point mutation mouse models

An alternative system has been developed to overcome the problem of neonatal lethality in Cx26-null mice. Thus far, four different conditional Cx26 knockout (cCx26) mouse lines have been developed in an attempt to model the DFNB1 deafness seen in humans. All four mouse models utilise the $Cx26^{loxP/loxP}$ mouse for tissue or cell-specific

Cx26 deletion via Cre-recombinase (Cohen-Salmon et al., 2002; Sun et al., 2009; Wang et al., 2009). In most of these studies the spatial or temporal deletion of the *Gjb2* gene was limited to cells comprising the epithelial gap junction network. All mutants had profound-to-severe hearing loss as characterised by a significant increase in auditory brainstem response (ABR) thresholds, but no vestibular defects. Although all the mouse models were significantly deaf, there were some differences reported in the type of pathology associated with deafness. The original cCx26-null mouse (Cohen-Salmon et al., 2002) showed normal development of the inner ear up until the point of hearing onset (P14). From this stage onwards, the authors reported cell death of the inner hair cell (IHC) supporting cells initially, followed by other supporting cells and outer hair cells (OHCs). Spaces of Nuel and tunnel of Corti collapsed from P15-P16 onwards and this was coupled with a loss of integrity of the reticular lamina at the apical end of hair cells. In addition, there was a marked reduction in both the EP and endolymphatic [K^+]. The authors propose that the onset of hearing around P14 triggers the death of IHC-supporting cells by oxidative stress, generated in response to accumulated K^+ interfering with the removal of the neurotransmitter glutamate (Cohen-Salmon et al., 2002).

Three other cCx26 mouse lines also have severe hearing impairment, confirming the essential need for Cx26 protein for cochlear function (Sun et al., 2009; Wang et al., 2009). Although these studies also showed supporting cell and OHC atrophy, the organ of Corti never fully developed in these mice. Nuel's space around OHCs and the tunnel of Corti never opened during postnatal development, suggesting a role for Cx26 in the maturation of the cochlear sensory epithelium (Wang et al., 2009). In agreement, a mouse line engineered to express a dominant-negative Cx26R75W mutation (model for DFNA3) also demonstrated impaired postnatal development of the organ of Corti (Kudo et al., 2003; Inoshita et al., 2008). Delayed organ of Corti maturation may occur because loss of Cx26 gap junctions leads to a disruption in biochemical coupling between supporting cells and reduced supply of growth factors and nutrients (Inoshita et al., 2008; Wang et al., 2009). In addition, Inoshita et al. (2008) also suggest decreased ATP release through connexin hemichannels in the Cx26R75W mouse may lead to disrupted development of both supporting cells and hair cells.

Surprisingly, Cx26R75W mice develop a normal EP, despite expression of the dominant-negative mutation throughout the lateral wall (Kudo et al., 2003). This is in contrast to the original cCx26 knockout study (Cohen-Salmon et al., 2002), where both

the EP and endolymphatic [K^+] were reduced in adult mice. The cCx26 models developed by Sun et al. (2009) and Wang et al. (2009) were not tested for EP or [K^+]. The normal EP values in the Cx26R75W mouse indicate that Cx26 may not be important for stria vascularis function. However, this theory needs to be confirmed with targeted deletion of Cx26 from the connective tissue gap junction system. It could also be possible that excess amounts of Cx30 or endogenous Cx26 are able to compensate for the mutation in the spiral ligament.

A recent study has developed the first mouse model of syndromic hearing loss (Schutz et al., 2011). A dominant-negative mutation, S17F, in the *Gjb2* gene causes sensorineural hearing loss and skin disease, recapitulating KID syndrome seen in humans (Richard et al., 2002). Homozygous mutants are not viable, but heterozygous mice display both symptoms, thus confirming the dominant effect of the mutation. Cx26S17F channels are non-functional and do not pass any current, contrary to the gain-of-function effect of increased hemichannel activity seen with other KID mutations (Lee et al., 2009). Heterozygous Cx26S17F mice have significantly elevated hearing thresholds and a reduced EP. Further detailed work is required to understand the mechanism of deafness in these mice, but it appears that cochlea development is not as severely affected in comparison to conditional knockouts. The authors propose that remaining wild-type Cx26 may be sufficient to stabilise Cx30 channels and partially maintain cochlear homeostasis (Schutz et al., 2011).

5.1.2.2 Cx30 mouse models of deafness

Cx30 is essential for hearing, and deletion of the *GJB6* gene in humans causes severe deafness (del Castillo et al., 2002). A Cx30 knockout (*Cx30*$^{-/-}$) mouse model also causes profound deafness and recapitulates the non-syndromic form (DFNB1) seen in humans. These mice never develop an EP and initially have hearing thresholds over 80 dB, despite apparently normal inner-ear development. In addition, the endolymphatic [K^+] develops normally (~100 mM) up until the onset of hearing (P13-P14), but then reduces (to ~44 mM) in the adult mouse. At this point the hearing thresholds are elevated above 100 dB, indicating profound deafness. Hair cell loss was reported relatively soon after the onset of hearing and gradually spread over several months (Teubner et al., 2003b). A separate study also showed that OHCs died quicker than IHCs, and that by 6 months all OHCs had degenerated. Loss of IHCs in contrast was

relatively slow. Cell death was first observed at P21 in the basal turn, but even after 18 months, many IHCs were still present in the middle and apical turns. In comparison with cCx26 mice, cell death was relatively slow and mild (Sun et al., 2009).

Interestingly, it has been shown that Cx26 protein levels are significantly reduced in the cochlea of *Cx30*$^{-/-}$ mice, even though mRNA levels remain unchanged (Ahmad et al., 2007). A large proportion of gap junctions in the cochlear duct are reported to consist of Cx26 and Cx30, which have been shown to form heteromeric channels (Lautermann et al., 1998; Ahmad et al., 2003; Forge et al., 2003b; Yum et al., 2007). Reduced Cx26 content, yet normal mRNA levels, in *Cx30*$^{-/-}$ mice suggests that homotypic Cx26 channels are relatively unstable at the cell surface, and that Cx30 in normal tissue may have a stabilising effect on functional cochlear gap junctions. Thus, loss of Cx30 is predicted to cause an overall reduction in gap junction numbers. In support of this hypothesis, an adapted *Cx30*$^{-/-}$ mouse model engineered to express extra copies of the Cx26 allele completely rescued hearing sensitivity and prevented hair cell death (Ahmad et al., 2007). The authors suggest that heteromeric Cx26/Cx30 channels are not essential for normal cochlear function. Although the instability and faster degradation of homotypic channels may account for cochlear pathology in cases where mutations lead to an inability to form heteromeric gap junctions, it does not account for deafness-causing connexin mutations that oligomerise into functional heteromeric gap junctions (Nickel and Forge, 2010). It may also be the case that particular cell types or regions of the cochlea express only Cx30 homotypic gap junctions and that over-expression of Cx26 in those cells leads to restored GJIC, rather than an overall increase in gap junction numbers.

A recent mouse model has been engineered to express the human non-syndromic Cx30T5M mutation under the control of the endogenous Cx30 promoter (Schutz et al., 2010). These mice have reduced levels of both Cx26 and Cx30 protein, suggesting that the T5M mutation also leads to gap junction instability, in agreement with reduced Cx26 channel numbers seen in *Cx30*$^{-/-}$ mice (Ahmad et al., 2007). Surprisingly, the Cx30T5M mice only exhibited a mild increase in hearing thresholds, up to ~15 dB across all frequencies (Schutz et al., 2010). This contrasts with the more severe, yet variable, deafness seen in human Cx30T5M carriers. Some carriers have been shown to have a 20-50 dB decrease in hearing levels at frequencies of 2-8 kHz, whereas some showed profound sensorineural deafness (Grifa et al., 1999). Differences in biochemical

coupling and gap junction permeabilities between mice and humans, as analysed previously (Beltramello et al., 2003), are suggested to account for the differences between species (Schutz et al., 2010). In addition, Cx30T5M mice develop a normal EP and exhibit normal electrical coupling between non-sensory cells. However, a marked reduction in the ability to transfer the fluorescent tracer calcein and reduction in intercellular Ca^{2+} signalling via ATP release from hemichannels have been suggested. This has led to the authors suggesting that impaired biochemical coupling is the cause of deafness in these mutants (Schutz et al., 2010).

That protein levels of both Cx26 and Cx30 are reduced in the T5M mouse model, yet hearing thresholds are not severely affected, may suggest that it is not necessarily reduced gap junction numbers in Cx30-mutant mice that cause deafness, as proposed by Ahmad et al. (2007). Instead, it seems likely that there are regions or cell types that express Cx30 specifically, which may be compensated for by over-expression of Cx26 in *Cx30*$^{-/-}$ mice. For example, Deiters' cells have been shown to express Cx30 predominantly over Cx26 (Sun et al., 2005; Jagger and Forge, 2006), thus a complete lack of Cx30 may lead to deficient K^+ homeostasis in this region. This may also explain why OHCs begin to degenerate after hearing onset and prior to IHCs in *Cx30*$^{-/-}$ mice.

The generation of EP is dependent on the intermediate cells of stria vascularis, and requires electrical isolation of the intrastrial compartment from the lumen of blood vessels, and both perilymph and endolymph (as discussed in the previous chapter). This isolation is conferred by tight junctions between endothelial cells, marginal cells and basal cells. A novel mechanism for the lack of EP in *Cx30*$^{-/-}$ mice was proposed by Cohen-Salmon et al. (2007) who suggested that Cx30 deficiency causes disruption of the stria vascularis endothelial barrier. The authors came to this conclusion based on three experimental results. Firstly, they suggested that strial endothelial cells were abnormal in *Cx30*$^{-/-}$ mice as observed using transmission electron microscopy. Secondly, albumin and IgG heavy and light chains (serum proteins that are usually impermeable across the endothelial barrier) were detected in the intrastrial space. Thirdly, qPCR analysis of strial tissue revealed changes in the transcriptional level of several genes involved in vascular physiology. The authors hypothesize that loss of Cx30 gap junctions or nonjunctional hemichannels may lead to an osmotic imbalance within stria vascularis. This in turn is thought to cause changes in transcriptional levels of certain genes downstream and an eventual build-up of homocysteine (a non-protein

sulphur amino acid) that is proposed to cause endothelial dysfunction. Loss of a tight endothelial barrier would then cause an electric shunt, thought to be sufficient to cause a loss of EP (Cohen-Salmon et al., 2007). Several queries arise in response to this interpretation. For example, neither Cx26 nor Cx30 are expressed in strial endothelial cells (Cohen-Salmon et al., 2007), making it difficult to understand how gap junction dysfunction can result in only endothelial damage. In addition, Hoang et al. (2009) raise the question as to why Cx26R75W mice do not present the same pathology considering the mutation is expressed throughout the lateral wall (Kudo et al., 2003) and is dominant-negative over wild-type Cx26 and Cx30 (Hoang et al., 2009). Although a hypothesised complex signalling pathway has been proposed, the exact mechanism of how the loss of Cx30 can lead to changes in transcriptional regulation of certain genes is unknown. It is also unknown as to whether Cx26/Cx30 hemichannels exist in the stria vascularis.

This chapter focuses on the *Cx30*$^{-/-}$ mouse model and investigates stria vascularis morphology and the expression of proteins involved in the generation and maintenance of endocochlear potential (EP). In addition, the endothelial breakage theory is addressed using alternative techniques to those used by Cohen-Salmon et al. (2007).

Cx (gene)	Mutation	Phenotype	Hearing threshold (ABR)	EP and endolymphatic [K^+] (control vs mutant)	Reference
Cx26 (*Gjb2*)	Null (double knockout)	Embryonic lethal at E6.	N/A	N/A	Gabriel *et al.* 2008
	Conditional Cx26-null (*Cx26*$^{Otog/Cre}$)	Non-syndromic deafness. IHC-SC loss at P14. Loss of OHCs and SCs from P15-P16 onwards.	Average thresholds elevated by 30-36 dB for sensitive frequencies.	**P12-P13**: EP, 56 vs 58 mV; [K^+], not recorded. **Adult**: EP, 110 vs 38 mV; [K^+], 153 vs 85 mM.	Cohen-Salmon *et al.* 2002
	Conditional Cx26-null (*Cx26*$^{loxP/loxP}$; *Rosa26*^{CreER})	Non-syndromic deafness. Delayed postnatal development.	Elevated by 30-50 dB across frequencies.	Not recorded.	Sun *et al.* 2009
	Conditional Cx26-null (foxg1-Cre and pax2-Cre lines)	Non-syndromic deafness. Delayed postnatal development. Supporting cell degeneration from P8 onwards. OHC death ~P13.	Elevated by 30-50 dB across all frequencies.	Not recorded.	Wang *et al.* 2009
	Cx26R75W	Non-syndromic deafness. Delayed postnatal development. Hair cell degeneration by 7 weeks.	Average threshold elevated by ~70 dB.	**16-21 weeks**: EP, 97.4 vs 87.7 mV; [K^+] not recorded.	Kudo *et al.* 2003
	Cx26S17F	Cx26$^{S17F/S17F}$ embryonic lethal. Cx26$^{+/S17F}$ similar phenotype to KID syndrome (deafness and skin disease).	Average threshold elevated by ~35-40 dB.	**Adult**: EP, reduced by 42 mV in 129Sv background, reduced by 25 mV in C57BL/6 background; [K^+] not recorded.	Schutz *et al.* 2011
Cx30 (*Gjb6*)	Null (double knockout)	Non-syndromic deafness. Normal development up to P17. Gradual loss of sensory cells from P18. Extensive HC loss by 4 months.	P17-P18 thresholds elevated from 31 dB in controls to 84 dB in mutant. Adult mutants had no detectable ABR up to 100 dB.	**P13-P14**: EP; 74 vs 0 mV, [K^+]; 102 mM vs 100 mM. **Adult**: EP; 83 vs 3 mV, [K^+]; 148 vs 44 mM.	Teubner *et al.* 2003
	Cx30T5M	Non-syndromic deafness.	Mild, but significant elevation of ~15 dB for most freq.	**P21-P28**: EP; 121.2 vs 122.2 mV.	Schutz *et al.* 2010

Table 5-1. Summary of Cx26 and Cx30 mutant mouse models.

ABR, auditory brainstem response; IHC/OHC, inner/outer hair cell; SC, supporting cell.

5.2 Results

5.2.1 Stria vascularis morphology in Cx30$^{-/-}$ mice

5.2.1.1 Stria vascularis is significantly thinner

During the investigation into the role of Cx30 in the development of cochlea function, a noticeable and consistent thinning of stria vascularis tissue in *Cx30* null (*Cx30*$^{-/-}$) mice was observed - which has not been reported in previous *Cx30*$^{-/-}$ studies. To quantify these findings, the distance between the apical surface of marginal cells and basal cells was measured in three locations along the width of the stria (Figure 5-2A) and then averaged, as implemented elsewhere (Wangemann et al., 2004). Representative fluorescence images show detailed measurements and confirm a statistically significant thinning of strial tissue in adult *Cx30*$^{-/-}$ cryosections (Figure 5-2B,C). To avoid potential influences from tissue preparation and processing artefacts, thickness measurements were also analysed from thin section, transmission electron micrographs (TEM). Strial thickness measured from TEM sections of Cx30 wild-type (*Cx30*$^{+/+}$) and *Cx30*$^{-/-}$ mice aged between post-natal day 30 (P30) and P37 were all significantly reduced in mutant mice (Figure 5-2D). Older mice, aged between P57 and P67, also displayed significant stria vascularis thinning in basal and apical coils of the cochlea (Figure 5-2E). To determine whether this morphology could be a consequence or cause of hearing impairment in these mice strial measurements were recorded from fluorescently-labelled cryosections taken within the first week of hearing onset (P13-P19). Strial thickness was significantly reduced in basal and apical turns of *Cx30*$^{-/-}$ mice (Figure 5-2F). This suggests that the tissue never reaches the mature thickness seen in *Cx30*$^{+/+}$ animals. Consistent with the TEM dimensions, aged *Cx30*$^{-/-}$ mice (P38 to P51) also had a considerably thinner stria vascularis in comparison to wild-type (Figure 5-2G).

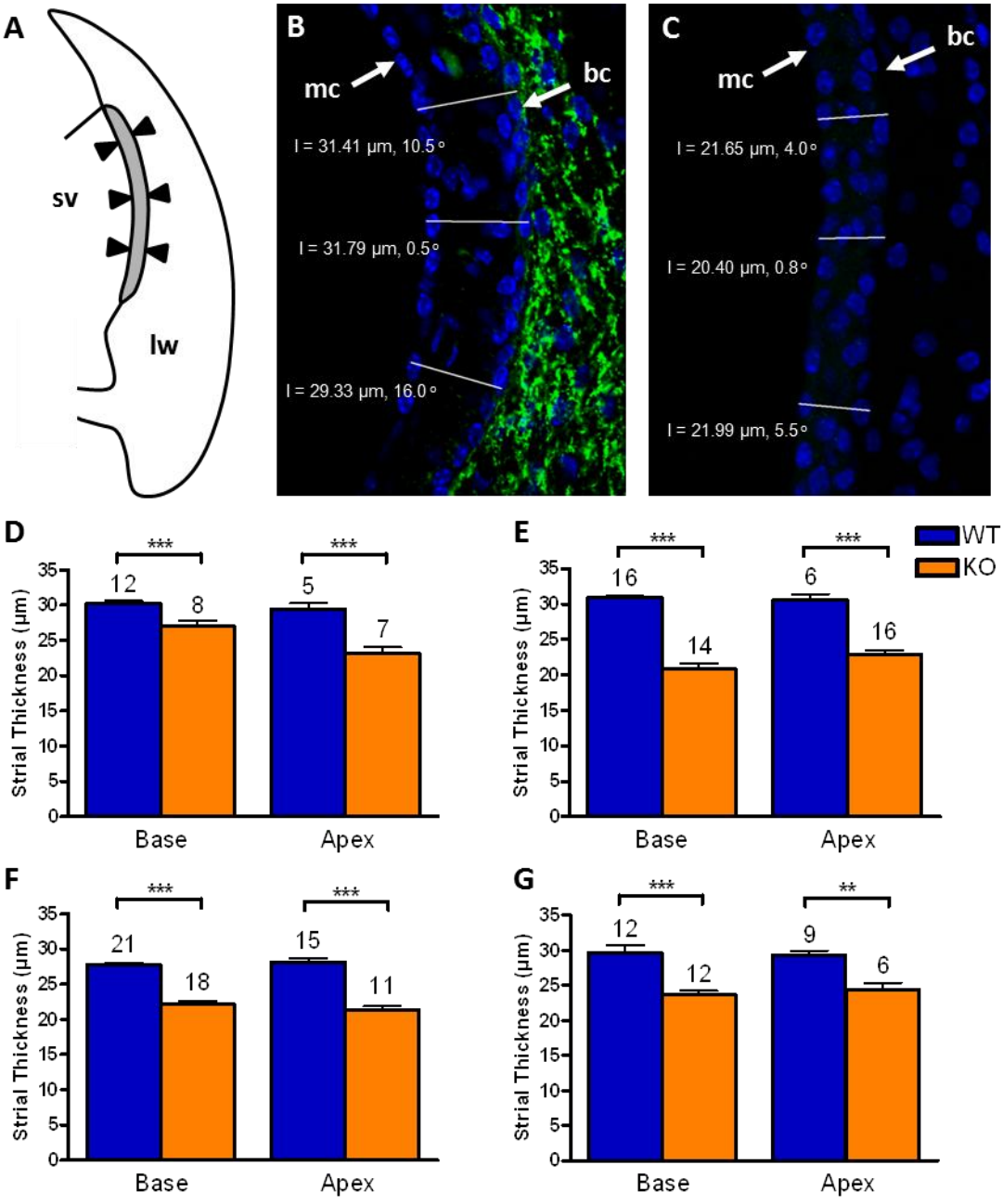

Figure 5-2. Thinning of stria vascularis in *Cx30*$^{-/-}$ (KO) mice.

(A) Schematic showing the locations of stria vascularis (sv) measurements. Thickness was determined from the average of three measurements recorded perpendicular to the surface of marginal cells. (B-C) Representative immunofluorescence images showing three distances measured from marginal cells (mc) to basal cells (bc) in *Cx30*$^{+/+}$ (B) and *Cx30*$^{-/-}$ (C) cochlear cryosections. Cx30 is labelled in green, nuclei in blue. (D-E) Strial thickness data pooled from P30 to P37 (D) and P57 to P67 mice (E) measured from transmission electron micrographs (WT, blue bars; KO, orange bars). (F-G) Strial thickness data pooled from P12 to P19 (F) and P38 to P51 mice (G) measured from immunofluorescent cochlear cryosections. Tissues for electron microscopy were prepared and processed by G. Nevill and A. Forge. Number above each column indicates the number of measurements. Each bar represents measurements from a minimum of 3 animals. *Cx30*$^{-/-}$ strial thickness was significantly thinner in all age sets (** $p<0.005$;*** $p<0.0005$).

5.2.1.2 Marginal cell nuclei appear abnormal

When measuring the thickness of the stria vascularis it also became apparent that, in most cases, the morphology of marginal cell nuclei in *Cx30*$^{-/-}$ mice appeared abnormal in comparison to those of age-matched *Cx30*$^{+/+}$ mice. This was consistent in both thin sections and cryosections of mutant cochleae. In mature (>P38) cochlear cryosections, control marginal cell nuclei were located at the apical surface facing scala media and appeared flattened and either ellipsoidal or plano-concave in shape (Figure 5-3Ai-Aii). In comparison, many of the nuclei in *Cx30*$^{-/-}$ marginal cells appeared more rounded and oval (Figure 5-3Bi-Bii) and were not ordered uniformly at the apical surface. To quantify these findings, the dimensions of marginal cell nuclei were calculated from magnified confocal images of cochlea cryosections. In both the younger (P17-P19) and older aged groups (P38-P51) the nuclear dimensions (calculated from the ratio of length to width) were significantly different in *Cx30*$^{-/-}$ mice (Figure 5-3C). *Cx30*$^{+/+}$ measurements for both age groups had dimensions in which the length of each nucleus was more than twice that of the width (P17-P19, 2.37 ±0.08; P38-P51, 2.37 ±0.15), giving a flattened appearance (as depicted in the figure key). In contrast, nuclei measured from *Cx30*$^{-/-}$ mice had dimensions in which the length was relatively equal to the width (P17-P19, 1.37 ±0.08; P38-P51, 1.20 ±0.06), thus giving a more rounded appearance. Marginal cell nuclei that are atypical in shape have been reported in other examples of stria vascularis abnormalities (Jagger et al., 2011). In addition, marginal cell nuclei are large and irregular in shape during early postnatal development and flatten out at the apical surface before strial maturation (Steel and Barkway, 1989; Souter and Forge, 1998). The observation of atypically shaped marginal cell nuclei in *Cx30*$^{-/-}$ mice may be consistent with those cells not reaching full maturity.

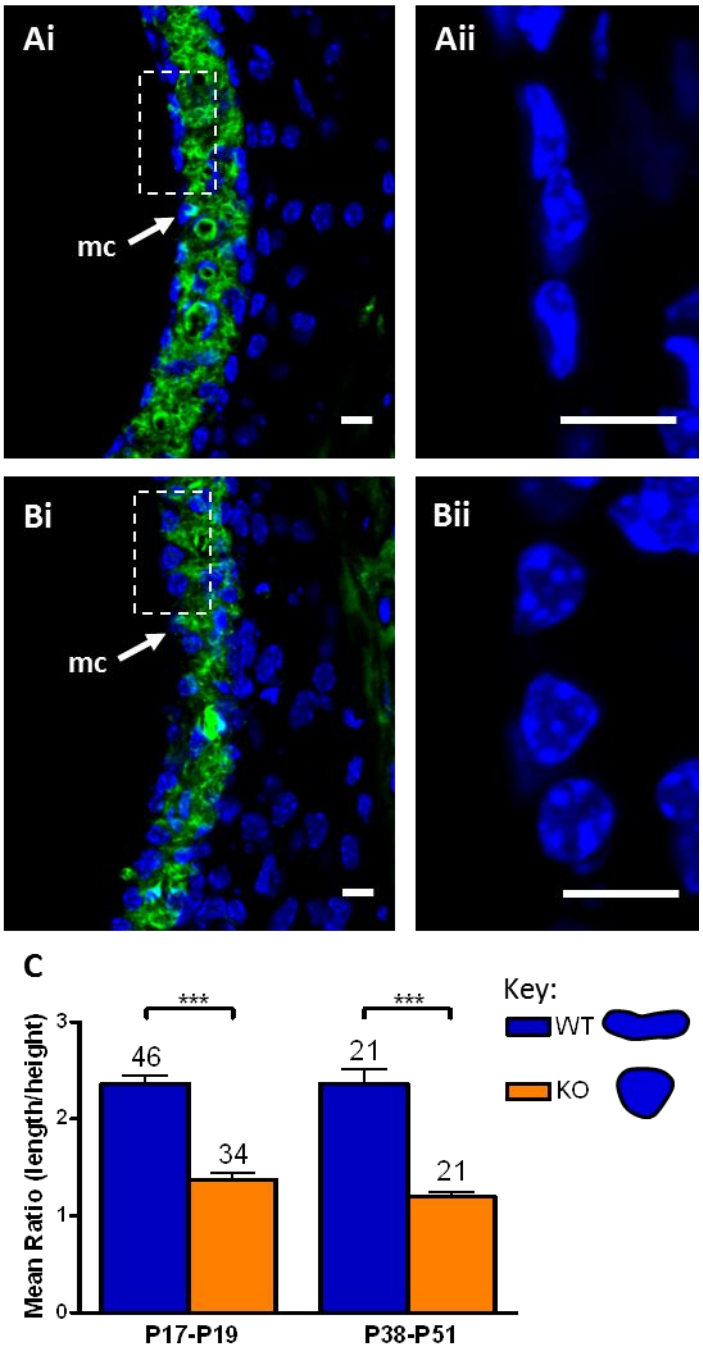

Figure 5-3. Abnormal marginal cell nuclei in Cx30$^{-/-}$ (KO) mice.

(Ai) A cryosection of the basal turn stria vascularis of a P42 Cx30$^{+/+}$ cochlea. Marginal cells (mc) were stained with an anti-NKCC1 antibody (green). Nuclei (blue) were stained with DAPI and were located at the apical surface of marginal cells. (Aii) A detailed view of the boxed area in (Ai) shows the characteristic flattened or ellipsoid-shaped nuclei of normal marginal cells. (Bi) A corresponding image from the basal turn of a P38 Cx30$^{-/-}$ cochlea. (Bii) A detailed view of the boxed area in (Bi) revealed abnormally shaped marginal cell nuclei, which appeared more rounded than ellipsoid in shape. (C) Marginal cell nuclei dimensions were quantified from young (P17-P19) and older (P38-P51) mice and displayed as a mean ratio of length/height. Number above each column indicates the number of measurements from 3 (P17-P19WT) or 2 animals (all other bars) respectively. Cx30$^{-/-}$ marginal cell nuclei had significantly different ratios from Cx30$^{+/+}$ in both age sets (*** $p<0.0001$). Scale bars, 10 µm.

5.2.2 Expression of strial cell proteins important in the generation of endocochlear potential

Cx30$^{-/-}$ mice do not generate an EP (Teubner et al., 2003b; Ahmad et al., 2007). The mice used in this study were obtained from the European Mouse Mutant Archive (www.emmanet.org, EM:00323) and originate from the same colony used in the studies where EP was recorded. All homozygous *Cx30*$^{-/-}$ mice were deaf, as determined by a lack of preyer reflex and were genotyped to confirm the deletion of *Gjb6* gene. It is important to note that EP was not measured here, but is assumed to be absent considering a lack of EP is sufficient to cause hearing loss and recordings from elsewhere have confirmed that *Cx30*$^{-/-}$ mice do not develop an EP (Teubner et al., 2003b; Ahmad et al., 2007). Stria vascularis is thinner in these animals (see 5.2.1.1), suggesting a lack of tissue maturation. Thus, the expression of genes and proteins involved in EP generation were investigated using immunofluorescence labelling and qPCR in both *Cx30*$^{+/+}$ and *Cx30*$^{-/-}$ strial tissue.

5.2.2.1 Reduced K_{ir}4.1 expression in Cx30$^{-/-}$ mice

K_{ir}4.1 is expressed in intermediate cells and is essential for EP generation (as described in the previous chapter) and is down regulated in various cochlear pathologies (Wangemann et al., 2004; Jin et al., 2008; Mustapha et al., 2009). Immunofluorescence labelling of adult *Cx30*$^{+/+}$ mice revealed extensive labelling for K_{ir}4.1 in intermediate cells of a basal turn cochlea (Figure 5-4A). In contrast, K_{ir}4.1 fluorescence in intermediate cells was markedly decreased in the basal turn of an age-matched *Cx30*$^{-/-}$ cochlea (Figure 5-4B). This was somewhat surprising given that a previous report suggested K_{ir}4.1 was not down-regulated in *Cx30*$^{-/-}$ mice (Cohen-Salmon et al., 2007). All cryosections were processed at the same time with the same conditions and prepared so that both wild-type and *Cx30*$^{-/-}$ cryosections were mounted on the same slide. This was to ensure that both genotypes were treated identically, including antibody concentrations and incubation times. In addition, all confocal imaging settings were constant between scans. This allowed for semi-quantitative comparison between samples. A line profile plotted along the width of the stria vascularis showed significantly higher peaks of pixel intensity in *Cx30*$^{+/+}$ compared to *Cx30*$^{-/-}$ (Figure 5-4C). The mean average of the recorded pixel intensities along the line profile was reduced by 63%, thus confirming a strong reduction of K_{ir}4.1 fluorescence in *Cx30*$^{-/-}$

stria (Figure 5-4D). Almost identical results were found in the apical region of the cochlea (Figure 5-4-H), indicating that the decrease in $K_{ir}4.1$ immunofluorescence intensity was consistent throughout the cochlea. Similar results were also found in younger mice (P19) where the average *Cx30*$^{-/-}$ $K_{ir}4.1$ grey level was reduced by ~55% in comparison to the measurements from wild-type, age-matched mice (data not shown).

In addition to immunofluorescence labelling, *$K_{ir}4.1$* mRNA levels were measured from isolated stria vascularis tissue by real-time qPCR (Figure 5-5). In comparison to age-matched *Cx30*$^{+/+}$ mice, *$K_{ir}4.1$* mRNA levels were 1.3 and 3.8-fold lower in P7 and P15 *Cx30*$^{-/-}$ stria respectively. In older mice (P38) the level of mRNA in the *Cx30*$^{-/-}$ stria had increased, but was still 1.3-fold lower in comparison to a P35 *Cx30*$^{+/+}$. These data appear correspond to the immunofluorescence data and indicate that mRNA and protein levels of $K_{ir}4.1$ are reduced in *Cx30*$^{-/-}$ mice. These data are preliminary experiments, of which one animal from each genotype was used for each age group. Therefore, statistical analyses were not performed. Although further experiments and animals are required for statistical significance, there does appear to be a general trend of reduced *$K_{ir}4.1$* mRNA levels in *Cx30*$^{-/-}$ mice. In comparison to protein levels, these reductions may not appear to be significant. However, a study by Wangemann et al. (2004) has shown normal mRNA expression of *$K_{ir}4.1$* in strial tissue of a Pendred syndrome mouse model, but an absence of $K_{ir}4.1$ protein, which would account for the observed loss of EP. The authors suggest that post-transcriptional regulation may have an effect on $K_{ir}4.1$ protein levels, which may also be the case here.

$K_{ir}4.1$ is also expressed in the organ of Corti (Hibino et al., 1997) and is thought to be involved in uptake of extracellular K^+ into supporting cells. Whether the loss of Cx30 affected $K_{ir}4.1$ expression in these cells was also investigated. $K_{ir}4.1$ immunofluorescence was detected in many supporting cells including pillar cells, Deiters' cells and Hensen's cells in a *Cx30*$^{+/+}$ apical turn (Figure 5-6Ai,ii). In contrast, supporting cells in a *Cx30*$^{-/-}$ mid turn had a marked reduction in $K_{ir}4.1$ fluorescence. Remnants of expression were only detectable in the inner pillar cells (Figure 5-6Bi,ii), suggesting that loss of Cx30 might also have an effect on cells in the organ of Corti. Notably, confocal images of spiral ganglion satellite cells had similar levels of $K_{ir}4.1$ immunofluorescence in both *Cx30*$^{+/+}$ (Figure 5-6C) and *Cx30*$^{-/-}$ (Figure 5-6D) mice. Thus, the reduction of $K_{ir}4.1$ appeared to be sight-specific.

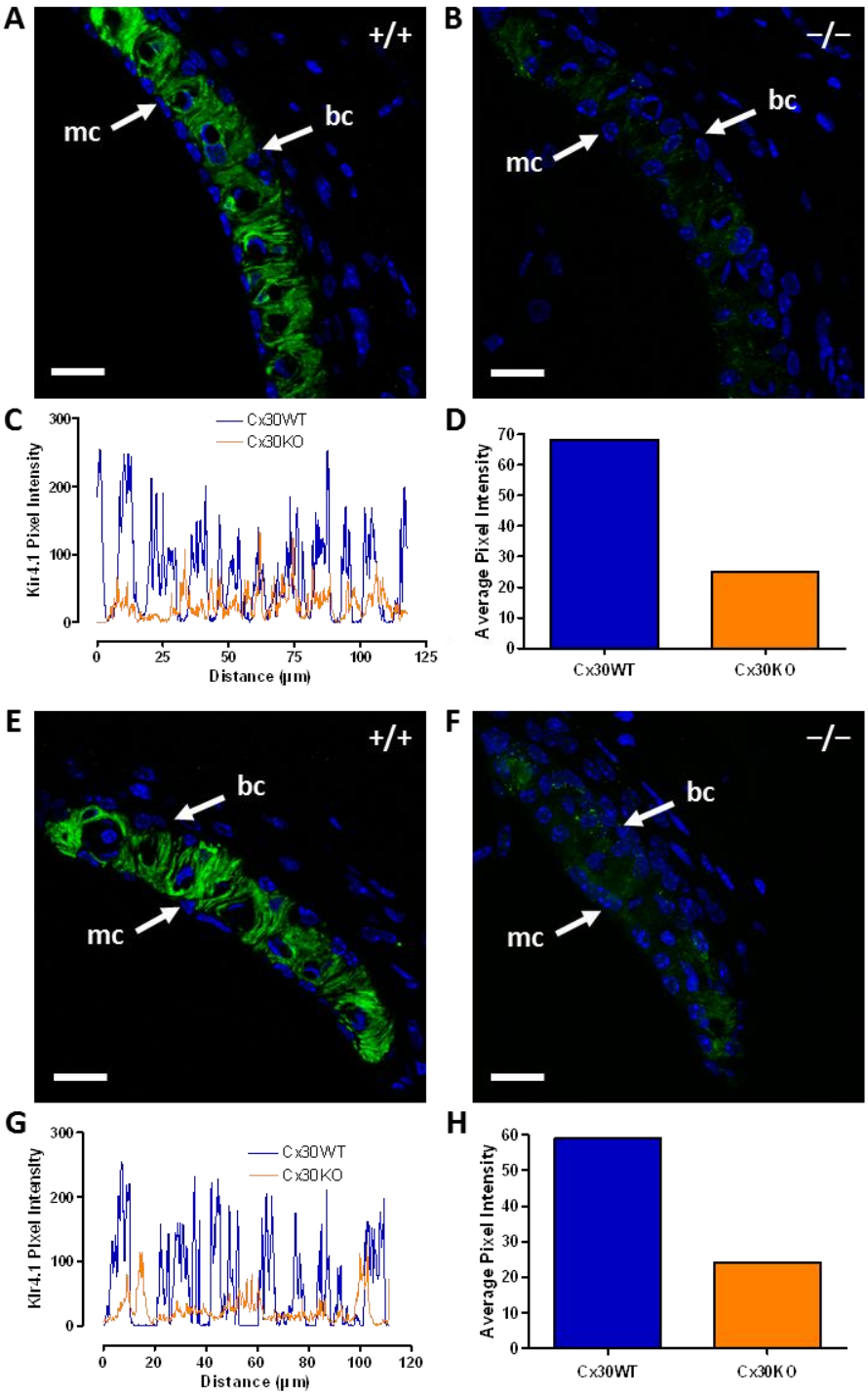

Figure 5-4. Reduced Kir4.1 protein expression in Cx30$^{-/-}$ (KO) mice.

(A) Cryosection of the basal turn stria vascularis from a P42 Cx30$^{+/+}$ (WT) mouse stained for Kir4.1 (green). Nuclei were counter-stained with DAPI (blue). Kir4.1 was strongly expressed in intermediate cells located between marginal cells (mc) and basal cells (bc). (B) A P38 Cx30$^{-/-}$ cryosection showed a marked reduction of Kir4.1 protein in the basal turn stria vascularis. (C) A semi-quantitative pixel intensity profile of Kir4.1 fluorescence plotted along the length of stria vascularis shows a strong reduction of Kir4.1 in the Cx30$^{-/-}$ mouse, confirmed also by the total average pixel intensity signal (D). Apical turns from Cx30$^{+/+}$ (E) and Cx30$^{-/-}$ (F) cryosections also show a strong reduction in Kir4.1 expression. Pixel intensity plot (G) and average pixel intensity (H) both confirm the reduction of Kir4.1. All settings were kept the same for each experiment. Scale bars, 20 µm.

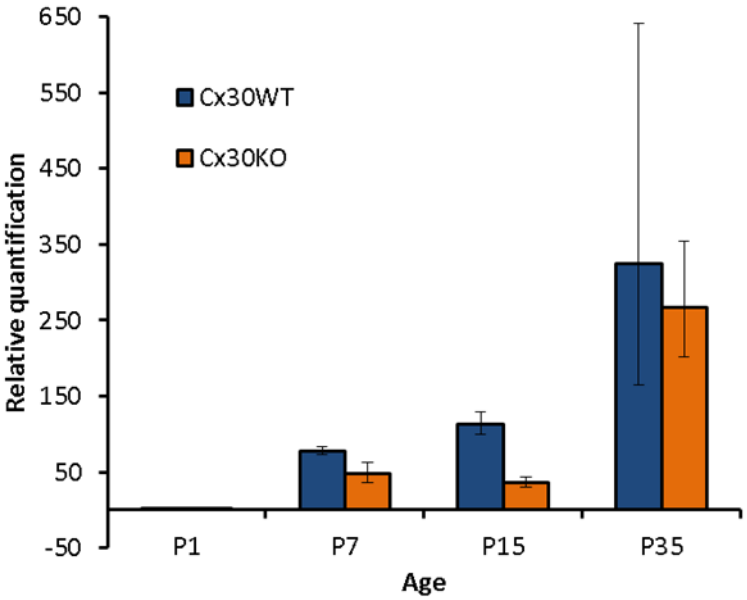

Figure 5-5. Reduction of Kir4.1 mRNA in Cx30$^{-/-}$ strial tissue.

Total mRNA was isolated from strips of stria vascularis from wild-type and Cx30$^{-/-}$ (KO) mice at the ages listed. At P1 expression of Kir4.1 was virtually absent, and was used as the calibrator. Expression increased from P7 up to P35 in wild-type mice (blue bars). In comparison, Cx30$^{-/-}$ mice of equivalent age had decreased levels of mRNA (orange bars), which was more pronounced at P15. For all experiments 18S rRNA was used as an endogenous control. Error bars represent 95% confidence intervals. These data are preliminary and represent data from one individual animal for each genotype and age, therefore statistical analyses were not performed.

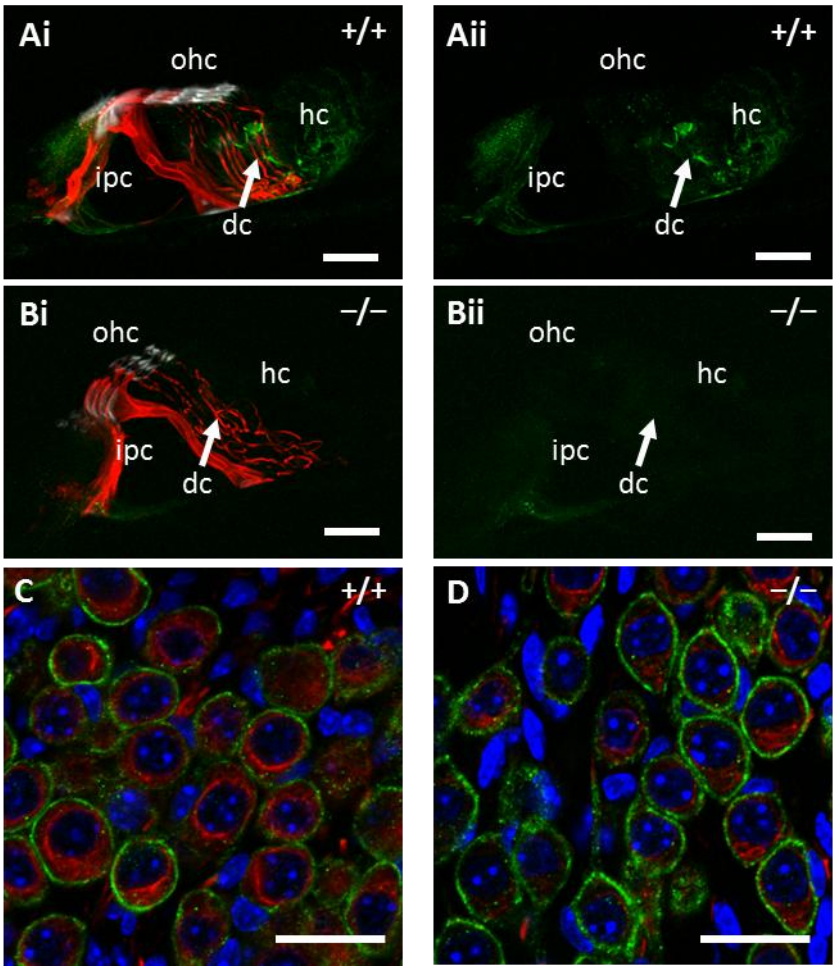

Figure 5-6. Reduced Kir4.1 expression in $Cx30^{-/-}$ supporting cells.

(Ai,ii) A confocal projection (18.5 µm depth) of a mid-turn organ of Corti from the same $Cx30^{+/+}$ cochlear cryosection as in Figure 5-4. The section was labelled for Kir4.1 (green), acetylated tubulin (red) and actin (white). Kir4.1 was detected in Deiters' cells (dc), pillar cells (pc) and Hensen's cells (hc) in the wild-type animal. The actin-rich stereocilia of outer hair cells (ohc) are also labelled. (Bi,ii) Kir4.1 was strongly reduced in the $Cx30^{-/-}$ mid-turn organ of Corti (18.5 µm projection). Expression was only detectable in the inner pillar cells and not in Deiters' cells or Hensen's cells. (C) Control image from the same wild-type cryosection showing normal Kir4.1 expression in spiral ganglion satellite cells (green). Nuclei were counter-stained with DAPI (blue). (D) Kir4.1 levels in $Cx30^{-/-}$ satellite cells were comparable to those of the wild-type. Scale bars, 20 µm.

5.2.2.2 Normal expression of other strial cell markers

Since $K_{ir}4.1$ expression was reduced in *Cx30*$^{-/-}$ mice, it was important to determine whether any other components of the EP generating machinery were affected. An immunofluorescence-labelling study was performed on adult *Cx30*$^{+/+}$ and *Cx30*$^{-/-}$ cryosections. Marginal cell proteins involved in K^+ transport were analysed. NKCC1, a Na^+-K^+-Cl^- co-transporter (Figure 5-7A) and Na^+-K^+-ATPase (Figure 5-7B) labelled the numerous in-foldings of marginal cell basolateral membranes. KCNQ1, a component of the KCNQ1/KCNE1 potassium channel important for pumping K^+ into endolymph, was expressed at the apical surface of marginal cells (Figure 5-7C). In comparison, expression of NKCC1 (Figure 5-7D), Na^+-K^+-ATPase (Figure 5-7E) and KCNQ1 (Figure 5-7F) were comparable in *Cx30*$^{-/-}$ mice. This suggests that even though marginal cell nuclei appeared atypical, expression of certain EP generating components appeared normal. Immunofluorescence analysis of other ion channels known to be expressed in marginal cells, including the Cl^- channel Barttin and H^+-K^+-ATPase have yet to be tested, although normal expression of the latter has been shown in a separate study (Cohen-Salmon et al., 2007).

Proteins normally expressed in the basal cell layer were also investigated. The tight-junction protein Claudin-11 (Figure 5-7G), glucose transporter-1 GLUT-1 (Figure 5-7H) and Cx26 (Figure 5-7I) were all expressed in *Cx30*$^{+/+}$ basal cells. Claudin-11 is the only known member of the claudin family found in the basal cell layer and is essential for stria vascularis integrity. Loss of claudin-11 in genetically engineered mice results in a loss of EP (Gow et al., 2004). In *Cx30*$^{-/-}$ mice, claudin-11 was expressed in a similar fashion to that of *Cx30*$^{+/+}$ mice (Figure 5-7J), suggesting that the basal cell tight-junction barrier is intact. GLUT-1 is an important glucose transporter in stria vascularis and is expressed in endothelial cells as well as basal cells (Ando et al., 2008). Comparable immunofluorescence-labelling was seen between *Cx30*$^{+/+}$ and *Cx30*$^{-/-}$ stria vascularis (Figure 5-7K). Finally, it is known that gap junctions are present between adjacent basal cells, between basal cells and intermediate cells and between basal cells and fibrocytes (Forge, 1984). Comparable expression patterns of Cx26 were apparent in *Cx30*$^{-/-}$ mice (Figure 5-7L), indicating that the basal layer is coupled to the underlying spiral ligament. Together, these data suggest that most of the proteins involved in generating the EP are normal in *Cx30*$^{-/-}$ mice, and from the markers tested, only $K_{ir}4.1$ expression is altered.

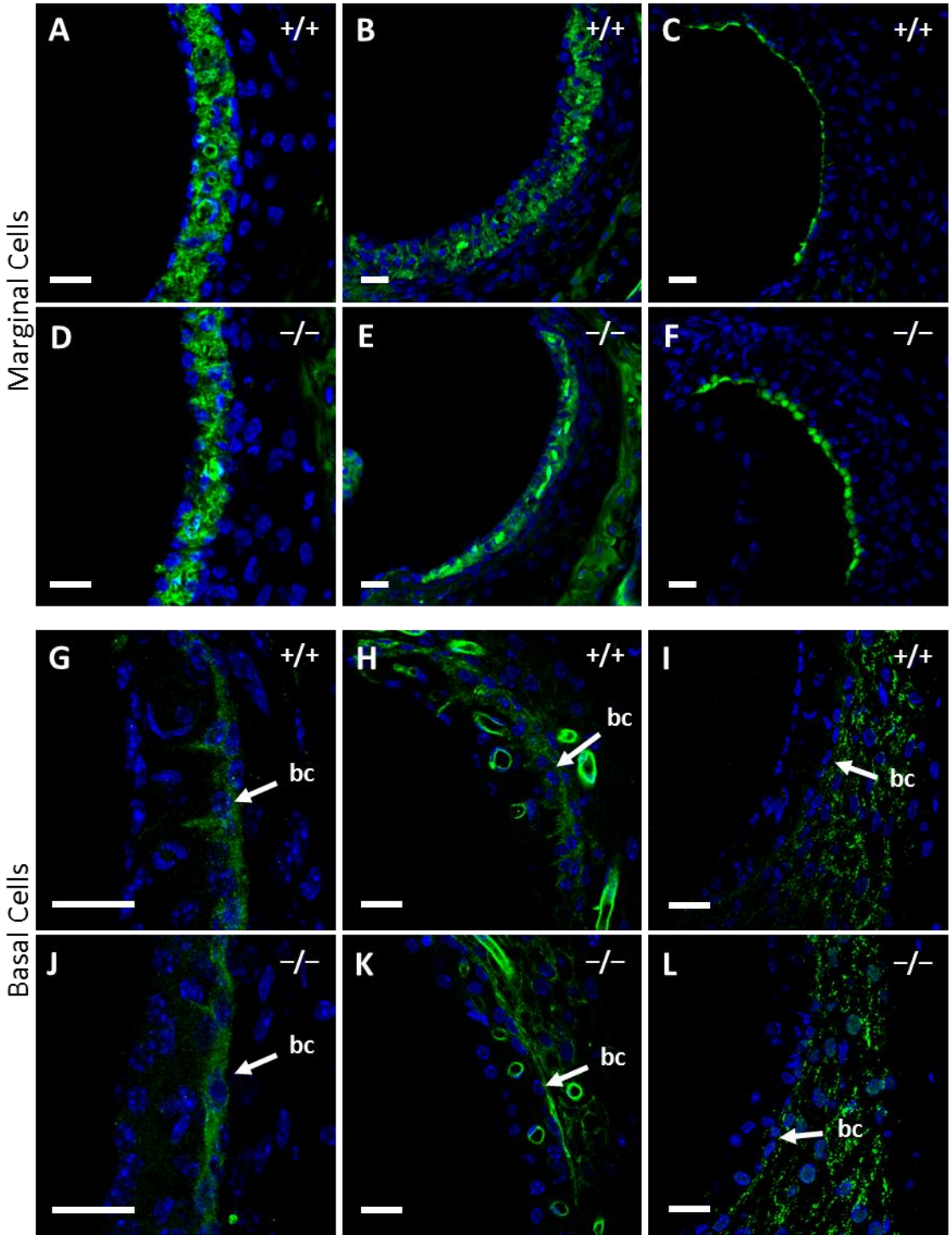

Figure 5-7. Normal expression of marginal and basal cell markers in Cx30$^{-/-}$ mice.

(A-F) Marginal cell proteins (green) were labelled with antibodies for NKCC1 (A,D), Na^{+}-K^{+}-ATPase (B,E) and KCNQ1 (C,F). Nuclei were counter-stained with DAPI (blue). Expression patterns were comparable between Cx30 wild-type (A-C, +/+) and knock-out (D-F, –/–) P38 animals. (G-L) Basal cell proteins (green) were labelled with antibodies for claudin-11 (G,J), GLUT-1 (H,K) and Cx26 (I,L). Protein expression was similar in Cx30$^{+/+}$ and Cx30$^{-/-}$ basal cells. Scale bars, 20 µm.

5.2.3 Endothelial barrier is unaffected in Cx30$^{-/-}$ mice

5.2.3.1 Tail-vein injection of a fluorescently-tagged bovine serum albumin conjugate

Disruption of the endothelial barrier of capillaries supplying the stria vascularis has been proposed as a mechanism for lack of EP development in *Cx30*$^{-/-}$ mice (Cohen-Salmon et al., 2007). Loss of the endothelial barrier would result in leakage of ions and proteins into the intrastrial space and would disrupt the specific properties of the electrically isolated intrastrial space. Disruption of the ionic composition and potential leakage would then cause an electric shunt and a complete loss of EP. However, endothelial cells in the stria vascularis do not express Cx26 or Cx30 (Cohen-Salmon et al., 2007). Therefore, the following question arises: how does loss of Cx30 cause disruption of the endothelial barrier? Firstly, to investigate whether capillaries were leaky in our *Cx30*$^{-/-}$ mice, a different approach to that of Cohen-Salmon et al. (2007) was implemented. Fluorescently tagged bovine serum albumin (BSA-FITC) was injected into the tail veins of both *Cx30*$^{+/+}$ and *Cx30*$^{-/-}$ mice. This protein is normally impermeant across the endothelial barrier and has been used elsewhere to investigate the leakiness of blood vessels in response to spinal cord injury (Cronin et al., 2008) and microvessel permeability in response to endothelin-1 (King-VanVlack et al., 2003). The potential for leakage of BSA-FITC into the intrastrial space was investigated.

Fixed cochleae were dissected and whole-mount strial tissue strips were analysed by confocal microscopy. A basal turn strip of tissue from an adult *Cx30*$^{+/+}$ mouse showed BSA-FITC fluorescence within the complex network of strial capillaries (**Figure 5-9**A). To detect whether BSA-FITC had leaked into the intrastrial space grey level intensities were plotted along a line profile (**Figure 5-9**B). The grey level peaks were sharp and corresponded well to each capillary intersected along the line profile. The intrastrial space between capillaries had no detectable amounts of BSA-FITC suggesting that the protein did not leak through the endothelial barrier in *Cx30*$^{+/+}$ mice. Equivalent images (**Figure 5-9**C) and grey level measurements (**Figure 5-9**D) in *Cx30*$^{-/-}$ mice were similar to those of *Cx30*$^{+/+}$. Grey levels were confined to capillaries, with no BSA-FITC detected in the intrastrial space. The images shown were taken from tissue fixed prior to dissection. In addition, live strial whole mounts were prepared from both *Cx30*$^{+/+}$ and *Cx30*$^{-/-}$ mice, which also showed labelling within capillaries and not

within the intrastrial space (data not shown). This confirmed that BSA-FITC was not washed out of the stria vascularis during the fixation step.

Cochlear cryosections were also prepared from BSA-FITC injected mice. BSA-FITC in a basal turn image was confined to the capillaries and was not detected in the intrastrial space of *Cx30*$^{+/+}$ mice (Figure 5-8Ai). The green channel was converted to a monochrome image (Figure 5-8Aii) and grey levels plotted along the width of the stria (Figure 5-8B). The fluorescent peaks corresponded well with the location of each capillary filled with BSA-FITC. In *Cx30*$^{-/-}$ mice, a similar pattern was found. BSA-FITC showed no signs of leakage into the intrastrial space (Figure 5-8Ci). A grey-scale image of BSA-FITC fluorescence and a line plot of pixel intensity confirmed a lack of fluorescence between capillaries (Figure 5-8Cii,D). If BSA-FITC was to leak into the intrastrial space, the profile peaks would be expected to appear broader and less sharp, indicating fluorescence between capillaries. However, this was not the case in any of the samples tested. These data suggest that the endothelial barrier is intact, and thus prevents leakage of fluorescently-tagged albumin into the intrastrial space.

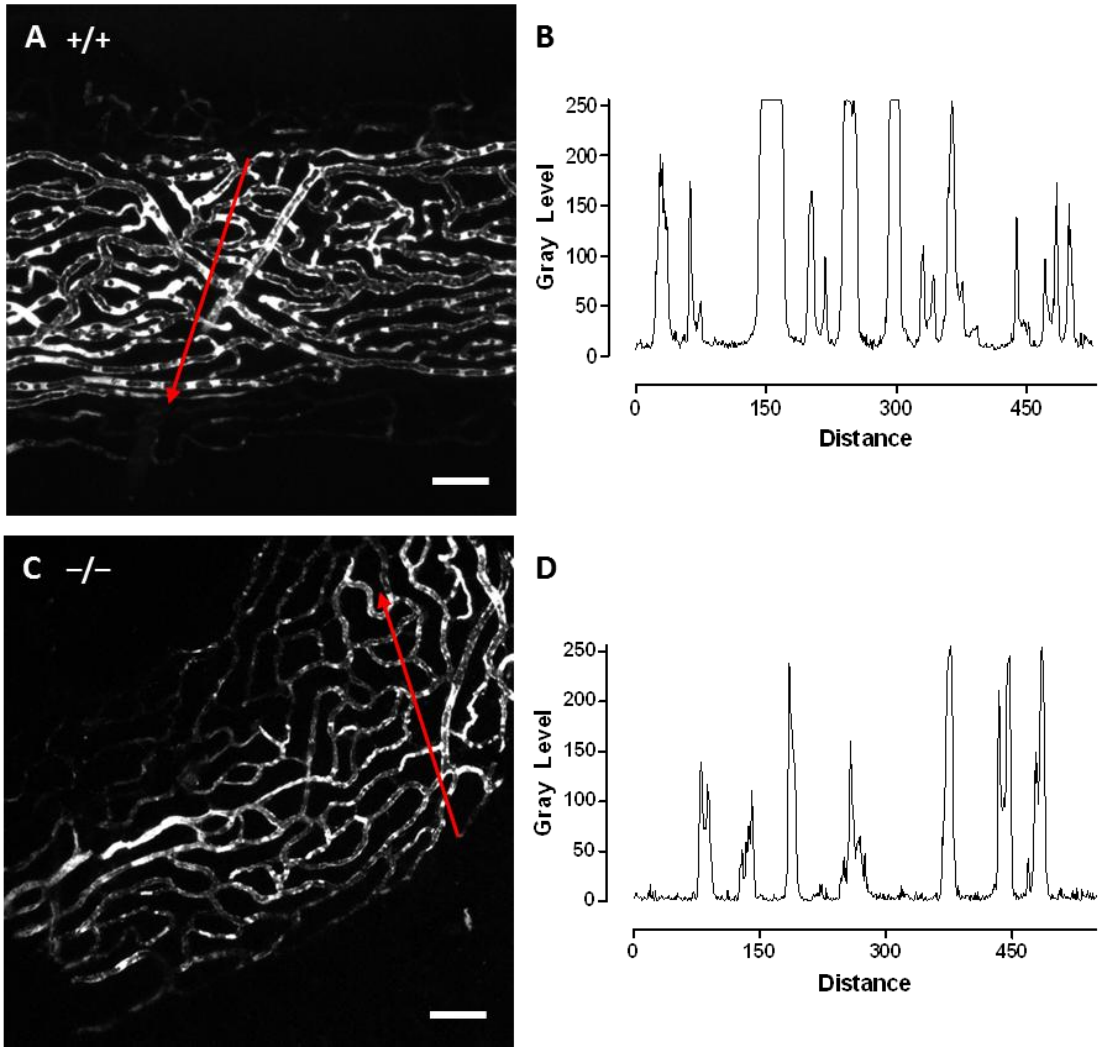

Figure 5-8. BSA-FITC is confined to capillaries in stria vascularis whole-mounts.

Adult mice were injected with BSA-FITC into the tail vein. Whole mounts of strial tissue were prepared post-fixation. Images are shown in monochrome format. (A) A face-on view of a basal turn coil from a $Cx30^{+/+}$ mouse. BSA-FITC (white) was strongly present within the capillary network. (B) Grey levels plotted from the red line in (A) reveal tall, sharp peaks corresponding to each capillary cross-section. There was no fluorescence in the intrastrial space. (C) Basal turn stria from a $Cx30^{-/-}$ mouse showed no obvious signs of leakage into the intrastrial space. (D) A line profile plot corresponding to (C) confirms that BSA-FITC was confined to strial capillaries. There was no detectable leakage into the intrastrial space. Grey levels were measured up to a maximum of 256 from an 8-bit image. Scale bars, 50 µm.

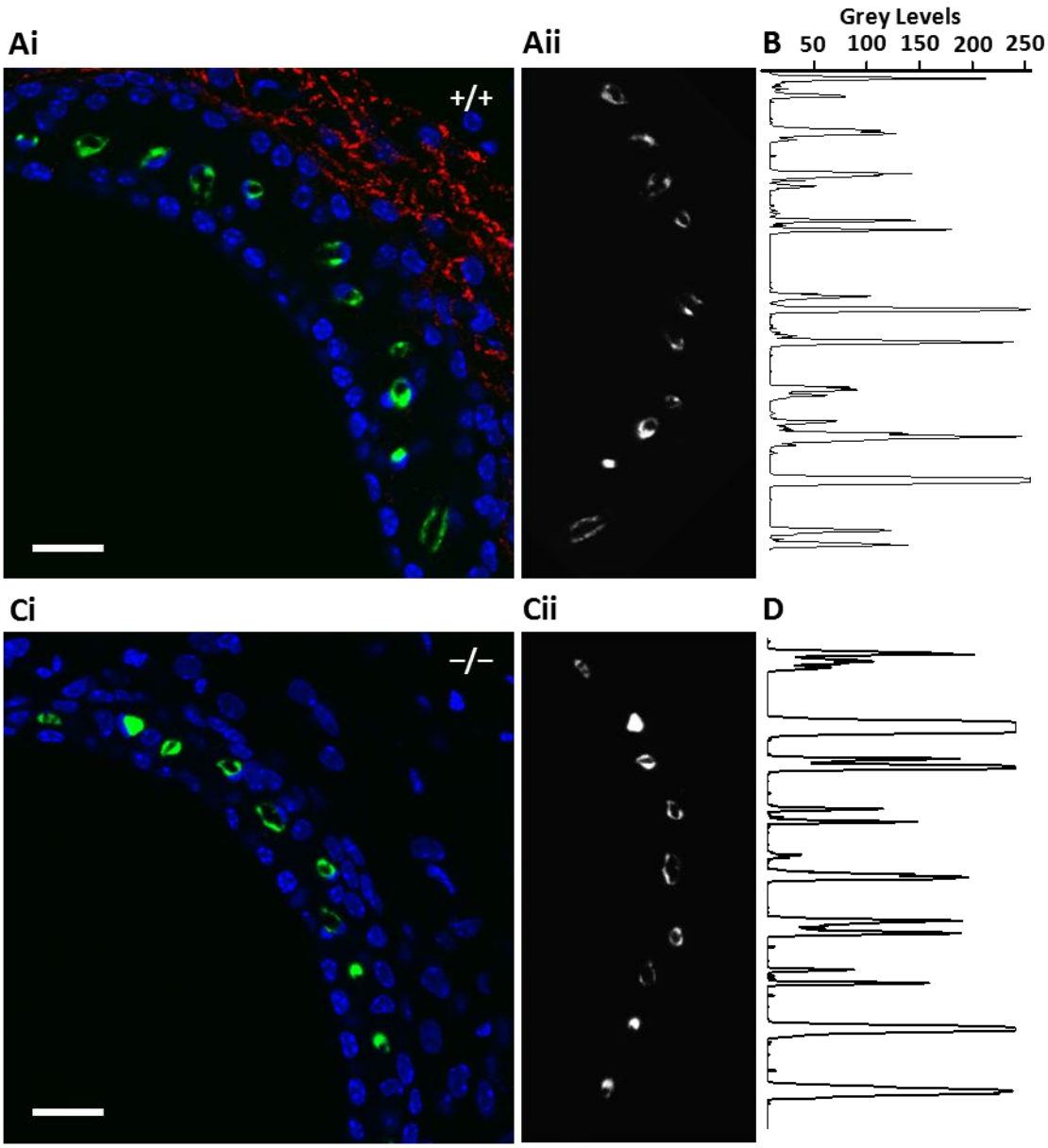

Figure 5-9. BSA-FITC is confined to capillaries and does not leak into the intrastrial space.

Cochlear cryosections were obtained from adult mice. Each mouse was injected with FITC-conjugated bovine serum albumin (BSA-FITC, green) into their tail vein. (Ai) A basal turn section from a wild-type (+/+) mouse labelled for Cx30 (red) and nuclei (blue). BSA-FITC was confined to the strial capillaries. To quantify, the BSA-FITC channel was converted into monochrome (Ai) and grey level intensity measured along a line profile passing through each capillary (B). Peaks correspond to each capillary. There was no detectable fluorescence between capillaries. (Ci) A $Cx30^{-/-}$ section, negative for Cx30 labelling (lack of red fluorescence), showed bright BSA-FITC fluorescence within strial capillaries. (Cii) Monochrome image used to detect grey levels (D) showed no leakage of BSA-FITC into the intrastrial space. Fluorescence was confined to sharp peaks corresponding to each capillary cross-section. Grey levels were measured up to a maximum of 256 from an 8-bit image. Scale bars, 20 µm.

5.2.3.2 Loop diuretic injection induces intrastrial oedema

The data presented here seem at odds with the results of Cohen-Salmon et al. (2007). Therefore, it was decided to assess strial blood vessel permeability from an additional approach. Adult *Cx30*$^{+/+}$ and *Cx30*$^{-/-}$ mice were treated with a loop diuretic (bumetanide) via intraperitoneal injection. Loop diuretics cause an acute swelling (oedema) within the intrastrial space (Santi and Duvall, III, 1979), by blocking the NKCC1 transporter found in the basolateral surface of marginal cells (Crouch et al., 1997; Azuma et al., 2002). Na^+ ions accumulate in the intrastrial space since NKCC1 is the only ion transporter responsible for Na^+ uptake into marginal cells (Wangemann and Schacht, 1996). The working hypothesis for this experiment suggests that if the endothelial barrier is intact, as it is in *Cx30*$^{+/+}$ mice, then ions will accumulate within the intrastrial space. In contrast, if the endothelial barrier is disrupted in *Cx30*$^{-/-}$ mice then ions and solutes would be able to dissipate into the vasculature, thus preventing an oedema.

TEM (prepared by G. Neville and A. Forge) images from a basal turn *Cx30*$^{+/+}$ mouse injected with a saline control, showed normal strial morphology (Figure 5-10A). The intrastrial space was not visible due to the tight compaction of marginal and intermediate cell processes. After treatment with bumetanide, numerous fluid-filled spaces (oedema) appeared within the stria vascularis (Figure 5-10B). TEM images from a basal turn *Cx30*$^{-/-}$ mouse showed characteristic morphologies such as a thinning of stria vascularis and abnormal marginal cell nuclei (Figure 5-10C), as reported above. Bumetanide injection into a *Cx30*$^{-/-}$ mouse also caused oedema in the intrastrial space (Figure 5-10D). Numerous fluid-filled spaces were apparent between marginal and intermediate cells. These data further suggest that the endothelial barrier is intact in the *Cx30*$^{-/-}$ mice.

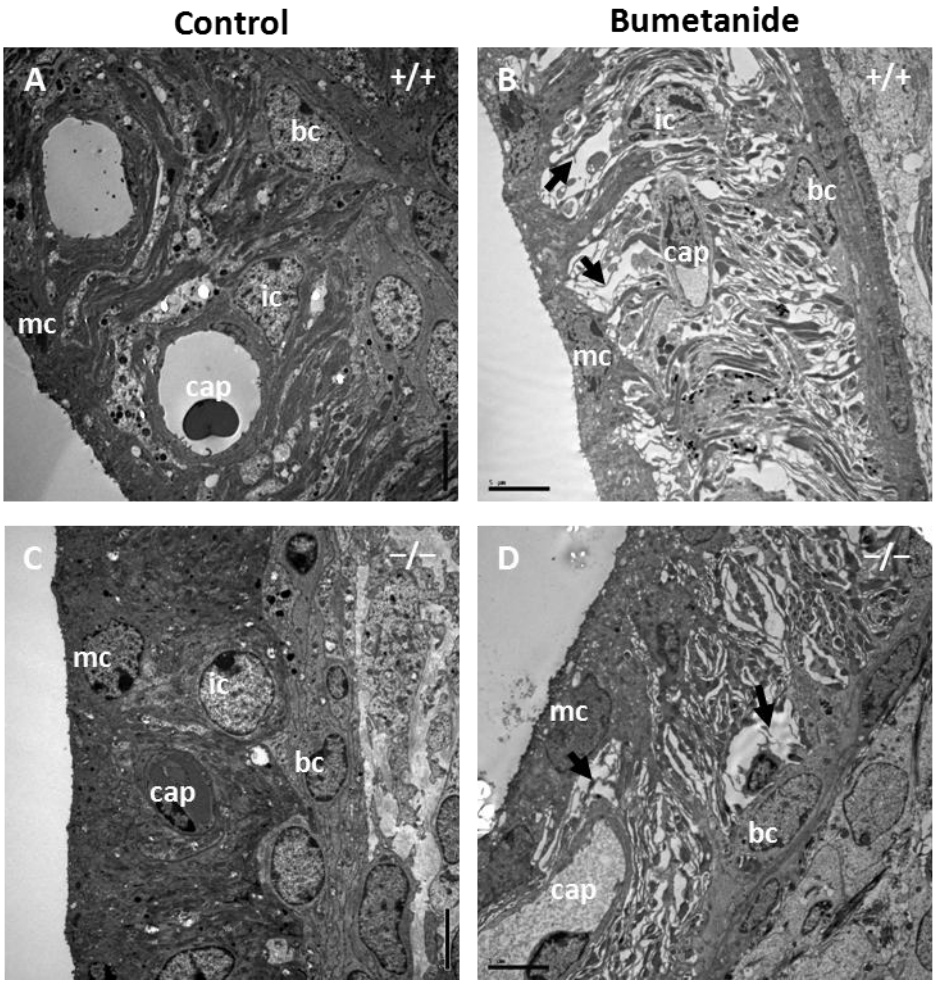

Figure 5-10. Loop diuretic injection causes intrastrial oedema in both $Cx30^{+/+}$ and $Cx30^{-/-}$ mice.

(A) TEM micrograph of basal turn stria vascularis from an adult $Cx30^{+/+}$ mouse. Projections from marginal cells (mc) and intermediate cells (ic) were interwoven and packed tightly within the intrastrial space and around capillaries (cap). bc, basal cells. (B) Intraperitoneal injection of a loop diuretic (bumetanide) caused oedema in the intrastrial space, noticeable as white spaces between marginal and intermediate cell processes (black arrows). (C) TEM micrograph of a $Cx30^{-/-}$ basal turn stria. Notice that the marginal cell nuclei are abnormal in shape and the strial compartment is thinner than the wild-type counterpart. (D) Administration of bumetanide also caused oedema within the intrastrial space in a similar fashion to wild-type (black arrows). Tissue preparation for EM imaging was carried out by G. Neville and A. Forge. Scale bars, 5 µm.

5.2.4 Disrupted epithelial repair in Cx30$^{-/-}$ mice

In addition to the abnormalities described in the stria vascularis, an unusual pathology of the sensory epithelium was observed in aged *Cx30*$^{-/-}$ mice. Supporting cells play a vital role in the repair and maintenance of the epithelium in response to hair cell death. In the organ of Corti, chronic aminoglycoside treatment causes the hair cell body to degenerate within the epithelium. In response, the supporting cells expand to close the space once occupied by the hair cell. During this process, an apical fragment of the hair cell is retained within the reticular lamina to maintain epithelial integrity. Only when supporting cells have expanded and formed new tight junctions is the apical fragment released into the *scala media*. This mechanism occurs through a controlled process that enables maintenance of the permeability barrier during structural reorganisation (Forge, 1985; McDowell et al., 1989; Raphael and Altschuler, 1991; Li et al., 1995; Ahmad et al., 2007).

The epithelial repair process in *Cx30*$^{-/-}$ mice appears to be defective, but still maintains an epithelial boundary. Cryosections of adult *Cx30*$^{-/-}$ cochleae showed a continuous epithelium of cells growing on the surface of the tectorial membrane from the attachment point after the third row of outer hair cells to the base of Reissner's membrane as early as P38 (Figure 5-11Ai-iii). By 8-months, the area below the ectopic epithelium was swollen and the majority of the organ of Corti was degenerated, except for the structure of inner and outer pillar cells. In addition, the epithelial cells surrounding the tectorial membrane expressed Cx26, whereas the rest of the outer sulcus supporting cell network had little discernable Cx26 labelling (Figure 5-11Bi-iii). Thin sections of older cochleae revealed a progressive pathological effect that worsens with age. A control section from a 15-month old *Cx30*$^{+/-}$ mouse showed a normal cochlear morphology with an intact tectorial membrane and supporting cell epithelium (Figure 5-11C). In contrast, an age-matched *Cx30*$^{-/-}$ section showed engulfment of the tectorial membrane, severe swelling and detachment of the supporting cell epithelium. Only the pillar cells remained attached to the basement membrane (Figure 5-11D). Additionally, a cochlear section from a 16-month old *Cx30*$^{-/-}$ mouse is shown as an example of a worsening phenotype (Figure 5-11E). The supporting cells appeared to scale Reissner's membrane, enclosing the tectorial membrane in a large cyst-like compartment. Again pillar cell remnants were left attached to the basement membrane.

These data suggest an important role for Cx30 in the maintenance of the sensory epithelium and in regulating repair after hair cell loss. In mice lacking Cx30 protein, it appears that the repair of the epithelium is abnormal, leads to engulfment of the tectorial membrane and the formation of a cyst-like compartment within the extracellular space of supporting and organ of Corti cells.

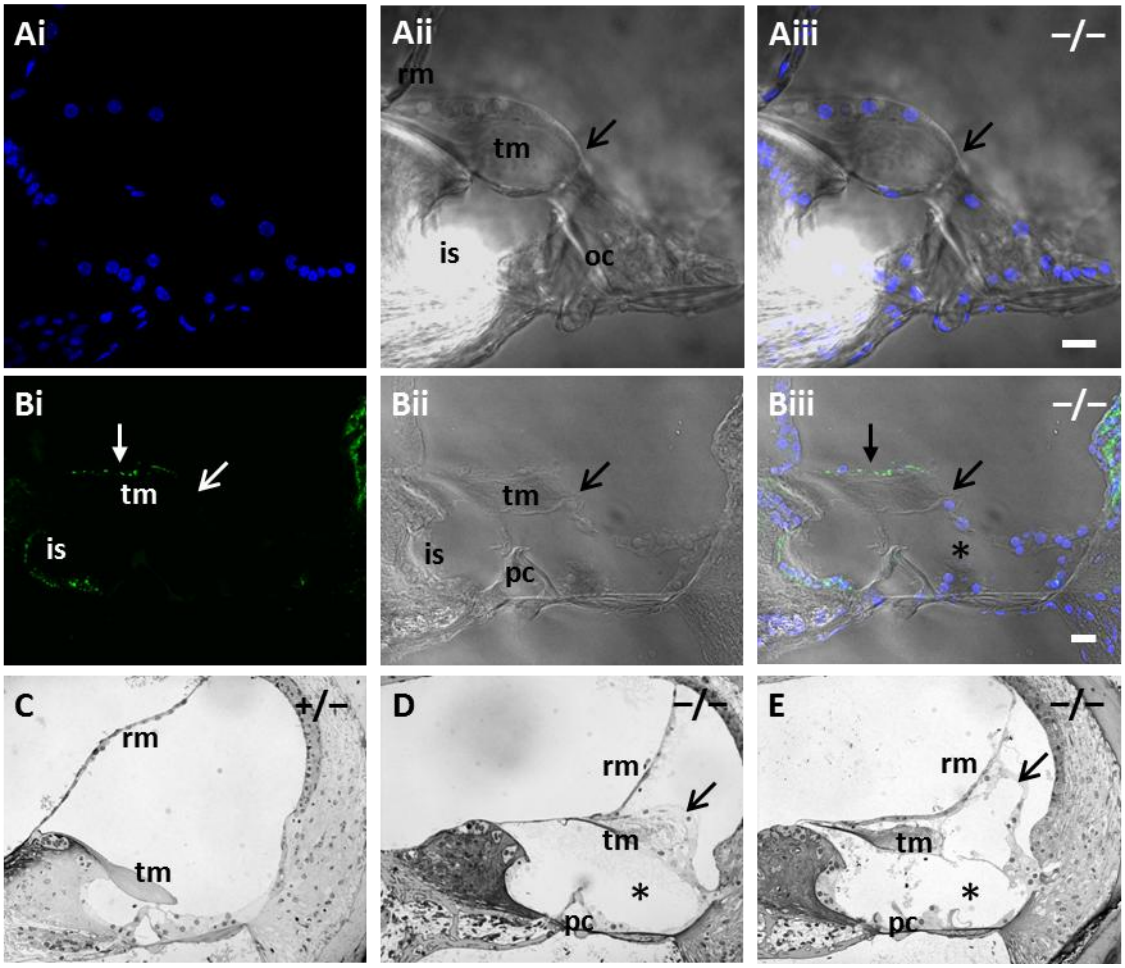

Figure 5-11. Degenerative response in the Cx30$^{-/-}$ organ of Corti.

Basal turn cochlear cryosections from P38 (A) and 8-month (B) old Cx30$^{-/-}$ mice. Basal turn thin sections from 15-month old Cx30$^{+/-}$ (C), 15-month old Cx30$^{-/-}$ (D) and 16-month old Cx30$^{-/-}$ (E) mice. (Ai) Nuclei were stained with DAPI (blue). (Aii) DIC image showing Reissner's membrane (rm), tectorial membrane (tm), inner sulcus (is) and organ of Corti (oc). (Aiii) Merged image showed an abnormal epithelial growth from the attachment point of tectorial membrane to organ of Corti (open arrow), over the tectorial membrane and towards the attachment point of Reissner's membrane. (Bi) Cryosection was immunolabelled for Cx26 (green). (Bii) Corresponding DIC image. (Biii) Merged image with DAPI (blue) channel showed a more severe epithelial pathology and a Cx26-expressing epithelium (closed arrow) had grown over the tectorial membrane (open arrow). In addition, the organ of Corti appeared degenerated, with only pillar cell (pc) remnants and a swelling of the extracellular space (asterisk). (C) A basal turn of a Cx30$^{+/-}$ mouse showed normal morphology and an intact tectorial membrane. (D) Abnormal epithelial growth (open arrow) and oedema (asterisk) in an age-matched Cx30$^{-/-}$ mouse. Pillar cell remnants were visible. (E) A Cx30$^{-/-}$ basal turn showed an even more severe phenotype. Epithelial cells appeared to have scaled the Reissner's membrane, enclosing the tectorial membrane and leaving pillar cell remnants. Scale bars, 20 µm.

5.3 Discussion

The data presented in this chapter indicates a disruption of homeostasis in the *Cx30*$^{-/-}$ stria vascularis. Thinning of the tissue, abnormal marginal cell nuclei and down-regulation of the potassium channel $K_{ir}4.1$ were apparent within the first week of hearing onset. Expression of other proteins important in the development and maintenance of EP were normal. In addition, and in contrast to a paper published by Cohen-Salmon et al. (2007), we found no evidence of capillary leakage in *Cx30*$^{-/-}$ stria vascularis. An abnormal pathology in the epithelial region of the organ of Corti was also found in aged *Cx30*$^{-/-}$ mice, which has not been reported previously. These differences and pathologies are discussed below.

5.3.1 Abnormalities in the stria vascularis of Cx30$^{-/-}$ *mice indicate retarded developmental*

5.3.1.1 Morphological differences in Cx30$^{-/-}$ *stria vascularis*

Thinning of stria vascularis has been shown in several cochlear pathologies and mutant mouse models. Taylor et al. (2008) have shown a thinning of stria in response to kanamycin-bumetanide treatment and suggest this is due to a reduction of marginal cell infoldings and apoptotic cell death (Taylor et al., 2008). This has also been shown for chronic aminoglycoside treatment (Forge et al., 1987) and with ageing (Spicer and Schulte, 2005). In addition, mouse (Steel and Barkway, 1989) and rat (Kitamura et al., 1994) models of deafness caused by melanocyte/intermediate cell defects have reduced or no EP and a thinner stria vascularis. A more recent study of a mouse model of secondary hypothyroidism has also demonstrated a thinning of stria vascularis, reduction of $K_{ir}4.1$ and reduced EP in mice (Mustapha et al., 2009). Thus, strial thinning and/or reduction in $K_{ir}4.1$ levels are associated with hearing loss.

During early stages of stria vascularis development, immature marginal cells are evident by the lack of processes projecting into the intrastrial space and by the rounded nuclei within the cell body. As marginal cells mature, basal projections gradually extend outwards into the intrastrial space and nuclei flatten at the apical surface (Steel and Barkway, 1989; Souter and Forge, 1998). Here, detailed analysis of the dimensions of marginal cell nuclei revealed a significant number in *Cx30*$^{-/-}$ animals were rounded in shape in comparison to flat or plano-concave nuclei in age-matched wild-types. This

phenotype suggests that marginal cells may not mature fully in the *Cx30*$^{-/-}$ mouse. Abnormal nuclei were noticed both in the younger (P17-P19) and older aged groups (P38-P51), yet cells expressed normal marginal cell proteins (including NKCC1, Na,K-ATPase and KCNQ1) in both genotypes. Marginal cells are not predicted to malfunction in *Cx30*$^{-/-}$ mice since the endolymphatic $[K^+]_{(e)}$ develops normally, and are unlikely to be responsible for the absence of EP. Further work, including measurements of strial cell numbers, volume fractions and fractions of unit area, determined by electron microscopy, would be useful for determining changes in cell structure (Forge et al., 1987).

5.3.1.2 Reduced K_{ir}4.1 expression and loss of EP

Data here suggests a reduction, though not complete loss of *Kir4.1* mRNA and protein in the stria vascularis. Since Kir4.1 channels are required for generating the high intrastrial potential across the intermediate cell membrane (Takeuchi et al., 2000), reduction in this protein may account for the lack of EP in *Cx30*$^{-/-}$ mice. Expression of K_{ir}4.1 in intermediate cells increases significantly at P7-P8 in mice and coincides with the onset and rise of EP (Hibino et al., 1997). Incidentally, $[K^+]_e$ has already reached adult levels by this stage (Bosher and Warren, 1971), indicating that the initial supply of K^+ required for development of endolymph may not be dependent on K_{ir}4.1. In the early stages of development (up to P7), marginal cells express the necessary K^+ transport proteins, such as Na^+-K^+-ATPase, to continuously transfer K^+ into endolymph (via KCNQ1/KCNE1 channels). Concurrently there is a steep rise in $[K^+]_e$. The source of K^+ for this process is predicted to be the perilymph (Marcus, 1986). Thus, in the early stages of development, marginal cells are comparable to vestibular dark cells, which are not part of an EP generating compartment and obtain K^+ from perilymph. The differences between marginal cells and dark cells arise when intermediate cells, capillaries and basal cells all migrate into position and undergo maturation to form a sealed compartment with marginal cells, consisting of tight junctions between basal cells and between endothelial cells. Tight junction formation between basal cells and between endothelial cells begins ~P7 and isolates the intrastrial space from perilymph and the lumen of capillaries – a process essential for EP generation (Souter and Forge, 1998). Consequently, the basal surfaces of marginal cells become isolated from perilymphatic fluid and are likely to require K^+ from an alternative source.

During the latter stages of cochlear development and once the high $[K^+]_e$ is reached around P7 (Bosher and Warren, 1971; Yamasaki et al., 2000), the EP is generated by expression of $K_{ir}4.1$ in intermediate cells (Hibino et al., 1997), sealing of basal cell tight junctions, and formation of gap junctions (Souter and Forge, 1998). These processes permit generation of the EP whilst also permitting K^+ recycling from the spiral ligament. In addition, $K_{ir}4.1$ channels now supply K^+ to marginal cells. Therefore, if the main source of K^+ in the adult mouse is from K^+ recycling via gap junctions and $K_{ir}4.1$ channels, then a reduction of $K_{ir}4.1$ in *Cx30*$^{-/-}$ mice can account for the lack of EP. This may also explain the reduction of $[K^+]_e$ in adult *Cx30*$^{-/-}$ mice, as described by Teubner et al. (2003). In agreement, *Kir4.1*$^{-/-}$ mice have a complete loss of EP and a partial, but not complete reduction in $[K^+]_e$ (Marcus et al., 2002).

The reason for a reduction of $K_{ir}4.1$ in *Cx30*$^{-/-}$ intermediate cells is not known. Recent studies have shown that mutation or loss of Cx30 leads to differences in the permselectivity of gap junction channels in the cochlea. In particular, one study (Chang et al., 2008) showed that intercellular transfer of a fluorescent, non-metabolizable D-glucose analogue (2-NBDG) was impaired in *Cx30*$^{-/-}$ mice. Similar decreases of glucose transfer were also seen with 1-octanol (a non-specific gap junction blocker). The authors suggest that functional Cx26/Cx30 gap junctions are required for efficient transfer of glucose from blood vessels into the supporting cell syncytium. In addition, the same study also showed that glucose deficiency resulted in an increase of reactive oxygen species (ROS) in *Cx30*$^{-/-}$ mice. Therefore, the loss of Cx30 might also affect the extent of glucose transfer between strial cells (basal and intermediate) that are coupled by gap junctions in *Cx30*$^{+/+}$ mice. As well as deficiencies in glucose transport, the metabolic coupling of second messengers involved in lateral wall development may be impaired. Ca^{2+} wave propagation or IP_3 transfer have not been investigated in lateral wall tissue. Therefore, it would be beneficial to investigate whether these signalling pathways are required for normal lateral wall development/reorganisation and whether these processes are altered in *Cx30*$^{-/-}$ mice.

There remains the possibility that intermediate cells are coupled by gap junctions to endothelial cells or pericytes in the stria vascularis (Takeuchi and Ando, 1998a), although this has been questioned by Cohen-Salmon et al. (2007) who did not find dye transfer between intermediate/basal cells and endothelial cells. If the former is true then Cx30 could have a role in forming gap junction channels between capillary

cells, which may be important for intermediate cell maturation and $K_{ir}4.1$ expression. If this is the case then it also raises the question as to why Cx26 cannot compensate for the loss of Cx30 in *Cx30*$^{-/-}$ mice. Both isoforms belong to the *beta* family of connexins and, as a result, would be expected to bind to similar connexin subtypes within the same family. One explanation could be that Cx30 has unique properties in respect to binding to an unknown connexin subtype in endothelial cells. These cells have been shown to express Cx45 with increasing expression from birth into adulthood (Cohen-Salmon et al. 2004). Whether Cx30 hemichannels could form heterotypic gap junctions with endothelial hemichannels such as Cx45 is unknown. This theory is unlikely, however, since both connexins belong to different connexin families (Cx45, *gamma*; Cx30, *beta*) and, to date, there is no evidence of cross-over between connexin families.

5.3.2 Endothelial barrier breakage theory

The differences seen here compared to the publication by Cohen-Salmon et al. (2007) could be due to differences in the experimental techniques used. Cohen-Salmon et al. detected IgG and albumin in the *Cx30*$^{-/-}$ stria vascularis with immuno-labelling after cardiac perfusion of PBS and 4% paraformaldehyde (PFA). It has been shown that the process of cardiac perfusion can cause an imbalance in the normal pressures within the vasculature, which may lead to tissue damage (Ohno et al., 2006). In particular, one study has shown leakage from blood vessels and variable albumin diffusion artefacts as a consequence of artificial perfusion pressures during fixation (Shi et al., 2011). Thus, the method of intracardiac perfusion used by Cohen-Salmon et al. (2007) may have led to a disruption of the endothelial barrier during the wash stage prior to fixation. Leakage of IgG and albumin into the extracellular space could have been directed by two factors during the perfusion-fixation step. Firstly, the change in normal capillary pressure may have damaged the endothelial barrier, thus enabling it to become leaky. Secondly, the continuous pumping of fluid, and likely high pressures incurred, may exacerbate the movement of both IgG and albumin through the damaged endothelial barrier into the intrastrial space prior to fixation. The differences seen between wild-type and *Cx30*$^{-/-}$ mice in the earlier study could be due to differences in perfusion-pressures between experiments and/or between different animals used. The same principle could also apply to the cardiac-perfused fixations used for EM processing, where the authors reported damage of endothelial cell tight junctions.

BSA-FITC injections into the vasculature have been used elsewhere to investigate blood vessel permeability (Cronin et al., 2008). This technique was applied here as an alternative method for investigating the theory of endothelial breakage in *Cx30*$^{-/-}$ mice. In the present study, the fixation (4% PFA) was carried out by gentle cochlea perfusion through the round/oval windows immediately after the animal's death followed by immersion in fixative for a further hour. Therefore, the pressure within strial capillaries was not altered in a way that might cause damage to the endothelial barrier. BSA-FITC was detected only within the capillaries of whole-mounts and cryosections of both genotypes. This would suggest that if BSA-FITC had leaked into the intrastrial space, it would have been readily detected. Additionally, live, unfixed strial tissue from mice injected with BSA-FITC showed bright fluorescence within strial capillaries, but not in the intrastrial space of either genotype (data not shown). Also, tight junctions between strial endothelial cells viewed by TEM were not disrupted in *Cx30*$^{-/-}$ mice (data from A. Forge, not shown).

The issue of capillary leakage was approached with a further alternative technique. Injection of a loop diuretic (Bumetanide) into normal mice has been shown to cause an oedema within the intrastrial space (Santi and Duvall, III, 1979), by blocking the function of marginal cell NKCC1 transporters. Oedema forms because the intrastrial compartment is structurally isolated from the lumen of blood vessels, perilymph and endolymph. If the endothelial barrier was disrupted in *Cx30*$^{-/-}$ mice it would be expected that the oedema would dissipate through the damaged blood vessel barrier and not accumulate in the intrastrial space. Results here demonstrate that oedema occurs in both *Cx30*$^{+/+}$ and *Cx30*$^{-/-}$ mice, adding further evidence for an intact endothelial barrier.

It is unclear in the publication by Cohen-Salmon et al. (2007) as to how gap junction dysfunction can result in damage to the endothelial barrier. They report high levels of homocysteine in *Cx30*$^{-/-}$ stria vascularis and suggest that this may cause endothelial damage. Cx26 and Cx30 are not expressed in strial endothelial cells. Therefore, the question arises as to how does the down-regulation of one connexin result in endothelial damage? The authors propose that Cx30 normally forms hemichannels (presumably in the intermediate or basal cell layers) and that a loss of Cx30 hemichannels may cause an osmotic imbalance, leading indirectly to an increase in homocysteine. These theories are somewhat ambiguous considering there has been

no evidence to suggest Cx30-hemichannels exist in the stria vascularis, and secondly, that Cx30-hemichannels should be closed under physiological conditions (Valiunas and Weingart, 2000). The authors do note however, that the mechanism requires further exploration. Results presented in this chapter argue against this mechanism as the cause of EP loss, and that further experiments are required to discover whether functional connexin hemichannels exist in the stria vascularis.

5.3.3 The epithelial barrier and repair in Cx30$^{-/-}$ mice

In unison with defects in the stria vascularis, it is conceivable that the loss of EP and death of hair cells are aided by a disrupted epithelial barrier separating perilymph from endolymph. Cx30 is known to be the predominant connexin expressed in Deiters' cells and is the only region in the cochlear duct where Cx26 does not significantly co-localise with Cx30 (Sun et al., 2005; Jagger and Forge, 2006). Studies here have identified an abnormal growth of epithelial cells from the Hensen's cell region to the Reissner's membrane attachment point. In conjunction with this abnormal pathological growth, which ensheathes the tectorial membrane and presents with swelling of the underlying epithelium, we found a reduction of $K_{ir}4.1$ expression in *Cx30*$^{-/-}$ Deiters' cells. Whether this reduction is a direct result of Cx30 loss or a secondary effect of hair cell loss and epithelial repair is currently unknown. It will be important to determine whether $K_{ir}4.1$ expression ever reaches mature levels in *Cx30*$^{-/-}$ Deiters' cells (i.e. at the age of hearing onset) or whether reduction of the potassium channel occurs before hair cell death, or as a consequence of hair cell death. Investigation of $K_{ir}4.1$ channel activity was attempted with the whole-cell patch clamp method. However, due to difficulties in obtaining intact Deiters' cells from aged cochleae and time constraints, these studies were unsuccessful. Work in our lab is on-going with regard to these queries.

The apparent down-regulation of Cx26 in outer sulcus supporting cells in older *Cx30*$^{-/-}$ animals suggests that Cx30 might have an important role in regulating the life cycle of Cx26 channels. This agrees with a previous report that showed ~3-fold reduction of Cx26 protein levels in *Cx30*$^{-/-}$ mice (Ahmad et al., 2007). The authors suggest that reduced availability of gap junctions may hinder the K^+ recycling pathway or intercellular movement of other molecules important for cell survival. This could also explain why the older *Cx30*$^{-/-}$ mice formed cyst-like compartments below the ectopic epithelium. A reduction of $K_{ir}4.1$ and lack of gap junction channels may result in an

accumulation of ions as a result of impaired homeostasis. In regard to this finding, future experiments will need to address whether the regulation of integrins, tight junction proteins, such as ZO-1, and other supporting cell markers important for cell adhesion and/or differentiation differ in the epithelium of *Cx30*$^{-/-}$ mice.

5.4 Conclusion

The data described in this chapter present novel mechanisms for deafness and lack of EP in the *Cx30*$^{-/-}$ mouse. Abnormalities including irregular shaped marginal cell nuclei, thinning of the stria vascularis and reduced expression of $K_{ir}4.1$ are most likely due to retarded development of the strial tissue. Marginal and basal cells expressed known protein markers important for EP generation, suggesting that the main developmental defect occurs within the intermediate cell. Although not shown in other *Cx30*$^{-/-}$ studies, these data suggest that Cx30 is important for stria vascularis maturation. In addition, an abnormal epithelial growth that encompass the tectorial membrane and leads to formation of cyst-like compartments has been identified in aged *Cx30*$^{-/-}$ mice, suggesting a role for Cx30 in epithelial repair. In contrast to a publication by Cohen-Salmon et al. (2007), capillary leakage in *Cx30*$^{-/-}$ stria was not observed here. This theory was investigated with two different approaches; injection of fluorescently-tagged BSA to visualise possible leakage and loop diuretic injection to induce oedema. Both techniques suggested that the *Cx30*$^{-/-}$ strial endothelial barrier was intact.

6 GENERAL DISCUSSION

This thesis has investigated the functions and properties of Cx26 and Cx30 using three experimental systems: *in vitro* studies to investigate the trafficking properties of Cx26 and Cx30; *in situ* studies to investigate GJIC during lateral wall development and *in vivo* studies to investigate the role of Cx30 in stria vascularis development. To fully understand the pathogenic effects of clinical connexin mutations, it is essential to elucidate the life-cycle, functions and properties of these proteins in cellular physiology. Since Kanno and Loewenstein first identified direct cell-to-cell communication over four decades ago (Kanno and Loewenstein, 1964a; Kanno and Loewenstein, 1964b), research in the field of connexins and gap junction biology has increased rapidly – and especially since connexin mutations were first associated with human disease. Gap junctions in the cochlea are predicted to play a role in electrical coupling, biochemical coupling, K^+ buffering and K^+ recycling. In addition, hemichannels are suggested to enable the release of second messengers required for organ of Corti development (Tritsch et al., 2007). In the mature cochlea, Cx26 and Cx30 are the predominant connexins expressed in the epithelial and connective tissue gap junction networks (Forge et al., 2003a). Mutations in these two subtypes account for most of the inherited cases of hearing loss, yet the exact mechanisms and functions underlying the disease phenotype are not clear.

6.1 Divergent Cx26 and Cx30 trafficking pathways: a mechanism for asymmetric coupling?

Gap junctions in cells engineered to express both Cx26 and Cx30 have different dye tracer permeabilities in comparison to those in cells expressing Cx26 (Marziano et al., 2003). In addition, gap junctions composed of Cx26/Cx30 heterotypic and/or heteromeric channels in organ of Corti supporting cells have electrically and chemically rectifying functions, which is proposed to lead to asymmetric current flow between supporting cells (Zhao and Santos-Sacchi, 2000; Zhao, 2000). This hypothesis is supported by selective dye transfer through medial and lateral compartments within the mature supporting cell syncytium (Jagger and Forge, 2006). This compartmentalisation is proposed to result from differential expression of Cx26/Cx30 heteromeric channels and Cx26 homotypic gap junctions in distinct regions of the supporting cell network. Therefore, the precise intermixing of connexins may be regulated so that

homotypic/heterotypic and/or heteromeric gap junctions are formed to direct current or biochemical intercellular transfer in a particular direction in the cochlea. Selective coupling has been shown to occur in other systems, such as glial cells of the central nervous system, which feature heterotypic gap junctions between different cell types (e.g. astrocytes and oligodendrocytes). These cell types express different connexin subtypes and it is this complexity that is thought to enable asymmetric coupling (Zahs, 1998).

Most of the cells within the epithelial and connective tissue gap junction networks of the cochlea express both Cx26 and Cx30. Therefore, intracellular regulatory mechanisms are likely required to produce specific heterotypic configurations for permselectivity and/or directional coupling. Regulating the trafficking pathways through specific organelles may be an evolutionary mechanism that permits or prevents connexin inter-mixing. Cx30 trafficking appears to be insensitive to the Golgi disrupting drug BFA, suggesting Cx30 can reach the plasma membrane independently of the Golgi apparatus. During the course of this study similar results have been reported elsewhere (Qu et al., 2009). These authors also suggest that Cx30 delivery and anchoring to the PM is dependent on actin, rather than microtubules. It is proposed that trafficking along actin cables could allow direct delivery of Cx30 from the endoplasmic reticulum to the PM.

There remains the possibility that Cx30 acts as a stabilising connexin, with an unusually long half-life at the PM. This seems unlikely though, since connexins generally have characteristically quick turn-over rates (Laird, 2006). However, data published elsewhere suggests that loss of Cx30 leads to unstable Cx26-containing gap junctions and an overall reduction in Cx26 protein (Ahmad et al., 2007). Cx30 could, therefore, act in the cochlea by exerting a longer half-life on Cx26 at the PM.

In the current study Cx26, in contrast to Cx30, was sensitive to BFA treatment, suggesting that it requires a functional Golgi apparatus for correct transport to the PM. In agreement with these data, a previous study has shown that Cx26 trafficking is dependent on a functional Golgi apparatus in transfected BICR-M1Rk cells (Thomas et al., 2005). In contrast, as discussed in chapter 3, Cx26 has also been suggested to traffic via a Golgi-independent pathway in transfected HeLa and COS-7 cells (Martin et al., 2001a). These conflicting results may represent direct examples of intracellular

regulation due to variability in conditions and cell types used. Regulation of Cx26 trafficking in cochlear cells deserves further study.

It is known that supporting cells and fibrocytes have intracellular mechanisms that permit both intermixing of Cx26 and Cx30 because heteromeric configurations have been detected using immunofluorescence co-localisation, immuno-gold labelling, co-immunoprecipitation, electrophysiology recordings, fluorescence resonance energy transfer (FRET) and dye permeability studies (Ahmad et al., 2003; Forge et al., 2003b; Jagger and Forge, 2006; Yum et al., 2007). Accordingly, separate trafficking pathways may also exist to prevent or reduce heteromeric connexon formation to maintain expression of some homotypic gap junctions. This novel mechanism could be similar to that of CD45 trafficking (as discussed in 3.1.2) which has been shown to occur both conventionally (through the Golgi) and non-conventionally (bypassing the Golgi) (Baldwin and Ostergaard, 2002).

6.2 Dye-coupling in the lateral wall supports a role for K^+ recycling

Data in this thesis has demonstrated compartmentalised GJIC in the lateral wall of rat cochlear slices as early as P2. From this stage onwards there is a rapid increase in connexin expression and gap-junctional coupling between type I, II and V fibrocytes. The connective tissue gap junction network appears to largely mature by P7, as shown by extensive dye spread throughout lateral wall fibrocytes and basal cells. In addition, intermediate cells are coupled to basal cells and are identifiable by $K_{ir}4.1$ expression at this stage (Hibino et al., 1997; Kelly et al., 2011). These data suggest that the connective tissue gap junction network matures several days in advance of hearing onset and is capable of re-circulating K^+ for secretion by intermediate cells as early as P7.

During earlier stages of development (from birth to P7), marginal cells are comparable to vestibular dark cells and continuously pump K^+ into endolymph. The source of K^+ during these early developmental stages and before strial maturation is predicted to be from perilymph (Marcus, 1986). However, it is also possible that compartmentalised regions of GJIC may act as a source of K^+ ions for marginal cells before formation of the sealed stria vascularis unit, which may coincide with a gradual increase of $K_{ir}4.1$ expression in developing intermediate cells. The temporal expression

of $K_{ir}4.1$ in developing intermediate cells requires further study to elucidate a role in providing K^+ to marginal cells in early developmental stages (<P7).

Once tight junctions begin to form between basal cells, and $K_{ir}4.1$ expression is upregulated (P7 onwards), EP generation advances to adult levels. At this stage, marginal cell access to perilymph is restricted and likely requires the gap junction network to provide a direct route of K^+ to intermediate cells. Our observations that the lateral wall GJIC pathway appears to largely mature by P7, and that intermediate cells are identifiable by Kir4.1 expression, both suggest that endolymphatic K^+ could be derived from the connective tissue gap junction network well in advance of hearing onset. Therefore, the lateral wall would be competent to receive and buffer K^+ derived from the supporting cells when that pathway is activated by air-borne sound (~P12). It would be beneficial to visualise these K^+ transport pathways in cochlear slices with K^+ sensitive dyes and/or K^+-selective electrodes, however these techniques are not yet available or are not yet precise enough to record such phenomena.

6.3 Cx30 is essential for cochlear physiology, strial maturation and EP generation

Recent studies and data in this thesis confirm that Cx26 and Cx30 are required for cochlear development and homeostasis and that the loss of one connexin cannot compensate for the other. Conditional Cx26 knockout and transgenic mice have impaired organ of Corti development in association with hair cell death (Inoshita et al., 2008; Sun et al., 2009; Wang et al., 2009). In contrast, Cx30-null mice appear to have normal organ of Corti development up to the age of hearing onset, but impaired stria vascularis and EP development. The changes described suggest a role for Cx30 in strial maturation and also K^+ recycling. Loss of Cx30 disrupts the normal expression of $K_{ir}4.1$ in intermediate cells and prevents generation of the EP (as measured by Teubner et al., 2003b).

Due to the extensive serial arrangement of gap junctions and the expression of K^+ transporters and channels in discrete regions of the cochlea, it is not surprising that a potassium recycling pathway is a popular hypothesis in cochlear physiology (Kikuchi et al., 2000; Wangemann, 2002; Hibino and Kurachi, 2006). However, some studies now suggest roles for gap junctions other than in K^+ recycling. One such study proposes that

lack of glucose and biochemical transport in *Cx30*$^{-/-}$ mice is the major cause of hearing loss (Chang et al., 2008). The authors suggest that there is no difference in the transjunctional whole-cell currents between Claudius/outer sulcus cells in *Cx30*$^{+/+}$ and *Cx30*$^{-/-}$ mice, which is understandable since any wild-type gap junction channel can pass K^+ ions and Cx26 homotypic channels are known to still exist in the absence of Cx30. Although the electrical coupling of Claudius/outer sulcus cells appears to be normal in *Cx30*$^{-/-}$ mice, the same cannot be said for Deiters' cells. Cx30 expression is dominant in these cells (Jagger and Forge, 2006) and only 5% of their gap junctions show Cx26 co-labelling (Sun et al., 2005). These authors did not carry out electrical recordings from this region; it will be important to determine whether the ionic coupling of Deiters' cells is different between *Cx30*$^{+/+}$ and *Cx30*$^{-/-}$ animals. A loss of Cx30 in these cell types may be detrimental to cochlear physiology and may explain the degeneration and swelling of the organ of Corti in aged *Cx30*$^{-/-}$ mice. K^+ buffering and recycling may be affected predominantly in Deiters' cells, which may lead to an accumulation of K^+ ions and homeostatic (e.g. osmolarity) deficits. The role of aquaporins in supporting cells during this process has not been investigated, but will be of interest for future studies.

One interesting question that arises from the study by Chang et al. (2008), is whether the permeability of glucose is determined by connexin subtype? The fluorescent glucose analogue (2-NBDG) used in that study has a molecular weight of 342 Da. This is only slightly larger than Neurobiotin^{TM} tracer (MW = 287 Da), which is known to permeate Cx26 and Cx30 homotypic, as well as heteromeric, gap junctions. Data suggests that in the absence of Cx30, 2-NBDG is less-permeable through remaining Cx26 homotypic gap junctions. It would be of interest to determine whether specific connexin subtypes regulate the permeability of glucose. Future studies could investigate 2-NBDG transfer in HeLa cells stably expressing Cx26 and/or Cx30 to determine their relative permeabilities.

Though evidence for functional Cx26/Cx30 gap junction channels in the regulation of biochemical transport now seems compelling (Beltramello et al., 2005), it does not rule out a parallel role in K^+ recycling. Biochemical coupling through gap junctions, or possibly hemichannels, may be essential for cochlear development and cell survival, but in addition, gap junctions are also likely to act both in a K^+ buffering and recycling syncytium. Transgenic mouse lines that specifically disrupt spiral ligament

fibrocytes support a K^+ recycling role for the connective tissue gap junction system. For example, deficiency of the transcription factor Brn-4 expression in type I, II, III and V fibrocytes leads to profound deafness and a dramatic reduction of EP (Minowa et al., 1999). Severe ultrastructural alterations and atrophy of fibrocytes, coupled with a reduction of Cx26 is proposed to disrupt GJIC specific to the lateral wall (Minowa et al., 1999; Xia et al., 2002). In addition, mice lacking Tbx18, a transcription factor expressed in mesenchymal fibrocytes, are profoundly deaf and do not have an EP. The authors propose that defective differentiation of fibrocytes, coupled with a resultant loss of Cx26 expression, interferes with strial generation and K^+ recycling through the connective tissue gap junction network (Trowe et al., 2008). However, direct evidence of K^+ flux through the epithelial and subsequently through the connective tissue gap junctions systems is lacking. Novel experimental techniques will be required to conclusively show a role for gap junctions in K^+ recycling.

7 REFERENCES

Abe,S., Usami,S., Shinkawa,H., Kelley,P.M., and Kimberling,W.J. (2000). Prevalent connexin 26 gene (GJB2) mutations in Japanese. *J. Med. Genet.* **37,** 41-43.

Ahmad,S., Chen,S., Sun,J., and Lin,X. (2003). Connexins 26 and 30 are co-assembled to form gap junctions in the cochlea of mice. *Biochem. Biophys. Res. Commun.* **307,** 362-368.

Ahmad,S., Diez,J.A., George,C.H., and Evans,W.H. (1999). Synthesis and assembly of connexins in vitro into homomeric and heteromeric functional gap junction hemichannels. *Biochem. J.* **339 (Pt 2),** 247-253.

Ahmad,S. and Evans,W.H. (2002). Post-translational integration and oligomerization of connexin 26 in plasma membranes and evidence of formation of membrane pores: implications for the assembly of gap junctions. *Biochem. J.* **365,** 693-699.

Ahmad,S., Tang,W., Chang,Q., Qu,Y., Hibshman,J., Li,Y., Sohl,G., Willecke,K., Chen,P., and Lin,X. (2007). Restoration of connexin26 protein level in the cochlea completely rescues hearing in a mouse model of human connexin30-linked deafness. *Proc. Natl. Acad. Sci. U. S. A* **104,** 1337-1341.

Alberts,B., Bray,D., Lewis,J., Raff,M., Roberts,K., and Watson,J.D. (1994). From Single Cells to Multicellular Organisms. In *Molecular Biology of the Cell*. New York: Garland Science.

Alexander,D.B. and Goldberg,G.S. (2003). Transfer of biologically important molecules between cells through gap junction channels. *Curr. Med. Chem.* **10,** 2045-2058.

Ando,M., Edamatsu,M., Fukuizumi,S., and Takeuchi,S. (2008). Cellular localization of facilitated glucose transporter 1 (GLUT-1) in the cochlear stria vascularis: its possible contribution to the transcellular glucose pathway. *Cell Tissue Res.* **331,** 763-769.

Ando,M. and Takeuchi,S. (1999). Immunological identification of an inward rectifier K+ channel (Kir4.1) in the intermediate cell (melanocyte) of the cochlear stria vascularis of gerbils and rats. *Cell Tissue Res.* **298,** 179-183.

Anselmi,F., Hernandez,V.H., Crispino,G., Seydel,A., Ortolano,S., Roper,S.D., Kessaris,N., Richardson,W., Rickheit,G., Filippov,M.A. et al. (2008). ATP release through connexin hemichannels and gap junction transfer of second messengers propagate Ca2+ signals across the inner ear. *Proc. Natl. Acad. Sci. U. S. A* **105,** 18770-18775.

Ashmore,J.F. (1987). A fast motile response in guinea-pig outer hair cells: the cellular basis of the cochlear amplifier. *J. Physiol* **388,** 323-347.

Azuma,H., Takeuchi,S., Higashiyama,K., Ando,M., Kakigi,A., Nakahira,M., Yamakawa,K., and Takeda,T. (2002). Bumetanide-induced enlargement of the intercellular space in the stria vascularis requires an active Na+-K+-ATPase. *Acta Otolaryngol.* **122,** 816-821.

Baldwin,T.A. and Ostergaard,H.L. (2002). The protein-tyrosine phosphatase CD45 reaches the cell surface via golgi-dependent and -independent pathways. *J. Biol. Chem.* **277,** 50333-50340.

Barbe,M.T., Monyer,H., and Bruzzone,R. (2006). Cell-cell communication beyond connexins: the pannexin channels. *Physiology. (Bethesda.)* **21,** 103-114.

Beardslee,M.A., Laing,J.G., Beyer,E.C., and Saffitz,J.E. (1998). Rapid turnover of connexin43 in the adult rat heart. *Circ. Res.* **83,** 629-635.

Beltramello,M., Bicego,M., Piazza,V., Ciubotaru,C.D., Mammano,F., and D'Andrea,P. (2003). Permeability and gating properties of human connexins 26 and 30 expressed in HeLa cells. *Biochem. Biophys. Res. Commun.* **305,** 1024-1033.

Beltramello,M., Piazza,V., Bukauskas,F.F., Pozzan,T., and Mammano,F. (2005). Impaired permeability to Ins(1,4,5)P3 in a mutant connexin underlies recessive hereditary deafness. *Nat. Cell Biol.* **7,** 63-69.

Benedetti,E.L. and Emmelot,P. (1965). Electron microscopic observations on negatively stained plasma membranes isolated from rat liver. *J. Cell Biol.* **26,** 299-305.

Bergoffen,J., Scherer,S.S., Wang,S., Scott,M.O., Bone,L.J., Paul,D.L., Chen,K., Lensch,M.W., Chance,P.F., and Fischbeck,K.H. (1993). Connexin mutations in X-linked Charcot-Marie-Tooth disease. *Science* **262,** 2039-2042.

Beurg,M., Fettiplace,R., Nam,J.H., and Ricci,A.J. (2009). Localization of inner hair cell mechanotransducer channels using high-speed calcium imaging. *Nat. Neurosci.* **12,** 553-558.

Beyer,E.C. and Berthoud,V.M. (2009). The family of connexin genes. In *Connexins: A guide*. (ed. Harris,A.L. and Locke,D.), pp. 3-26. New York: Humana Press.

Bitner-Glindzicz,M. (2002). Hereditary deafness and phenotyping in humans. *Br. Med. Bull.* **63,** 73-94.

Boettger,T., Hubner,C.A., Maier,H., Rust,M.B., Beck,F.X., and Jentsch,T.J. (2002). Deafness and renal tubular acidosis in mice lacking the K-Cl co-transporter Kcc4. *Nature* **416,** 874-878.

Boettger,T., Rust,M.B., Maier,H., Seidenbecher,T., Schweizer,M., Keating,D.J., Faulhaber,J., Ehmke,H., Pfeffer,C., Scheel,O. et al. (2003). Loss of K-Cl co-transporter KCC3 causes deafness, neurodegeneration and reduced seizure threshold. *EMBO J.* **22,** 5422-5434.

Bok,D., Galbraith,G., Lopez,I., Woodruff,M., Nusinowitz,S., BeltrandelRio,H., Huang,W., Zhao,S., Geske,R., Montgomery,C. et al. (2003). Blindness and auditory

impairment caused by loss of the sodium bicarbonate cotransporter NBC3. *Nat. Genet.* **34,** 313-319.

Bosher,S.K. and Warren,R.L. (1971). A study of the electrochemistry and osmotic relationships of the cochlear fluids in the neonatal rat at the time of the development of the endocochlear potential. *J. Physiol* **212,** 739-761.

Brobby,G.W., Muller-Myhsok,B., and Horstmann,R.D. (1998). Connexin 26 R143W mutation associated with recessive nonsyndromic sensorineural deafness in Africa. *N. Engl. J. Med.* **338,** 548-550.

Bruzzone,R. and Dermietzel,R. (2006). Structure and function of gap junctions in the developing brain. *Cell Tissue Res.* **326,** 239-248.

Bruzzone,R., White,T.W., and Paul,D.L. (1996). Connections with connexins: the molecular basis of direct intercellular signaling. *Eur. J. Biochem.* **238,** 1-27.

Cali,T., Galli,C., Olivari,S., and Molinari,M. (2008). Segregation and rapid turnover of EDEM1 by an autophagy-like mechanism modulates standard ERAD and folding activities. *Biochem. Biophys. Res. Commun.* **371,** 405-410.

Chalcroft,J.P. and Bullivant,S. (1970). An interpretation of liver cell membrane and junction structure based on observation of freeze-fracture replicas of both sides of the fracture. *J. Cell Biol.* **47,** 49-60.

Chang,Q., Tang,W., Ahmad,S., Stong,B., Leu,G., and Lin,X. (2009). Functional studies reveal new mechanisms for deafness caused by connexin mutations. *Otol. Neurotol.* **30,** 237-240.

Chang,Q., Tang,W., Ahmad,S., Zhou,B., and Lin,X. (2008). Gap junction mediated intercellular metabolite transfer in the cochlea is compromised in connexin30 null mice. *PLoS. One.* **3,** e4088.

Chittka,L. and Brockmann,A. (2005). Perception space--the final frontier. *PLoS. Biol.* **3,** e137.

Cohen-Salmon,M., Maxeiner,S., Kruger,O., Theis,M., Willecke,K., and Petit,C. (2004). Expression of the connexin43- and connexin45-encoding genes in the developing and mature mouse inner ear. *Cell Tissue Res.* **316,** 15-22.

Cohen-Salmon,M., Ott,T., Michel,V., Hardelin,J.P., Perfettini,I., Eybalin,M., Wu,T., Marcus,D.C., Wangemann,P., Willecke,K. et al. (2002). Targeted ablation of connexin26 in the inner ear epithelial gap junction network causes hearing impairment and cell death. *Curr. Biol.* **12,** 1106-1111.

Cohen-Salmon,M., Regnault,B., Cayet,N., Caille,D., Demuth,K., Hardelin,J.P., Janel,N., Meda,P., and Petit,C. (2007). Connexin30 deficiency causes instrastrial fluid-blood barrier disruption within the cochlear stria vascularis. *Proc. Natl. Acad. Sci. U. S. A* **104,** 6229-6234.

Common,J.E., Becker,D., Di,W.L., Leigh,I.M., O'Toole,E.A., and Kelsell,D.P. (2002). Functional studies of human skin disease- and deafness-associated connexin 30 mutations. *Biochem. Biophys. Res. Commun.* **298,** 651-656.

Common,J.E., Bitner-Glindzicz,M., O'Toole,E.A., Barnes,M.R., Jenkins,L., Forge,A., and Kelsell,D.P. (2005). Specific loss of connexin 26 expression in ductal sweat gland epithelium associated with the deletion mutation del(GJB6-D13S1830). *Clin. Exp. Dermatol.* **30,** 688-693.

Common,J.E., Di,W.L., Davies,D., and Kelsell,D.P. (2004). Further evidence for heterozygote advantage of GJB2 deafness mutations: a link with cell survival. *J. Med. Genet.* **41,** 573-575.

Cooper,D.N. and Barondes,S.H. (1990). Evidence for export of a muscle lectin from cytosol to extracellular matrix and for a novel secretory mechanism. *J. Cell Biol.* **110,** 1681-1691.

Cronin,M., Anderson,P.N., Cook,J.E., Green,C.R., and Becker,D.L. (2008). Blocking connexin43 expression reduces inflammation and improves functional recovery after spinal cord injury. *Mol. Cell Neurosci.* **39,** 152-160.

Crouch,J.J., Sakaguchi,N., Lytle,C., and Schulte,B.A. (1997). Immunohistochemical localization of the Na-K-Cl co-transporter (NKCC1) in the gerbil inner ear. *J. Histochem. Cytochem.* **45,** 773-778.

D'Souza,M., Miller,J., Mcgowan,K., Schneider,G.D., and Frisina,R. Connexin-26 Expression in the LLC-PK1-CL-4 Epithelial Cell Line. Association for Research in Otolaryngology. 17-2-2008. 17-2-2008.
Ref Type: Conference Proceeding

Dahl,G., Werner,R., Levine,E., and Rabadan-Diehl,C. (1992). Mutational analysis of gap junction formation. *Biophys. J.* **62,** 172-180.

Dallos,P. (1978). Cochlear Electrophysiology. In *Evoked Electrical Activity in the Auditory Nervous System*. (ed. Naunton,R.F. and Fernández,C.), pp. 141-150. New York: Academic Press.

Darrow,B.J., Laing,J.G., Lampe,P.D., Saffitz,J.E., and Beyer,E.C. (1995). Expression of multiple connexins in cultured neonatal rat ventricular myocytes. *Circ. Res.* **76,** 381-387.

Das,S., Smith,T.D., Sarma,J.D., Ritzenthaler,J.D., Maza,J., Kaplan,B.E., Cunningham,L.A., Suaud,L., Hubbard,M.J., Rubenstein,R.C. et al. (2009). ERp29 restricts Connexin43 oligomerization in the endoplasmic reticulum. *Mol. Biol. Cell* **20,** 2593-2604.

Davies,C., Tingley,D., Kachar,B., Wenthold,R.J., and Petralia,R.S. (2001). Distribution of members of the PSD-95 family of MAGUK proteins at the synaptic region of inner and outer hair cells of the guinea pig cochlea. *Synapse* **40,** 258-268.

De Mello,W.C. (1983). The influence of pH on the healing-over of mammalian cardiac muscle. *J. Physiol* **339,** 299-307.

del Castillo,F.J., Rodriguez-Ballesteros,M., Alvarez,A., Hutchin,T., Leonardi,E., de Oliveira,C.A., Azaiez,H., Brownstein,Z., Avenarius,M.R., Marlin,S. et al. (2005). A novel deletion involving the connexin-30 gene, del(GJB6-d13s1854), found in trans with mutations in the GJB2 gene (connexin-26) in subjects with DFNB1 non-syndromic hearing impairment. *J. Med. Genet.* **42,** 588-594.

del Castillo,I., Villamar,M., Moreno-Pelayo,M.A., del Castillo,F.J., Alvarez,A., Telleria,D., Menendez,I., and Moreno,F. (2002). A deletion involving the connexin 30 gene in nonsyndromic hearing impairment. *N. Engl. J. Med.* **346,** 243-249.

Denoyelle,F., Lina-Granade,G., Plauchu,H., Bruzzone,R., Chaib,H., Levi-Acobas,F., Weil,D., and Petit,C. (1998). Connexin 26 gene linked to a dominant deafness. *Nature* **393,** 319-320.

Denoyelle,F., Marlin,S., Weil,D., Moatti,L., Chauvin,P., Garabedian,E.N., and Petit,C. (1999). Clinical features of the prevalent form of childhood deafness, DFNB1, due to a connexin-26 gene defect: implications for genetic counselling. *Lancet* **353,** 1298-1303.

Di,W.L., Rugg,E.L., Leigh,I.M., and Kelsell,D.P. (2001). Multiple epidermal connexins are expressed in different keratinocyte subpopulations including connexin 31. *J. Invest Dermatol.* **117,** 958-964.

Diez,J.A., Ahmad,S., and Evans,W.H. (1999). Assembly of heteromeric connexons in guinea-pig liver en route to the Golgi apparatus, plasma membrane and gap junctions. *Eur. J. Biochem.* **262,** 142-148.

Dodson,K.M., Blanton,S.H., Welch,K.O., Norris,V.W., Nuzzo,R.L., Wegelin,J.A., Marin,R.S., Nance,W.E., Pandya,A., and Arnos,K.S. (2011). Vestibular dysfunction in DFNB1 deafness. *Am. J. Med. Genet. A* **155A,** 993-1000.

Eckert,R., Dunina-Barkovskaya,A., and Hulser,D.F. (1993). Biophysical characterization of gap-junction channels in HeLa cells. *Pflugers Arch.* **424,** 335-342.

Egan,M.E., Pearson,M., Weiner,S.A., Rajendran,V., Rubin,D., Glockner-Pagel,J., Canny,S., Du,K., Lukacs,G.L., and Caplan,M.J. (2004). Curcumin, a major constituent of turmeric, corrects cystic fibrosis defects. *Science* **304,** 600-602.

Eiberger,J., Kibschull,M., Strenzke,N., Schober,A., Bussow,H., Wessig,C., Djahed,S., Reucher,H., Koch,D.A., Lautermann,J. et al. (2006). Expression pattern and functional characterization of connexin29 in transgenic mice. *Glia* **53,** 601-611.

Elfgang,C., Eckert,R., Lichtenberg-Frate,H., Butterweck,A., Traub,O., Klein,R.A., Hulser,D.F., and Willecke,K. (1995). Specific permeability and selective formation of gap junction channels in connexin-transfected HeLa cells. *J. Cell Biol.* **129,** 805-817.

Essenfelder,G.M., Bruzzone,R., Lamartine,J., Charollais,A., Blanchet-Bardon,C., Barbe,M.T., Meda,P., and Waksman,G. (2004). Connexin30 mutations responsible for hidrotic ectodermal dysplasia cause abnormal hemichannel activity. *Hum. Mol. Genet.* **13,** 1703-1714.

Falk,M.M., Buehler,L.K., Kumar,N.M., and Gilula,N.B. (1997). Cell-free synthesis and assembly of connexins into functional gap junction membrane channels. *EMBO J.* **16,** 2703-2716.

Falk,M.M., Kumar,N.M., and Gilula,N.B. (1994). Membrane insertion of gap junction connexins: polytopic channel forming membrane proteins. *J. Cell Biol.* **127,** 343-355.

Fallon,R.F. and Goodenough,D.A. (1981). Five-hour half-life of mouse liver gap-junction protein. *J. Cell Biol.* **90,** 521-526.

Fatal,N., Karhinen,L., Jokitalo,E., and Makarow,M. (2004). Active and specific recruitment of a soluble cargo protein for endoplasmic reticulum exit in the absence of functional COPII component Sec24p. *J. Cell Sci.* **117,** 1665-1673.

Feldmann,D., Le,M.C., Jonard,L., Thierry,P., Czajka,C., Couderc,R., Ferec,C., Denoyelle,F., Marlin,S., and Fellmann,F. (2009). A new large deletion in the DFNB1 locus causes nonsyndromic hearing loss. *Eur. J. Med. Genet.* **52,** 195-200.

Fettiplace,R. and Ricci,A.J. (2006). Mechanoelectrical transduction in auditory hair cells. In *Vertebrate Hair Cells*. (ed. Eatock,R.A., Fay,R.R., and Popper,A.N.), pp. 154-203. New York: Springer.

Forge,A. (1984). Gap junctions in the stria vascularis and effects of ethacrynic acid. *Hear. Res.* **13,** 189-200.

Forge,A. (1985). Outer hair cell loss and supporting cell expansion following chronic gentamicin treatment. *Hear. Res.* **19,** 171-182.

Forge,A., Becker,D., Casalotti,S., Edwards,J., Marziano,N., and Nevill,G. (2003a). Gap junctions in the inner ear: comparison of distribution patterns in different vertebrates and assessement of connexin composition in mammals. *J. Comp Neurol.* **467,** 207-231.

Forge,A., Marziano,N.K., Casalotti,S.O., Becker,D.L., and Jagger,D. (2003b). The inner ear contains heteromeric channels composed of cx26 and cx30 and deafness-related mutations in cx26 have a dominant negative effect on cx30. *Cell Commun. Adhes.* **10,** 341-346.

Forge,A., Wright,A., and Davies,S.J. (1987). Analysis of structural changes in the stria vascularis following chronic gentamicin treatment. *Hear. Res.* **31,** 253-265.

Forge,A. and Wright,T. (2002). The molecular architecture of the inner ear. *Br. Med. Bull.* **63,** 5-24.

Franz,A., Maass,K., and Seedorf,M. (2007). A complex peptide-sorting signal, but no mRNA signal, is required for the Sec-independent transport of Ist2 from the yeast ER to the plasma membrane. *FEBS Lett.* **581,** 401-405.

Furness,D.N., Lawton,D.M., Mahendrasingam,S., Hodierne,L., and Jagger,D.J. (2009). Quantitative analysis of the expression of the glutamate-aspartate transporter

and identification of functional glutamate uptake reveal a role for cochlear fibrocytes in glutamate homeostasis. *Neuroscience* **162,** 1307-1321.

Furshpan,E.J. and Potter,D.D. (1959). Transmission at the giant motor synapses of the crayfish. *J. Physiol* **145,** 289-325.

Gabriel,H.D., Jung,D., Butzler,C., Temme,A., Traub,O., Winterhager,E., and Willecke,K. (1998). Transplacental uptake of glucose is decreased in embryonic lethal connexin26-deficient mice. *J. Cell Biol.* **140,** 1453-1461.

Gaietta,G., Deerinck,T.J., Adams,S.R., Bouwer,J., Tour,O., Laird,D.W., Sosinsky,G.E., Tsien,R.Y., and Ellisman,M.H. (2002). Multicolor and electron microscopic imaging of connexin trafficking. *Science* **296,** 503-507.

Gale,J.E., Piazza,V., Ciubotaru,C.D., and Mammano,F. (2004). A mechanism for sensing noise damage in the inner ear. *Curr. Biol.* **14,** 526-529.

Geleoc,G.S. and Holt,J.R. (2003). Auditory amplification: outer hair cells pres the issue. *Trends Neurosci.* **26,** 115-117.

George,C.H., Kendall,J.M., and Evans,W.H. (1999). Intracellular trafficking pathways in the assembly of connexins into gap junctions. *J. Biol. Chem.* **274,** 8678-8685.

Gillespie,P.G., Dumont,R.A., and Kachar,B. (2005). Have we found the tip link, transduction channel, and gating spring of the hair cell? *Curr. Opin. Neurobiol.* **15,** 389-396.

Goodenough,D.A. (1974). Bulk isolation of mouse hepatocyte gap junctions. Characterization of the principal protein, connexin. *J. Cell Biol.* **61,** 557-563.

Goodenough,D.A., Goliger,J.A., and Paul,D.L. (1996). Connexins, connexons, and intercellular communication. *Annu. Rev. Biochem.* **65,** 475-502.

Goodenough,D.A. and Revel,J.P. (1970). A fine structural analysis of intercellular junctions in the mouse liver. *J. Cell Biol.* **45,** 272-290.

Goodenough,D.A. and Stoeckenius,W. (1972). The isolation of mouse hepatocyte gap junctions. Preliminary chemical characterization and x-ray diffraction. *J. Cell Biol.* **54,** 646-656.

Gow,A., Davies,C., Southwood,C.M., Frolenkov,G., Chrustowski,M., Ng,L., Yamauchi,D., Marcus,D.C., and Kachar,B. (2004). Deafness in Claudin 11-null mice reveals the critical contribution of basal cell tight junctions to stria vascularis function. *J. Neurosci.* **24,** 7051-7062.

Gratton,M.A., Schulte,B.A., and Hazen-Martin,D.J. (1996). Characterization and development of an inner ear type I fibrocyte cell culture. *Hear. Res.* **99,** 71-78.

Grieve,AG. and Rabouille,C. (2011). Golgi bypass: skirting around the heart of classical secretion. *Cold Spring Harbor Perspectives in Biology* **3**.

Grifa,A., Wagner,C.A., D'Ambrosio,L., Melchionda,S., Bernardi,F., Lopez-Bigas,N., Rabionet,R., Arbones,M., Monica,M.D., Estivill,X. et al. (1999). Mutations in GJB6 cause nonsyndromic autosomal dominant deafness at DFNA3 locus. *Nat. Genet.* **23,** 16-18.

Griffiths,G., Fuller,S.D., Back,R., Hollinshead,M., Pfeiffer,S., and Simons,K. (1989). The dynamic nature of the Golgi complex. *J. Cell Biol.* **108,** 277-297.

Guggino,W.B. and Stanton,B.A. (2006). New insights into cystic fibrosis: molecular switches that regulate CFTR. *Nat. Rev. Mol. Cell Biol.* **7,** 426-436.

Guilford,P., Ben,A.S., Blanchard,S., Levilliers,J., Weissenbach,J., Belkahia,A., and Petit,C. (1994). A non-syndrome form of neurosensory, recessive deafness maps to the pericentromeric region of chromosome 13q. *Nat. Genet.* **6,** 24-28.

Gulley,R.L. and Reese,T.S. (1976). Intercellular junctions in the reticular lamina of the organ of Corti. *J. Neurocytol.* **5,** 479-507.

Harris,A.L. (2001). Emerging issues of connexin channels: biophysics fills the gap. *Q. Rev. Biophys.* **34,** 325-472.

Hasdemir,B., Fitzgerald,D.J., Prior,I.A., Tepikin,A.V., and Burgoyne,R.D. (2005). Traffic of Kv4 K+ channels mediated by KChIP1 is via a novel post-ER vesicular pathway. *J. Cell Biol.* **171,** 459-469.

Helms,J.B. and Rothman,J.E. (1992). Inhibition by brefeldin A of a Golgi membrane enzyme that catalyses exchange of guanine nucleotide bound to ARF. *Nature* **360,** 352-354.

Hequembourg,S. and Liberman,M.C. (2001). Spiral ligament pathology: a major aspect of age-related cochlear degeneration in C57BL/6 mice. *J. Assoc. Res. Otolaryngol.* **2,** 118-129.

Hibino,H., Higashi-Shingai,K., Fujita,A., Iwai,K., Ishii,M., and Kurachi,Y. (2004). Expression of an inwardly rectifying K+ channel, Kir5.1, in specific types of fibrocytes in the cochlear lateral wall suggests its functional importance in the establishment of endocochlear potential. *Eur. J. Neurosci.* **19,** 76-84.

Hibino,H., Horio,Y., Inanobe,A., Doi,K., Ito,M., Yamada,M., Gotow,T., Uchiyama,Y., Kawamura,M., Kubo,T. et al. (1997). An ATP-dependent inwardly rectifying potassium channel, KAB-2 (Kir4. 1), in cochlear stria vascularis of inner ear: its specific subcellular localization and correlation with the formation of endocochlear potential. *J. Neurosci.* **17,** 4711-4721.

Hibino,H. and Kurachi,Y. (2006). Molecular and physiological bases of the K+ circulation in the mammalian inner ear. *Physiology. (Bethesda.)* **21,** 336-345.

Hibino,H., Nin,F., Tsuzuki,C., and Kurachi,Y. (2010). How is the highly positive endocochlear potential formed? The specific architecture of the stria vascularis and the roles of the ion-transport apparatus. *Pflugers Arch.* **459,** 521-533.

Hoang,D.E., Ahmad,S., Chang,Q., Tang,W., Stong,B., and Lin,X. (2009). Diverse deafness mechanisms of connexin mutations revealed by studies using in vitro approaches and mouse models. *Brain Res.* **1277,** 52-69.

Hoh,J.H., Sosinsky,G.E., Revel,J.P., and Hansma,P.K. (1993). Structure of the extracellular surface of the gap junction by atomic force microscopy. *Biophys. J.* **65,** 149-163.

Hong,H.M., Yang,J.J., Shieh,J.C., Lin,M.L., and Li,S.Y. (2010). Novel mutations in the connexin43 (GJA1) and GJA1 pseudogene may contribute to nonsyndromic hearing loss. *Hum. Genet.* **127,** 545-551.

Inoshita,A., Iizuka,T., Okamura,H.O., Minekawa,A., Kojima,K., Furukawa,M., Kusunoki,T., and Ikeda,K. (2008). Postnatal development of the organ of Corti in dominant-negative Gjb2 transgenic mice. *Neuroscience* **156,** 1039-1047.

Ishii,M., Fujita,A., Iwai,K., Kusaka,S., Higashi,K., Inanobe,A., Hibino,H., and Kurachi,Y. (2003). Differential expression and distribution of Kir5.1 and Kir4.1 inwardly rectifying K+ channels in retina. *Am. J. Physiol Cell Physiol* **285,** C260-C267.

Iurato,S., Franke,K., Luciano,L., Wermbter,G., Pannese,E., and Reale,E. (1976). Intercellular junctions in the organ of Corti as revealed by freeze fracturing. *Acta Otolaryngol.* **82,** 57-69.

Jagger,D., Collin,G., Kelly,J., Towers,E., Nevill,G., Longo-Guess,C., Benson,J., Halsey,K., Dolan,D., Marshall,J. et al. (2011). Alstrom Syndrome protein ALMS1 localizes to basal bodies of cochlear hair cells and regulates cilium-dependent planar cell polarity. *Hum. Mol. Genet.* **20,** 466-481.

Jagger,D.J. and Forge,A. (2006). Compartmentalized and signal-selective gap junctional coupling in the hearing cochlea. *J. Neurosci.* **26,** 1260-1268.

Jagger,D.J., Nevill,G., and Forge,A. (2010). The Membrane Properties of Cochlear Root Cells are Consistent with Roles in Potassium Recirculation and Spatial Buffering. *J. Assoc. Res. Otolaryngol.*

Jagger,D.J., Robertson,D., and Housley,G.D. (2000). A technique for slicing the rat cochlea around the onset of hearing. *J. Neurosci. Methods* **104,** 77-86.

Jahnke,K. (1975). The fine structure of freeze-fractured intercellular junctions in the guinea pig inner ear. *Acta Otolaryngol. Suppl* **336,** 1-40.

Janecke,A.R., Hennies,H.C., Gunther,B., Gansl,G., Smolle,J., Messmer,E.M., Utermann,G., and Rittinger,O. (2005). GJB2 mutations in keratitis-ichthyosis-deafness syndrome including its fatal form. *Am. J. Med. Genet. A* **133A,** 128-131.

Jin,Z., Ulfendahl,M., and Jarlebark,L. (2008). Spatiotemporal loss of K+ transport proteins in the developing cochlear lateral wall of guinea pigs with hereditary deafness. *Eur. J. Neurosci.* **27,** 145-154.

John,S.A. and Revel,J.P. (1991). Connexon integrity is maintained by non-covalent bonds: intramolecular disulfide bonds link the extracellular domains in rat connexin-43. *Biochem. Biophys. Res. Commun.* **178,** 1312-1318.

Juschke,C., Ferring,D., Jansen,R.P., and Seedorf,M. (2004). A novel transport pathway for a yeast plasma membrane protein encoded by a localized mRNA. *Curr. Biol.* **14,** 406-411.

Kanno,Y. and Loewenstein,W.R. (1964a). INTERCELLULAR DIFFUSION. *Science* **143,** 959-960.

Kanno,Y. and Loewenstein,W.R. (1964b). LOW-RESISTANCE COUPLING BETWEEN GLAND CELLS. SOME OBSERVATIONS ON INTERCELLULAR CONTACT MEMBRANES AND INTERCELLULAR SPACE. *Nature* **201,** 194-195.

Kelly,J.J., Forge,A., and Jagger,D.J. (2011). Development of gap junctional intercellular communication within the lateral wall of the rat cochlea. *Neuroscience* **180,** 360-369.

Kelsell,D.P., Di,W.L., and Houseman,M.J. (2001). Connexin mutations in skin disease and hearing loss. *Am. J. Hum. Genet.* **68,** 559-568.

Kelsell,D.P., Dunlop,J., Stevens,H.P., Lench,N.J., Liang,J.N., Parry,G., Mueller,R.F., and Leigh,I.M. (1997). Connexin 26 mutations in hereditary non-syndromic sensorineural deafness. *Nature* **387,** 80-83.

Kelsell,D.P., Wilgoss,A.L., Richard,G., Stevens,H.P., Munro,C.S., and Leigh,I.M. (2000). Connexin mutations associated with palmoplantar keratoderma and profound deafness in a single family. *Eur. J. Hum. Genet.* **8,** 469-472.

Kharkovets,T., Dedek,K., Maier,H., Schweizer,M., Khimich,D., Nouvian,R., Vardanyan,V., Leuwer,R., Moser,T., and Jentsch,T.J. (2006). Mice with altered KCNQ4 K+ channels implicate sensory outer hair cells in human progressive deafness. *EMBO J.* **25,** 642-652.

Kidder,G.M. (2009). Toward a new nomenclature for connexin genes. In *Connexins: A guide*. (ed. Harris,A.L. and Locke,D.), pp. 543-545. New York: Humana Press.

Kikuchi,K. and Hilding,D.A. (1966). The development of the stria vascularis in the mouse. *Acta Otolaryngol.* **62,** 277-291.

Kikuchi,T., Adams,J.C., Miyabe,Y., So,E., and Kobayashi,T. (2000). Potassium ion recycling pathway via gap junction systems in the mammalian cochlea and its interruption in hereditary nonsyndromic deafness. *Med. Electron Microsc.* **33,** 51-56.

Kikuchi,T., Adams,J.C., Paul,D.L., and Kimura,R.S. (1994). Gap junction systems in the rat vestibular labyrinth: immunohistochemical and ultrastructural analysis. *Acta Otolaryngol.* **114,** 520-528.

Kikuchi,T., Kimura,R.S., Paul,D.L., and Adams,J.C. (1995). Gap junctions in the rat cochlea: immunohistochemical and ultrastructural analysis. *Anat. Embryol. (Berl)* **191,** 101-118.

King-VanVlack,C.E., Mewburn,J.D., Chapler,C.K., and MacDonald,P.H. (2003). Hemodynamic and proinflammatory actions of endothelin-1 in guinea pig small intestine submucosal microcirculation. *Am. J. Physiol Gastrointest. Liver Physiol* **284,** G940-G948.

Kitajiri,S., Miyamoto,T., Mineharu,A., Sonoda,N., Furuse,K., Hata,M., Sasaki,H., Mori,Y., Kubota,T., Ito,J. et al. (2004). Compartmentalization established by claudin-11-based tight junctions in stria vascularis is required for hearing through generation of endocochlear potential. *J. Cell Sci.* **117,** 5087-5096.

Kitamura,K., Sakagami,M., Umemoto,M., Takeda,N., Doi,K., Kasugai,T., and Kitamura,Y. (1994). Strial dysfunction in a melanocyte deficient mutant rat (Ws/Ws rat). *Acta Otolaryngol.* **114,** 177-181.

Klausner,R.D., Donaldson,J.G., and Lippincott-Schwartz,J. (1992). Brefeldin A: insights into the control of membrane traffic and organelle structure. *J. Cell Biol.* **116,** 1071-1080.

Klumperman,J., Schweizer,A., Clausen,H., Tang,B.L., Hong,W., Oorschot,V., and Hauri,H.P. (1998). The recycling pathway of protein ERGIC-53 and dynamics of the ER-Golgi intermediate compartment. *J. Cell Sci.* **111 (Pt 22),** 3411-3425.

Kofuji,P. and Newman,E.A. (2004). Potassium buffering in the central nervous system. *Neuroscience* **129,** 1045-1056.

Kojima,T., Mitaka,T., Shibata,Y., and Mochizuki,Y. (1995). Induction and regulation of connexin26 by glucagon in primary cultures of adult rat hepatocytes. *J. Cell Sci.* **108 (Pt 8),** 2771-2780.

Konishi,T., Hamrick,P.E., and Walsh,P.J. (1978). Ion transport in guinea pig cochlea. I. Potassium and sodium transport. *Acta Otolaryngol.* **86,** 22-34.

Koval,M. (2006). Pathways and control of connexin oligomerization. *Trends Cell Biol.* **16,** 159-166.

Koval,M., Harley,J.E., Hick,E., and Steinberg,T.H. (1997). Connexin46 is retained as monomers in a trans-Golgi compartment of osteoblastic cells. *J. Cell Biol.* **137,** 847-857.

Kressin,K., Kuprijanova,E., Jabs,R., Seifert,G., and Steinhauser,C. (1995). Developmental regulation of Na+ and K+ conductances in glial cells of mouse hippocampal brain slices. *Glia* **15,** 173-187.

Kudo,T., Ikeda,K., Kure,S., Matsubara,Y., Oshima,T., Watanabe,K., Kawase,T., Narisawa,K., and Takasaka,T. (2000). Novel mutations in the connexin 26 gene (GJB2) responsible for childhood deafness in the Japanese population. *Am. J. Med. Genet.* **90,** 141-145.

Kudo,T., Kure,S., Ikeda,K., Xia,A.P., Katori,Y., Suzuki,M., Kojima,K., Ichinohe,A., Suzuki,Y., Aoki,Y. et al. (2003). Transgenic expression of a dominant-negative connexin26 causes degeneration of the organ of Corti and non-syndromic deafness. *Hum. Mol. Genet.* **12,** 995-1004.

Kumar,N.M. and Gilula,N.B. (1992). Molecular biology and genetics of gap junction channels. *Semin. Cell Biol.* **3,** 3-16.

Kumar,N.M. and Gilula,N.B. (1986). Cloning and characterization of human and rat liver cDNAs coding for a gap junction protein. *J. Cell Biol.* **103,** 767-776.

Kunzelmann,P., Schroder,W., Traub,O., Steinhauser,C., Dermietzel,R., and Willecke,K. (1999). Late onset and increasing expression of the gap junction protein connexin30 in adult murine brain and long-term cultured astrocytes. *Glia* **25,** 111-119.

Laciano,L., Franke,K., Iurato,S., and Reale,E. (1977). Freeze-fracture study of the cell junctions in the utricle and saccule. *Acta Otolaryngol.* **83,** 79-84.

Laing,J.G. and Beyer,E.C. (1995). The gap junction protein connexin43 is degraded via the ubiquitin proteasome pathway. *J. Biol. Chem.* **270,** 26399-26403.

Laird,D.W. (2010). The gap junction proteome and its relationship to disease. *Trends Cell Biol.* **20,** 92-101.

Laird,D.W. (2006). Life cycle of connexins in health and disease. *Biochem. J.* **394,** 527-543.

Laird,D.W., Castillo,M., and Kasprzak,L. (1995). Gap junction turnover, intracellular trafficking, and phosphorylation of connexin43 in brefeldin A-treated rat mammary tumor cells. *J. Cell Biol.* **131,** 1193-1203.

Laird,D.W., Puranam,K.L., and Revel,J.P. (1991). Turnover and phosphorylation dynamics of connexin43 gap junction protein in cultured cardiac myocytes. *Biochem. J.* **273(Pt 1),** 67-72.

Lamartine,J., Munhoz,E.G., Kibar,Z., Lanneluc,I., Callouet,E., Laoudj,D., Lemaitre,G., Hand,C., Hayflick,S.J., Zonana,J. et al. (2000). Mutations in GJB6 cause hidrotic ectodermal dysplasia. *Nat. Genet.* **26,** 142-144.

Lautermann,J., Frank,H.G., Jahnke,K., Traub,O., and Winterhager,E. (1999). Developmental expression patterns of connexin26 and -30 in the rat cochlea. *Dev. Genet.* **25,** 306-311.

Lautermann,J., ten Cate,W.J., Altenhoff,P., Grummer,R., Traub,O., Frank,H., Jahnke,K., and Winterhager,E. (1998). Expression of the gap-junction connexins 26 and 30 in the rat cochlea. *Cell Tissue Res.* **294,** 415-420.

Lee,J.R., Derosa,A.M., and White,T.W. (2009). Connexin mutations causing skin disease and deafness increase hemichannel activity and cell death when expressed in Xenopus oocytes. *J. Invest Dermatol.* **129,** 870-878.

Lee,M.C., Miller,E.A., Goldberg,J., Orci,L., and Schekman,R. (2004). Bi-directional protein transport between the ER and Golgi. *Annu. Rev. Cell Dev. Biol.* **20,** 87-123.

Lerer,I., Sagi,M., Ben-Neriah,Z., Wang,T., Levi,H., and Abeliovich,D. (2001). A deletion mutation in GJB6 cooperating with a GJB2 mutation in trans in non-syndromic deafness: A novel founder mutation in Ashkenazi Jews. *Hum. Mutat.* **18,** 460.

Levine,T. and Rabouille,C. (2005). Endoplasmic reticulum: one continuous network compartmentalized by extrinsic cues. *Curr. Opin. Cell Biol.* **17,** 362-368.

Li,L., Nevill,G., and Forge,A. (1995). Two modes of hair cell loss from the vestibular sensory epithelia of the guinea pig inner ear. *J. Comp Neurol.* **355,** 405-417.

Liang,F., Niedzielski,A., Schulte,B.A., Spicer,S.S., Hazen-Martin,D.J., and Shen,Z. (2003). A voltage- and Ca2+-dependent big conductance K channel in cochlear spiral ligament fibrocytes. *Pflugers Arch.* **445,** 683-692.

Liberman,M.C., Gao,J., He,D.Z., Wu,X., Jia,S., and Zuo,J. (2002). Prestin is required for electromotility of the outer hair cell and for the cochlear amplifier. *Nature* **419,** 300-304.

Lin,H.W., Schneider,M.E., and Kachar,B. (2005). When size matters: the dynamic regulation of stereocilia lengths. *Curr. Opin. Cell Biol.* **17,** 55-61.

Lippincott-Schwartz,J., Donaldson,J.G., Schweizer,A., Berger,E.G., Hauri,H.P., Yuan,L.C., and Klausner,R.D. (1990). Microtubule-dependent retrograde transport of proteins into the ER in the presence of brefeldin A suggests an ER recycling pathway. *Cell* **60,** 821-836.

Liu,X.Z., Xia,X.J., Adams,J., Chen,Z.Y., Welch,K.O., Tekin,M., Ouyang,X.M., Kristiansen,A., Pandya,A., Balkany,T. et al. (2001). Mutations in GJA1 (connexin 43) are associated with non-syndromic autosomal recessive deafness. *Hum. Mol. Genet.* **10,** 2945-2951.

Loewenstein,W.R. (1966). Permeability of membrane junctions. *Ann. N. Y. Acad. Sci.* **137,** 441-472.

Lopez-Bigas,N., Melchionda,S., Gasparini,P., Borragan,A., Arbones,M.L., and Estivill,X. (2002). A common frameshift mutation and other variants in GJB4 (connexin 30.3): Analysis of hearing impairment families. *Hum. Mutat.* **19,** 458.

Maeda,S., Nakagawa,S., Suga,M., Yamashita,E., Oshima,A., Fujiyoshi,Y., and Tsukihara,T. (2009). Structure of the connexin 26 gap junction channel at 3.5 A resolution. *Nature* **458,** 597-602.

Majumder,P., Crispino,G., Rodriguez,L., Ciubotaru,C.D., Anselmi,F., Piazza,V., Bortolozzi,M., and Mammano,F. (2010). ATP-mediated cell-cell signaling in the organ of Corti: the role of connexin channels. *Purinergic. Signal.* **6,** 167-187.

Makowski,L., Caspar,D.L., Phillips,W.C., and Goodenough,D.A. (1977). Gap junction structures. II. Analysis of the x-ray diffraction data. *J. Cell Biol.* **74,** 629-645.

Man,Y.K., Trolove,C., Tattersall,D., Thomas,A.C., Papakonstantinopoulou,A., Patel,D., Scott,C., Chong,J., Jagger,D.J., O'Toole,E.A. et al. (2007). A deafness-

associated mutant human connexin 26 improves the epithelial barrier in vitro. *J. Membr. Biol.* **218,** 29-37.

Manthey,D., Banach,K., Desplantez,T., Lee,C.G., Kozak,C.A., Traub,O., Weingart,R., and Willecke,K. (2001). Intracellular domains of mouse connexin26 and -30 affect diffusional and electrical properties of gap junction channels. *J. Membr. Biol.* **181,** 137-148.

Marazita,M.L., Ploughman,L.M., Rawlings,B., Remington,E., Arnos,K.S., and Nance,W.E. (1993). Genetic epidemiological studies of early-onset deafness in the U.S. school-age population. *Am. J. Med. Genet.* **46,** 486-491.

Marcus,D.C. (1986). Non-sensory electrophysiology of the cochlea: stria vascularis. In *Neurobiology of Hearing: The Cochlea*. (ed. Altschuler,R.A., Hoffman,D.W., and Bobbin,R.P.), pp. 123-137. New York: Raven.

Marcus,D.C., Marcus,N.Y., and Thalmann,R. (1981). Changes in cation contents of stria vascularis with ouabain and potassium-free perfusion. *Hear. Res.* **4,** 149-160.

Marcus,D.C., Rokugo,M., and Thalmann,R. (1985). Effects of barium and ion substitutions in artificial blood on endocochlear potential. *Hear. Res.* **17,** 79-86.

Marcus,D.C., Wu,T., Wangemann,P., and Kofuji,P. (2002). KCNJ10 (Kir4.1) potassium channel knockout abolishes endocochlear potential. *Am. J. Physiol Cell Physiol* **282,** C403-C407.

Martin,P.E., Blundell,G., Ahmad,S., Errington,R.J., and Evans,W.H. (2001a). Multiple pathways in the trafficking and assembly of connexin 26, 32 and 43 into gap junction intercellular communication channels. *J. Cell Sci.* **114,** 3845-3855.

Martin,P.E., Coleman,S.L., Casalotti,S.O., Forge,A., and Evans,W.H. (1999). Properties of connexin26 gap junctional proteins derived from mutations associated with non-syndromal heriditary deafness. *Hum. Mol. Genet.* **8,** 2369-2376.

Martin,P.E., Errington,R.J., and Evans,W.H. (2001b). Gap junction assembly: multiple connexin fluorophores identify complex trafficking pathways. *Cell Commun. Adhes.* **8,** 243-248.

Martinez,A.D., Acuna,R., Figueroa,V., Maripillan,J., and Nicholson,B. (2009). Gap-junction channels dysfunction in deafness and hearing loss. *Antioxid. Redox. Signal.* **11,** 309-322.

Martinez-Alonso,E., Egea,G., Ballesta,J., and Martinez-Menarguez,J.A. (2005). Structure and dynamics of the Golgi complex at 15 degrees C: low temperature induces the formation of Golgi-derived tubules. *Traffic.* **6,** 32-44.

Marziano,N.K., Casalotti,S.O., Portelli,A.E., Becker,D.L., and Forge,A. (2003). Mutations in the gene for connexin 26 (GJB2) that cause hearing loss have a dominant negative effect on connexin 30. *Hum. Mol. Genet.* **12,** 805-812.

Mathias,R.T., White,T.W., and Gong,X. (2010). Lens gap junctions in growth, differentiation, and homeostasis. *Physiol Rev.* **90,** 179-206.

Matlin,K.S. and Simons,K. (1983). Reduced temperature prevents transfer of a membrane glycoprotein to the cell surface but does not prevent terminal glycosylation. *Cell* **34,** 233-243.

Maxfield,F.R. and McGraw,T.E. (2004). Endocytic recycling. *Nat. Rev. Mol. Cell Biol.* **5,** 121-132.

Maza,J., Das,S.J., and Koval,M. (2005). Defining a minimal motif required to prevent connexin oligomerization in the endoplasmic reticulum. *J. Biol. Chem.* **280,** 21115-21121.

Maza,J., Mateescu,M., Das,S.J., and Koval,M. (2003). Differential oligomerization of endoplasmic reticulum-retained connexin43/connexin32 chimeras. *Cell Commun. Adhes.* **10,** 319-322.

McDowell,B., Davies,S., and Forge,A. (1989). The effect of gentamicin-induced hair cell loss on the tight junctions of the reticular lamina. *Hear. Res.* **40,** 221-232.

Medzihradszky,K.F. (2005). Characterization of protein N-glycosylation. *Methods Enzymol.* **405,** 116-138.

Melichar,I. and Syka,J. (1987). Electrophysiological measurements of the stria vascularis potentials in vivo. *Hear. Res.* **25,** 35-43.

Mellman,I. and Warren,G. (2000). The road taken: past and future foundations of membrane traffic. *Cell* **100,** 99-112.

Meyer,C.G., Amedofu,G.K., Brandner,J.M., Pohland,D., Timmann,C., and Horstmann,R.D. (2002). Selection for deafness? *Nat. Med.* **8,** 1332-1333.

Minowa,O., Ikeda,K., Sugitani,Y., Oshima,T., Nakai,S., Katori,Y., Suzuki,M., Furukawa,M., Kawase,T., Zheng,Y. et al. (1999). Altered cochlear fibrocytes in a mouse model of DFN3 nonsyndromic deafness. *Science* **285,** 1408-1411.

Mistrik,P. and Ashmore,J. (2009). The role of potassium recirculation in cochlear amplification. *Curr. Opin. Otolaryngol. Head Neck Surg.* **17,** 394-399.

Mistrik,P., Mullaley,C., Mammano,F., and Ashmore,J. (2009). Three-dimensional current flow in a large-scale model of the cochlea and the mechanism of amplification of sound. *J. R. Soc. Interface* **6,** 279-291.

Misumi,Y., Misumi,Y., Miki,K., Takatsuki,A., Tamura,G., and Ikehara,Y. (1986). Novel blockade by brefeldin A of intracellular transport of secretory proteins in cultured rat hepatocytes. *J. Biol. Chem.* **261,** 11398-11403.

Morell,R.J., Kim,H.J., Hood,L.J., Goforth,L., Friderici,K., Fisher,R., Van,C.G., Berlin,C.I., Oddoux,C., Ostrer,H. et al. (1998). Mutations in the connexin 26 gene (GJB2) among Ashkenazi Jews with nonsyndromic recessive deafness. *N. Engl. J. Med.* **339,** 1500-1505.

Morton,C.C. and Nance,W.E. (2006). Newborn hearing screening--a silent revolution. *N. Engl. J. Med.* **354,** 2151-2164.

Musil,L.S. and Goodenough,D.A. (1993). Multisubunit assembly of an integral plasma membrane channel protein, gap junction connexin43, occurs after exit from the ER. *Cell* **74,** 1065-1077.

Mustapha,M., Fang,Q., Gong,T.W., Dolan,D.F., Raphael,Y., Camper,S.A., and Duncan,R.K. (2009). Deafness and permanently reduced potassium channel gene expression and function in hypothyroid Pit1dw mutants. *J. Neurosci.* **29,** 1212-1223.

Mutai,H., Nagashima,R., Fujii,M., and Matsunaga,T. (2009). Mitotic activity and specification of fibrocyte subtypes in the developing rat cochlear lateral wall. *Neuroscience* **163,** 1255-1263.

Nakano,A. and Luini,A. (2010). Passage through the Golgi. *Curr. Opin. Cell Biol.* **22,** 471-478.

Nakano,Y., Kim,S.H., Kim,H.M., Sanneman,J.D., Zhang,Y., Smith,R.J., Marcus,D.C., Wangemann,P., Nessler,R.A., and Banfi,B. (2009). A claudin-9-based ion permeability barrier is essential for hearing. *PLoS. Genet.* **5,** e1000610.

Nebenfuhr,A., Ritzenthaler,C., and Robinson,D.G. (2002). Brefeldin A: deciphering an enigmatic inhibitor of secretion. *Plant Physiol* **130,** 1102-1108.

Nehring,R.B., Wischmeyer,E., Doring,F., Veh,R.W., Sheng,M., and Karschin,A. (2000). Neuronal inwardly rectifying K(+) channels differentially couple to PDZ proteins of the PSD-95/SAP90 family. *J. Neurosci.* **20,** 156-162.

Newman,E.A., Frambach,D.A., and Odette,L.L. (1984). Control of extracellular potassium levels by retinal glial cell K+ siphoning. *Science* **225,** 1174-1175.

Nickel,R. and Forge,A. (2010). Gap Junctions and Connexins: The Molecular Genetics of Deafness. Chichester: John Wiley & Sons, Ltd.

Nickel,R. and Forge,A. (2008). Gap junctions and connexins in the inner ear: their roles in homeostasis and deafness. *Curr. Opin. Otolaryngol. Head Neck Surg.* **16,** 452-457.

Nickel,R., Forge,A., and Jagger,D. (2009). Connexins in the inner ear. In *Connexins: A guide*. (ed. Harris,A.L. and Locke,D.), pp. 419-434. New York: Humana Press.

Nickel,W. and Rabouille,C. (2009). Mechanisms of regulated unconventional protein secretion. *Nat. Rev. Mol. Cell Biol.* **10,** 148-155.

Nickel,W. and Seedorf,M. (2008). Unconventional mechanisms of protein transport to the cell surface of eukaryotic cells. *Annu. Rev. Cell Dev. Biol.* **24,** 287-308.

Nin,F., Hibino,H., Doi,K., Suzuki,T., Hisa,Y., and Kurachi,Y. (2008). The endocochlear potential depends on two K+ diffusion potentials and an electrical barrier in the stria vascularis of the inner ear. *Proc. Natl. Acad. Sci. U. S. A* **105,** 1751-1756.

Ohno,N., Terada,N., and Ohno,S. (2006). Histochemical analyses of living mouse liver under different hemodynamic conditions by "in vivo cryotechnique". *Histochem. Cell Biol.* **126,** 389-398.

Ohno,Y., Hibino,H., Lossin,C., Inanobe,A., and Kurachi,Y. (2007). Inhibition of astroglial Kir4.1 channels by selective serotonin reuptake inhibitors. *Brain Res.* **1178,** 44-51.

Okiyoneda,T., Harada,K., Yamahira,K., Wada,I., Hashimoto,Y., Ueno,K., Suico,M.A., Shuto,T., and Kai,H. (2004). Characterization of the trafficking pathway of cystic fibrosis transmembrane conductance regulator in baby hamster kidney cells. *J. Pharmacol. Sci.* **95,** 471-475.

Orkand,R.K., Nicholls,J.G., and Kuffler,S.W. (1966). Effect of nerve impulses on the membrane potential of glial cells in the central nervous system of amphibia. *J. Neurophysiol.* **29,** 788-806.

Ortolano,S., Di,P.G., Crispino,G., Anselmi,F., Mammano,F., and Chiorini,J.A. (2008). Coordinated control of connexin 26 and connexin 30 at the regulatory and functional level in the inner ear. *Proc. Natl. Acad. Sci. U. S. A* **105,** 18776-18781.

Palade,G. (1975). Intracellular aspects of the process of protein synthesis. *Science* **189,** 867.

Pallares-Ruiz,N., Blanchet,P., Mondain,M., Claustres,M., and Roux,A.F. (2002). A large deletion including most of GJB6 in recessive non syndromic deafness: a digenic effect? *Eur. J. Hum. Genet.* **10,** 72-76.

Paul,D.L. (1986). Molecular cloning of cDNA for rat liver gap junction protein. *J. Cell Biol.* **103,** 123-134.

Paznekas,W.A., Boyadjiev,S.A., Shapiro,R.E., Daniels,O., Wollnik,B., Keegan,C.E., Innis,J.W., Dinulos,M.B., Christian,C., Hannibal,M.C. et al. (2003). Connexin 43 (GJA1) mutations cause the pleiotropic phenotype of oculodentodigital dysplasia. *Am. J. Hum. Genet.* **72,** 408-418.

Paznekas,W.A., Karczeski,B., Vermeer,S., Lowry,R.B., Delatycki,M., Laurence,F., Koivisto,P.A., Van,M.L., Boyadjiev,S.A., Bodurtha,J.N. et al. (2009). GJA1 mutations, variants, and connexin 43 dysfunction as it relates to the oculodentodigital dysplasia phenotype. *Hum. Mutat.* **30,** 724-733.

Penuela,S., Bhalla,R., Gong,X.Q., Cowan,K.N., Celetti,S.J., Cowan,B.J., Bai,D., Shao,Q., and Laird,D.W. (2007). Pannexin 1 and pannexin 3 are glycoproteins that exhibit many distinct characteristics from the connexin family of gap junction proteins. *J. Cell Sci.* **120,** 3772-3783.

Perkins,G.A., Goodenough,D.A., and Sosinsky,G.E. (1998). Formation of the gap junction intercellular channel requires a 30 degree rotation for interdigitating two apposing connexons. *J. Mol. Biol.* **277,** 171-177.

Phelan,P. (2005). Innexins: members of an evolutionarily conserved family of gap-junction proteins. *Biochim. Biophys. Acta* **1711,** 225-245.

Pickles,J.O., Comis,S.D., and Osborne,M.P. (1984). Cross-links between stereocilia in the guinea pig organ of Corti, and their possible relation to sensory transduction. *Hear. Res.* **15,** 103-112.

Plum,A., Winterhager,E., Pesch,J., Lautermann,J., Hallas,G., Rosentreter,B., Traub,O., Herberhold,C., and Willecke,K. (2001). Connexin31-deficiency in mice causes transient placental dysmorphogenesis but does not impair hearing and skin differentiation. *Dev. Biol.* **231,** 334-347.

Prazma,J. (1975). Electroanatomy of the lateral wall of the cochlea. *Arch. Otorhinolaryngol.* **209,** 1-13.

Prydz,K., Dick,G., and Tveit,H. (2008). How many ways through the Golgi maze? *Traffic.* **9,** 299-304.

Qu,C., Gardner,P., and Schrijver,I. (2009). The role of the cytoskeleton in the formation of gap junctions by Connexin 30. *Exp. Cell Res.* **315,** 1683-1692.

Qu,C., Liang,F., Smythe,N.M., and Schulte,B.A. (2007). Identification of ClC-2 and CIC-K2 chloride channels in cultured rat type IV spiral ligament fibrocytes. *J. Assoc. Res. Otolaryngol.* **8,** 205-219.

Rabionet,R., Lopez-Bigas,N., Arbones,M.L., and Estivill,X. (2002). Connexin mutations in hearing loss, dermatological and neurological disorders. *Trends Mol. Med.* **8,** 205-212.

Raphael,Y. and Altschuler,R.A. (1991). Reorganization of cytoskeletal and junctional proteins during cochlear hair cell degeneration. *Cell Motil. Cytoskeleton* **18,** 215-227.

Raphael,Y. and Altschuler,R.A. (2003). Structure and innervation of the cochlea. *Brain Res. Bull.* **60,** 397-422.

Reale,E., Luciano,L., Franke,K., Pannese,E., Wermbter,G., and Iurato,S. (1975). Intercellular junctions in the vascular stria and spiral ligament. *J. Ultrastruct. Res.* **53,** 284-297.

Revel,J.P. and Karnovsky,M.J. (1967). Hexagonal array of subunits in intercellular junctions of the mouse heart and liver. *J. Cell Biol.* **33,** C7-C12.

Richard,G., Rouan,F., Willoughby,C.E., Brown,N., Chung,P., Ryynanen,M., Jabs,E.W., Bale,S.J., DiGiovanna,J.J., Uitto,J. et al. (2002). Missense mutations in GJB2 encoding connexin-26 cause the ectodermal dysplasia keratitis-ichthyosis-deafness syndrome. *Am. J. Hum. Genet.* **70,** 1341-1348.

Robertson,J.D. (1963). THE OCCURRENCE OF A SUBUNIT PATTERN IN THE UNIT MEMBRANES OF CLUB ENDINGS IN MAUTHNER CELL SYNAPSES IN GOLDFISH BRAINS. *J. Cell Biol.* **19,** 201-221.

Rothman,J.E. (1994). Mechanisms of intracellular protein transport. *Nature* **372,** 55-63.

Rouan,F., White,T.W., Brown,N., Taylor,A.M., Lucke,T.W., Paul,D.L., Munro,C.S., Uitto,J., Hodgins,M.B., and Richard,G. (2001). trans-dominant inhibition of connexin-43 by mutant connexin-26: implications for dominant connexin disorders affecting epidermal differentiation. *J. Cell Sci.* **114,** 2105-2113.

Rubartelli,A., Cozzolino,F., Talio,M., and Sitia,R. (1990). A novel secretory pathway for interleukin-1 beta, a protein lacking a signal sequence. *EMBO J.* **9,** 1503-1510.

Ruggero,M.A. and Rich,N.C. (1991). Furosemide alters organ of corti mechanics: evidence for feedback of outer hair cells upon the basilar membrane. *J. Neurosci.* **11,** 1057-1067.

Rybak,L.P., Weberg,A., and Whitworth,C. (1991). Development of the stria vascularis in the rat. *ORL J. Otorhinolaryngol. Relat Spec.* **53,** 72-77.

Rybak,L.P., Whitworth,C., and Scott,V. (1992). Development of endocochlear potential and compound action potential in the rat. *Hear. Res.* **59,** 189-194.

Saez,J.C., Berthoud,V.M., Branes,M.C., Martinez,A.D., and Beyer,E.C. (2003). Plasma membrane channels formed by connexins: their regulation and functions. *Physiol Rev.* **83,** 1359-1400.

Sakaguchi,N., Crouch,J.J., Lytle,C., and Schulte,B.A. (1998). Na-K-Cl cotransporter expression in the developing and senescent gerbil cochlea. *Hear. Res.* **118,** 114-122.

Salt,A.N., Melichar,I., and Thalmann,R. (1987). Mechanisms of endocochlear potential generation by stria vascularis. *Laryngoscope* **97,** 984-991.

Santi,P.A. and Duvall,A.J., III (1979). Morphological alteration of the stria vascularis after administration of the diuretic bumetanide. *Acta Otolaryngol.* **88,** 1-12.

Santos-Sacchi,J. and Dallos,P. (1983). Intercellular communication in the supporting cells of the organ of Corti. *Hear. Res.* **9,** 317-326.

Saraste,J. and Kuismanen,E. (1984). Pre- and post-Golgi vacuoles operate in the transport of Semliki Forest virus membrane glycoproteins to the cell surface. *Cell* **38,** 535-549.

Sato,I., Obata,Y., Kasahara,K., Nakayama,Y., Fukumoto,Y., Yamasaki,T., Yokoyama,K.K., Saito,T., and Yamaguchi,N. (2009). Differential trafficking of Src, Lyn, Yes and Fyn is specified by the state of palmitoylation in the SH4 domain. *J. Cell Sci.* **122,** 965-975.

Scemes,E. (2011). Nature of plasmalemmal functional "hemichannels". *Biochim. Biophys. Acta*.

Schulte,B.A. and Schmiedt,R.A. (1992). Lateral wall Na,K-ATPase and endocochlear potentials decline with age in quiet-reared gerbils. *Hear. Res.* **61,** 35-46.

Schutz,M., Auth,T., Gehrt,A., Bosen,F., Korber,I., Strenzke,N., Moser,T., and Willecke,K. (2011). The connexin26 S17F mouse mutant represents a model for the human hereditary keratitis-ichthyosis-deafness syndrome. *Hum. Mol. Genet.* **20,** 28-39.

Schutz,M., Scimemi,P., Majumder,P., De Siati,R.D., Crispino,G., Rodriguez,L., Bortolozzi,M., Santarelli,R., Seydel,A., Sonntag,S. et al. (2010). The human deafness-associated connexin 30 T5M mutation causes mild hearing loss and reduces

biochemical coupling among cochlear non-sensory cells in knock-in mice. *Hum. Mol. Genet.* **19,** 4759-4773.

Scott,C.A. and Kelsell,D.P. (2011). Key functions for gap junctions in skin and hearing. *Biochem. J.* **438,** 245-254.

Segretain,D. and Falk,M.M. (2004). Regulation of connexin biosynthesis, assembly, gap junction formation, and removal. *Biochim. Biophys. Acta* **1662,** 3-21.

Shen,Z., Liang,F., Hazen-Martin,D.J., and Schulte,B.A. (2004). BK channels mediate the voltage-dependent outward current in type I spiral ligament fibrocytes. *Hear. Res.* **187,** 35-43.

Shi,L., Terada,N., Saitoh,Y., Saitoh,S., and Ohno,S. (2011). Immunohistochemical distribution of serum proteins in living mouse heart with In vivo cryotechnique. *Acta Histochem. Cytochem.* **44,** 61-72.

Singh,R. and Wangemann,P. (2008). Free radical stress-mediated loss of Kcnj10 protein expression in stria vascularis contributes to deafness in Pendred syndrome mouse model. *Am. J. Physiol Renal Physiol* **294,** F139-F148.

Smith,F.J., Morley,S.M., and McLean,W.H. (2002). A novel connexin 30 mutation in Clouston syndrome. *J. Invest Dermatol.* **118,** 530-532.

Sohl,G. and Willecke,K. (2003). An update on connexin genes and their nomenclature in mouse and man. *Cell Commun. Adhes.* **10,** 173-180.

Sonntag,S., Sohl,G., Dobrowolski,R., Zhang,J., Theis,M., Winterhager,E., Bukauskas,F.F., and Willecke,K. (2009). Mouse lens connexin23 (Gje1) does not form functional gap junction channels but causes enhanced ATP release from HeLa cells. *Eur. J. Cell Biol.* **88,** 65-77.

Sosinsky,G.E., Boassa,D., Dermietzel,R., Duffy,H.S., Laird,D.W., MacVicar,B., Naus,C.C., Penuela,S., Scemes,E., Spray,D.C. et al. (2011). Pannexin channels are not gap junction hemichannels. *Channels (Austin.)* **5,** 193-197.

Souter,M. and Forge,A. (1998). Intercellular junctional maturation in the stria vascularis: possible association with onset and rise of endocochlear potential. *Hear. Res.* **119,** 81-95.

Spector,G.J. and Carr,C. (1979). The ultrastructural cytochemistry of peroxisomes in the guinea pig cochlea: a metabolic hypothesis for the stria vascularis. *Laryngoscope* **89,** 1-38.

Spicer,S.S. and Schulte,B.A. (1991). Differentiation of inner ear fibrocytes according to their ion transport related activity. *Hear. Res.* **56,** 53-64.

Spicer,S.S. and Schulte,B.A. (1996). The fine structure of spiral ligament cells relates to ion return to the stria and varies with place-frequency. *Hear. Res.* **100,** 80-100.

Spicer,S.S. and Schulte,B.A. (2005). Pathologic changes of presbycusis begin in secondary processes and spread to primary processes of strial marginal cells. *Hear. Res.* **205,** 225-240.

Spoendlin,H. (1972). Innervation densities of the cochlea. *Acta Otolaryngol.* **73,** 235-248.

Steel,K.P. and Barkway,C. (1989). Another role for melanocytes: their importance for normal stria vascularis development in the mammalian inner ear. *Development* **107,** 453-463.

Sterkers,O., Saumon,G., Tran Ba,H.P., and Amiel,C. (1982). K, Cl, and H2O entry in endolymph, perilymph, and cerebrospinal fluid of the rat. *Am. J. Physiol* **243,** F173-F180.

Suko,T., Ichimiya,I., Yoshida,K., Suzuki,M., and Mogi,G. (2000). Classification and culture of spiral ligament fibrocytes from mice. *Hear. Res.* **140,** 137-144.

Sun,J., Ahmad,S., Chen,S., Tang,W., Zhang,Y., Chen,P., and Lin,X. (2005). Cochlear gap junctions coassembled from Cx26 and 30 show faster intercellular Ca2+ signaling than homomeric counterparts. *Am. J. Physiol Cell Physiol* **288,** C613-C623.

Sun,Y., Tang,W., Chang,Q., Wang,Y., Kong,W., and Lin,X. (2009). Connexin30 null and conditional connexin26 null mice display distinct pattern and time course of cellular degeneration in the cochlea. *J. Comp Neurol.* **516,** 569-579.

Suzuki,T., Takamatsu,T., and Oyamada,M. (2003). Expression of gap junction protein connexin43 in the adult rat cochlea: comparison with connexin26. *J. Histochem. Cytochem.* **51,** 903-912.

Swanson,G.J., Howard,M., and Lewis,J. (1990). Epithelial autonomy in the development of the inner ear of a bird embryo. *Dev. Biol.* **137,** 243-257.

Tachibana,M. and Morioka,H. (1976). Well developed gap junctions between Deiter's cells of the organ of Corti. *J. Electron Microsc. (Tokyo)* **25,** 95-97.

Takeuchi,S. and Ando,M. (1998a). Dye-coupling of melanocytes with endothelial cells and pericytes in the cochlea of gerbils. *Cell Tissue Res.* **293,** 271-275.

Takeuchi,S. and Ando,M. (1998b). Inwardly rectifying K+ currents in intermediate cells in the cochlea of gerbils: a possible contribution to the endocochlear potential. *Neurosci. Lett.* **247,** 175-178.

Takeuchi,S., Ando,M., and Kakigi,A. (2000). Mechanism generating endocochlear potential: role played by intermediate cells in stria vascularis. *Biophys. J.* **79,** 2572-2582.

Tanemoto,M., Fujita,A., Higashi,K., and Kurachi,Y. (2002). PSD-95 mediates formation of a functional homomeric Kir5.1 channel in the brain. *Neuron* **34,** 387-397.

Tanemoto,M., Kittaka,N., Inanobe,A., and Kurachi,Y. (2000). In vivo formation of a proton-sensitive K+ channel by heteromeric subunit assembly of Kir5.1 with Kir4.1. *J. Physiol* **525 Pt 3,** 587-592.

Tang,W., Zhang,Y., Chang,Q., Ahmad,S., Dahlke,I., Yi,H., Chen,P., Paul,D.L., and Lin,X. (2006). Connexin29 is highly expressed in cochlear Schwann cells, and it is required for the normal development and function of the auditory nerve of mice. *J. Neurosci.* **26,** 1991-1999.

Tasaki,I. and Spyropoulos,C.S. (1959). Stria vascularis as source of endocochlear potential. *J. Neurophysiol.* **22,** 149-155.

Taylor,R.R., Nevill,G., and Forge,A. (2008). Rapid hair cell loss: a mouse model for cochlear lesions. *J. Assoc. Res. Otolaryngol.* **9,** 44-64.

Teubner,B., Michel,V., Pesch,J., Lautermann,J., Cohen-Salmon,M., Sohl,G., Jahnke,K., Winterhager,E., Herberhold,C., Hardelin,J.P. et al. (2003b). Connexin30 (Gjb6)-deficiency causes severe hearing impairment and lack of endocochlear potential. *Hum. Mol. Genet.* **12,** 13-21.

Teubner,B., Michel,V., Pesch,J., Lautermann,J., Cohen-Salmon,M., Sohl,G., Jahnke,K., Winterhager,E., Herberhold,C., Hardelin,J.P. et al. (2003a). Connexin30 (Gjb6)-deficiency causes severe hearing impairment and lack of endocochlear potential. *Hum. Mol. Genet.* **12,** 13-21.

Theis,M., Magin,T.M., Plum,A., and Willecke,K. (2000). General or cell type-specific deletion and replacement of connexin-coding DNA in the mouse. *Methods* **20,** 205-218.

Thomas,T., Jordan,K., Simek,J., Shao,Q., Jedeszko,C., Walton,P., and Laird,D.W. (2005). Mechanisms of Cx43 and Cx26 transport to the plasma membrane and gap junction regeneration. *J. Cell Sci.* **118,** 4451-4462.

Thomas,T., Telford,D., and Laird,D.W. (2004). Functional domain mapping and selective trans-dominant effects exhibited by Cx26 disease-causing mutations. *J. Biol. Chem.* **279,** 19157-19168.

Traub,O., Look,J., Paul,D., and Willecke,K. (1987). Cyclic adenosine monophosphate stimulates biosynthesis and phosphorylation of the 26 kDa gap junction protein in cultured mouse hepatocytes. *Eur. J. Cell Biol.* **43,** 48-54.

Tritsch,N.X., Yi,E., Gale,J.E., Glowatzki,E., and Bergles,D.E. (2007). The origin of spontaneous activity in the developing auditory system. *Nature* **450,** 50-55.

Trowe,M.O., Maier,H., Schweizer,M., and Kispert,A. (2008). Deafness in mice lacking the T-box transcription factor Tbx18 in otic fibrocytes. *Development* **135,** 1725-1734.

Tveit,H., Akslen,L.K., Fagereng,G.L., Tranulis,M.A., and Prydz,K. (2009). A secretory Golgi bypass route to the apical surface domain of epithelial MDCK cells. *Traffic.* **10,** 1685-1695.

Unger,V.M., Kumar,N.M., Gilula,N.B., and Yeager,M. (1999). Three-dimensional structure of a recombinant gap junction membrane channel. *Science* **283,** 1176-1180.

Unwin,P.N. and Ennis,P.D. (1984). Two configurations of a channel-forming membrane protein. *Nature* **307,** 609-613.

Valiunas,V. and Weingart,R. (2000). Electrical properties of gap junction hemichannels identified in transfected HeLa cells. *Pflugers Arch.* **440,** 366-379.

Vanslyke,J.K., Naus,C.C., and Musil,L.S. (2009). Conformational maturation and post-ER multisubunit assembly of gap junction proteins. *Mol. Biol. Cell* **20,** 2451-2463.

von Békésy,G. (1952). Resting potentials inside the cochlear partition of the guinea pig. *Nature* **169,** 241-242.

Wada,J., Kambayashi,J., Marcus,D.C., and Thalmann,R. (1979). Vascular perfusion of the cochlea: effect of potassium-free and rubidium-substituted media. *Arch. Otorhinolaryngol.* **225,** 79-81.

Wang,W.H., Yang,J.J., Lin,Y.C., Yang,J.T., and Li,S.Y. (2010). Novel expression patterns of connexin 30.3 in adult rat cochlea. *Hear. Res.* **265,** 77-82.

Wang,X., Matteson,J., An,Y., Moyer,B., Yoo,J.S., Bannykh,S., Wilson,I.A., Riordan,J.R., and Balch,W.E. (2004). COPII-dependent export of cystic fibrosis transmembrane conductance regulator from the ER uses a di-acidic exit code. *J. Cell Biol.* **167,** 65-74.

Wang,Y., Chang,Q., Tang,W., Sun,Y., Zhou,B., Li,H., and Lin,X. (2009). Targeted connexin26 ablation arrests postnatal development of the organ of Corti. *Biochem. Biophys. Res. Commun.* **385,** 33-37.

Wangemann,P. (2002). K+ cycling and the endocochlear potential. *Hear. Res.* **165,** 1-9.

Wangemann,P. (2006). Supporting sensory transduction: cochlear fluid homeostasis and the endocochlear potential. *J. Physiol* **576,** 11-21.

Wangemann,P., Itza,E.M., Albrecht,B., Wu,T., Jabba,S.V., Maganti,R.J., Lee,J.H., Everett,L.A., Wall,S.M., Royaux,I.E. et al. (2004). Loss of KCNJ10 protein expression abolishes endocochlear potential and causes deafness in Pendred syndrome mouse model. *BMC. Med.* **2,** 30.

Wangemann,P. and Schacht,J. (1996). Homeostatic Mechanisms in the Cochlea. In *Springer Handbook of Auditory Research: The Cochlea*. (ed. Dallos,P., Popper,A.N., and Fay,R.R.), pp. 130-185. New York: Springer.

Weber,P.C., Cunningham,C.D., III, and Schulte,B.A. (2001). Potassium recycling pathways in the human cochlea. *Laryngoscope* **111,** 1156-1165.

Weidmann,S. (1952). The electrical constants of Purkinje fibres. *J. Physiol* **118,** 348-360.

White,T.W. and Paul,D.L. (1999). Genetic diseases and gene knockouts reveal diverse connexin functions. *Annu. Rev. Physiol* **61,** 283-310.

White,T.W., Paul,D.L., Goodenough,D.A., and Bruzzone,R. (1995). Functional analysis of selective interactions among rodent connexins. *Mol. Biol. Cell* **6,** 459-470.

Willecke,K., Eiberger,J., Degen,J., Eckardt,D., Romualdi,A., Guldenagel,M., Deutsch,U., and Sohl,G. (2002). Structural and functional diversity of connexin genes in the mouse and human genome. *Biol. Chem.* **383,** 725-737.

Wu,T. and Marcus,D.C. (2003). Age-related changes in cochlear endolymphatic potassium and potential in CD-1 and CBA/CaJ mice. *J. Assoc. Res. Otolaryngol.* **4,** 353-362.

Xia,A.P., Ikeda,K., Katori,Y., Oshima,T., Kikuchi,T., and Takasaka,T. (2000). Expression of connexin 31 in the developing mouse cochlea. *Neuroreport* **11,** 2449-2453.

Xia,A.P., Kikuchi,T., Minowa,O., Katori,Y., Oshima,T., Noda,T., and Ikeda,K. (2002). Late-onset hearing loss in a mouse model of DFN3 non-syndromic deafness: morphologic and immunohistochemical analyses. *Hear. Res.* **166,** 150-158.

Xia,J.H., Liu,C.Y., Tang,B.S., Pan,Q., Huang,L., Dai,H.P., Zhang,B.R., Xie,W., Hu,D.X., Zheng,D. et al. (1998). Mutations in the gene encoding gap junction protein beta-3 associated with autosomal dominant hearing impairment. *Nat. Genet.* **20,** 370-373.

Yamaji,S., Droggiti,A., Lu,S.C., Martinez-Chantar,M.L., Warner,A., and Varela-Rey,M. (2010). S-Adenosylmethionine regulates connexins sub-types expressed by hepatocytes. *Eur. J. Cell Biol.*

Yamasaki,M., Komune,S., Shimozono,M., Matsuda,K., and Haruta,A. (2000). Development of monovalent ions in the endolymph in mouse cochlea. *ORL J. Otorhinolaryngol. Relat Spec.* **62,** 241-246.

Yang,J.J., Huang,S.H., Chou,K.H., Liao,P.J., Su,C.C., and Li,S.Y. (2007). Identification of mutations in members of the connexin gene family as a cause of nonsyndromic deafness in Taiwan. *Audiol. Neurootol.* **12,** 198-208.

Yeager,M., Unger,V.M., and Falk,M.M. (1998). Synthesis, assembly and structure of gap junction intercellular channels. *Curr. Opin. Struct. Biol.* **8,** 517-524.

Yoo,J.S., Moyer,B.D., Bannykh,S., Yoo,H.M., Riordan,J.R., and Balch,W.E. (2002). Non-conventional trafficking of the cystic fibrosis transmembrane conductance regulator through the early secretory pathway. *J. Biol. Chem.* **277,** 11401-11409.

Yoshida,K., Ichimiya,I., Suzuki,M., and Mogi,G. (1999). Effect of proinflammatory cytokines on cultured spiral ligament fibrocytes. *Hear. Res.* **137,** 155-159.

Yum,S.W., Zhang,J., Valiunas,V., Kanaporis,G., Brink,P.R., White,T.W., and Scherer,S.S. (2007). Human connexin26 and connexin30 form functional heteromeric and heterotypic channels. *Am. J. Physiol Cell Physiol* **293,** C1032-C1048.

Zahs,K.R. (1998). Heterotypic coupling between glial cells of the mammalian central nervous system. *Glia* **24,** 85-96.

Zaman,K., McPherson,M., Vaughan,J., Hunt,J., Mendes,F., Gaston,B., and Palmer,L.A. (2001). S-nitrosoglutathione increases cystic fibrosis transmembrane regulator maturation. *Biochem. Biophys. Res. Commun.* **284,** 65-70.

Zdebik,A.A., Wangemann,P., and Jentsch,T.J. (2009). Potassium ion movement in the inner ear: insights from genetic disease and mouse models. *Physiology. (Bethesda.)* **24,** 307-316.

Zelante,L., Gasparini,P., Estivill,X., Melchionda,S., D'Agruma,L., Govea,N., Mila,M., Monica,M.D., Lutfi,J., Shohat,M. et al. (1997). Connexin26 mutations associated with the most common form of non-syndromic neurosensory autosomal recessive deafness (DFNB1) in Mediterraneans. *Hum. Mol. Genet.* **6,** 1605-1609.

Zhang,Y., Tang,W., Ahmad,S., Sipp,J.A., Chen,P., and Lin,X. (2005). Gap junction-mediated intercellular biochemical coupling in cochlear supporting cells is required for normal cochlear functions. *Proc. Natl. Acad. Sci. U. S. A* **102,** 15201-15206.

Zhao,H.B. (2000). Directional rectification of gap junctional voltage gating between dieters cells in the inner ear of guinea pig. *Neurosci. Lett.* **296,** 105-108.

Zhao,H.B., Kikuchi,T., Ngezahayo,A., and White,T.W. (2006). Gap junctions and cochlear homeostasis. *J. Membr. Biol.* **209,** 177-186.

Zhao,H.B. and Santos-Sacchi,J. (2000). Voltage gating of gap junctions in cochlear supporting cells: evidence for nonhomotypic channels. *J. Membr. Biol.* **175,** 17-24.

Zhao,H.B., Yu,N., and Fleming,C.R. (2005). Gap junctional hemichannel-mediated ATP release and hearing controls in the inner ear. *Proc. Natl. Acad. Sci. U. S. A* **102,** 18724-18729.

Zheng-Fischhofer,Q., Schnichels,M., Dere,E., Strotmann,J., Loscher,N., McCulloch,F., Kretz,M., Degen,J., Reucher,H., Nagy,J.I. et al. (2007). Characterization of connexin30.3-deficient mice suggests a possible role of connexin30.3 in olfaction. *Eur. J. Cell Biol.* **86,** 683-700.

Zimmer,D.B., Green,C.R., Evans,W.H., and Gilula,N.B. (1987). Topological analysis of the major protein in isolated intact rat liver gap junctions and gap junction-derived single membrane structures. *J. Biol. Chem.* **262,** 7751-7763.

Zuber,C., Cormier,J.H., Guhl,B., Santimaria,R., Hebert,D.N., and Roth,J. (2007). EDEM1 reveals a quality control vesicular transport pathway out of the endoplasmic reticulum not involving the COPII exit sites. *Proc. Natl. Acad. Sci. U. S. A* **104,** 4407-4412.